INVESTIGATING THE CELL-SPECIFIC MECHANISMS THAT DRIVE SEX DIFFERENCES DURING NEUROPATHIC PAIN DEVELOPMENT

by

Thomas Alexander Szabo-Pardi

APPROVED BY SUPERVISORY COMMITTEE:

_____

Michael Burton, Chair

_____

Theodore Price

_____

Gregory Dussor

_____

Millie Rincón-Cortés

A családomnak

INVESTIGATING THE CELL-SPECFICI MECHANISMS THAT DRIVE SEX

DIFFERENCES DURING NEUROPATHIC PAIN DEVELOPMENT

by

THOMAS ALEXANDER SZABO-PARDI, BS

DISSERTATION

Presented to the Faculty of

The University of Texas at Dallas

in Partial Fulfillment

of the Requirements

for the Degree of

DOCTOR OF PHILOSOPHY IN

COGNITION AND NEUROSCIENCE

THE UNIVERSITY OF TEXAS AT DALLAS

August 2022

ACKNOWLEDGMENTS

INVESTIGATING THE CELL-SPECIFIC MECHANISMS THAT DRIVE SEX

DIFFERENCES DURING NEUROPATHIC PAIN DEVELOPMENT

Thomas Alexander Szabo-Pardi, PhD
The University of Texas at Dallas, 2022

Supervising Professor: Michael Burton

Chronic pain patients often suffer from a decline in quality of life due to a lack of efficacious long-term therapeutics. Moreover, the prevalence of chronic pain conditions is on the rise, with an average increase of nearly 10 percent in patients per decade. This, coupled with the devastating impact of the opioid crisis, highlights the need for novel pain therapeutics. An extensive literature has placed microglia, the resident immune cells of the central nervous system, at the forefront of male-specific mechanisms that mediate chronic pain plasticity. Recently, efforts have been made to design studies aimed at dissecting female specific mechanisms in pain plasticity. Evidence suggests that immune-related components of nociceptors are heavily dysregulated following insult and are more directly responsible for changes in female-specific sensitization. Despite advances in the field of pain neurobiology, there remains a clear disconnect between the cellular mechanisms that underlie maladaptive chronic pain in males and females. Moreover, a lack of studies directed towards interventions during early neuropathic pain development make it difficult to assess how functional changes in cellular phenotypes following injury can be manipulated to prevent maladaptive pain plasticity from taking place. The goal of our research was to use an innovative

approach to identify nociceptor and immune cell-specific mechanisms in both the peripheral and central nervous systems that mediate sex differences during neuropathic pain development. Our findings suggest that the initial phase of neuropathic development is sexually dimorphic, characterized by nociceptor-specific signaling mechanisms in females and immune cell mediated sensitization in males which may be modulated by genetic and pharmacological manipulation of toll-like receptor 4 signaling.

TABLE OF CONTENTS

LIST OF FIGURES

LIST OF TABLES

CHAPTER 1

INTRODUCTION

Prevalence of Pain

Pain is a multi-faceted, subjective experience that involves the integration of sensory systems and higher order processing centers in the brain. Pain is recognized as a biological benefit that induces defensive behaviors following injury which helps to facilitate the healing process. Dysregulation of the nervous and immune systems can often lead to maladaptive plasticity which translates to long lasting, or idiopathic pain. Chronic pain is characterized by pain that persists beyond a biological benefit and is clinically defined when symptoms are present for more than 3 months. Chronic pain is a pervasive disease that affects 10% of the world's population, with a prevalence of closer to 20-25% in some countries (Goldberg & McGee, 2011). In the United States, the Centers for Disease Control and Prevention (CDC) lists chronic pain as the number one cause of long-term disability and loss of productivity (Dahlhamer et al., 2018). For example, neuropathic pain, a major chronic pain sub-type, results from disease or trauma to the central and peripheral nervous systems and can occur in up to 30% of patients following routine operation (Kehlet, 2006). People who suffer from chronic pain often report significantly reduced quality of life which is often comorbid with other diseases (Hadi et al., 2019). Moreover, the estimated socioeconomic burden associated with chronic pain in the United States alone is between $530 and $635 billion per year, which is comprised of days of work missed, lost wages and direct medical costs (Smith & Hillner, 2019). The issue only becomes more complex given the lack of effective, long-term pain therapeutics.

Efficacy of Current Chronic Pain Pharmacotherapies

Despite widespread research efforts, treatments for chronic pain remain largely ineffective. Acetaminophen (paracetamol) is a staple medication in the arsenal of clinicians used to manage patients pain symptoms. While it's one of the oldest analgesics used in the clinic, there is still debate centered around the specific mechanism of action. It is posited that acetaminophen's analgesic effects are derived from a combination of direct and indirect inhibition of central cyclo-oxygenase 1 & 2, and modulation of the endocannabinoid system (Graham et al., 2013). While these drugs have a proven record of providing positive pain management to patients suffering from acute pain, particularly when administered perioperatively, their use is often accompanied by potentially life-threating side effects such as hepatotoxicity, in a dose-dependent manner (Scarpignato et al., 2015). These effects may be mitigated by limiting use; however, patients often require daily dosages of pain medication to effectively manage their symptoms.

COX2-selective and nonselective nonsteroidal anti-inflammatory drugs (NSAIDs) are a group of medicines used to treat acute pain and inflammation but have shown little to no benefit when used to treat chronic pain (Finnerup, 2019). While their efficacy regarding managing acute pain symptoms is undisputed, NSAID use is often accompanied by a myriad of off-target effects which can be life-threatening. For example, NSAID use may lead to increased risk of gastrointestinal hemorrhage when used perioperatively (Hadjicharalambous et al., 2016). Additionally, NSAID use carries significant cardiovascular risk, particularly when used in a chronic setting (Wang et al., 2022). Furthermore, these off-target effects prove to be highly problematic given the target populations for these medications often have cardiovascular comorbidities. These side effects

impose a significant burden on the quality of life of chronic pain patients. Even in cases where desired levels of analgesia are achieved, the multitude off-target effects may cause unintended functional disabilities or even death.

Interestingly, some of the most widely prescribed chronic pain drugs are anticonvulsants and antidepressants, specifically gabapentin and duloxetine. Anticonvulsants typically mediate analgesia through inhibition of the alpha-2-delta subunit of voltage-gated calcium channels in the central nervous system which reduces excitatory neurotransmission (Sills & Rogawski, 2020). Antidepressants such as duloxetine have FDA approval for the treatment of chronic and acute pain and work by inhibiting reuptake of serotonin and norepinephrine during synaptic transmission (Wright et al., 2010). While gabapentin has been shown to possess efficacy when used as a pain therapeutic for conditions such as diabetic neuropathy and neuralgia, it's use is often accompanied by cognitive impairments such as depression, sedation and confusion which significantly diminish quality of life (Mellegers et al., 2001). Use of gabapentin as an analgesic during surgery-induced neuropathy may also worsen cognitive impairment comorbidities (Shiers et al., 2018). Moreover, it was initially thought that gabapentin does not have addictive properties, but recent evidence suggests there is potential for misuse or abuse (Chiappini & Schifano, 2016).

Opioid-based therapies are often used to manage chronic pain and are typically effective in the short-term; however, their continued use is associated with devastating consequences. Over the last 20 years, more than 700,000 people have died from drug overdose, with 68% of those deaths linked to prescription opioid misuse (Gaskin & Richard, 2012). Moreover, long-term opioid usage

induces hyperalgesia, which leads to a cycle of heightened pain responses necessitating increased dosages (Finnerup, 2015). The eventual dependence on and tolerance of opioids from long-term usage is a sad reality for many patients suffering from chronic pain. Also, there is a marked lack of long-term, rigorous scientific studies aimed towards discovering the best clinical practice when it comes to opioid prescription. A recent review examined over 60 clinical trials, many of which were non-randomized open trials, which provided moderate evidence of long-term efficacy and low incidence of tolerance, however; this cannot serve as a substitute for randomized clinical trials (Furlan et al., 2011). Additionally, the overwhelming majority of these trials lasted for less than a month; too short to determine the lasting effects of opioid use in chronic pain management. Studies like this bring to light the complexity of the issues surrounding chronic pain management, especially when considering the enormous variability in a patients biological and affective responses to opioid administration.

Sex Differences in the Clinic

Until a 2015 mandate that outlined the necessity to include biological sex as a variable in NIH-funded research, the majority of pain research had only been in males. Recent literature has highlighted major sexual dimorphisms that alter the way researchers and clinicians alike must approach pain treatments. Consequently, the sexually dimorphic mechanisms that regulate plastic changes in cells involved in neuropathic pain development are not well understood.

Epidemiological studies have found that the prevalence of chronic pain in women is far greater than in men. Women are more likely to develop conditions that may lead to nociception or pain,

especially diseases that affect the musculoskeletal system such as fibromyalgia, osteoarthritis, and low back pain (Ruau et al., 2012). In general, female patients are also more likely to seek medical attention, 20% more likely to report experience of pain symptoms and have even been found to be more sensitive to painful stimuli than men (Steingrímsdóttir et al., 2017). Moreover, women tend to experience greater levels of cancer pain than men (Chou et al., 2018). In the clinic, women typically have worse outcomes regarding therapeutic intervention than men (Templeton, 2020). For example, women are more likely to develop chronic knee pain following total knee arthroplasty (TKA) (Vina et al., 2020). Women also report greater levels of idiopathic pain following TKA and are less responsive to pain therapeutics such as low efficacy opioids. These drugs are often less effective in women and may even function as receptor antagonists as opposed to agonists in males, highlighting fundamental sex differences in opioid system functionality (Barrett, 2006).

The influence of hormones has always been a potential culprit; however, recent evidence suggests that transient shifts in sex hormones like estrogen during the phasic nature of the estrus cycle may not be directly responsible. In fact, the dichotomy in sex-based nociception may be hardwired at birth and modulated to some degree by hormones during adulthood. A recent clinical study discovered that widespread cortical responses in pre- and full-term infants to nociceptive stimulation are different between sexes. Interestingly, no differences were found in respond to innocuous touch, indicating that the signaling pathways between the sensory and nociceptive systems are not mutually exclusive (Verriotis et al., 2018). However, many preclinical studies have shown that estrogens play a significant role in pain management. For example, ovariectomized

female rodents can manifest mechanical and thermal hyperalgesia and are often more sensitive to noxious stimuli while supplementation with estrogen may reverse these effects (Chen et al., 2012; Zhang et al., 2020). Moreover, evidence suggests that the estrus cycle may modulate the biological response to pharmacological stimulation. Specifically, administration of the neurotransmitter, 5-HT, can induce more robust pain behaviors during proestrus and estrus and may be reversed by an appropriate antagonist (Kaur et al., 2018). Nonetheless, the mechanisms by which estrogen modulates nociception remain largely unknown and are an underrepresented area of pain research considering the number of conflicting findings.

Discovery of Toll-Like Receptors

Toll, which is a *D. melanogaster* type-1 transmembrane protein, was initially ascribed to regulate dorsal-ventral polarity during development (Anderson et al., 1985). It was later found to facilitate antifungal response elements that protected the host against fungal infection (Lemaitre et al., 1996). The *D. melanogaster* toll protein is similar to the interleukin-1 receptor (IL-1R) which mediates inflammation through a variety of intracellular signaling processes, one of them being activation and nuclear localization of the pro-inflammatory transcription factor nuclear factor-kappa B (NF-κB) (Gay & Keith, 1991; Ghosh et al., 1990). Shortly after this discovery, a human homologue of the Toll protein was identified on chromosome 4p14 which indicated that a human "toll-like" protein could be responsible for initiating the innate immune response to foreign pathogens (Taguchi et al., 1996). Moreover, the human toll protein was found to also activate NF-κB and upregulate expression of proinflammatory cytokines such as Il-1, IL-6, and tumor necrosis factor-α (TNF- α) (Medzhitov et al., 1997).

The TLR family consists of a multitude of both extra (TLR1, 2, 4, 5 and 6) and intracellular (TLR3, 7, 8 and 9) receptor subtypes with a molecular weight ranging from 84-121 kD and are evolutionarily conserved (Bauer et al., 2012; Werling & Jungi, 2003). They are known as pattern-recognition receptors (PRRs) with an extracellular leucine-rich repeat (LRR) domain which is involved in both endogenous and exogenous ligand recognition, ranging from foreign pathogenic components like lipopolysaccharide (LPS) to nucleic acids such as viral RNA and CpG DNA (Uematsu & Akira, 2008). Interestingly, TLRs also contain an intracellular toll/interleukin-1 (IL-1) receptor-like (TIR) domain which is a highly conserved motif that facilitates signal transduction through a variety of protein kinases (Akira & Takeda, 2004).

It was not until the turn of the 21st century that the specific role of TLR4 in LPS detection and signal transduction was discovered (Du et al., 1999; Hoshino et al., 1999). Structurally, TLR4 forms a multi-receptor complex on the surface of a cell's extracellular membrane or endosomal compartments within the cell. It is coupled with several other proteins and adaptors such and cluster of differentiation 14 (CD14) and myeloid differentiation factor-2 (MD-2) (Kawasaki & Kawai, 2014). CD14 is a glycosylphosphatidylinositol (GPI)-anchored receptor which is known to be a co-receptor to TLR4 and is required for LPS-induced TLR4 activation (Zanoni et al., 2011). Since CD14 does not contain an intracellular tail, it cannot facilitate intracellular signaling without forming a receptor complex with TLR4/MD-2, or other toll-like receptors (Ulevitch & Tobias, 1995). LPS is a relatively large glycolipid comprised of 3 primary structural domains: lipid A tail, the core oligosaccharide, and the O antigen (Raetz et al., 2006). The lipid A tail typically forms the hydrophobic portion of the molecule and consists of an acetylated β-1'-6-linked glucosamine

disaccharide that forms the outer leaflet of the membrane (Raetz et al., 2006). The fundamental function of LPS in gram-negative bacteria is to serve as the structural foundation of the outer cell membrane and to establish a permeability barrier preventing entry of toxic molecules (Carpenter et al., 2016). It was discovered that mutations in the murine TLR4 gene of a hypo responsive strain (C3H/HeJ) led to a reduction in sickness behaviors in response to administration of LPS (Poltorak et al., 1998). This provided robust evidence to suggest that TLR4 is responsible for mediating the pro-inflammatory phenotype caused by LPS. Being a PRR, it was postulated that TLR4 could recognize and respond to a multitude of ligands which may mediate other cellular processes beyond just the innate immune response. Moreover, TLR4 has been shown to be expressed on a host of cells in both the central nervous system (CNS) and periphery. These include microglia (Olson & Miller, 2004), astrocytes (Bowman et al., 2003), neurons (Tang et al., 2007), macrophages (Kawai et al., 1999), dendritic cells (Ketloy et al., 2008), endothelial cells (Lu et al., 2012), fibroblasts (Bhattacharyya et al., 2018) and many more. Since TLR4 is expressed on a variety of cells with specific biological functions, considerations must be made on a per cell basis when interpreting the effects of TLR4 signaling in disease pathology. To begin to dissect the sex- and cell-specific role of TLR4 signaling in pain development our lab utilized two novel transgenic models that enable reactivation of a TLR4 allele using a cell-specific locus to drive expression of cre recombinase. Here we are able to reactivate TLR4 expression in a whole-body null background in either Nav1.8 expressing nociceptors or LysozymeM expressing peripheral macrophages. Initial characterization of these lines revealed significant sex differences in response to intraplantar administration of LPS. We find that both male and female mice lacking whole-body TLR4 do not develop mechanical hypersensitivity in response to intraplantar LPS injection (Figure 1.1A-F;

Table 1.1). Interestingly, reactivation of TLR4 on peripheral macrophages only recapitulates a wild type behavioral phenotype in male, but not females (Figure 1.1A-C; Table 1.1). This suggests that the TLR4-dependent signaling mechanisms activated by LPS between male and female macrophages differs. Moreover, reactivation of TLR4 on Nav1.8 nociceptors only recapitulates a wild type phenotype in females (Figure 1.1D-F; Table 1.1). We believe that direct activation of nociceptors by TLR4 ligands in females initiates inflammatory pathways necessary for the development of inflammatory pain. This initial endeavor has laid the foundation for future studies present in this dissertation.
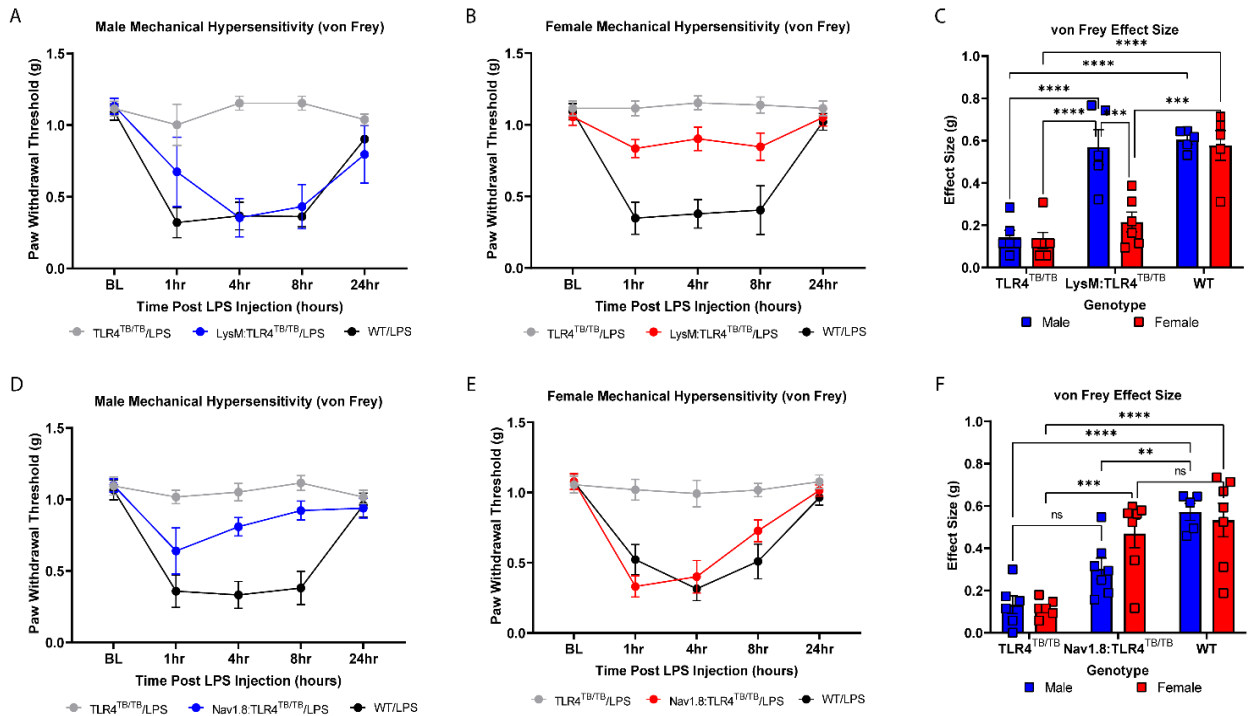
Figure 1.1. Sex- and cell-specific effects of TLR4 activation by LPS in DRG nociceptors and peripheral macrophages. Hind paw mechanical thresholds were measured prior to intraplantar injection of LPS and on timepoints: 1hr, 4hr, 8 hr and 24hrs post-injection. **A)** Representative von Frey plot of Male TLR4$^{TB/TB}$ (n=6), LysM:TLR4$^{TB/TB}$ (n=5) and WT (n=5) mice injected with intraplantar LPS. **B)** Representative von Frey plot of female TLR4$^{TB/TB}$ (n=6), LysM:TLR4$^{TB/TB}$ (n=6) and WT (n=5) mice injected with intraplantar LPS. **C)** Representative plot of mechanical hypersensitivity effect sizes with sexes combined. **D)** Representative von Frey plot of Male

TLR4$^{TB/TB}$ (n=6), Nav1.8:TLR4$^{TB/TB}$ (n=7) and WT (n=) mice injected with intraplantar LPS. **E)** Representative von Frey plot of female TLR4$^{TB/TB}$ (n=6), Nav1.8:TLR4$^{TB/TB}$ (n=7) and WT (n=7) mice injected with intraplantar LPS. **F)** Representative plot of mechanical hypersensitivity effect sizes with sexes combined. Statistical comparisons are described in Table 1.1. Data were analyzed using a 2way ANOVA.

Table 1.1. Statistical values corresponding to the data represented in Figure 1.1.

Tukey's multiple comparisons test	Mean Diff.	95.00% CI of diff.	Below threshold?	Summary	Adjusted P Value
Figure 1.1A					
BL					
TLR4$^{TB/TB}$ vs. LysM:TLR4$^{TB/TB}$	-0.01757	-0.2278 to 0.1927	No	ns	0.9702
TLR4$^{TB/TB}$ vs. WT	0.02303	-0.1919 to 0.2379	No	ns	0.9514
LysM:TLR4$^{TB/TB}$ vs. WT	0.0406	-0.1834 to 0.2646	No	ns	0.8649
1hr					
TLR4$^{TB/TB}$ vs. LysM:TLR4$^{TB/TB}$	0.3282	-0.5068 to 1.163	No	ns	0.5065
TLR4$^{TB/TB}$ vs. WT	0.6823	0.1821 to 1.182	Yes	*	0.0107
LysM:TLR4$^{TB/TB}$ vs. WT	0.3541	-0.4748 to 1.183	No	ns	0.4273
4hr					
TLR4$^{TB/TB}$ vs. LysM:TLR4$^{TB/TB}$	0.7996	0.3396 to 1.260	Yes	**	0.0055
TLR4$^{TB/TB}$ vs. WT	0.787	0.4546 to 1.119	Yes	***	0.0009
LysM:TLR4$^{TB/TB}$ vs. WT	-0.0126	-0.4930 to 0.4678	No	ns	0.9968
8hr					
TLR4$^{TB/TB}$ vs. LysM:TLR4$^{TB/TB}$	0.7224	0.1883 to 1.256	Yes	*	0.0165
TLR4$^{TB/TB}$ vs. WT	0.7919	0.5419 to 1.042	Yes	****	<0.0001
LysM:TLR4$^{TB/TB}$ vs. WT	0.06958	-0.4615 to 0.6006	No	ns	0.9129
24hr					
TLR4$^{TB/TB}$ vs. LysM:TLR4$^{TB/TB}$	0.2429	-0.4583 to 0.9441	No	ns	0.5119
TLR4$^{TB/TB}$ vs. WT	0.1355	-0.1979 to 0.4688	No	ns	0.4516
LysM:TLR4$^{TB/TB}$ vs. WT	-0.1074	-0.7950 to 0.5802	No	ns	0.8812
Figure 1.1B					
BL					

TLR4$^{TB/TB}$ vs. LysM:TLR4$^{TB/TB}$	0.05927	-0.1936 to 0.3121	No	ns	0.841
TLR4$^{TB/TB}$ vs. WT	0.02309	-0.2421 to 0.2883	No	ns	0.9763
LysM:TLR4$^{TB/TB}$ vs. WT	-0.03618	-0.3014 to 0.2290	No	ns	0.9429
1hr					
TLR4$^{TB/TB}$ vs. LysM:TLR4$^{TB/TB}$	0.2808	0.02791 to 0.5336	Yes	*	0.026
TLR4$^{TB/TB}$ vs. WT	0.7669	0.5017 to 1.032	Yes	****	<0.0001
LysM:TLR4$^{TB/TB}$ vs. WT	0.4861	0.2210 to 0.7513	Yes	***	0.0001
4hr					
TLR4$^{TB/TB}$ vs. LysM:TLR4$^{TB/TB}$	0.2513	-0.001543 to 0.5041	No	ns	0.0518
TLR4$^{TB/TB}$ vs. WT	0.775	0.5098 to 1.040	Yes	****	<0.0001
LysM:TLR4$^{TB/TB}$ vs. WT	0.5237	0.2585 to 0.7889	Yes	****	<0.0001
8hr					
TLR4$^{TB/TB}$ vs. LysM:TLR4$^{TB/TB}$	0.2687	0.01589 to 0.5216	Yes	*	0.0347
TLR4$^{TB/TB}$ vs. WT	0.7109	0.4457 to 0.9761	Yes	****	<0.0001
LysM:TLR4$^{TB/TB}$ vs. WT	0.4421	0.1770 to 0.7073	Yes	***	0.0005
24hr					
TLR4$^{TB/TB}$ vs. LysM:TLR4$^{TB/TB}$	0.0636	-0.1892 to 0.3164	No	ns	0.8193
TLR4$^{TB/TB}$ vs. WT	0.09415	-0.1710 to 0.3593	No	ns	0.6733
LysM:TLR4$^{TB/TB}$ vs. WT	0.03055	-0.2346 to 0.2957	No	ns	0.9589
Figure 1.1C					
TLR4$^{TB/TB}$:Male vs. TLR4$^{TB/TB}$:Female	0.01529	-0.1970 to 0.2275	No	ns	>0.9999
TLR4$^{TB/TB}$:Male vs. LysM:TLR4$^{TB/TB}$:Male	-0.4257	-0.6483 to -0.2031	Yes	****	<0.0001
TLR4$^{TB/TB}$:Male vs. LysM:TLR4$^{TB/TB}$:Female	-0.07188	-0.2841 to 0.1404	No	ns	0.9009
TLR4$^{TB/TB}$:Male vs. WT:Male	-0.461	-0.6836 to -0.2384	Yes	****	<0.0001
TLR4$^{TB/TB}$:Male vs. WT:Female	-0.4337	-0.6563 to -0.2111	Yes	****	<0.0001
TLR4$^{TB/TB}$:Female vs. LysM:TLR4$^{TB/TB}$:Male	-0.441	-0.6636 to -0.2183	Yes	****	<0.0001
TLR4$^{TB/TB}$:Female vs. LysM:TLR4$^{TB/TB}$:Female	-0.08717	-0.2994 to 0.1251	No	ns	0.8042
TLR4$^{TB/TB}$:Female vs. WT:Male	-0.4763	-0.6989 to -0.2536	Yes	****	<0.0001
TLR4$^{TB/TB}$:Female vs. WT:Female	-0.449	-0.6716 to -0.2264	Yes	****	<0.0001
LysM:TLR4$^{TB/TB}$:Male vs. LysM:TLR4$^{TB/TB}$:Female	0.3538	0.1312 to 0.5764	Yes	***	0.0006

LysM:TLR4$^{TB/TB}$:Male vs. WT:Male	-0.03531	-0.2678 to 0.1972	No	ns	0.997
LysM:TLR4$^{TB/TB}$:Male vs. WT:Female	-0.008063	-0.2406 to 0.2244	No	ns	>0.9999
LysM:TLR4$^{TB/TB}$:Female vs. WT:Male	-0.3891	-0.6117 to -0.1665	Yes	***	0.0002
LysM:TLR4$^{TB/TB}$:Female vs. WT:Female	-0.3618	-0.5845 to -0.1392	Yes	***	0.0004
WT:Male vs. WT:Female	0.02725	-0.2053 to 0.2598	No	ns	0.9991
Figure 1.1D					
TLR4$^{TB/TB}$ vs. Nav1.8:TLR4$^{TB/TB}$	-0.00434	-0.2222 to 0.2135	No	ns	0.9983
TLR4$^{TB/TB}$ vs. WT	0.0272	-0.2400 to 0.2944	No	ns	0.956
Nav1.8:TLR4$^{TB/TB}$ vs. WT	0.03154	-0.2144 to 0.2774	No	ns	0.9267
1hr					
TLR4$^{TB/TB}$ vs. Nav1.8:TLR4$^{TB/TB}$	0.3778	-0.1159 to 0.8716	No	ns	0.1293
TLR4$^{TB/TB}$ vs. WT	0.6587	0.2685 to 1.049	Yes	**	0.0057
Nav1.8:TLR4$^{TB/TB}$ vs. WT	0.2809	-0.2607 to 0.8225	No	ns	0.3656
4hr					
TLR4$^{TB/TB}$ vs. Nav1.8:TLR4$^{TB/TB}$	0.2423	0.0007893 to 0.4838	Yes	*	0.0493
TLR4$^{TB/TB}$ vs. WT	0.719	0.3888 to 1.049	Yes	***	0.0009
Nav1.8:TLR4$^{TB/TB}$ vs. WT	0.4767	0.1458 to 0.8075	Yes	**	0.0087
8hr					
TLR4$^{TB/TB}$ vs. Nav1.8:TLR4$^{TB/TB}$	0.1928	-0.03355 to 0.4191	No	ns	0.0975
TLR4$^{TB/TB}$ vs. WT	0.7345	0.3346 to 1.134	Yes	**	0.0037
Nav1.8:TLR4$^{TB/TB}$ vs. WT	0.5417	0.1408 to 0.9426	Yes	*	0.0135
24hr					
TLR4$^{TB/TB}$ vs. Nav1.8:TLR4$^{TB/TB}$	0.07799	-0.1511 to 0.3071	No	ns	0.6344
TLR4$^{TB/TB}$ vs. WT	0.05717	-0.2304 to 0.3448	No	ns	0.8261
Nav1.8:TLR4$^{TB/TB}$ vs. WT	-0.02082	-0.3252 to 0.2835	No	ns	0.9799
Figure 1.1E					
TLR4$^{TB/TB}$ vs. Nav1.8:TLR4$^{TB/TB}$	-0.02165	-0.2416 to 0.1983	No	ns	0.9617
TLR4$^{TB/TB}$ vs. WT	-0.02101	-0.2368 to 0.1948	No	ns	0.9624
Nav1.8:TLR4$^{TB/TB}$ vs. WT	0.0006429	-0.2071 to 0.2084	No	ns	>0.9999

1hr					
TLR4$^{TB/TB}$ vs. Nav1.8:TLR4$^{TB/TB}$	0.6886	0.4033 to 0.9738	Yes	***	0.0001
TLR4$^{TB/TB}$ vs. WT	0.4973	0.1423 to 0.8523	Yes	**	0.0082
Nav1.8:TLR4$^{TB/TB}$ vs. WT	-0.1912	-0.5450 to 0.1625	No	ns	0.3446
4hr					
TLR4$^{TB/TB}$ vs. Nav1.8:TLR4$^{TB/TB}$	0.5921	0.1899 to 0.9943	Yes	**	0.0057
TLR4$^{TB/TB}$ vs. WT	0.6781	0.3354 to 1.021	Yes	***	0.0007
Nav1.8:TLR4$^{TB/TB}$ vs. WT	0.08599	-0.3000 to 0.4720	No	ns	0.8221
8hr					
TLR4$^{TB/TB}$ vs. Nav1.8:TLR4$^{TB/TB}$	0.2901	0.04358 to 0.5366	Yes	*	0.0227
TLR4$^{TB/TB}$ vs. WT	0.5081	0.1265 to 0.8896	Yes	*	0.0131
Nav1.8:TLR4$^{TB/TB}$ vs. WT	0.218	-0.1803 to 0.6162	No	ns	0.3314
24hr					
TLR4$^{TB/TB}$ vs. Nav1.8:TLR4$^{TB/TB}$	0.06172	-0.1102 to 0.2336	No	ns	0.604
TLR4$^{TB/TB}$ vs. WT	0.1121	-0.08621 to 0.3103	No	ns	0.3166
Nav1.8:TLR4$^{TB/TB}$ vs. WT	0.05033	-0.1335 to 0.2342	No	ns	0.7457
Figure 1.1F					
Male					
TLR4$^{TB/TB}$ vs. Nav1.8:TLR4$^{TB/TB}$	-0.1711	-0.3708 to 0.02849	No	ns	0.1108
TLR4$^{TB/TB}$ vs. WT	-0.4388	-0.6561 to -0.2215	Yes	****	<0.0001
Nav1.8:TLR4$^{TB/TB}$ vs. WT	-0.2677	-0.4778 to -0.05757	Yes	**	0.009
Female					
TLR4$^{TB/TB}$ vs. Nav1.8:TLR4$^{TB/TB}$	-0.3515	-0.5512 to -0.1519	Yes	***	0.0003
TLR4$^{TB/TB}$ vs. WT	-0.4154	-0.6150 to -0.2158	Yes	****	<0.0001
Nav1.8:TLR4$^{TB/TB}$ vs. WT	-0.06386	-0.2557 to 0.1279	No	ns	0.7923

Beyond the recognition of LPS, TLR4 is also capable of binding a multitude of pathogenic components such as teichuronic acid from gram-positive bacteria and the *Dengue virus* NS1 protein (Modhiran et al., 2015; Yang et al., 2001). The extracellular domain of TLR4 exhibits a significant amount of sequence divergence due to the polymorphic nature of the LRR (Thomas et

al., 2006; Werling et al., 2009). This is typically comprised of the first 82 amino acids within the proximal region of the extracellular domain, and is involved in recognition and response to TLR4 ligands (Alvarez et al., 2006). The intra and inter-species variation in response to LPS, and other ligands, is attributed to the poor conservation of this extracellular amino acid sequence. In addition to the previously discussed exogenous pathogen-associated molecular patterns (PAMPs), TLR4 also recognizes endogenous danger-associated molecular patterns (DAMPs) such as heat shock proteins (HSPs), high mobility group box 1 (HMGB1) and fibronectin (Chase et al., 2007; Gondokaryono et al., 2007; Yu et al., 2006). Moreover, TLR4 has been shown to recognize long-chain saturated fatty acids. The principal component of LPS that carries its immunostimulatory activity is the lipid A moiety which contains numerous saturated fatty acyl chains required for interaction with the TLR4/MD-2 receptor complex (Steimle et al., 2016). Evidence suggest inhibition of microglial TLR4 by neutralizing antibodies prevents initiation of a pro-inflammatory phenotype following palmitic acid or fatty acid exposure which is typically found in the western diet (Nicholas et al., 2017; Shi et al., 2006). This indicates that TLR4 plays a critical role in the innate immune system's ability to recognize and respond to foreign pathogens and facilitate host defense, but it is also crucial for the detection of endogenous signals related to tissue injury, sterile inflammation, and obesity-induced inflammation.

TLR4 Signaling: MyD88- and TRIF-Dependent Pathways

TLR4 signaling pathways can generally be classified into two categories: MyD88- and TRIF-dependent pathways. These two pathways are responsible for activation of various intracellular signaling cascades based on specific adaptor protein recruitment. Upon activation of the

TLR4/MD-2 heterodimer and internalization, MyD88 forms a complex with a family of IRAK kinases. Following formation of this complex, IRAK4 activates IRAK1 which becomes phosphorylated and is subsequently released from MyD88 (Jiang et al., 2002; Kollewe et al., 2004). IRAK1 then associates with the RING-domain E3 ubiquitin ligase TRAF6. The ubiquitin-conjugating enzymes, UBC13 and UEV1A, along with TRAF6 promote the K63-linked polyubiquitin chains generated by TRAF6 which facilitates activation of TAK1 (Ajibade et al., 2013; Chen, 2012). Activation of TAK1 leads to association with the IKK complex, allowing for activation of the NF-κB and MAPK pathways. The IKK complex is comprised of a regulatory subunit, IKKγ, and two catalytic subunits: IKKα and IKKβ. TAK1 interacts with the IKK complex through ubiquitin chains which enable the phosphorylation of serine residues on KKβ and facilitates its activation (Kawai & Akira, 2010). The IKK complex phosphorylates IκBα, which constitutively prevents NF-κB nuclear translocation. NF-κB is a dimeric transcription factor that is part of the Rel-homology domain-containing protein family. This includes RelB, c-Rel, p50/NF-κB1, p52/ NF-κB2, and p65/RelA. The prototypical version of NF-κB is a heterodimer comprised of the p50 and p65 subunits (Hayden & Ghosh, 2004). Phosphorylation of IκBα facilitates proteasome degradation by 26S, which allows NF-κB to translocate to the nucleus of the cell and bind to κB sites that initiate inflammatory gene transcription such as TNFα, IL-1, IL-6 and IL-12 (Ferreiro & Komives, 2010). TAK1 activation can also lead to intracellular signaling through MAPKs such as JNK, ERK1, ERK2, and p38 which facilitate activation of AP-1 transcription factors that regulate inflammatory processes (Gunnell et al., 2010). Interestingly, TAK1 deficiency has been shown to reduce or even inhibit inflammatory cytokine production in mouse embryonic fibroblasts (Lluis et al., 2010). However, deficiency of TAK1 in mouse neutrophils does not

recapitulate this reduction in inflammatory signaling, suggesting that TLR4 may have cell-specific differences in signaling capabilities (Ajibade et al., 2012).

During endosomal TLR4 signaling, the TIR domain uses TRAM to recruit TRIF. Interaction between TRIF and TRAF6 leads to the recruitment of kinase RIP-1 which activates the TAK1 complex by facilitating association between TAB1-3 and TAK1, similar to the MyD88-dependent pathway (Kagan et al., 2008). This, in turn, leads to activation of the previously discussed NF-κB and AP-1 pathways and the induction of inflammatory cytokines. Conversely, interaction between TRIF and TRAF3 facilitates recruitment of IKK-related kinases such as TBK1 and IKKi. These are directly responsible for IRF3 phosphorylation (Fitzgerald et al., 2003). Like NF-κB, IRF3 forms a dimer upon activation and translocates to the nucleus of the cell where it induces expression of type-1 interferons (Kolb et al., 2014).

Modulation of Pain by TLR4

Over the last decade evidence has been mounting which suggests TLR4 that is a critical mediator of the nervous and immune systems inflammatory response during pain (DeLeo et al., 2004; Guo & Schluesener, 2007; Heiman et al., 2014). During peripheral inflammation, TLR4 and CD14 gene expression is increased in the spinal cord of rats injected with intraplantar complete Freund's adjuvant (CFA) (Raghavendra et al., 2004). These results were confirmed nearly a decade later where another group had shown an increase in microglia reactivity following intraplantar CFA injection by measuring upregulation of OX-42 and TLR4 expression in the dorsal spinal cord (Zhao et al., 2015). Moreover, intraplantar or intraoral injection of LPS induces robust mechanical

and thermal hypersensitivity which is accompanied by upregulation of various inflammatory cytokines. The observed phenotypes are blocked by modulation of TLR4 activity or MyD88 deficiency (Araya et al., 2020; Calil et al., 2014). Taken together, these suggest that both central and peripherally expressed TLR4 mediates acute inflammatory pain.

In addition to inflammatory pain, TLR4 has also been shown to be involved in chemotherapy-induced peripheral neuropathy (CIPN). Paclitaxel, a taxol-based chemotherapeutic, engages similar inflammatory intracellular signaling pathways as the classical TLR4 ligand, LPS (Zaks-Zilberman et al., 2001). This is evident by paclitaxel utilizing the same MD-2 accessory protein required for LPS signal transduction and upregulating inflammatory cytokines such as IL-1, TNFα and IL-6 in the blood (O'Brien et al., 1995; Resman et al., 2008). More recently, paclitaxel has been shown to interact with TLR4 in the DRG and spinal cord. Paclitaxel treatment upregulates TLR4 expression in these tissues and facilitates canonical activation of MyD88-medaited signaling pathways which results in a behavioral pain phenotype (Li et al., 2014). Blockade of TLR4 signaling using LPS-RS seemingly reverses the pain phenotype, which further implicates the direct activation of TLR4 by chemotherapeutics in peripheral CIPN development (Illias et al., 2022). While evidence suggests that these effects may be neuronally mediated by subpopulations of IB4 and CGRP expressing nociceptors, paclitaxel has also been shown to modulate pro-inflammatory, or M1, polarization of peripheral macrophages in a TLR4-dependent manner (Wanderley et al., 2018). As M1-polarized macrophages produce a multitude of neuromodulatory cytokines, it's likely that the effects of chemotherapeutics on TLR4 activation in immune cells also contributes CIPN development.

TLR4 has also been shown to play a significant role in opioid-induced hyperalgesia. While this seems paradoxical, evidence suggests that mu opioids can lead to increased pain sensitivity (Weber et al., 2017). It is believed that certain opioids can bind to TLR4 using the MD-2 adaptor, similar to LPS, which facilitates inflammatory signaling (J. Li et al., 2016). By acting as TLR4 ligands, traditional opioid receptor agonists may induce a pain phenotype, or enhance sensitivity through hyperalgesic priming (Ellis et al., 2016). These effects can be reversed or blocked by inhibiting activation of TLR4 using pharmacological antagonists such as TAK-242 or LPS-RS (Grace et al., 2016).

Neuroimmune Modulation of Chronic Pain

Within the last decade there have been numerous studies aimed towards dissecting sex differences in chronic pain development. While the scientific community has made significant progress towards addressing nearly a century of male-biased pain research, there are still many questions left unanswered and mechanisms that remain unclear. Given the disproportionate number of women impacted by chronic pain and the lack of effective therapeutics, understanding the sex- and cell-specific differences in neuroimmune modulation of pain is necessary to appropriately design and execute research targeted at therapeutic development (Bartley & Fillingim, 2013).

It is now widely appreciated that the nervous and immune systems communicate with one another to coordinate their dynamic responses to stimulation. Immune cells can modulate the activity of pain-sensing neurons, nociceptors, by releasing pro- or anti-inflammatory cytokines. In turn, nociceptors communicate with immune cells by releasing immunomodulatory neuropeptides, chemokines, cytokines, and microRNAs (Talbot et al., 2016). Emerging evidence suggests that the

interaction between the nervous and immune systems is bidirectional, indicating that crosstalk between these systems is necessary to not only maintain homeostasis, but also respond appropriately to tissue injury and infection (Pinho-Ribeiro et al., 2017). To understand how these systems interact with one another, we must first discuss how they individually sense danger signals.

Within the dorsal root ganglia (DRG) there exists a heterogenous population of nociceptive neurons that are characterized by their varying degrees of myelination, size and signaling capabilities (Alshawaf et al., 2018). Recent single-cell RNA-sequencing (scRNA-seq) data indicates that there are 10 major populations of nociceptive neurons in the murine DRG, with numerous subtypes that further distinguish their unique physiological properties (C. L. Li et al., 2016). These nociceptors actively respond to external stimuli such as changes in temperature, mechanical or chemical thresholds. At baseline, these cells play a necessary role in alerting the individual to potentially harmful situations and inducing defensive behaviors. However, dysregulation of peripheral nociceptive circuitry may lead to maladaptive plasticity and chronic pain. The mechanism by which chronic pain occurs in the periphery is likely due to ectopic activity of peripheral nerves, or the DRG, which is generated as a result of Na^+ channel upregulation and hypersensitization to neuromodulators (Black et al., 2008). Transient receptor potential channels (TRP channels), specifically TRPA1 and TRPV1, are crucial components of nociceptor signaling as they regulate pain and temperature sensation through Ca^{2+} influx (Song & Yuan, 2010). These TRP channels have been implicated in the pathogenesis of both acute and chronic pain making them a prime candidate for pain therapeutics (Duitama et al., 2020). Nociceptors also express a

host of PRRs like TLRs, Nod-like receptors (NLRs), C-type lectin receptors (CLRs) and cytosolic DNA sensory (CDSs) that are responsible for mediating changes in nociceptor sensitivity during tissue injury or infection (Ackland et al., 2013). Out of these PRRs, TLR4, specifically, has been shown to possess the highest expression levels in DRG neurons (Zheng et al., 2019). Interestingly, evidence suggests that in the DRG and trigeminal ganglia (TG) TLR4 and TRPV1 are functionally coupled, meaning that TLR4 can directly modulate activity of TRPV1. Infusion of LPS in dissociated TG and DRG neurons potentiated capsaicin-induced responses such as rapid Ca^{2+} influx and calcitonin gene-related peptide (CGRP) release, both of which are not directly linked to TLR4 signaling cascades (Diogenes et al., 2011; Wu et al., 2019). In TLR4 knockout mice, capsaicin-induced pain is significantly reduced, which is intriguing given that capsaicin is known to signal exclusively through TRPV1. Moreover, these findings suggest that the TIR adaptor molecule, a specific component of TRIF-dependent TLR4 intracellular signaling, is responsible for preventing activation-induced endocytosis of TRPV1 (Min et al., 2018). Taken together, these studies reveal a unique interaction between TLR4 and TRPV1 which enhance the context by which we understand nociceptor physiology. While TLR4 does not contain any electrically-coupled signaling mechanisms, it possesses the ability to modulate Na_v channel activity—an essential component of nociceptive transmission. Phosphorylated-p65 (p-p65), an active subunit of NF-κB, can reversibly interact with $Na_v1.7$ sodium channels in DRG nociceptors within minutes of phosphorylation. This interaction increases $Na_v1.7$ currents by slowing inactivation and facilitating recovery following depolarization (Xie et al., 2019). While the direct mechanisms involved are yet to be elucidated, this work demonstrates regulation of voltage-dependent nociceptor activity in a

transcription-independent manner. These data highlight the ability of TLR4 to modulate nociceptor signaling in numerous ways.

While the basic mechanisms of neuroimmune modulation of chronic pain are well appreciated, not all is equal between sexes. For example, microglia in the CNS were thought to possess a more male-specific role in mediating the development of chronic pain (Inyang, 2019; Sorge, 2011; Sorge, 2015). Conversely, a study that compared central and peripheral immune cell transcriptional profiles following spinal-nerve ligation (SNL) found that peripheral immune cells were considerably more dysregulated following injury and highlighted sex-specific differences in the adaptive immune response (Lopes, 2017). RNA-seq analysis of both male and female DRG neurons following peripheral chronic constriction injury (CCI) revealed sex-specific differences in gene expression. For example, colony-stimulating factor 1 (CSF1) is expressed de-novo following nerve injury in the DRG and is transported to the spinal cord where it acts on dorsal horn microglia (Guan et al., 2016). In this study, CSF1 was shown to be expressed at much higher quantities in females than males suggesting that regulation of CSF1 signaling during neuropathic injury may be a sex-dependent mechanism (Stephens et al., 2019). Intrathecal administration of CSF1 has been shown to induce a robust pro-inflammatory phenotype in male microglia characterized by amoeboid morphology and an inflammatory transcript profile. While microglia are neuromodulatory in nature, they also respond to signals sent from other immune cells. Foxp3-expressing regulatory T cells (Tregs) have been shown to suppress inflammatory activation of microglia and limit pain hypersensitivity (Wan, 2010). Results from this study indicate that CSF1 can mediate crosstalk between lymphocytes and spinal cord microglia in females by acting as a

modulator of Treg immunosuppressive activity (Kuhn et al., 2021). As peripheral macrophages also express the receptor for CSF1 (CSF1R), a follow-up study was conducted to delineate the sex-specific role of microglia vs. macrophages in CSF1-mediated neuropathic. Interestingly, it was found that deletion of CSF1 in sensory neurons only reduced tissue-resident macrophage (Ki67$^+$) expansion in the DRG of males, but not females following spared-nerve injury (SNI). It was also demonstrated that macrophages in the DRG of both sexes contribute to the initiation and maintenance of neuropathic pain, although, it seemed to be a more male-biased mechanism (Yu et al., 2020). Taken together, these data suggest that other sensory neuron derived mechanisms differentiate male and female neuropathic pain development.

Sex Differences in TLR4-Mediated Neuropathic Pain Development

Over the last decade TLR4 has made its way into the spotlight of pain research. Although, its exact sex- and cell-specific role in mediating chronic pain development and maintenance have been controversial. One of the first studies to implicate TLR4 signaling in neuropathic pain development sought to characterize the functional role of microglia TLR4 in response to spinal nerve ligation (SNL). They found that TLR4 whole body null mice not only attenuated the inflammatory response of spinal microglia, but also reduced the nociceptive behavioral phenotype seen after nerve injury (Tanga et al., 2005). Subsequent studies have corroborated these findings by pharmacologically inhibiting spinal TLR4 activation with LPS-RS, naloxone, naltrexone, and FP-1—all of which function as TLR4 antagonists with varying degrees of specificity and efficacy (Bettoni et al., 2008; Hutchinson et al., 2008). Lastly, chemotherapy-induced neuropathic pain is one of the major dose-limiting side effects of cancer treatments. TLR4 has been shown to recognize various taxol-based

chemotherapeutics and engage inflammatory intracellular signaling mechanisms similar to LPS and HMGB1 (Szajnik et al., 2009). It was found that activation of TLR4 expressed by CGRP and isolectin B4 (IB4) positive nociceptive neurons in the DRG induced acute sensitization of TRPV1-mediated Ca^{2+} responses (Li, Adamek, et al., 2015; Li et al., 2014). Moreover, early nociceptive behaviors were correlated with increased activity of the MyD88-dependent pathway and activity of the TRIF-dependent pathway was elevated during later time points. This suggests that signal transduction by TLR4 is dynamic in nature and differences in the specific pathways activated may be responsible for the initiation vs. maintenance of neuropathic pain. While these studies do provide convincing evidence that suggests immune-mediated TLR4 signaling contributes to neuropathic pain development, biological sex was not considered as a variable. It was not until a few years later that the sex-specific contribution of TLR4 in both inflammatory and neuropathic pain was addressed. It was found that intrathecal administration of LPS induced a robust pain phenotype in male, but not female mice and antagonism of spinal TLR4 reversed this effect in only males. Moreover, SNI induced neuropathic pain behaviors in both male and female mice, but only male mice showed transient attenuation of pain behaviors following intrathecal LPS-RS injection (Sorge, 2011). Some data suggest that the role of TLR4 in inflammatory and neuropathic pain development is reliant on the timing of TLR4 modulation. Intrathecal LPS facilitated mechanical hypersensitivity development in both male and female mice; however, inhibition of spinal TLR4 signaling by TAK-242 prevented development of allodynia but could not reverse established allodynia in males (Woller et al., 2016). These results were confirmed using TLR4 whole body knockout mice. While these results seem contradictory, they may be explained by differences in the strain of mouse used and serotype and dose of LPS. In accordance with the previously

discussed study, another group had demonstrated a sex-specific role of TLR4 in SNL-induced neuropathic pain. Their data suggests that TLR4 whole body null females do not exhibit a reduction in mechanical hypersensitivity like their male counterparts (Stokes et al., 2013). Interestingly, they also show that MyD88-deficient mice have a reduction in activated transcription factor 3 (ATF3) expression in DRG neurons. This was one of the first studies to suggest that TLR4 either directly, or indirectly influences expression of neuronal injury markers in the periphery. However, these findings are not always recapitulated in subsequent studies.

To date, almost all studies had been focused on central effects of TLR4 signaling. To address this, a research group had generated a unique transgenic model to assess the role of both central microglia and peripheral macrophages and TLR4 signaling in chronic pain. Interestingly, their results suggest that microglia equally participate in the imitation of neuropathic mechanical hypersensitivity in both males and females, but different cell types mediate its maintenance. Moreover, they show that ablation of microglia prior to injury only delays the onset of neuropathic pain, but synergistic ablation of both microglia and macrophages prevents neuropathic pain development (Peng, 2016). To address discrepancies in the temporal and cell-specific role TLR4 in neuropathic pain, a recent study used a conditional knockout mouse line which enabled deletion of TLR4 from microglia, specifically. They found that systemic antagonism of TLR4 is effective at improving chronic pain outcomes in both sexes when administered at the time of injury as opposed to when pain is already established. Their data shows that late conditional knockout of TLR4 only results in partial improvement in allodynia of both sexes, suggesting that microglia TLR4 plays less of a role in the maintenance of neuropathic pain (Huck et al., 2021).

An important consideration is the model and inflammatory mediators used to study the effects of TLR4 in chronic pain. HMGB1, also known as amphoterin, is a highly dynamic nuclear chromatin-binding protein that orchestrates key biological events such as sterile inflammation and chemoattraction based on its redox biology (Kwak et al., 2020). HMGB1 is capable of signaling through multiple receptors, including TLR2, TLR4 and the receptor for glycation and end products (RAGE) (Hori et al., 1995; Park et al., 2004). HMGB1 may be released from the nuclear envelope of cells in two primary ways: active release and passive secretion. Active release of HMGB1 is reliant on hyperacetylation of two nuclear localization sequence (NLS) sites which allows it to accumulate in the cytoplasm (Youn & Shin, 2006). Passive secretion of HMGB1 results from cell death, including apoptosis, autophagy, and necrosis (Qin et al., 2006; Quarato et al., 2016; Thorburn et al., 2009). Intracellular HMGB1 exists in its all thiol form (at-HMGB1) and can be oxidized to the disulfide form (ds-HMGB1) when reactive oxygen species (ROS) present in the extracellular matrix facilitate disulfide bridge formation between cysteine residues 23 and 45 (Venereau et al., 2013). Ds-HMGB1 functions as an inflammatory cytokine that induces preferential activation of TLR4 (Yamasoba et al., 2016). HMGB1 has been shown to be upregulated in both sensory neurons in the DRG, as well as peripheral immune cells and glia in response to neuropathic injury. Upregulation of HMGB1 was also associated with a transition from nuclear to cytosolic localization which is indicative of active release (Müller et al., 2004). Inhibition of HMGB1 signaling by a neutralizing antibody prevented mechanical allodynia development and cytosolic localization of the protein, suggesting that peripheral HMGB1 signaling plays a significant role in the development of neuropathic pain (Shibasaki et al., 2010). Interestingly, this study was focused entirely on the effects of HMGB1 signaling through RAGE,

and not TLR4. Moreover, only male rats were used in these experiments. Another study demonstrates that administration of dsHMGB1 was shown to increase excitability of dissociated DRG neurons. Treatment with an HMGB1 inhibitor, glycyrrhizin (GL), was able to reverse the HMGB1-dependent increase in neuronal excitability. Moreover, systemic inhibition of HMGB1 signaling was able to reverse mechanical allodynia resulting from tibial nerve injury (TNI) which is a model of neuropathic pain (Feldman et al., 2012). Distinct from the previously discussed study, these effects were interpreted more so in the context of TLR4-dependent signaling and were done in female rats. A more recent study highlights the effects of central HMGB1-TLR4 signaling on collagen antibody -induced arthritic (CAIA) pain. They also demonstrate that intrathecal administration of dsHMGB1 induces pain-like behaviors in mice of both sexes, and it TLR4-dependent. Moreover, pharmacological inhibition of spinal HMGB1 signaling reverses CAIA pain (Agalave et al., 2014). This study provides additional evidence to support the role of HMGB1 in inflammatory and neuropathic pain, but it was also one of the first to directly assess sex-differences in HMGB1-TLR4 signaling. Although these findings do not seem to recapitulate the Sorge et al., 2011 study that found robust sex differences in spinal TLR4 signaling, it does seem suggest that there may be mechanistic differences in the specific ligands, signaling pathways, and cell types responsible for neuropathic pain development between males and females. The involvement of sex- and cell-specific HGMB1 signaling in the periphery has not been extensively reported on until recently.

Our initial investigations were aimed at studying the underlying mechanisms that may attribute to the protective effect of upstream TLR4 inhibition. As an initial endeavor, we utilized two

transgenic models that allow for conditional deletion of TLR4 from a cell-specific locus: Nav1.8 (Jia et al., 2021) on peripheral nociceptors or LysozymeM (Jia et al., 2014) on peripheral macrophages. As previously discussed, evidence suggests that HMGB1 is heavily involved in mediating inflammation through TLR4 signaling. Since TLR4 is expressed on neuron and immune cells, we sought to dissect the sex- and cell-specific effects of intraplanar HMGB1 administration on mechanical hypersensitivity. We discovered that TLR4 on macrophages were necessary in males (Fig. 1.2A & C; Table 1.2) and TLR4 on nociceptors were necessary in females to induce a painful behavior phenotype (Fig. 1.2B & D; Table 1.2). Additionally, we wanted to characterize the role of TLR4 in hyperalgesic priming which may reveal insights as to the mechanisms that underlie the transition from acute to chronic pain. Once the animals had returned to baseline, we performed an intraplanar injection of a subthreshold dose of prostaglandin E2 and measured mechanical hypersensitivity. Again, we found that TLR4 activation by HMGB1 on macrophages was necessary to elicit the primed phenotype in males (Fig. 1.2A & C; Table 1.2), but it was TLR4 activation by HMGB1 on nociceptors for females (Fig. 1.2B & D; Table 1.2). More recently, a study found that inhibition of TLR4 signaling in peripheral macrophages attenuated dsHMGB1-induced pain behaviors in male, but not female mice, suggesting that the cell types responsible for mediating peripheral pain mechanisms differs between sexes (Rudjito, 2020). Using conditional TLR4 knockout in DRG nociceptors, they also demonstrate that HMGB1 mediates CAIA pain through TLR4 signaling in both sexes. Another study confirmed these findings by using a similar genetic and CAIA pain model. Moreover, by conditional deletion of HMGB1 from the whole DRG neuron population, they confirm that HMGB1 is also responsible for neuropathic pain development during SNI in females. The specific receptors for HMGB1, neuronal subtypes, and

male-specific mechanisms were not addressed (Yang et al., 2021). Therefore, studies that evaluate

the effectiveness of inhibiting both TLR4 and HMGB1 signaling will shed light on the sex- and

cell-specific mechanisms of chronic pain.
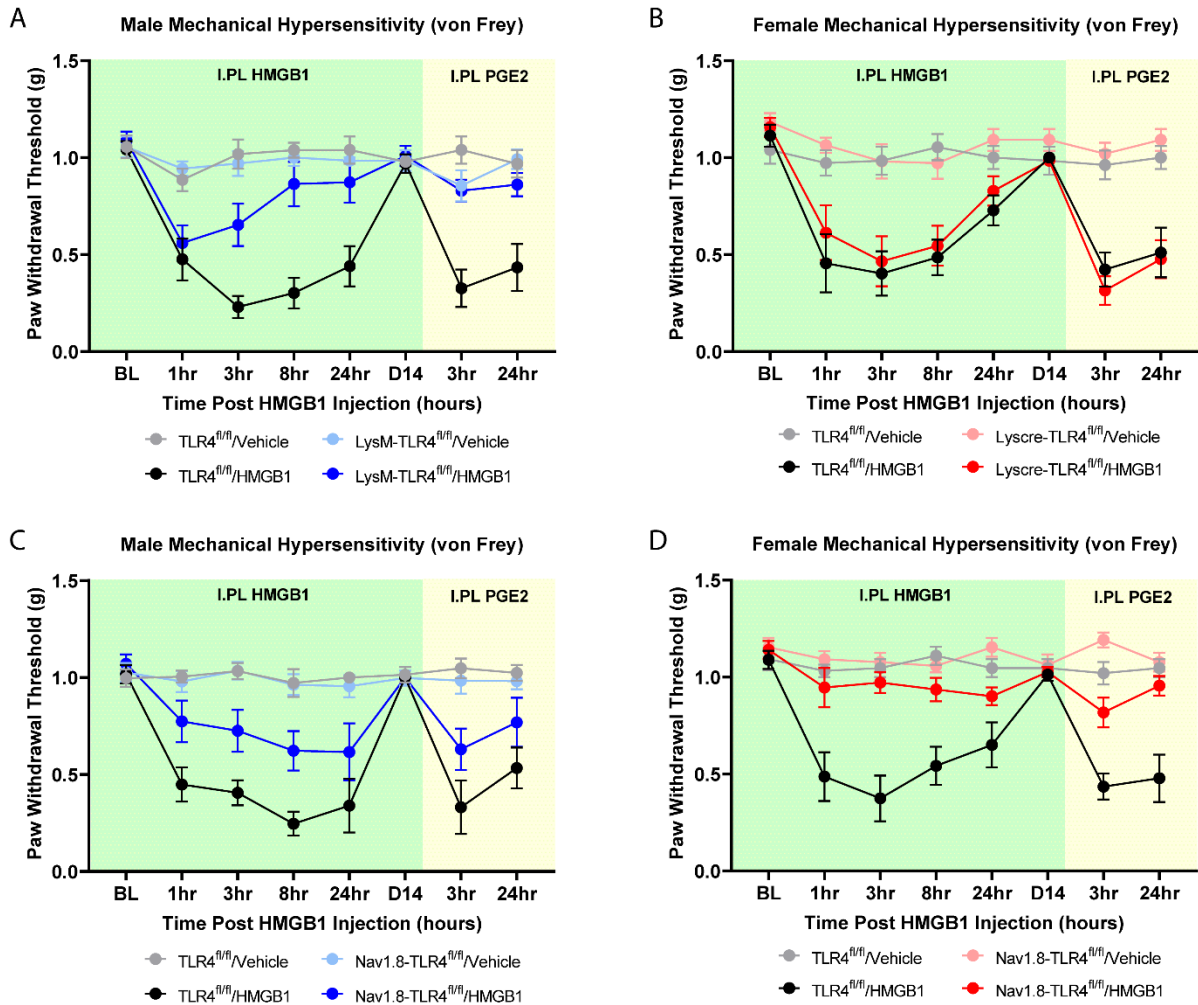
Figure 1.2. Sex- and cell-specific effects of TLR4 activation by HMGB1 in DRG nociceptors and peripheral macrophages. A) Hind paw mechanical withdrawal thresholds were measured prior to 1 µg HMGB1 injection and at 1hr, 3hr, 8hr, 24hr and day 14 post injection in male TLR4$^{fl/fl}$ vehicle (n=6), TLR4$^{fl/fl}$ HMGB1 (n=8), LysM-TLR4$^{fl/fl}$ vehicle (n=8), LysM-TLR4$^{fl/fl}$ HMGB1 (n=9) mice. On day 14 mice were injected with a subthreshold dose of PGE2 and mechanical withdrawal thresholds were measured at 3hr and 24hr post injection. **B)** Hind paw mechanical withdrawal thresholds were measured prior to 1 µg HMGB1 injection and at 1hr, 3hr, 8hr, 24hr and day 14 post injection in female TLR4$^{fl/fl}$ vehicle (n=6), TLR4$^{fl/fl}$ HMGB1 (n=7), LysM-TLR4$^{fl/fl}$ vehicle (n=5), LysM-TLR4$^{fl/fl}$ HMGB1 (n=8) mice. On day 14 mice were injected with a

28

subthreshold dose of PGE2 and mechanical withdrawal thresholds were measured at 3hr and 24hr post injection. **C)** Hind paw mechanical withdrawal thresholds were measured prior to 1 µg HMGB1 injection and at 1hr, 3hr, 8hr, 24hr and day 14 post injection in male TLR4$^{fl/fl}$ vehicle (n=7), TLR4$^{fl/fl}$ HMGB1 (n=6), Nav1.8-TLR4$^{fl/fl}$ vehicle (n=8), Nav1.8-TLR4$^{fl/fl}$ HMGB1 (n=8) mice. On day 14 mice were injected with a subthreshold dose of PGE2 and mechanical withdrawal thresholds were measured at 3hr and 24hr post injection. **D)** Hind paw mechanical withdrawal thresholds were measured prior to 1 µg HMGB1 injection and at 1hr, 3hr, 8hr, 24hr and day 14 post injection in female TLR4$^{fl/fl}$ vehicle (n=5), TLR4$^{fl/fl}$ HMGB1 (n=9), Nav1.8-TLR4$^{fl/fl}$ vehicle (n=6), Nav1.8-TLR4$^{fl/fl}$ HMGB1 (n=9) mice. On day 14 mice were injected with a subthreshold dose of PGE2 and mechanical withdrawal thresholds were measured at 3hr and 24hr post injection. Data are represented as the standard error of the mean and were analyzed using a 2-way ANOVA and Tukey's *post-hoc* comparisons. Statistical comparisons are provided in Table 1.2.

Table 1.2. Statistical comparisons of the data represented in Figure 1.2.

Tukey's multiple comparisons test	Mean Diff.	95.00% CI of diff.	Below threshold?	Summary	Adjusted P Value
Figure 1.2A					
BL					
TLR4$^{fl/fl}$/Vehicle vs. TLR4$^{fl/fl}$/HMGB1	0.01398	-0.2101 to 0.2381	No	ns	0.9974
TLR4$^{fl/fl}$/Vehicle vs. LysM-TLR4$^{fl/fl}$/Vehicle	0.0008208	-0.2387 to 0.2404	No	ns	>0.9999
TLR4$^{fl/fl}$/Vehicle vs. LysM-TLR4$^{fl/fl}$/HMGB1	-0.0325	-0.2591 to 0.1941	No	ns	0.9714
TLR4$^{fl/fl}$/HMGB1 vs. LysM-TLR4$^{fl/fl}$/Vehicle	-0.01316	-0.2175 to 0.1912	No	ns	0.9975
TLR4$^{fl/fl}$/HMGB1 vs. LysM-TLR4$^{fl/fl}$/HMGB1	-0.04648	-0.2312 to 0.1382	No	ns	0.8854
LysM-TLR4$^{fl/fl}$/Vehicle vs. LysM-TLR4$^{fl/fl}$/HMGB1	-0.03332	-0.2413 to 0.1747	No	ns	0.9657
1hr					
TLR4$^{fl/fl}$/Vehicle vs. TLR4$^{fl/fl}$/HMGB1	0.4098	0.03891 to 0.7808	Yes	*	0.0298
TLR4$^{fl/fl}$/Vehicle vs. LysM-TLR4$^{fl/fl}$/Vehicle	-0.05834	-0.2740 to 0.1573	No	ns	0.8304
TLR4$^{fl/fl}$/Vehicle vs. LysM-TLR4$^{fl/fl}$/HMGB1	0.3251	0.008911 to 0.6413	Yes	*	0.0432
TLR4$^{fl/fl}$/HMGB1 vs. LysM-TLR4$^{fl/fl}$/Vehicle	-0.4682	-0.8260 to -0.1104	Yes	*	0.0123
TLR4$^{fl/fl}$/HMGB1 vs. LysM-TLR4$^{fl/fl}$/HMGB1	-0.08471	-0.4917 to 0.3223	No	ns	0.9291
LysM-TLR4$^{fl/fl}$/Vehicle vs. LysM-TLR4$^{fl/fl}$/HMGB1	0.3835	0.08851 to 0.6784	Yes	*	0.0113

3hr					
TLR4^{fl/fl}/Vehicle vs. TLR4^{fl/fl}/HMGB1	0.7881	0.4998 to 1.076	Yes	****	<0.0001
TLR4^{fl/fl}/Vehicle vs. LysM-TLR4^{fl/fl}/Vehicle	0.04833	-0.2504 to 0.3470	No	ns	0.9601
TLR4^{fl/fl}/Vehicle vs. LysM-TLR4^{fl/fl}/HMGB1	0.3648	-0.02587 to 0.7554	No	ns	0.0704
TLR4^{fl/fl}/HMGB1 vs. LysM-TLR4^{fl/fl}/Vehicle	-0.7398	-0.9892 to -0.4904	Yes	****	<0.0001
TLR4^{fl/fl}/HMGB1 vs. LysM-TLR4^{fl/fl}/HMGB1	-0.4234	-0.7895 to -0.05729	Yes	*	0.0223
LysM-TLR4^{fl/fl}/Vehicle vs. LysM-TLR4^{fl/fl}/HMGB1	0.3164	-0.05690 to 0.6897	No	ns	0.1085
8hr					
TLR4^{fl/fl}/Vehicle vs. TLR4^{fl/fl}/HMGB1	0.7364	0.4680 to 1.005	Yes	****	<0.0001
TLR4^{fl/fl}/Vehicle vs. LysM-TLR4^{fl/fl}/Vehicle	0.03768	-0.1335 to 0.2089	No	ns	0.9122
TLR4^{fl/fl}/Vehicle vs. LysM-TLR4^{fl/fl}/HMGB1	0.1741	-0.1967 to 0.5450	No	ns	0.5032
TLR4^{fl/fl}/HMGB1 vs. LysM-TLR4^{fl/fl}/Vehicle	-0.6987	-0.9695 to -0.4280	Yes	****	<0.0001
TLR4^{fl/fl}/HMGB1 vs. LysM-TLR4^{fl/fl}/HMGB1	-0.5623	-0.9663 to -0.1583	Yes	**	0.0059
LysM-TLR4^{fl/fl}/Vehicle vs. LysM-TLR4^{fl/fl}/HMGB1	0.1364	-0.2358 to 0.5087	No	ns	0.6875
24hr					
TLR4^{fl/fl}/Vehicle vs. TLR4^{fl/fl}/HMGB1	0.599	0.2250 to 0.9730	Yes	**	0.0024
TLR4^{fl/fl}/Vehicle vs. LysM-TLR4^{fl/fl}/Vehicle	0.05494	-0.2009 to 0.3107	No	ns	0.8671
TLR4^{fl/fl}/Vehicle vs. LysM-TLR4^{fl/fl}/HMGB1	0.1667	-0.2067 to 0.5400	No	ns	0.5705
TLR4^{fl/fl}/HMGB1 vs. LysM-TLR4^{fl/fl}/Vehicle	-0.5441	-0.8871 to -0.2010	Yes	**	0.0047
TLR4^{fl/fl}/HMGB1 vs. LysM-TLR4^{fl/fl}/HMGB1	-0.4323	-0.8590 to -0.005626	Yes	*	0.0466
LysM-TLR4^{fl/fl}/Vehicle vs. LysM-TLR4^{fl/fl}/HMGB1	0.1117	-0.2269 to 0.4504	No	ns	0.7286
D14					
TLR4^{fl/fl}/Vehicle vs. TLR4^{fl/fl}/HMGB1	0.009717	-0.1512 to 0.1706	No	ns	0.9975
TLR4^{fl/fl}/Vehicle vs. LysM-TLR4^{fl/fl}/Vehicle	-0.005808	-0.1833 to 0.1716	No	ns	0.9996
TLR4^{fl/fl}/Vehicle vs. LysM-TLR4^{fl/fl}/HMGB1	-0.03003	-0.2022 to 0.1421	No	ns	0.9496

TLR4$^{fl/fl}$/HMGB1 vs. LysM-TLR4$^{fl/fl}$/Vehicle	-0.01552	-0.2229 to 0.1918	No	ns	0.9962
TLR4$^{fl/fl}$/HMGB1 vs. LysM-TLR4$^{fl/fl}$/HMGB1	-0.03975	-0.2444 to 0.1649	No	ns	0.9424
LysM-TLR4$^{fl/fl}$/Vehicle vs. LysM-TLR4$^{fl/fl}$/HMGB1	-0.02423	-0.2394 to 0.1910	No	ns	0.9877
3hr					
TLR4$^{fl/fl}$/Vehicle vs. TLR4$^{fl/fl}$/HMGB1	0.7128	0.3568 to 1.069	Yes	***	0.0004
TLR4$^{fl/fl}$/Vehicle vs. LysM-TLR4$^{fl/fl}$/Vehicle	0.1838	-0.1327 to 0.5003	No	ns	0.3539
TLR4$^{fl/fl}$/Vehicle vs. LysM-TLR4$^{fl/fl}$/HMGB1	0.2098	-0.06243 to 0.4821	No	ns	0.1519
TLR4$^{fl/fl}$/HMGB1 vs. LysM-TLR4$^{fl/fl}$/Vehicle	-0.529	-0.8963 to -0.1618	Yes	**	0.0046
TLR4$^{fl/fl}$/HMGB1 vs. LysM-TLR4$^{fl/fl}$/HMGB1	-0.503	-0.8387 to -0.1673	Yes	**	0.004
LysM-TLR4$^{fl/fl}$/Vehicle vs. LysM-TLR4$^{fl/fl}$/HMGB1	0.02601	-0.2630 to 0.3150	No	ns	0.9932
24hr					
TLR4$^{fl/fl}$/Vehicle vs. TLR4$^{fl/fl}$/HMGB1	0.534	0.1123 to 0.9558	Yes	*	0.0132
TLR4$^{fl/fl}$/Vehicle vs. LysM-TLR4$^{fl/fl}$/Vehicle	-0.02355	-0.2911 to 0.2440	No	ns	0.9925
TLR4$^{fl/fl}$/Vehicle vs. LysM-TLR4$^{fl/fl}$/HMGB1	0.1074	-0.1704 to 0.3853	No	ns	0.6611
TLR4$^{fl/fl}$/HMGB1 vs. LysM-TLR4$^{fl/fl}$/Vehicle	-0.5576	-0.9621 to -0.1531	Yes	**	0.0085
TLR4$^{fl/fl}$/HMGB1 vs. LysM-TLR4$^{fl/fl}$/HMGB1	-0.4266	-0.8358 to -0.01737	Yes	*	0.0406
LysM-TLR4$^{fl/fl}$/Vehicle vs. LysM-TLR4$^{fl/fl}$/HMGB1	0.131	-0.09325 to 0.3552	No	ns	0.3649
Figure 1.2B					
BL					
TLR4$^{fl/fl}$/HMGB1 vs. Lyscre-TLR4$^{fl/fl}$/HMGB1	-0.04336	-0.2665 to 0.1798	No	ns	0.938
TLR4$^{fl/fl}$/HMGB1 vs. TLR4$^{fl/fl}$/Vehicle	0.07453	-0.2015 to 0.3506	No	ns	0.8419
TLR4$^{fl/fl}$/HMGB1 vs. Lyscre-TLR4$^{fl/fl}$/Vehicle	-0.07038	-0.2949 to 0.1542	No	ns	0.7748
Lyscre-TLR4$^{fl/fl}$/HMGB1 vs. TLR4$^{fl/fl}$/Vehicle	0.1179	-0.1468 to 0.3825	No	ns	0.5418
Lyscre-TLR4$^{fl/fl}$/HMGB1 vs. Lyscre-TLR4$^{fl/fl}$/Vehicle	-0.02702	-0.2316 to 0.1776	No	ns	0.9772
TLR4$^{fl/fl}$/Vehicle vs. Lyscre-TLR4$^{fl/fl}$/Vehicle	-0.1449	-0.4111 to 0.1213	No	ns	0.3685

1hr					
$TLR4^{fl/fl}$/HMGB1 vs. Lyscre-$TLR4^{fl/fl}$/HMGB1	-0.1576	-0.7626 to 0.4475	No	ns	0.868
$TLR4^{fl/fl}$/HMGB1 vs. $TLR4^{fl/fl}$/Vehicle	-0.5171	-1.039 to 0.004877	No	ns	0.0522
$TLR4^{fl/fl}$/HMGB1 vs. Lyscre-$TLR4^{fl/fl}$/Vehicle	-0.6087	-1.126 to -0.09116	Yes	*	0.0242
Lyscre-$TLR4^{fl/fl}$/HMGB1 vs. $TLR4^{fl/fl}$/Vehicle	-0.3596	-0.8357 to 0.1166	No	ns	0.1589
Lyscre-$TLR4^{fl/fl}$/HMGB1 vs. Lyscre-$TLR4^{fl/fl}$/Vehicle	-0.4511	-0.9175 to 0.01521	No	ns	0.0579
$TLR4^{fl/fl}$/Vehicle vs. Lyscre-$TLR4^{fl/fl}$/Vehicle	-0.09157	-0.3349 to 0.1518	No	ns	0.6405
3hr					
$TLR4^{fl/fl}$/HMGB1 vs. Lyscre-$TLR4^{fl/fl}$/HMGB1	-0.0629	-0.5693 to 0.4435	No	ns	0.9827
$TLR4^{fl/fl}$/HMGB1 vs. $TLR4^{fl/fl}$/Vehicle	-0.5812	-0.9968 to -0.1656	Yes	**	0.0074
$TLR4^{fl/fl}$/HMGB1 vs. Lyscre-$TLR4^{fl/fl}$/Vehicle	-0.578	-1.021 to -0.1349	Yes	*	0.0115
Lyscre-$TLR4^{fl/fl}$/HMGB1 vs. $TLR4^{fl/fl}$/Vehicle	-0.5183	-0.9658 to -0.07073	Yes	*	0.0228
Lyscre-$TLR4^{fl/fl}$/HMGB1 vs. Lyscre-$TLR4^{fl/fl}$/Vehicle	-0.5151	-0.9865 to -0.04377	Yes	*	0.0314
$TLR4^{fl/fl}$/Vehicle vs. Lyscre-$TLR4^{fl/fl}$/Vehicle	0.003167	-0.3609 to 0.3672	No	ns	>0.9999
8hr					
$TLR4^{fl/fl}$/HMGB1 vs. Lyscre-$TLR4^{fl/fl}$/HMGB1	-0.05954	-0.4637 to 0.3447	No	ns	0.9718
$TLR4^{fl/fl}$/HMGB1 vs. $TLR4^{fl/fl}$/Vehicle	-0.5683	-0.9116 to -0.2250	Yes	**	0.0021
$TLR4^{fl/fl}$/HMGB1 vs. Lyscre-$TLR4^{fl/fl}$/Vehicle	-0.4857	-0.8566 to -0.1148	Yes	*	0.0112
Lyscre-$TLR4^{fl/fl}$/HMGB1 vs. $TLR4^{fl/fl}$/Vehicle	-0.5088	-0.8785 to -0.1390	Yes	**	0.0074
Lyscre-$TLR4^{fl/fl}$/HMGB1 vs. Lyscre-$TLR4^{fl/fl}$/Vehicle	-0.4262	-0.8194 to -0.03293	Yes	*	0.0328
$TLR4^{fl/fl}$/Vehicle vs. Lyscre-$TLR4^{fl/fl}$/Vehicle	0.08259	-0.2495 to 0.4147	No	ns	0.8578
24hr					
$TLR4^{fl/fl}$/HMGB1 vs. Lyscre-$TLR4^{fl/fl}$/HMGB1	-0.1008	-0.4187 to 0.2170	No	ns	0.7883
$TLR4^{fl/fl}$/HMGB1 vs. $TLR4^{fl/fl}$/Vehicle	-0.2729	-0.5668 to 0.02100	No	ns	0.0711

TLR4$^{fl/fl}$/HMGB1 vs. Lyscre-TLR4$^{fl/fl}$/Vehicle	-0.3641	-0.6575 to -0.07061	Yes	*	0.0156
Lyscre-TLR4$^{fl/fl}$/HMGB1 vs. TLR4$^{fl/fl}$/Vehicle	-0.1721	-0.4564 to 0.1123	No	ns	0.3209
Lyscre-TLR4$^{fl/fl}$/HMGB1 vs. Lyscre-TLR4$^{fl/fl}$/Vehicle	-0.2632	-0.5468 to 0.02036	No	ns	0.0715
TLR4$^{fl/fl}$/Vehicle vs. Lyscre-TLR4$^{fl/fl}$/Vehicle	-0.09117	-0.3455 to 0.1632	No	ns	0.6872
D14					
TLR4$^{fl/fl}$/HMGB1 vs. Lyscre-TLR4$^{fl/fl}$/HMGB1	0.01563	-0.03610 to 0.06735	No	ns	0.7545
TLR4$^{fl/fl}$/HMGB1 vs. TLR4$^{fl/fl}$/Vehicle	0.01578	-0.2513 to 0.2829	No	ns	0.9959
TLR4$^{fl/fl}$/HMGB1 vs. Lyscre-TLR4$^{fl/fl}$/Vehicle	-0.09212	-0.3218 to 0.1375	No	ns	0.4552
Lyscre-TLR4$^{fl/fl}$/HMGB1 vs. TLR4$^{fl/fl}$/Vehicle	0.0001583	-0.2642 to 0.2645	No	ns	>0.9999
Lyscre-TLR4$^{fl/fl}$/HMGB1 vs. Lyscre-TLR4$^{fl/fl}$/Vehicle	-0.1077	-0.3307 to 0.1152	No	ns	0.3622
TLR4$^{fl/fl}$/Vehicle vs. Lyscre-TLR4$^{fl/fl}$/Vehicle	-0.1079	-0.3954 to 0.1796	No	ns	0.6558
3hr					
TLR4$^{fl/fl}$/HMGB1 vs. Lyscre-TLR4$^{fl/fl}$/HMGB1	0.1082	-0.2298 to 0.4461	No	ns	0.7803
TLR4$^{fl/fl}$/HMGB1 vs. TLR4$^{fl/fl}$/Vehicle	-0.5396	-0.8852 to -0.1941	Yes	**	0.0031
TLR4$^{fl/fl}$/HMGB1 vs. Lyscre-TLR4$^{fl/fl}$/Vehicle	-0.5971	-0.9196 to -0.2745	Yes	**	0.0011
Lyscre-TLR4$^{fl/fl}$/HMGB1 vs. TLR4$^{fl/fl}$/Vehicle	-0.6478	-0.9591 to -0.3366	Yes	***	0.0003
Lyscre-TLR4$^{fl/fl}$/HMGB1 vs. Lyscre-TLR4$^{fl/fl}$/Vehicle	-0.7053	-0.9856 to -0.4249	Yes	****	<0.0001
TLR4$^{fl/fl}$/Vehicle vs. Lyscre-TLR4$^{fl/fl}$/Vehicle	-0.05743	-0.3516 to 0.2367	No	ns	0.9257
24hr					
TLR4$^{fl/fl}$/HMGB1 vs. Lyscre-TLR4$^{fl/fl}$/HMGB1	0.03377	-0.4468 to 0.5143	No	ns	0.9966
TLR4$^{fl/fl}$/HMGB1 vs. TLR4$^{fl/fl}$/Vehicle	-0.4901	-0.9363 to -0.04386	Yes	*	0.032
TLR4$^{fl/fl}$/HMGB1 vs. Lyscre-TLR4$^{fl/fl}$/Vehicle	-0.5812	-1.027 to -0.1351	Yes	*	0.0131
Lyscre-TLR4$^{fl/fl}$/HMGB1 vs. TLR4$^{fl/fl}$/Vehicle	-0.5238	-0.8685 to -0.1792	Yes	**	0.0038
Lyscre-TLR4$^{fl/fl}$/HMGB1 vs. Lyscre-TLR4$^{fl/fl}$/Vehicle	-0.615	-0.9590 to -0.2711	Yes	**	0.0012
TLR4$^{fl/fl}$/Vehicle vs. Lyscre-TLR4$^{fl/fl}$/Vehicle	-0.09117	-0.3455 to 0.1632	No	ns	0.6872

Figure 1.2C					
BL					
TLR4$^{fl/fl}$/Vehicle vs. TLR4$^{fl/fl}$/HMGB1	-0.02029	-0.3196 to 0.2790	No	ns	0.9981
TLR4$^{fl/fl}$/Vehicle vs. Nav1.8-TLR4$^{fl/fl}$/Vehicle	-0.02907	-0.3075 to 0.2494	No	ns	0.9931
TLR4$^{fl/fl}$/Vehicle vs. Nav1.8-TLR4$^{fl/fl}$/HMGB1	-0.07348	-0.3519 to 0.2049	No	ns	0.9032
TLR4$^{fl/fl}$/HMGB1 vs. Nav1.8-TLR4$^{fl/fl}$/Vehicle	-0.008775	-0.2993 to 0.2818	No	ns	0.9998
TLR4$^{fl/fl}$/HMGB1 vs. Nav1.8-TLR4$^{fl/fl}$/HMGB1	-0.05319	-0.3437 to 0.2374	No	ns	0.9647
Nav1.8-TLR4$^{fl/fl}$/Vehicle vs. Nav1.8-TLR4$^{fl/fl}$/HMGB1	-0.04441	-0.3134 to 0.2246	No	ns	0.9737
1hr					
TLR4$^{fl/fl}$/Vehicle vs. TLR4$^{fl/fl}$/HMGB1	0.5563	0.2570 to 0.8556	Yes	****	<0.0001
TLR4$^{fl/fl}$/Vehicle vs. Nav1.8-TLR4$^{fl/fl}$/Vehicle	0.02511	-0.2533 to 0.3035	No	ns	0.9955
TLR4$^{fl/fl}$/Vehicle vs. Nav1.8-TLR4$^{fl/fl}$/HMGB1	0.2307	-0.04777 to 0.5091	No	ns	0.1422
TLR4$^{fl/fl}$/HMGB1 vs. Nav1.8-TLR4$^{fl/fl}$/Vehicle	-0.5312	-0.8217 to -0.2406	Yes	****	<0.0001
TLR4$^{fl/fl}$/HMGB1 vs. Nav1.8-TLR4$^{fl/fl}$/HMGB1	-0.3256	-0.6161 to -0.03507	Yes	*	0.0212
Nav1.8-TLR4$^{fl/fl}$/Vehicle vs. Nav1.8-TLR4$^{fl/fl}$/HMGB1	0.2056	-0.06344 to 0.4745	No	ns	0.1991
3hr					
TLR4$^{fl/fl}$/Vehicle vs. TLR4$^{fl/fl}$/HMGB1	0.6276	0.3283 to 0.9269	Yes	****	<0.0001
TLR4$^{fl/fl}$/Vehicle vs. Nav1.8-TLR4$^{fl/fl}$/Vehicle	-0.001661	-0.2801 to 0.2768	No	ns	>0.9999
TLR4$^{fl/fl}$/Vehicle vs. Nav1.8-TLR4$^{fl/fl}$/HMGB1	0.3078	0.02935 to 0.5862	Yes	*	0.0238
TLR4$^{fl/fl}$/HMGB1 vs. Nav1.8-TLR4$^{fl/fl}$/Vehicle	-0.6293	-0.9198 to -0.3387	Yes	****	<0.0001
TLR4$^{fl/fl}$/HMGB1 vs. Nav1.8-TLR4$^{fl/fl}$/HMGB1	-0.3198	-0.6104 to -0.02930	Yes	*	0.0246
Nav1.8-TLR4$^{fl/fl}$/Vehicle vs. Nav1.8-TLR4$^{fl/fl}$/HMGB1	0.3094	0.04045 to 0.5784	Yes	*	0.0169
8hr					
TLR4$^{fl/fl}$/Vehicle vs. TLR4$^{fl/fl}$/HMGB1	0.7258	0.4265 to 1.025	Yes	****	<0.0001
TLR4$^{fl/fl}$/Vehicle vs. Nav1.8-TLR4$^{fl/fl}$/Vehicle	0.008861	-0.2696 to 0.2873	No	ns	0.9998

TLR4$^{fl/fl}$/Vehicle vs. Nav1.8-TLR4$^{fl/fl}$/HMGB1	0.3496	0.07120 to 0.6281	Yes	**	0.0073
TLR4$^{fl/fl}$/HMGB1 vs. Nav1.8-TLR4$^{fl/fl}$/Vehicle	-0.717	-1.007 to -0.4264	Yes	****	<0.0001
TLR4$^{fl/fl}$/HMGB1 vs. Nav1.8-TLR4$^{fl/fl}$/HMGB1	-0.3762	-0.6667 to -0.08566	Yes	**	0.0052
Nav1.8-TLR4$^{fl/fl}$/Vehicle vs. Nav1.8-TLR4$^{fl/fl}$/HMGB1	0.3408	0.07178 to 0.6097	Yes	**	0.0066
24hr					
TLR4$^{fl/fl}$/Vehicle vs. TLR4$^{fl/fl}$/HMGB1	0.6599	0.3606 to 0.9592	Yes	****	<0.0001
TLR4$^{fl/fl}$/Vehicle vs. Nav1.8-TLR4$^{fl/fl}$/Vehicle	0.04464	-0.2338 to 0.3231	No	ns	0.9758
TLR4$^{fl/fl}$/Vehicle vs. Nav1.8-TLR4$^{fl/fl}$/HMGB1	0.3836	0.1051 to 0.6620	Yes	**	0.0025
TLR4$^{fl/fl}$/HMGB1 vs. Nav1.8-TLR4$^{fl/fl}$/Vehicle	-0.6153	-0.9058 to -0.3248	Yes	****	<0.0001
TLR4$^{fl/fl}$/HMGB1 vs. Nav1.8-TLR4$^{fl/fl}$/HMGB1	-0.2764	-0.5669 to 0.01418	No	ns	0.0688
Nav1.8-TLR4$^{fl/fl}$/Vehicle vs. Nav1.8-TLR4$^{fl/fl}$/HMGB1	0.3389	0.06995 to 0.6079	Yes	**	0.007
D14					
TLR4$^{fl/fl}$/Vehicle vs. TLR4$^{fl/fl}$/HMGB1	0.01504	-0.2843 to 0.3143	No	ns	0.9992
TLR4$^{fl/fl}$/Vehicle vs. Nav1.8-TLR4$^{fl/fl}$/Vehicle	0.01754	-0.2609 to 0.2960	No	ns	0.9984
TLR4$^{fl/fl}$/Vehicle vs. Nav1.8-TLR4$^{fl/fl}$/HMGB1	0.01504	-0.2634 to 0.2935	No	ns	0.999
TLR4$^{fl/fl}$/HMGB1 vs. Nav1.8-TLR4$^{fl/fl}$/Vehicle	0.0025	-0.2880 to 0.2930	No	ns	>0.9999
TLR4$^{fl/fl}$/HMGB1 vs. Nav1.8-TLR4$^{fl/fl}$/HMGB1	0	-0.2905 to 0.2905	No	ns	>0.9999
Nav1.8-TLR4$^{fl/fl}$/Vehicle vs. Nav1.8-TLR4$^{fl/fl}$/HMGB1	-0.0025	-0.2715 to 0.2665	No	ns	>0.9999
3hr					
TLR4$^{fl/fl}$/Vehicle vs. TLR4$^{fl/fl}$/HMGB1	0.7165	0.4172 to 1.016	Yes	****	<0.0001
TLR4$^{fl/fl}$/Vehicle vs. Nav1.8-TLR4$^{fl/fl}$/Vehicle	0.06383	-0.2146 to 0.3423	No	ns	0.9338
TLR4$^{fl/fl}$/Vehicle vs. Nav1.8-TLR4$^{fl/fl}$/HMGB1	0.4175	0.1390 to 0.6959	Yes	***	0.0008
TLR4$^{fl/fl}$/HMGB1 vs. Nav1.8-TLR4$^{fl/fl}$/Vehicle	-0.6527	-0.9432 to -0.3622	Yes	****	<0.0001
TLR4$^{fl/fl}$/HMGB1 vs. Nav1.8-TLR4$^{fl/fl}$/HMGB1	-0.2991	-0.5896 to -0.008533	Yes	*	0.041
Nav1.8-TLR4$^{fl/fl}$/Vehicle vs. Nav1.8-TLR4$^{fl/fl}$/HMGB1	0.3536	0.08464 to 0.6226	Yes	**	0.0044

24hr					
TLR4$^{fl/fl}$/Vehicle vs. TLR4$^{fl/fl}$/HMGB1	0.4912	0.1919 to 0.7905	Yes	***	0.0002
TLR4$^{fl/fl}$/Vehicle vs. Nav1.8-TLR4$^{fl/fl}$/Vehicle	0.04266	-0.2358 to 0.3211	No	ns	0.9788
TLR4$^{fl/fl}$/Vehicle vs. Nav1.8-TLR4$^{fl/fl}$/HMGB1	0.255	-0.02341 to 0.5334	No	ns	0.0857
TLR4$^{fl/fl}$/HMGB1 vs. Nav1.8-TLR4$^{fl/fl}$/Vehicle	-0.4485	-0.7391 to -0.1580	Yes	***	0.0005
TLR4$^{fl/fl}$/HMGB1 vs. Nav1.8-TLR4$^{fl/fl}$/HMGB1	-0.2362	-0.5267 to 0.05439	No	ns	0.1548
Nav1.8-TLR4$^{fl/fl}$/Vehicle vs. Nav1.8-TLR4$^{fl/fl}$/HMGB1	0.2124	-0.05662 to 0.4813	No	ns	0.175
Figure 1.2D					
BL					
TLR4$^{fl/fl}$/HMGB1 vs. Nav1.8-TLR4$^{fl/fl}$/HMGB1	-0.05109	-0.2405 to 0.1383	No	ns	0.8659
TLR4$^{fl/fl}$/HMGB1 vs. TLR4$^{fl/fl}$/Vehicle	-0.003538	-0.2311 to 0.2240	No	ns	>0.9999
TLR4$^{fl/fl}$/HMGB1 vs. Nav1.8-TLR4$^{fl/fl}$/Vehicle	-0.06491	-0.2647 to 0.1349	No	ns	0.7719
Nav1.8-TLR4$^{fl/fl}$/HMGB1 vs. TLR4$^{fl/fl}$/Vehicle	0.04755	-0.1802 to 0.2753	No	ns	0.9135
Nav1.8-TLR4$^{fl/fl}$/HMGB1 vs. Nav1.8-TLR4$^{fl/fl}$/Vehicle	-0.01382	-0.2139 to 0.1862	No	ns	0.9968
TLR4$^{fl/fl}$/Vehicle vs. Nav1.8-TLR4$^{fl/fl}$/Vehicle	-0.06137	-0.2968 to 0.1741	No	ns	0.8413
1hr					
TLR4$^{fl/fl}$/HMGB1 vs. Nav1.8-TLR4$^{fl/fl}$/HMGB1	-0.4591	-0.9231 to 0.004942	No	ns	0.053
TLR4$^{fl/fl}$/HMGB1 vs. TLR4$^{fl/fl}$/Vehicle	-0.5452	-0.9494 to -0.1410	Yes	*	0.01
TLR4$^{fl/fl}$/HMGB1 vs. Nav1.8-TLR4$^{fl/fl}$/Vehicle	-0.605	-1.012 to -0.1978	Yes	**	0.0051
Nav1.8-TLR4$^{fl/fl}$/HMGB1 vs. TLR4$^{fl/fl}$/Vehicle	-0.08612	-0.4152 to 0.2429	No	ns	0.849
Nav1.8-TLR4$^{fl/fl}$/HMGB1 vs. Nav1.8-TLR4$^{fl/fl}$/Vehicle	-0.1459	-0.4795 to 0.1878	No	ns	0.5676
TLR4$^{fl/fl}$/Vehicle vs. Nav1.8-TLR4$^{fl/fl}$/Vehicle	-0.05976	-0.2265 to 0.1070	No	ns	0.6848
3hr					
TLR4$^{fl/fl}$/HMGB1 vs. Nav1.8-TLR4$^{fl/fl}$/HMGB1	-0.5974	-0.9852 to -0.2096	Yes	**	0.0034
TLR4$^{fl/fl}$/HMGB1 vs. TLR4$^{fl/fl}$/Vehicle	-0.6717	-1.057 to -0.2866	Yes	**	0.0015

$TLR4^{fl/fl}$/HMGB1 vs. Nav1.8-$TLR4^{fl/fl}$/Vehicle	-0.7024	-1.088 to -0.3165	Yes	**	0.001
Nav1.8-$TLR4^{fl/fl}$/HMGB1 vs. $TLR4^{fl/fl}$/Vehicle	-0.0743	-0.2853 to 0.1367	No	ns	0.7242
Nav1.8-$TLR4^{fl/fl}$/HMGB1 vs. Nav1.8-$TLR4^{fl/fl}$/Vehicle	-0.105	-0.3178 to 0.1079	No	ns	0.4925
$TLR4^{fl/fl}$/Vehicle vs. Nav1.8-$TLR4^{fl/fl}$/Vehicle	-0.03067	-0.2395 to 0.1781	No	ns	0.9662
8hr					
$TLR4^{fl/fl}$/HMGB1 vs. Nav1.8-$TLR4^{fl/fl}$/HMGB1	-0.3936	-0.7309 to -0.05636	Yes	*	0.0205
$TLR4^{fl/fl}$/HMGB1 vs. $TLR4^{fl/fl}$/Vehicle	-0.5678	-0.8952 to -0.2404	Yes	**	0.0014
$TLR4^{fl/fl}$/HMGB1 vs. Nav1.8-$TLR4^{fl/fl}$/Vehicle	-0.515	-0.8332 to -0.1967	Yes	**	0.0028
Nav1.8-$TLR4^{fl/fl}$/HMGB1 vs. $TLR4^{fl/fl}$/Vehicle	-0.1742	-0.4016 to 0.05319	No	ns	0.1586
Nav1.8-$TLR4^{fl/fl}$/HMGB1 vs. Nav1.8-$TLR4^{fl/fl}$/Vehicle	-0.1214	-0.3265 to 0.08379	No	ns	0.3376
$TLR4^{fl/fl}$/Vehicle vs. Nav1.8-$TLR4^{fl/fl}$/Vehicle	0.05284	-0.1330 to 0.2387	No	ns	0.7926
24hr					
$TLR4^{fl/fl}$/HMGB1 vs. Nav1.8-$TLR4^{fl/fl}$/HMGB1	-0.2508	-0.6298 to 0.1283	No	ns	0.245
$TLR4^{fl/fl}$/HMGB1 vs. $TLR4^{fl/fl}$/Vehicle	-0.3958	-0.7766 to -0.01492	Yes	*	0.0413
$TLR4^{fl/fl}$/HMGB1 vs. Nav1.8-$TLR4^{fl/fl}$/Vehicle	-0.5031	-0.8847 to -0.1214	Yes	*	0.0104
Nav1.8-$TLR4^{fl/fl}$/HMGB1 vs. $TLR4^{fl/fl}$/Vehicle	-0.145	-0.3410 to 0.05103	No	ns	0.1743
Nav1.8-$TLR4^{fl/fl}$/HMGB1 vs. Nav1.8-$TLR4^{fl/fl}$/Vehicle	-0.2523	-0.4500 to -0.05463	Yes	*	0.012
$TLR4^{fl/fl}$/Vehicle vs. Nav1.8-$TLR4^{fl/fl}$/Vehicle	-0.1073	-0.3161 to 0.1015	No	ns	0.4222
D14					
$TLR4^{fl/fl}$/HMGB1 vs. Nav1.8-$TLR4^{fl/fl}$/HMGB1	-0.01358	-0.1277 to 0.1005	No	ns	0.9858
$TLR4^{fl/fl}$/HMGB1 vs. $TLR4^{fl/fl}$/Vehicle	-0.03408	-0.2134 to 0.1452	No	ns	0.9236
$TLR4^{fl/fl}$/HMGB1 vs. Nav1.8-$TLR4^{fl/fl}$/Vehicle	-0.05062	-0.2506 to 0.1494	No	ns	0.8488
Nav1.8-$TLR4^{fl/fl}$/HMGB1 vs. $TLR4^{fl/fl}$/Vehicle	-0.0205	-0.1982 to 0.1572	No	ns	0.9783
Nav1.8-$TLR4^{fl/fl}$/HMGB1 vs. Nav1.8-$TLR4^{fl/fl}$/Vehicle	-0.03704	-0.2354 to 0.1613	No	ns	0.9247
$TLR4^{fl/fl}$/Vehicle vs. Nav1.8-$TLR4^{fl/fl}$/Vehicle	-0.01654	-0.2400 to 0.2069	No	ns	0.9953

3hr					
TLR4$^{fl/fl}$/HMGB1 vs. Nav1.8-TLR4$^{fl/fl}$/HMGB1	-0.3827	-0.6737 to -0.09170	Yes	**	0.0084
TLR4$^{fl/fl}$/HMGB1 vs. TLR4$^{fl/fl}$/Vehicle	-0.5848	-0.8482 to -0.3215	Yes	***	0.0001
TLR4$^{fl/fl}$/HMGB1 vs. Nav1.8-TLR4$^{fl/fl}$/Vehicle	-0.7567	-0.9855 to -0.5278	Yes	****	<0.0001
Nav1.8-TLR4$^{fl/fl}$/HMGB1 vs. TLR4$^{fl/fl}$/Vehicle	-0.2021	-0.4861 to 0.08180	No	ns	0.2035
Nav1.8-TLR4$^{fl/fl}$/HMGB1 vs. Nav1.8-TLR4$^{fl/fl}$/Vehicle	-0.3739	-0.6297 to -0.1182	Yes	**	0.0048
TLR4$^{fl/fl}$/Vehicle vs. Nav1.8-TLR4$^{fl/fl}$/Vehicle	-0.1718	-0.3988 to 0.05521	No	ns	0.1447
24hr					
TLR4$^{fl/fl}$/HMGB1 vs. Nav1.8-TLR4$^{fl/fl}$/HMGB1	-0.4775	-0.8771 to -0.07785	Yes	*	0.019
TLR4$^{fl/fl}$/HMGB1 vs. TLR4$^{fl/fl}$/Vehicle	-0.568	-0.9670 to -0.1690	Yes	**	0.0065
TLR4$^{fl/fl}$/HMGB1 vs. Nav1.8-TLR4$^{fl/fl}$/Vehicle	-0.5987	-0.9985 to -0.1989	Yes	**	0.0045
Nav1.8-TLR4$^{fl/fl}$/HMGB1 vs. TLR4$^{fl/fl}$/Vehicle	-0.09053	-0.2948 to 0.1138	No	ns	0.5644
Nav1.8-TLR4$^{fl/fl}$/HMGB1 vs. Nav1.8-TLR4$^{fl/fl}$/Vehicle	-0.1212	-0.3273 to 0.08488	No	ns	0.347
TLR4$^{fl/fl}$/Vehicle vs. Nav1.8-TLR4$^{fl/fl}$/Vehicle	-0.03067	-0.2395 to 0.1781	No	ns	0.9662

CHAPTER 2

THE ROLE OF MICROGLIA VERSUS PERIPHERAL MACROPHAGES IN

MALADAPTIVE PLASTICITY AFTER NERVE INJURY

Authors – Thomas A. Szabo-Pardi, Nilesh M. Agalave, Michael D. Burton

The Department of Neuroscience, BSB10.537

The University of Texas at Dallas

800 West Campbell Road

Richardson, Texas 75080-3021

Microglia and macrophages in the development of maladaptive plastic changes after peripheral nerve injury

Microglia and macrophages encompass the innate immune response to injury in the central and peripheral nervous systems, respectively, and are intimately involved in the pathogenesis of maladaptive changes (Tsuda, 2019). These dynamic cells can influence neuronal activity in active and quiescent states. Conflicting findings argue that peripheral macrophages facilitate the development of nerve injury-induced neuropathic pain, as opposed to central microglia (Lopes, 2017; Yu et al., 2020). It is imperative to discern their spatiotemporal contributions to the development and maintenance of maladaptive conditions, such as neuropathic pain (Inoue & Tsuda, 2018). The individual role of these cell types is difficult to parse out because both microglia and macrophages exhibit a keen ability to react quickly to injury and remain reactive after injury-induced changes. Appropriate methods to isolate and characterize these cells in downstream applications is necessary to uncover key findings (Agalave, 2020).

While the location and time points these cells mediate maladaptive changes remain unclear, it is obvious that certain neuroimmune activation pathways, such as Fractalkine (CX_3CL1)-Fractalkine receptor (CX_3CR1), high mobility group box 1 (HMGB1)-toll-like receptor 4 (TLR4), ATP-Purinergic channels, and HMGB1-protease activated receptor 2 (PAR2), are important in the neuroimmune signaling process. Interestingly, along with cell-type etiology of maladaptive plasticity, evidence points to an underlying sexual dimorphic mechanism in immune cell signaling

in response to injury. This sex difference can be attributed to "biased signaling" processing in similar cell types or different cell types altogether.

Contribution of macrophages and microglia in nerve injury-induced neuropathic pain models

Several experimental nerve injury models are commonly used to study neuropathic pain, such as spared nerve injury, spinal nerve ligation, and chronic constriction injury (**Figure 2.1A**). In these models, markers of macrophage activation such as ED-1, MHC-II and Iba1 are increased from days to weeks in lumbar dorsal root ganglia (DRG) (Ristoiu, 2013). Additionally, microglia in the spinal cord exhibit similar activation kinetics as macrophages during the development of neuropathic pain following nerve injury (Ristoiu, 2013). However, it remains unclear what these cell types respective roles are in the onset and maintenance of neuropathic pain. Several inflammatory mediators such as chemokine (CC motif) ligand 2, interleukin (IL)-6, IL-1β, matrix metallopeptidases-2, and -9, and CX_3CL1 are released following nerve injury and facilitate the activation of macrophages and microglia (Zhao et al., 2017). Activation of these cells upregulates factors that increase central excitatory neurotransmission, decrease inhibitory tone of interneurons, and promote nociceptor plasticity (Bennett et al., 2016). During the pathogenesis of nerve injury, macrophages in periphery, and microglia in the spinal cord, polarize to facilitate inflammation, neuroprotection, and tissue-repair. These cells polarize into an M1 (pro-inflammatory) or M2 (anti-inflammatory) phenotype. Typically, polarized macrophages are further classified into several subtypes which depend on the makeup of the inflammatory milieu (Martinez & Gordon, 2014). Despite substantive research regarding macrophage polarization in response to injury, it remains unclear how these cells, and their subtypes, are polarized during the development and resolution

41

of injury-induced neuropathic pain. Clarifying this dynamic response to injury will help improve our understanding of sexual dimorphisms that have been implicated in neuropathic pain. Moreover, polarization of microglia in the central nervous system is controversial (Ransohoff, 2016). It is difficult to discern a distinct phenotype in these cells as they often concurrently express markers of both pro-inflammatory and anti-inflammatory polarization following injury. Noteworthy, microglia are similarly active in males and females following nerve injury, however, blocking microglial activity through inhibitors such as TAK 242 (TLR4 inhibitor), CSFR1, BDNF-TrkB and p38 MAPK shows reversal of pain behaviors only in males (Tsuda, 2019). This suggests the central immune system exhibits a "biased" signaling pathway in the development of injury-induced neuropathic pain that is different between sexes. Thus, a need exists to explore these biased-intracellular signaling cascades in the context of maladaptive plasticity.
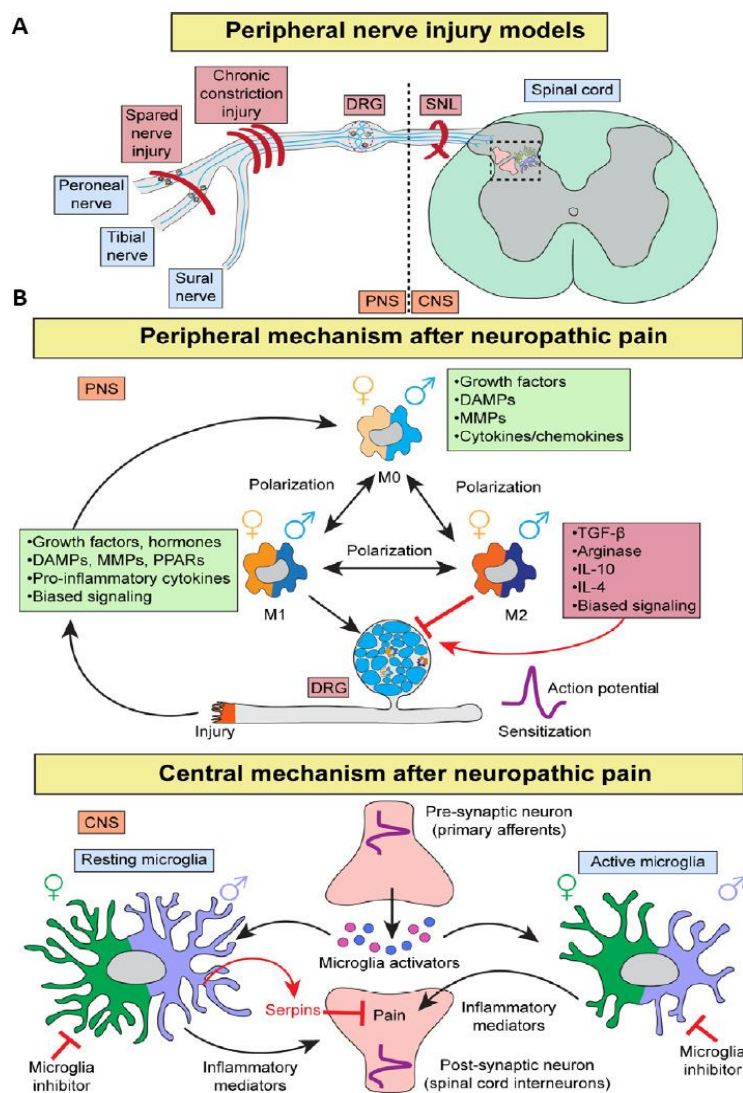
Figure 2.1. A graphic depicting peripheral macrophage *versus* central microglia during a peripheral nerve injury and possible sex differences in biased signaling pathways. (A) An illustration of different peripheral nerve injury experimental models of neuropathic pain. A prominent version of spared nerve injury (SNI) is the ligation and transection of the peroneal and tibial nerve, leaving the sural nerve intact to be sensitized. Chronic constriction injury utilizes 3 loose ligatures around the sciatic nerve trunk. The spinal nerve ligation model ligates the spinal nerve. (B) A depiction of how early peripheral nerve injury depicts how early peripheral nerve injury recruits macrophages/monocytes to the site of injury and dorsal root ganglia (DRG), which are activated and release inflammatory mediators such as growth factors, cytokines, danger associated molecular patterns (DAMPS) and matrix metalloproteins (MMPs). These mediators bind to their respective receptors expressed on the DRGs neuron to mediate nociception. (C) A depiction of what happens at central terminals depicts action at central terminals in the spinal cord where persistent activation of primary afferent neurons stimulates the release of inflammatory mediators that activate microglia in the dorsal horn of the spinal cord.

43

Acute-to-chronic effect of neuropathic pain on macrophage and microglia

Timing and signaling (biased): Microglia in the dorsal horn of the spinal cord facilitate chronic pain development in both sexes but inhibiting certain second messenger systems has shown promise in males only (Tsuda, 2019). Surprisingly, no studies have found differences in altered genes between males and females in microglia after neuropathic injury, suggesting similar phenotypic profiles. It is important to note that although the authors did not map the estrus cycle over the course of the entire study, there are no differences in basal sensitivity throughout each phase of the cycle (Sorge, 2011). Moreover, there is evidence to suggest that levels of microgliosis are similar in the spinal cord of males in females after nerve injury and is not estrus cycle dependent (Taves et al., 2016; Tsuda, 2019). However, the timing post-injury could reveal a therapeutic window that explains the etiology of sex differences. Based on this principle, a recent study revealed an increase in macrophage infiltration within the DRG in males 8 days after spinal nerve ligation, suggesting sexual dimorphic mechanisms in the recruitment of macrophages in the early phase of nerve injury (Lopes, 2017). While these immune cells are activated in both sexes after nerve injury, intracellular signaling cascades may facilitate maladaptive plasticity differently in males and females. Recent evidence highlights sex-biased signaling in various immune pathways. In males, elevated androgens enhance peroxisome proliferator activated receptor (PPAR) a expression that consequently inhibits nuclear factor-κB activity and interferon-γ production. In contrast, estrogens in females induce PPAR to exhibit similar anti-inflammatory actions as PPARa (Park & Choi, 2017) (**Figure 2.1B**). Activated macrophages in the DRG express proteins that help facilitate recruitment of various immune cells. This indicates alternative activation kinetics of the immune system where cell recruitment has a sexual dimorphic role in maladaptive plasticity. Thus,

activation of nociceptors may be different in male and female following nerve injury. The mechanisms involved in the development and maintenance of neuropathic pain are different, however, the spatiotemporal role of macrophages and microglia in the DRG and spinal cord are poorly documented. A need exists to examine the early recruitment/activation of macrophages and microglia in both sexes, and how these cells' phenotypes are altered over the pathogenesis of neuropathic pain.

The importance of differentiating neuropathic *versus* post-surgery/injury (sham effects) and the importance of therapeutic window of opportunity in the early stage

Since most studies investigate the therapeutic potential of altering immune cell signaling and activation after injury-induced neuropathy has developed, we sit at an important crossroad where we are able to answer questions as to how microglia and macrophages contribute to the onset of neuropathic pain. Moreover, the maladaptive/plastic effects of post-operative pain are often overlooked in studies focusing on neuropathic pain. It is imperative to discern the etiology of neuropathic, as opposed to post-operative pain. This presents a potential point of unbiased therapeutic intervention where we may attenuate, or even prevent the manifestation of neuropathic pain behaviors in both sexes. Macrophages in the DRG and microglia in spinal cord are activated early in response to nerve injury and remain active throughout its pathogenesis. Chronic activation of macrophages and microglia facilitate recruitment of other immune cells which leads to long lasting neuroimmune interactions. This reciprocal signaling maintains chronicity in nociceptive plasticity. Moreover, our lab has shown the direct involvement of HMGB1-TLR4 signaling in female nociceptors during neuropathic pain development (Szabo-Pardi et al., 2021). Thus,

modulating the early activation of macrophages and microglia may present a therapeutic approach to prevent neuropathic pain and avoid sexually biased signaling. However, we must first understand the respective contributions of these cells during the onset of injury to make conjecture as to how we should develop effective therapeutic approaches.

What are some differentiating factors between peripheral *versus* central immune cells and how they could reveal therapeutic targets?

The mechanisms of microglia polarization are not well understood. Traditional views regarding immune cell polarization are not well adapted to microglia. These cells are dynamic and present a spectrum of polarization markers making it difficult to distinguish phenotypes. This is compounded by evidence that suggests microglia are similarly active during the onset of neuropathic injury in both sexes. Previous therapeutic approaches using tetracycline antibiotics to inhibit microglia were unspecific and alleviate pain only in males. More recent endeavors utilize specific markers to identify microglia, which allows for a more direct therapeutic approach. In nerve injury models, activation of Kir2.1 resulted in proliferation and activation of microglia in both males and females. Additionally, TMEM119 has been identified as a specific marker for microglia in mice and humans. This allows for clear dissection of microglia from infiltrating peripheral monocytes and perivascular macrophages (Bennett et al., 2016). Lastly, P2RY12 has also been identified as a microglia specific marker and has been shown to be downregulated after nerve injury. Pharmacological manipulation of these proteins may help clarify the role of microglia specifically in central sensitization and maladaptive plasticity in response to nerve injury (**Figure 2.1**).

CHAPTER 3

USE OF INTEGRATED OPTICAL CLEARING AND 2-PHOTON IMAGING TO INVESTIGATE SEX DIFFERENCES IN NEUROIMMUNE INTERACTIONS AFTER PERIPHERAL NERVE INJURY

Authors – Thomas A. Szabo-Pardi, Umar M. Syed, Zachary W. Castillo, Michael D. Burton

The Department of Neuroscience, BSB10.537

The University of Texas at Dallas

800 West Campbell Road

Richardson, Texas 75080-3021

ABSTRACT

Peripheral nerve injury induces a myriad of immune-derived symptoms that negatively impacts pain, depression, and overall quality of life. Neuroimmune differences underlie sexual dimorphisms in various pain states. The innate immune system is a source of these sex differences, which promotes inflammation and pro-nociception through bidirectional signaling with the nervous system. Spatiotemporal interactions between leukocytes and sensory neurons could hold the key to explain ascribed differences between sexes. To date, studies have found it difficult to display these interactions. We are poised to answer important questions regarding the recruitment of peripheral leukocytes to key tissues of the pain system, the dorsal root ganglia (DRG) and sciatic nerve after nerve injury. We optically clear whole DRGs and sciatic nerves and concomitantly use multi-photon microscopy and transgenic reporter lines, to visualize leukocyte dynamics involved in neuropathic pain development following nerve injury. We observed robust sexual dimorphisms in leukocyte recruitment to the lumbar DRGs after nerve injury. We also assessed immune cell size and morphology to understand activation states in the context of nervous tissue inflammation. The altered mechanisms by which the male and female immune systems respond to nerve injury are still topics of further research, however; the continued use of next-generation imaging with advanced whole tissue image analysis remains an important tool in understanding the reciprocal interactions between neuronal and non-neuronal cells.

INTRODUCTION

Peripheral nerve injury often results in neuropathic pain, which is defined by trauma or lesions that disrupt the somatosensory systems. Injury-induced neuropathic pain is estimated to occur in over

48

30% of patients following routine operations (Kehlet, 2006). Patients often report higher levels of comorbidities, such as depression and sleep disorders which further contribute to increased pathological clinical outcomes and significantly reduce quality of life (McDermott et al., 2006). Although the prevalence of chronic pain continues to rise, the number and effectiveness of existing therapeutics remains limited (Finnerup, 2015). The increasing incidence of neuropathic pain has piqued interest in understanding the key immunologic processes involved. Previous studies have found a clinically observed difference in the prevalence and perception of pain in males vs. females (Fillingim, 2009; Mogil, 2012). However, there is still a dearth of knowledge on the sexual dimorphisms observed in leukocyte trafficking, morphology, and neuroimmune interaction.

Macrophages, key myeloid-derived leukocytes have been shown to play a key role in facilitating maladaptive nociception following nerve injury (Zhuo, 2011). Moreover, the peripheral immune system, specifically macrophages, play a pivotal role in sensitization of sensory neurons (Lindborg, 2018). Macrophages in the dorsal root ganglia (DRG) and sciatic nerve (ScN) play a critical role in both the initiation and maintenance of neuropathic pain by enhancing sensory neuron transduction and excitability (Basbaum, 2009). We hypothesize that using intact tissue for 3D rendering and morphologic analysis; we will be able to differentiate spatial resolution of macrophage infiltration and their interactions with sensory neurons in a sex-specific fashion. Recent studies have shown that these macrophages demonstrate robust molecular crosstalk with sensory neurons (Yu, 2020). This remains an integral process of not only pain induction as a protective mechanism, but also a transition to maladaptive chronic pain in some instances (Renthal et al., 2020). Discovering the sex-dependent roles of macrophages in tissue injury is paramount as

the incidence macrophage-dependent chronic pain in females is lower than in males (Agalave, 2020; Rudjito, 2020; Wiesenfeld-Hallin, 2005). As such, identifying sex differences in macrophage biology will serve as a foundation for future studies aimed at exploiting immunological regulation in pain and will serve to create a more tailored approach to therapeutics.

Our group has recently developed a technique for intravital imaging using transgenic reporter mice and multiphoton microscopy (Szabo-Pardi, 2019). We wanted to adapt these methods to conceptualize the immune response to injury. Changes in cellular morphology has been associated with changes in functionality of cells (McWhorter, 2013). We used transgenic reporter animals, fluorescently labeled (ROSA26^{tdTomatoLSL}) $\times$ LysozymeM:cre (LysM$^+$)-expressing leukocytes (LysM^{tdT+}). LysM is an antimicrobial enzyme (encoded by the *Lyz2* gene) that breaks down gram-positive bacterial cell walls and is predominately expressed by circulating neutrophils and tissue macrophages (Goren, 2009). Tissue macrophages have been shown to be upregulated within days after peripheral injury and are known to play a role in injury-induced sensitization of sensory neurons (Clausen, 1999; Kiguchi et al., 2018; Rittner, 2005). Prior studies have used techniques, such as flow cytometric analysis to quantify recruitment or infiltration of macrophages into peripheral nervous tissue, however, there are inherent limitations using this method (Ghasemlou, 2015; Lopes, 2017). Notably, a lack of clarity regarding pathogenesis and spatiotemporal visualization of macrophages in the extracellular space. Moreover, studies that investigate recruitment of any immune cell to peripheral nervous tissues rarely use both sexes, making it difficult to draw apt comparisons (Kwon, 2013; Schmid, 2013).

To provide a more robust understanding of interactions in nervous tissue after injury, we cleared tissue (Sca*l*eS1) to enable visualization of tdTomato-tagged macrophages via multiphoton microscopy. Not only does this technique preserve the integrity of extracted tissues, but it also provides an accurate representation of cell dynamics in a diseased state (Gmez-Gaviro, 2020). The ability to use whole, unsectioned tissue provides a clear advantage over conventional methods, which is made possible by visualizing the spatial relation of neuronal and non-neuronal immune cells in a three-dimensional (3-D) model. In this study, we find that male mice exhibit more robust infiltration of LysM[tdT+] macrophages after injury as compared to females. Additionally, we took advantage of advanced image analysis in concert with our experimental approach to group and classify the morphology of these macrophages. Recent literature has shown that macrophages exemplify distinct morphological changes differentiating into M1 and M2 phenotypes, pro-inflammatory or anti-inflammatory functions, respectively (McWhorter, 2013). In response to physiological changes and cytokine signaling, M2 macrophages are associated with an elongated, prolate morphology while M1 macrophages are associated with an oblate, flattened morphology (Bertani, 2017). This serves as an indispensable tool in our approach to elucidate sex differences after nerve injury and can be adapted to address the gap in understanding the intimate interactions between leukocytes and neurons in other aspects in neuroimmunology research.

MATERIALS AND METHODS

Laboratory Animals

All animal experiments were carried out in accordance with protocols approved by the Institutional Animal Care and Use Committee of the University of Texas at Dallas. Mice were housed (4–5 per

cage) in a temperature-controlled facility (20–25°C) and maintained on a 12-h light/dark cycle (lights on: 6 a.m./lights off: 6 p.m.). Mice had *ad-libitum* access to food and water and were 8–12-weeks-old during the experiments (male, 25–30 g; female, 20–25 g). Transgenic mice expressing NLS-Cre recombinase under control of the endogenous *Lyz2* promoter/enhancer elements (LysM) were obtained commercially from Jackson (Stock no: 004781). Characterization of these mice showed that heterozygous cre animals have no pain phenotype and normal electrophysiological properties (Clausen, 1999). Furthermore, transgenic mice expressing a loxP-flanked *STOP* cassette preventing expressing of tdTomato (red fluorescent protein) were purchased from Jackson (Stock no: 007909) and bred with LysM^{cre+} animals in-house (LysM^{cre+} × ROSA26^{LSLtdTomato} = LysM^{tdT}) and used for all behavioral and biochemical assays. All animals used were heterozygous for LysM^{cre} and had at least one copy of tdTomato. All strains were backcrossed to maintain C57BL/6J genetic background with animals from Jackson Lab (stock no. 000664).

Surgical Procedures

The spared nerve injury (SNI) model of neuropathic pain was used. Baseline values for behavioral experiments were established 24-h prior to surgery. Mice were anesthetized under isoflurane anesthesia (1.0–2.5%). The ipsilateral thigh was shaved and cleaned with betadine (Dynarex, NY, USA; cat no. 1425) and 70% ethanol (Decon Labs, PA, USA; cat no. 2701). The skin and muscle of the ipsilateral thigh were incised with a #11 scalpel (Thermo Fisher, MA, USA; cat no. 22-079-691) and the sciatic nerve along its three branches (common peroneal, tibial, and sural) were exposed. A tight ligature using a 5-0 silk suture (VWR, PA, USA; cat no. MV-682) was placed

around the proximal tibial and common peroneal branches, after which the nerves distal to the ligature were transected, taking care to not stretch or damage the sural nerve. The skin was closed using an auto clip (Fine Science Tools, CA, USA; cat no. 12022-09) and mice were returned to their home cages to recover (Decosterd, 2000). Sham surgeries were done identically to the SNI surgery; however, no portion of the sciatic nerve was ligated or transected. Following surgery, mice are subcutaneously administered a single dose of Gentamicin (5 mg/mL) (Sigma-Aldrich, CA, USA; cat no. G1272) as a prophylactic antibiotic. All mice were then returned to their home cages for recovery and monitored daily.

Behavioral Testing

To measure mechanical hypersensitivity, mice were individually placed on an elevated wire grid inside acrylic behavior racks and allowed to habituate for ~2-h. Behavior racks were cleaned with a 1:3 ratio of a natural all-purpose and deodorant-free cleaner (Seventh Generation™, VT, USA; cat no. 22719BK-5) and DI water and wiped dry to eliminate odor cues between each reading, baseline, and experiment. The ipsilateral hind paw was then stimulated with von Frey filaments (Stoelting Co., IL, USA; cat no. 58011) using the up-down experimental paradigm (Chaplan, 1994). To assess cold allodynia (cold response) in our SNI model, mice were individually placed on the same elevated wire grid and behavior racks and allowed to habituate for ~2-h before testing. Approximately 100 μL of biological grade acetone (Fisher Scientific, MA, USA; cat no. AI6P-4) was then applied to the lateral aspect of the ipsilateral hind paw using a 1 mL syringe (VWR, PA, USA; cat no. 309659) attached to a blunted 25 G needle (VWR, PA, USA; cat no. 305125). Cold response was assessed by paw licking, shaking, grooming behaviors and were measured over a 60-

s period (Yoon, 1994). Baseline values were taken 24-h prior to performing surgery. Mechanical hypersensitivity and cold allodynia were then measured on post-operative days 1, 3, and 5. Mechanical measures were always taken before cold response. All behavioral testing was done between 10 a.m. and 2:00 p.m. Experimenters were blinded to genotype, surgery, or both.

Optical Clearing

Five days post-SNI, mice were deeply anesthetized using a mixture of ketamine (80 mg/kg) and xylazine (12 mg/kg), injected intraperitoneally, and were transcardially perfused with 10 mL of ice cold $1 \times$ PBS (Thermofisher, MA, USA; cat no. BP3994) and then 10 mL of ice cold 4% paraformaldehyde (Sigma-Aldrich, CA, USA; cat no. F8775) using a 25G winged infusion set (Thermofisher, MA, USA; cat no. 14-840-37). Lumbar dorsal root ganglia (DRGs) (L4-5) and sciatic nerves (ScNs) were collected in 2 mL microcentrifuge tubes (Eppendorf, CT, USA; cat no. 022-43-104-8) and post-fixed in 1.5 mL of 4% paraformaldehyde (Sigma-Aldrich, CA, USA; cat no. F8775) (made in $1 \times$ PBS) for 4-h. Fixed tissues were then transferred to a 2 mL microcentrifuge tube containing 1.5 mL of 20% sucrose solution (VWR, PA, USA; cat no. 0335-1KG) (made in $1 \times$ PBS) for 48 h. Following cryoprotection, tissues were then transferred to a 5 mL microcentrifuge tube (Eppendorf, CT, USA; cat no. 0030-119-401), immersed in 1.5–4 mL of Sca*l*eS1 solution and placed on a tissue nutator for ~10–14 days to achieve optimal tissue clarity (Hama, 2015). This was to enhance perfusion of the extracted tissues. Sca*l*eS1 solution was aspirated and replaced every 48-h with fresh solution. The following reagents were used to prepare Sca*l*eS1 solution: 4 M urea crystals (Thermofischer, MA, USA; cat no. 29700), 0.1% (wt/vol) Triton X-100 (Sigma-Aldrich, CA, USA; cat no. X100), and 10% (wt/wt) glycerol (Fischer

Scientific, MA, USA; cat no. BP229-1). In brief, urea crystals were dissolved in water using a stir

bar Thermofisher, MA, USA; cat no. F37180). Next, the triton x-100 was added along with

glycerol and was left to mix for an hour. The solution was made and allowed a minimum of 48-h

to equilibrate before use and stored at room temperature.

Multiphoton Microscopy

Optically cleared DRGs and ScNs were embedded in single 13 mm glass-bottomed cell culture

plates (Thermofisher, MA, USA; cat no. 150680) using 0.5% (w/v) agarose (VWR, PA, USA; cat

no. MPN605) (dissolved in ultra-pure ddH$_2$O) as an immobilization medium. Upon polymerization

of the agarose, ~1 mL of Sca*l*eS1 solution was pipetted into the culture plates to ensure coverage

and adequate hydration of immobilized samples. Samples were individually imaged using an

Olympus MPE-RS TWIN multiphoton microscope outfitted with dual excitation lasers (Spectra

Physics INSIGHT DS+ -OL pulsed IR LASER, tunable from 680 to 1,300 nm, 120 fs pulse width

at specimen plane and SPECTRA PHYSICS MAI TAI HP DEEP SEE-OL pulsed IR LASER,

tunable from 690 to 1,040 nm, 100 fs pulse width at specimen plane). We have established optimal

parameters for multiphoton microscopy in a previous study (Szabo-Pardi et al., 2019). In brief,

using these excitation lasers in combination with a XLPLN25XWMP2 Olympus ultra $25 \times$ MPE

water-immersion objective (1.05 NA, 2 mm WD) we were able to image tdTomato-positive

LysM$^+$ cells (LysM^{tdT+}) (1,100 nm). Tissues were scanned using a galvanometer scanning unit at

10 us/pixel; 1:1 aspect ratio; 0.5 step size; 512×512 area and images were acquired with 2-channel

multi-alkali photomultiplier tubes (PMTs). Z-stack images were acquired of the entire sample (Y-

plane) of the DRG and distal/proximal portions of the ScN. A step size of 1 um per slice was used

and images were between 300 and 400 slices. FVMPE-RS system software (FluoView) was used to acquire images. Raw Z-stack images were then exported to Imaris imaging software for appropriate processing and analysis. Images were acquired by a blinded experimenter.

Image Analysis

Analysis of ScN and DRG tissues LysM^{tdT+} labeled macrophages was done with Imaris Software (Oxford Instruments, version 9.0.1). Previously acquired z-stacks are put into Imaris where each pixel from the 2D section was converted into a 3D voxel. This information was then used to reconstruct the original 3D object that spanned across the z-stacks. Images were imported into Imaris's Arena and viewed within the 3-D view of the Surpass. The Surfaces visualization is a computer-generated representation of the specified gray value range in the data set. In order to visualize the range of interest of an object's volume, an artificial solid object is created from which measurements can be derived. Surfaces were created using background subtraction for td-Tomato positive cells in the Z-stack images. A filter based on number of voxels was used to remove both artifacts and large neuronal cells within the image. Using the most representative image for DRGs and ScNs, creation parameters were made using the corresponding creation wizard in Imaris's Surfaces feature. Surfaces of the LysM^{tdT+} macrophages were then measured for cell count, ellipticity, volume, and sphericity. In order to normalize cell count via volume of tissue, surfaces were created for the whole DRG and sections of ScN using absolute intensity thresholding. Both proximal and distal sections of ScN were analyzed and data points were labeled accordingly to determine spatial differences in macrophage infiltration and activation along the ScN. All analyses were performed by an experimenter blinded to sex, genotype, treatment, and tissue type.

56

1. Sphericity—Given as a value from 0.01 to 1.00 with 1.00 being a perfect sphere in which the x, y, and z axes are all equal length. The sphericity of a particle is the ratio of the surface area of an equal-volume sphere to the actual surface area of the particle. The closer to 0 this value is the less spherical and more ellipsoid the shape is.

2. Prolate ellipticity—Given as a value from 0.01 to 1.00 with 1.00 representing an ellipsoid with one axis significantly longer than the others. A prolate ellipticity value moving toward 0 represents the lengths of the x, y, and z axes becoming more even. Values closer to 0 represent a more spherical shape while values closer to 1 represent a more elongated shape. A more elongated shape is typically associated with an M2 phenotype.

3. Oblate ellipticity—Given as a value from 0.01 to 1.00 with 1.00 representing an ellipsoid with two axes equal in length but longer than the third. An oblate ellipticity value moving toward 0 represents the lengths of the x, y, and z axes becoming more even. Values closer to 0 represent a more spherical shape while values closer to 1 represent a more flattened shape. A more flattened shape is typically associated with an M1 phenotype.

Statistical Analysis

Prism 8.01 software (GraphPad, San Diego, CA, USA) was utilized to generate all graphs and statistical analysis. Single comparisons were performed using Student's *t*-test, and multiple comparisons were performed using a one-way or two-way ANOVA with Bonferroni *post-hoc* tests for across-group comparisons. All data are represented as the standard error of the mean (SEM).

A *p*-value of <0.05 was used to determine statistical significance. Blinded experimenters performed all experiments and analysis.

RESULTS

Use of Interdisciplinary Techniques to Investigate the Macrophage Response During Peripheral Nerve Injury

Macrophages are implicated in the development of pain following nerve injury and have complex immunologic, neurologic, and physical facets (Raoof, 2018). To improve our understanding of the dynamic immune response after peripheral nerve injury, we designed an interdisciplinary approach combining advanced multiphoton microscopy, Sca*l*eS1 tissue clearing and a well-established nerve injury model (SNI) Using these techniques, we were able to address some of the limitations of previous studies investigating the macrophage response to nerve injury. Primarily, these limitations include: a lack of appropriate male and female representation in data sets, an inability to assess morphological changes in macrophages while preserving the integrity of the microenvironment, and skewed information resulting from single-slice imaging analysis as opposed to whole tissue. While these studies greatly improve our understanding on the dynamic nature of macrophage recruitment and activation, they highlight a need to develop integrative techniques to improve our approach.

Male and Female Mice Exhibit Robust Pain Behaviors Following SNI

To adequately assess the macrophage response to nerve injury, spared nerve injury (SNI) was performed to induce a pain state in both sexes. We chose this specific model of neuropathic pain because it has been shown to cause prolonged changes in behavioral phenotypes as well as immune

cell activation (Raoof, 2018). Moreover, the etiology of neuropathic pain that develops after SNI closely mimics the cardinal symptoms of clinically described neuropathic pain (Chen, 2015). In order to confirm that our procedure induced a pain state, we assessed mechanical hypersensitivity and cold allodynia in mice that received either SNI or sham. As expected, we found that males that received SNI exhibited significantly reduced paw withdrawal thresholds on days 1, 3 and 5 as compared to their sham counterparts. We report similar results in females where mice that received SNI had significantly reduced paw withdrawal thresholds on day 1, 3, and 5 as compared to sham controls (Figures 3.1A,C). Moreover, male mice that received SNI exhibited an elevated behavioral response to application of acetone to the ipsilateral hind paw on days 3 and 5 as compared to their sham counterparts. Similarly, female mice that received SNI exhibited an elevated behavioral response to application of acetone to the ipsilateral hind paw on days 1, 3, and 5 as compared to sham controls (Figures 3.1B,C). Lastly, we find no significant sex differences in the onset of mechanical hypersensitivity or cold allodynia after SNI. Taken together, these data indicate SNI induced robust pain behaviors before, and up to the day mice were euthanized and tissues were collected for analysis.
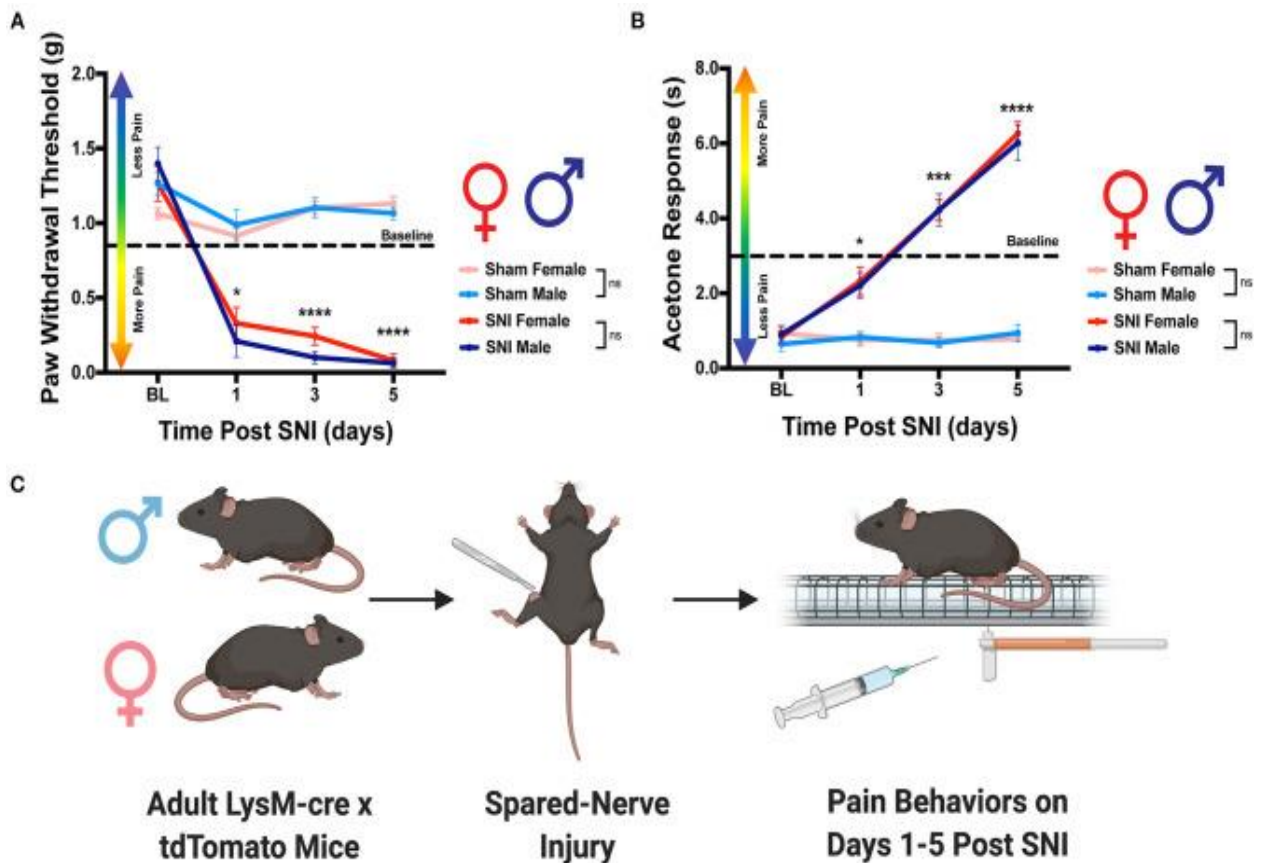
Figure 3.1. Development of neuropathic pain behaviors following SNI. Male and female LysM^{tdT+} mice were tested for mechanical hypersensitivity and cold allodynia on days 1, 3, and 5 post-SNI. (A) Male ($n = 7$) and Female ($n = 7$) LysM^{tdT+} mice exhibit significantly reduced mechanical withdrawal thresholds post-SNI as compared to their respective sham controls ($n = 7$). **(B)** Male ($n = 7$) and Female ($n = 7$) LysM^{tdT+} mice exhibit significantly elevated response latency to acetone application as compared to their respective sham controls ($n = 7$). **(C)** Graphical representation of the experimental timeline where male ($n = 7$) and Female ($n = 7$) LysM^{tdT+} mice were given SNI and were assessed for mechanical hypersensitivity and cold allodynia on days 1, 3, and 5 post-SNI. $^{*}p < 0.05$; $^{***}p < 0.001$; $^{****}p < 0.0001$. BL, Baseline. Made using BioRender.com.

SNI Induces Macrophage Recruitment, Activation, and Morphological Changes in the DRG

To explore our initial hypothesis regarding sex differences in macrophage infiltration, lumbar

DRGs (L4-5) were harvested from male and female LysM^{tdT+} reporter mice 5 days post-SNI. We

integrated Sca*l*eS1 whole tissue clearing with multiphoton imaging in both male and female DRGs

to visualize macrophage recruitment, activation, and changes in morphology (Figure 3.2A). Imaris image analyses revealed significant differences in macrophage recruitment to the DRG following SNI. We found that injured (SNI) male ipsilateral DRGs displayed significantly increased amounts of LysM^{tdT+} macrophages compared to the contralateral (uninjured) DRGs. Moreover, SNI induced significantly elevated LysM^{tdT+} macrophage recruitment to the ipsilateral DRG as compared to the sham surgery. Surprisingly, we do not report a significant increase in LysM^{tdT+} macrophage recruitment to the ipsilateral DRG in female mice after SNI. This remains true in the sham groups as well (Figure 3.2C). To account for differences in resident and infiltrating macrophages, we assessed the ratio of LysM^{tdT+} macrophages in the ipsilateral (injured) DRG with the contralateral (uninjured) DRG. Again, we found that males display significantly upregulated LysM^{tdT+} macrophages to the ipsilateral DRG. This is indicative of an upregulation of infiltrating macrophages (Figure 3.2D). To better understand the activation states of these infiltration macrophages, we analyzed the distribution and relative frequencies of LysM^{tdT+} macrophage volumes after SNI. We report no significant findings; however, male mice exhibit a trend of larger cell volumes in the injured ipsilateral DRG (Figures 3.2B,E,F). While these findings are not statistically significant, considered with the robust recruitment of LysM^{tdT+} macrophages, we can conclude that there is a biologically relevant upregulation and activation of macrophages in the DRG following SNI in male mice.
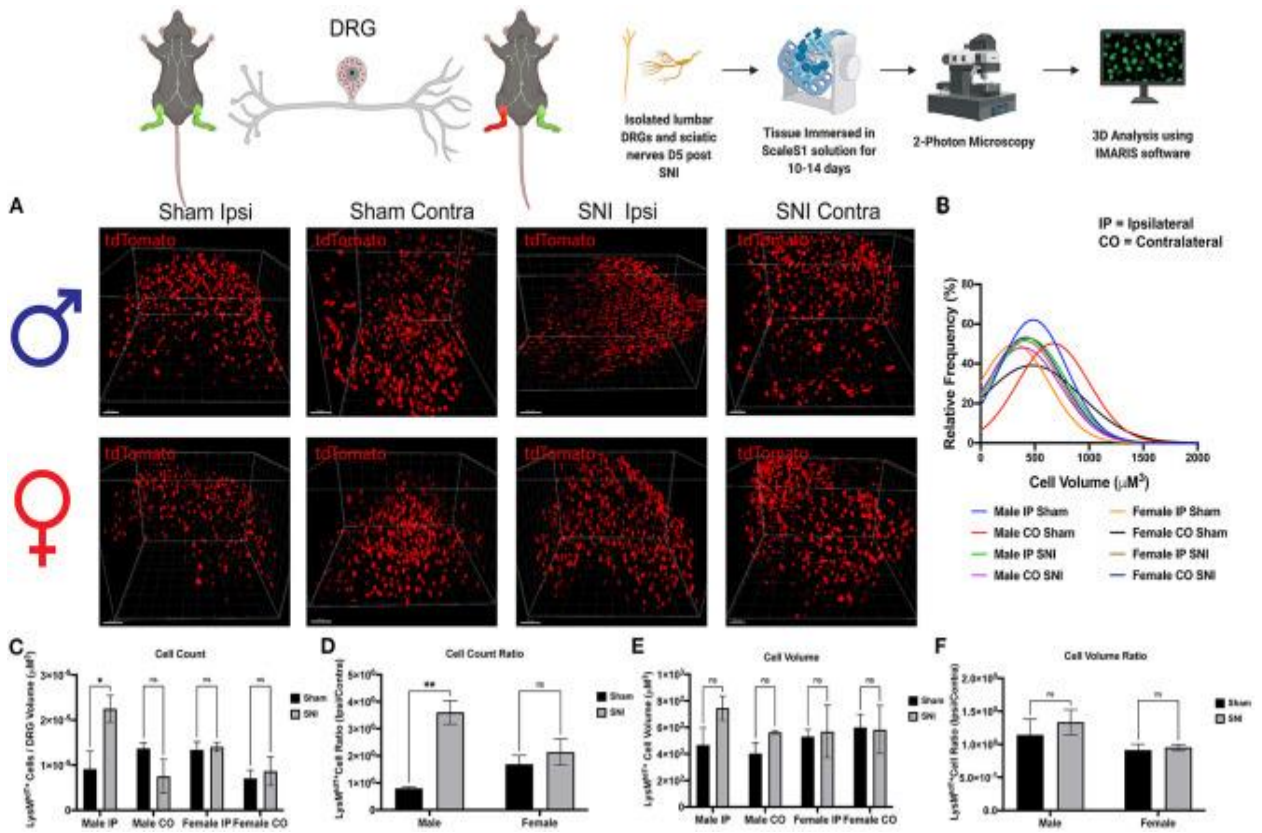
Figure 3.2. Infiltration of LysM^{tdT+} macrophages in the lumbar DRGs 5 days post-SNI. Male and female LysM^{tdT+} mice had DRGs harvested 5 days post-SNI. Tissues were processed and cleared using ScaleS1 solution for 10–14 days and imaged using 2-photon microscopy. **(A)** Representative images from male and female LysM^{tdT+} (red; 1,100 nm) DRGs ($n = 3$). **(B)** Frequency distribution histogram comparing the frequencies of LysM^{tdT+} cell volumes in control and injured male and female lumbar DRGs. **(C)** Quantification of LysM^{tdT+} macrophage infiltration in the lumbar DRGs 5 days post-SNI ($n = 3$) in males and females. **(D)** Quantification of LysM^{tdT+} macrophage infiltration in the lumbar DRGs 5 days post-SNI as a ratio of ipsilateral over contralateral DRG ($n = 3$) in males and females. **(E)** Quantification of LysM^{tdT+} macrophage volume in the lumbar DRGs 5 days post-SNI ($n = 3$) in males and females. **(F)** Quantification of LysM^{tdT+} macrophage cell volumes in the lumbar DRGs 5 days post-SNI as a ratio of ipsilateral over contralateral DRG ($n = 3$) in males and females. $^{*}p < 0.05$; $^{**}p < 0.01$. Scale Bar: 100 μm. IP, Ipsilateral; CO, Contralateral. Made using BioRender.com.

Next, we wanted to identify changes in macrophage morphology after SNI as these changes can be correlated with shifts in pro-(M1) and anti-(M2) inflammatory polarization. Macrophages have been shown to play a key role in regulating homeostasis and tissue repair after nerve injury, and polarization plays an integral role in this process (Chernykh, 2016). We may map changes in geometric profiles of macrophages using measures of oblate (flattened) ellipticity, prolate (elongated) ellipticity, and sphericity (Iwata, 2017). In response to physiologic input and cytokine signaling, M2 polarized macrophages are associated with an elongated, prolate morphology while M1 macrophages are associated with an oblate, flattened morphology (Bertani, 2017). Drawing upon these recent discoveries and classifications, we assessed the geometrics of these recruited LysM^{tdT+} macrophages in the DRG using Imaris analysis (Figure 3.3A). We found differences in the clustering of LysM^{tdT+} macrophages in mice that received SNI, which take on a more oblate (flattened) morphology after nerve injury. This is indicative of an M1 polarized phenotype. Moreover, we found that LysM^{tdT+} macrophages in animals that received a sham surgery take on a more prolate (elongated) morphology. This is indicative of an M2 polarized phenotype (Figure 3.3C). Lastly, we assessed sphericity of LysM^{tdT+} macrophages after nerve injury (Figure 3.3B). Although we find no significant differences, cells that take on a more prolate (flattened) shape after injury are also more spherical, indicating a more active phenotype (Sen, 2016). Taken together, we conclude that macrophages have a dynamic morphological response to injury and may be characterized based on their geometric shape.
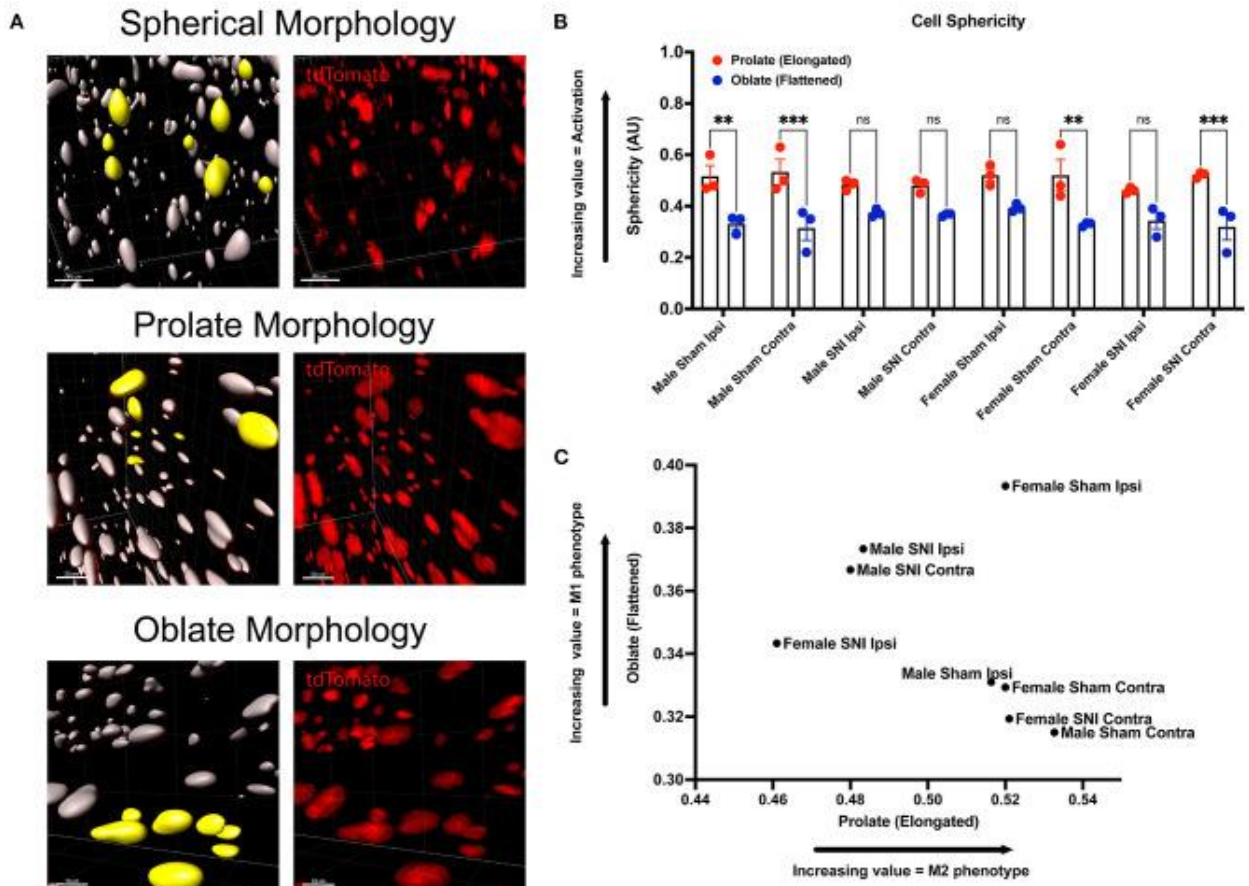
Figure 3.3. Morphology of LysM^{tdT+} macrophages in the lumbar DRGs 5 days post-SNI. Male and female LysM^{tdT+} mice had DRGs harvested 5 days post-SNI. Tissues were processed and cleared using ScaleS1 solution for 10–14 days and imaged using 2-photon microscopy. **(A)** Representative morphology from male and female LysM^{tdT+} (red; 1,100 nm) DRGs ($n = 3$). **(B)** Imaris analysis of LysM^{tdT+} cell morphology in male and female DRGs. Cells were analyzed for three morphologic parameters (sphericity, prolate, and oblate) and are displayed comparing oblateness and prolateness with respect to sphericity. **(C)** Scatter plot of DRG LysM^{+} cell oblateness with respect to prolateness in both male and female injury and control groups. $^{**}p < 0.01$; $^{***}p < 0.001$. Scale Bar: 100 μm. IP, Ipsilateral; CO, Contralateral.

SNI Induces Dynamic Changes in Macrophage Morphology in the ScN

To further identify the dynamic role of macrophages in response to nerve injury, we looked closer to the site of injury in the ScN. Here, we sought to distinguish the LysM^{tdT+} macrophage response between the DRG and ScN. Using the same principles, whole ScNs were harvested from male and female LysM^{tdT+} mice 5 days after SNI and were cleared using ScaleS1. Tissues were cleared and

imaged using multiphoton imaging and tissues were analyzed using Imaris (Figure 3.4A). Analyses revealed no significant differences in LysM^{tdT+} macrophage recruitment to the distal or proximal ScN. Although, both male female mice exhibit elevated LysM^{tdT+} macrophages in the ipsilateral ScN as compared to the contralateral control. While not significant, this does indicate a surgery-induced upregulation in macrophage recruitment to the ScN in males and females (Figures 3.4C, D). We report no differences in the volumes of these recruited LysM^{tdT+} macrophages (Figure 3.4D). Moreover, we do not report any differences in the distribution or relative frequencies of LysM^{tdT+} macrophage volumes after SNI in the ScN. However, female mice exhibit a larger distribution of LysM^{tdT+} cell volumes after SNI in the ipsilateral ScN as compared to other groups, indicating increased classical activation of macrophages (Figure 3.4B). Lastly, we report no differences in the cell volumes of LysM^{tdT+} macrophages in the ScN after SNI in both males and females (Figures 3.4E,F). Taken together, we can conclude there are dynamic biological changes that occur in the ScN following SNI in males and females.

Figure 3.4. Infiltration of LysM^tdT+ immune cells in the ScNs 5 days post-SNI. Male and female LysM-cre × tdTomato mice had ScNs harvested 5 days post-SNI. Tissues were processed and cleared using ScaleS1 solution for 10–14 days and imaged using 2-photon microscopy. (**A**) Representative images from male and female LysM^tdT+ (red; 1,100 nm) ScNs ($n = 3$). (**B**) Frequency distribution histogram comparing the frequencies of LysM^tdT+ cell volumes in control and injured male and female lumbar ScNs. (**C**) Quantification of LysM+ immune cell infiltration in the lumbar ScNs 5 days post-SNI ($n = 3$) in males and females. (**D**) Quantification of LysM^tdT+ macrophage infiltration in the lumbar ScNs 5 days post-SNI as a ratio of ipsilateral over contralateral ScN ($n = 3$) in males and females. (**E**) Quantification of LysM^tdT+ macrophage volume in the lumbar ScNs 5 days post-SNI ($n = 3$) in males and females. (**F**) Quantification of LysM^tdT+ macrophage cell volumes in the ScN 5 days post-SNI as a ratio of ipsilateral over contralateral ScN ($n = 3$) in males and females. Scale Bar: 100 μm. IP, Ipsilateral; CO, Contralateral. Made using BioRender.com.

We incorporated our geometric analyses to better understand the morphological changes that may occur in macrophages in the ScN (Figure 3.5A). While we report no differences in recruitment, there may be morphological changes that are biologically relevant (Cobos, 2018). We investigated

the sphericity of LysM^{tdT+} macrophages in the ScN and found that there were no differences between sexes or injury. Typically, a more spherical, or round, macrophage is classically activated, however, this does not mean that these macrophages have not altered their contractile state in response to injury. We report that there is a sexual dimorphism in the morphology of LysM^{tdT+} macrophages in the sciatic nerve 5 days after SNI. Male LysM^{tdT+} macrophages on the injured side exhibit more oblate, or flattened, cell morphology as opposed to females that exhibit a more prolate, or elongated, cell morphology (Figure 3.5C). This is indicative of an M1 polarization state in males as opposed to an M2 state in females. This idea has been a dogma in the field of neuroimmunology for decades (Li, 2009). Lastly, we find no differences in the sphericity of LysM^{tdT+} macrophages in the ScN (Figure 3.5B). This data indicates a distinction in macrophages in the DRG vs. ScN, where DRG macrophages are more M1 polarized in both sexes after surgery, and ScN macrophages are M1 polarized in males vs. M2 polarized in females.
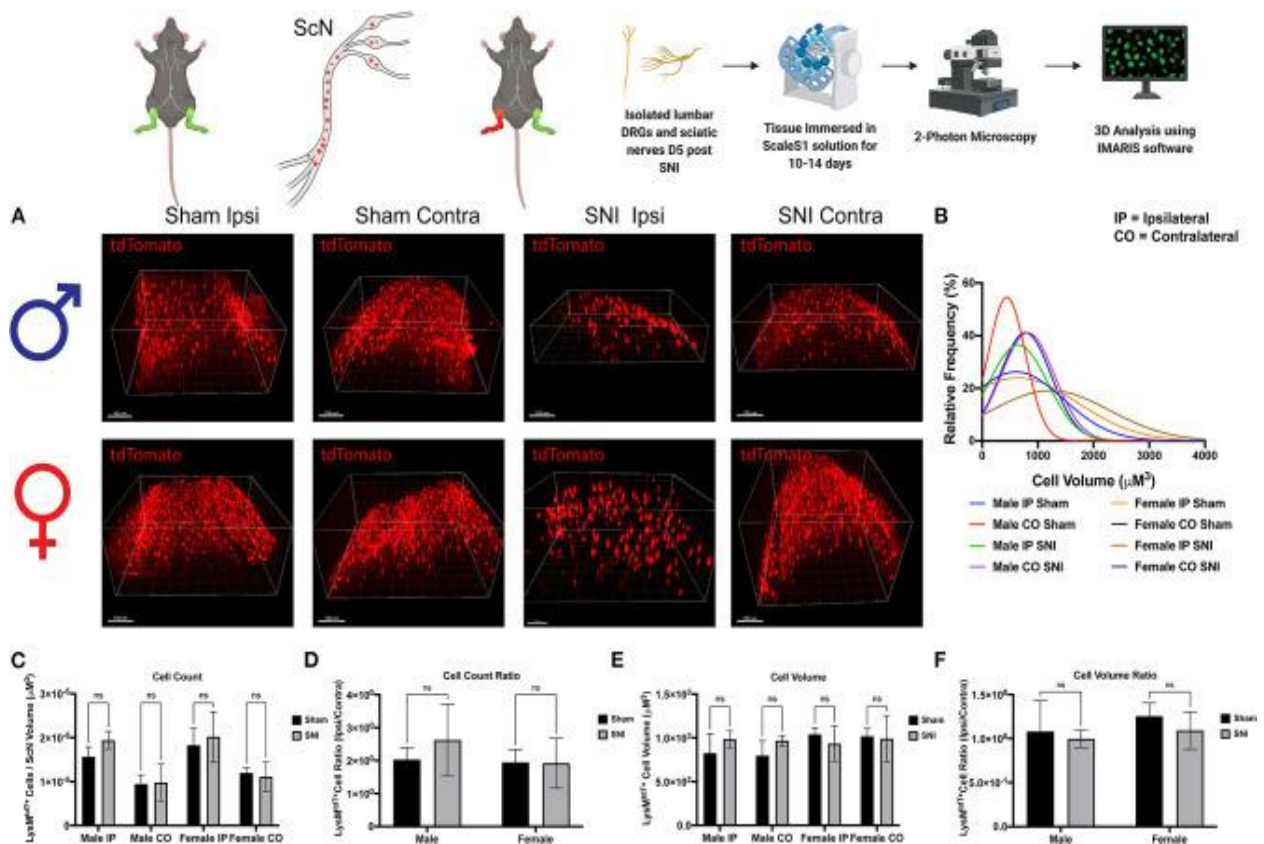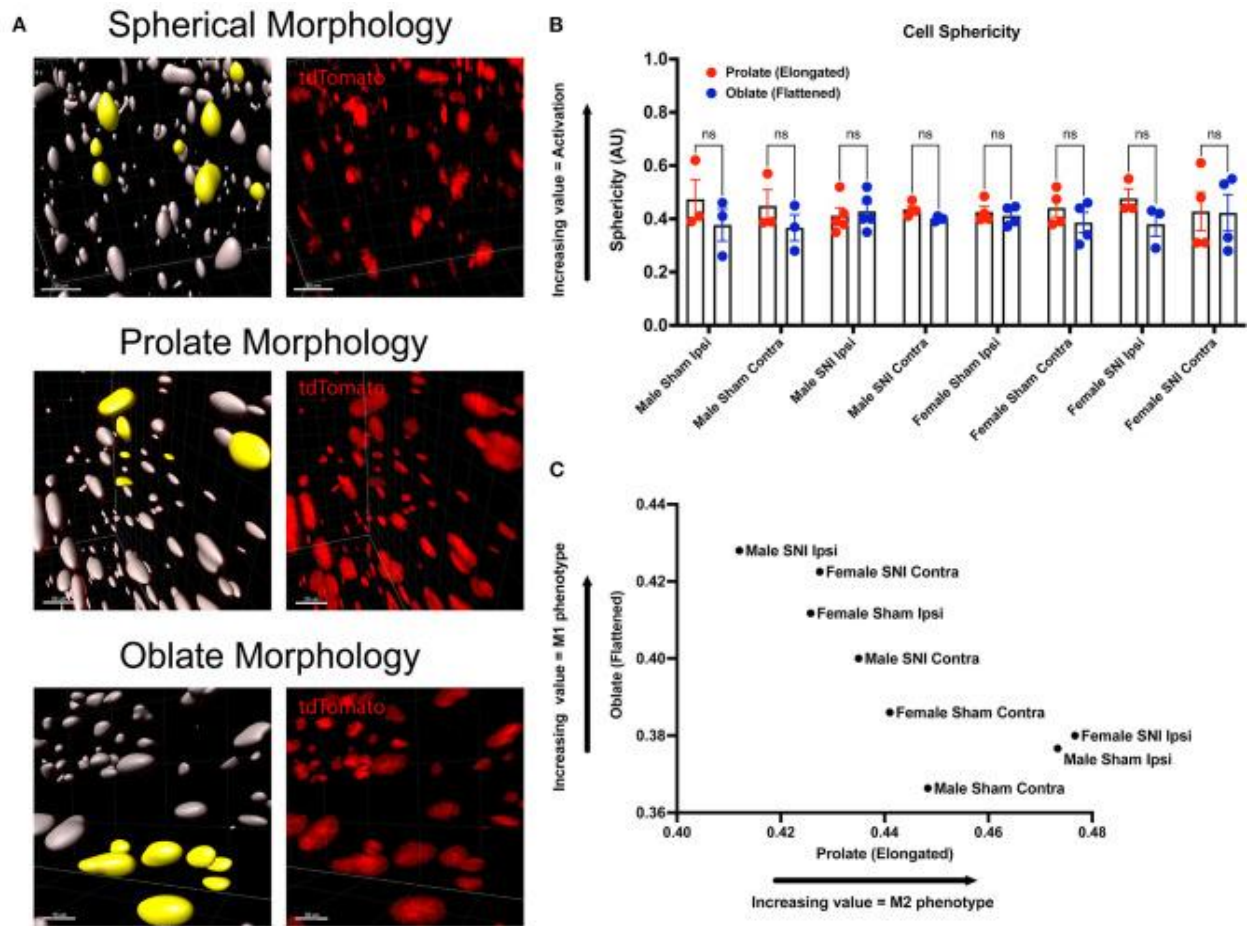
Figure 3.5. Morphology of LysM^{tdT+} macrophages in the ScN 5 days post-SNI. Male and female LysM^{tdT+} mice had ScNs harvested 5 days post-SNI. Tissues were processed and cleared using ScaleS1 solution for 10–14 days and imaged using 2-photon microscopy. **(A)** Representative morphology from male and female LysM^{tdT+} (red; 1,100 nm) ScNs ($n = 3$). **(B)** Imaris analysis of LysM^{tdT+} cell morphology in male and female ScNs. Cells were analyzed for three morphologic parameters (sphericity, prolate, and oblate) and are displayed comparing oblateness and prolateness with respect to sphericity. **(C)** Scatter plot of ScN LysM$^+$ cell oblateness with respect to prolateness in both male and female injury and control groups. Scale Bar: 100 μm. IP, Ipsilateral; CO, Contralateral.

DISCUSSION

Whole tissue *in-situ* visualization can reveal neuroimmune interactions that have been overlooked in the past. The goal of the present study was to analyze the sex-dependent dynamics of macrophage recruitment and changes in morphology after injury utilizing next generation tissue

clearing and imaging techniques. We performed SNI on male and female transgenic reporter mice constitutively expressing tdTomato, a red fluorescent protein, in macrophages under the LysM promoter. We then harvested lumbar DRGs and ScNs from these animals 5 days after the surgery and optically cleared the tissues using Sca*l*eS1. Macrophage recruitment and subsequent expansion peaks between days 3 and 7 after injury, therefore we chose day 5 to assess their physical characteristics (Chen, 2015). We then acquired high resolution Z-stack images of the cleared tissues using multiphoton microscopy and performed extensive analyses using Imaris Imaging Software to understand the dynamics of macrophage recruitment, activation, and morphology after injury. In this study, we found that males have higher LysM^{tdT+} macrophage counts in the lumbar DRGs (L4/5), expanding upon current literature that suggests females have alternative neuroimmune mechanisms that contribute to pain states. Moreover, we find dynamic changes in LysM^{tdT+} macrophage morphology, with SNI inducing a more pro-inflammatory, or M1, phenotype measured by cell shape (Figure 3.6). This highlights the need to improve our understanding of the sex-dependent distribution and role of other immune cells in pain. From a therapeutic perspective, there is a potential to harness the abilities of macrophages to induce anti-nociception and tissue repair after injury (Yu et al., 2020). The vast majority of our current understanding in macrophage functionality is reliant on soluble factors, such as cytokine production and cell surface protein expression. While this information is useful in providing the necessary framework to investigate the molecular underpinnings of macrophage activation in response to injury, bridging the gap between functionality and physical characteristics will discern the full spectrum of their involvement in tissue injury.
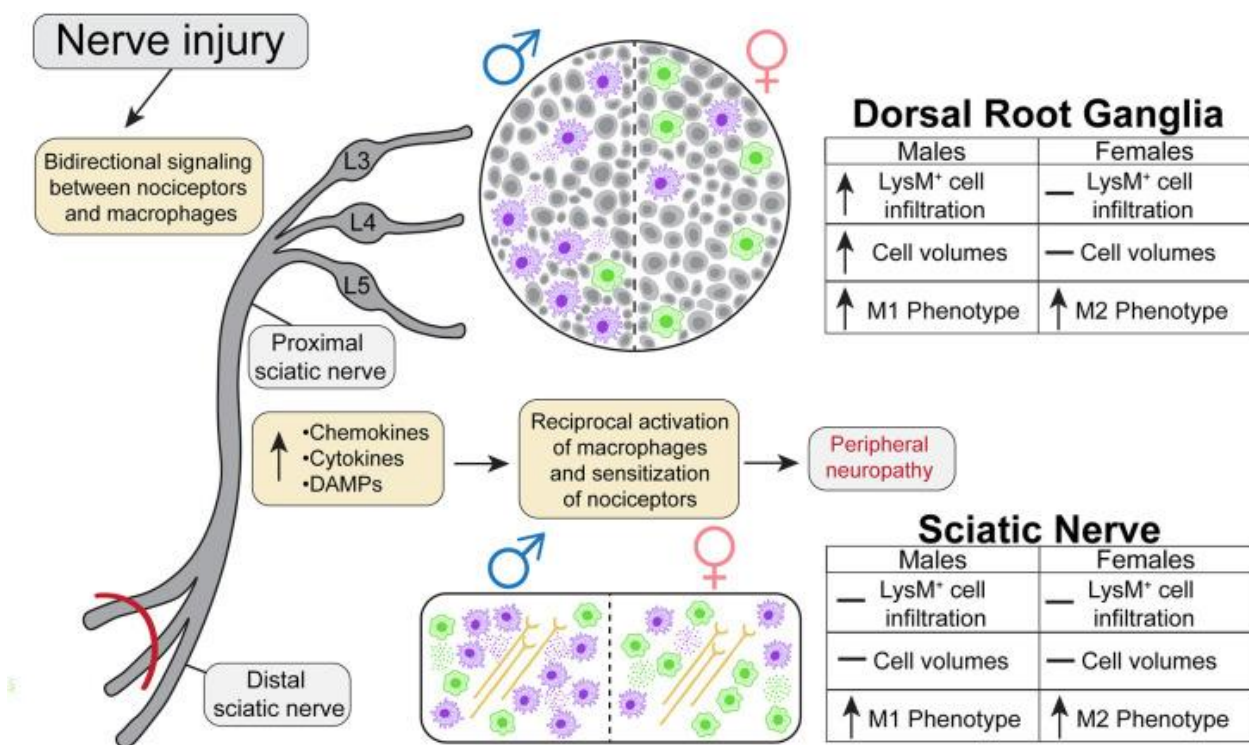
Figure 3.6. Graphical abstract representing the dynamic nature of macrophage recruitment and morphological changes following SNI in males and females.

Bi-directional communication between neuronal and non-neuronal cells in the DRG is a core mechanism in mediating the mammalian response to injury (Lopes, 2017). Current literature highlights the complex role that macrophages play in regulating inflammation and pro-nociception following injury, but the relevant sites of action remains unclear (Echeverry, 2013). Moreover, the current dogma in the field dictates males utilize a myeloid cell driven mechanism of neuronal sensitization to drive neuroinflammation (McWhorter, 2013). Although the reported behavioral contribution of these DRG macrophages is not dimorphic in nature, there exists a key cellular difference in their recruitment a morphology, lending to the idea that etiology differences can influence pain perception over time. Our data shows the magnitude of injury-induced macrophage expansion in the lumbar DRGs is significantly higher in males than in females. These findings are

also supported by a paper that characterizes sex differences in immune cell recruitment to both central and peripheral nervous tissues through flow cytometric analyses (Mosser, 2008). They demonstrate an upregulation of macrophages in both males and females after peripheral nerve injury in the lumbar DRGs, with key sex differences in the adaptive immune response. However, the adaptive immune response to injury was not the focus of our study. Collectively, these studies support the idea that macrophage recruitment to the DRG plays a critical role in neuroinflammation. Furthermore, we utilized sham and contralateral data to determine that no conclusive sex differences exist in baseline cell size and volumes further strengthening our premise that immune response to injury is sex dependent.

Conflicting reports about the role of macrophages in the ScN after nerve injury has groups reporting that macrophages do not play an important role in the pathogenesis of nerve injury-induced pain (Yu, 2020), while other reports found that inhibiting local macrophages in the ScN impairs development of neuropathic pain following nerve injury (Paul, 2013). An important distinction here is that we assessed the recruitment and morphological changes in macrophages at both distal ScN and proximal ScN. Here we assessed differences in macrophage activity with more granularity than previous studies. We find no significant recruitment of LysM^{tdT+} macrophages in the ScN 5 days after SNI, however, this does not equate to a lack of biological significance. It is a potential that the differences in macrophage morphology after SNI may alter cytokine signaling. Certain M2 macrophages phenotypes, or cells that have an elongated shape, retain the ability to produce pro-inflammatory cytokines and may be a differentiating factor in the immune response to injury in males vs. females (De Paoli et al., 2014). Despite our collective efforts, a rift exits in

our understanding of the role of macrophages in the ScN, but with every advance we are able to better understand the nuances of macrophages recruitment, activation and subsequent biological implications.

While the aforementioned studies have significantly improved our understanding of the dynamic nature of macrophage recruitment to peripheral nervous tissues, they have inherent limitations that we have addressed using our model. Geometric alteration of macrophages in response to injury has the ability regulate their functional phenotype (Tauer, 2002). However, it is impossible to discern this type of information by using typical immunohistochemical or flow cytometric analyses. Macrophages exhibit an elongated shape when polarized to an M2 phenotype, as opposed to a flattened shape when polarized to an M1 phenotype (Bronte, 2015). These polarization states are involved in a myriad of biological processes related to inflammation and tissue repair and are often indicative of a macrophages change in contractility as they interact with the extracellular matrix and cell adhesion molecules (Jensen, 2017). *In vivo* these polarization states are not dichotomous, but targeted therapeutics may be better tailored to treat each sex individually. Moreover, traditional imaging acquisition and analysis techniques are not well-suited to investigate changes in cellular shape as there are significant limitations in the resolution and depth of acquired images. This severely dampens the ability of researchers to utilize common image analysis software for this purpose. Therefore, we sought to address this lack of granularity by improving our understanding of the physical characteristics of macrophages in response to nerve injury utilizing Imaris image analysis (Belle, 2017).

72

Optical clearing techniques provide additional clarity in resolving cell to cell interactions by circumventing the limitations of traditional 2-dimensional (2-D) imaging. Typically, 2-D image reconstruction of limited z-frames provides biased information as cellular density is not uniform throughout select regions of interest. By using Sca*l*eS1 optical tissue clearing in combination with deep tissue multiphoton microscopy, we were able to create a 3-D model of whole DRGs and ScNs. This allowed us to accurately assess the infiltration of immune cells to these tissues following peripheral nerve injury. Multiphoton microscopy may be used to image thicker tissue slices, but image quality quickly deteriorates when focusing deeper into a sample (Renier, 2014). To circumvent this limitation, we chose to utilize Sca*l*eS1 as our method of optical tissue clearing. Sca*l*eS1 was our preferred method of optical tissue clearing as it has been shown to avoid tissue expansion, preserve lipids and provide a safe immersion-medium for objectives (Hama, 2015). We also took into consideration other clearing methods, such as DBE or CLARITY. These alternate clearing methods offered a shorter clearing time and work better on larger tissue sizes, however they had considerable limitations with regard to preservation of fluorescence and tissue integrity (Jensen, 2017). Another clearing method we considered was DISCO which utilizes a de-lipidating agent to enhance the refractory index of the tissue (Belle, 2017). Similar to previously discussed alternatives, this method allows for faster clearing times, however it is accompanied with significant amounts of tissue distortion making it suboptimal for our study. Current use of this method is better suited for larger tissues, such as brain or embryos (Renier, 2014). Furthermore, Sca*l*eS1 utilizes materials that are inexpensive and commonly found in research labs making it easy to use and more accessible to a wider audience. Moreover, Sca*l*eS1 is well-suited for imaging fluorescent proteins, which was the primary focus of our study.

73

In conclusion, the combined use of our genetic model, tissue clearing, and multiphoton microscopy serves as a powerful tool for investigating neuroimmune spatiotemporal relationships and provides a versatile framework to further our understanding of the role macrophages play in pain development. Moreover, we further delineate the sexual dimorphisms that exist in the physical phenotype of macrophages in response to nerve injury.

CHAPTER 4

SEX DIFFERENCES IN PACLITAXEL-INDUCED NEUROPATHIC PAIN ARE

DRIVEN BY TLR4 SIGNALING ON MACROPAGES

Authors – Thomas A. Szabo-Pardi, Ileana Cruz, Dana M. Jenkins, Ruchira Gundlapally, Han S. Jeong, Salim Megat, Jia Lin, Theodore J. Price, Michael D. Burton.

The Department of Neuroscience, BSB10.537

The University of Texas at Dallas

800 West Campbell Road

Richardson, Texas 75080-3021

ABSTRACT

Chemotherapy-induced peripheral neuropathy (CIPN) persists in over a third of patients exposed to chemotherapeutics and is linked to the generation of chronic pain long after cessation of treatment. While paclitaxel activates toll like receptor 4 (TLR4) on macrophages, the sex-specific mechanisms of macrophage activation during chemotherapy treatment and its effects on both behavioral and molecular pain phenotypes remains elusive. Uncovering how cells recognize and respond to chemotherapeutics will lead to improved understanding of the mechanisms in pain plasticity and ultimately better therapies. We hypothesized that activation of TLR4 on macrophages facilitates a sex-dependent transition in the cellular machinery required to establish neuropathic pain during chemotherapy. In this study, we used LysM^{TLR4Flox} mice which allow for cre-mediated deletion of a floxed TLR4 allele by utilizing cre-recombinase in the LysozymeM promoter in peripheral macrophages. Therefore, we are able to assess the role of TLR4 activation on macrophages during systemic paclitaxel treatment. Interestingly, we observed a reversal of mechanical hypersensitivity when TLR4 is removed from macrophages in males, but not females. Moreover, we found that paclitaxel drives a shift towards a pro-inflammatory cellular phenotype in male macrophages. We identified an increase in dorsal root ganglia (DRG) macrophages and neuronal activating transcription factor 3 (ATF3) expression after paclitaxel treatment in both sexes. These increases are dependent on macrophage TLR4 in males only. Lastly, we observed a reduction in hind paw intraepidermal nerve fiber density following paclitaxel treatment in both sexes, however; this effect is reversed only in male macrophage TLR4 knockouts. Taken together, this work demonstrates a sex-specific effect on macrophage TLR4 in paclitaxel-induced peripheral

neuropathy; highlighting the need to delve deeper to uncover the mechanisms behind sex differences observed in the promotion of chronic pain states.

INTRODUCTION

Chemotherapy-induced peripheral neuropathy (CIPN) is one of the major dose-limiting side effects of chemotherapy treatment in cancer patients (Oun et al., 2018). Patients often report pain and numbness, coined "pins and needles" by many physicians, in the affected extremities (Wolf et al., 2012). More than 70% of cancer patients present with these symptoms in the clinic during routine treatments, which often predicates poor disease prognosis (Seretny et al., 2014). Moreover, exposure to chemotherapeutics is closely linked to neural plasticity underlying chronic pain long after cessation of treatment, making CIPN a long-term morbidity in many cancer survivors (Hershman et al., 2016). Therefore, elucidating the sex-specific mechanisms that regulate the development of CIPN may present a point of personalized therapeutic intervention in which pain comorbidities may be alleviated, allowing for extended periods of chemotherapy regiments and significantly improved quality of life.

With 2015 NIH mandate necessitating the inclusion of sex as a biological factor in peer-reviewed studies, there has been a marked improvement in the quality of studies in pain research. This recent renewal has shed light on discoveries which suggest the neuroimmune mechanisms that regulate chronic pain between sexes is varied (Mogil, 2020). Conversely, inconsistencies in both clinical and pre-clinical literature investigating sex differences during CIPN development highlight the dire need for comprehensive studies aimed at effectively dissecting the complex nature of CIPN

(Gewandter et al., 2020; Naji-Esfahani et al., 2016). One of the most broadly prescribed chemotherapeutic agents used to treat solid tumors is paclitaxel, an antineoplastic agent, which primarily acts through microtubule destabilization and cell-cycle arrest (Zhu & Chen, 2019). Interestingly, an alternative mechanism of paclitaxel treatment engages inflammatory signaling through toll like receptor 4 (TLR4), similar to lipopolysaccharide (LPS) (Byrd-Leifer et al., 2001). We recently published a study that demonstrates cap-dependent protein translation, regulated by eukaryotic translation initiation factor 4E (eIF4E), possesses a pivotal role in paclitaxel-induced neuropathy development, with nuanced sex- and cell-specific differences (Agalave et al., 2021; Megat et al., 2019). Specifically, T-cell subpopulations in the lymph nodes are dysregulated after paclitaxel treatment and are modulated by expression eIF4E. These physiological changes attenuate nociceptive behavioral phenotypes in response to paclitaxel treatment in both sexes. This suggests that inflammatory signaling pathways mediated by the eIF4E complex, many of which are downstream of TLR4 activation, are closely involved in pain plasticity during chemotherapy treatment.

Not unlike T-cells, macrophages have been shown to regulate pain and inflammation in a sex-dependent manner (Yu et al., 2020). As part of the innate immune system, macrophages can adopt diverse functional phenotypes in response to stimulation. These shifts in cellular phenotypes can be attributed to their expression of M1 or M2 biomarkers, and can represent a broad spectrum of opposing biological functions (Murray, 2017). M1 macrophages exhibit pro-inflammatory properties, such as upregulated cytokine production, antigen presentation, and phagocytic activity, whereas M2 macrophages are more anti-inflammatory in nature and promote tissue regeneration

through immunosuppression (Mendoza-Coronel & Ortega, 2017). A driving force in macrophage polarization is the activation of pattern recognition receptors (PRRs), which possess a crucial role in initiating the innate immune response to infection and tissue injury (Srivastava et al., 2017). TLR4, a PRR, has been implicated in numerous studies investigating the effects of chemotherapeutics on CIPN development (Li et al., 2014; Rajput et al., 2013; Son et al., 2019). Activation of TLR4 on male macrophages by paclitaxel treatment induces pro-inflammatory polarization and prevents anti-inflammatory polarization (Wanderley et al., 2018). Dysregulated inflammation from macrophages in the dorsal root ganglia (DRG), specifically, can influence the activity of nociceptors through release of inflammatory mediators in response to paclitaxel treatment (Zhang et al., 2016). Reciprocal interaction between these two populations could contribute to maladaptive nociceptor plasticity during CIPN development. An inherent limitation in many of the previously mentioned studies is the lack of female representation. Although the incidence and mortality of cancer is higher in men than women, understanding the mechanisms that contribute to CIPN, a major dose-limiting side effect of chemotherapeutics, would allow for more personalized therapeutics and improved disease prognoses for both men and women (Kim et al., 2018).

Therefore, we sought to elucidate the sex-specific role of TLR4 activation during CIPN which may mediate crosstalk between activated immune and neuronal populations in the DRG. We utilized LysozymeMcre $\times$ TLR4$^{fl/fl}$ (LysM^{TLR4Flox}) mice as a genetic tool, which allow for cre-mediated deletion of a floxed TLR4 allele by utilizing LysM as a promoter for cre expression in macrophages and monocytes, specifically (Jia et al., 2014). Given the lack of studies adequately powered to

assess sex differences in CIPN, we investigated if there was a sex-dependent role of TLR4 activation during paclitaxel-induced neuropathic pain development, phagocytic capacity of macrophages, and intraepidermal nerve fiber (IENF) density in the paw skin. We hypothesized that paclitaxel regulates activation of macrophages through TLR4 signaling in males, which facilitates dysregulated communication between these cells and nociceptive neurons in the DRG. These bi-directional inflammatory signaling processes promote inflammatory polarization and antigen presentation in male macrophages, which leads to upregulated incidence of neuronal injury, retraction of IENFs and subsequent CIPN development.

MATERIALS AND METHODS

Animals

All experiments utilizing animals were performed accordance with ARRIVE guidelines and the National Institutes of Health guide for the care and use of Laboratory animals (NIH Publications No. 8023, revised 1978). Adult male and female mice between 8 and 14 weeks old (20-30g weight) were used for all behavioral and molecular experiments; a general timeline is detailed in Figure 4.1. In this study we utilized LysozymeMcre $\times$ TLR4$^{fl/fl}$ mice as a genetic tool to dissect the cell-specific role of TLR4 on myeloid cells. In brief, these mice allow for cre-mediated deletion of a floxed TLR4 allele in macrophages and monocytes by utilizing LysM as a promoter for expression of a cre recombinase enzyme (Figure 4.2A). These mice were originally obtained as a generous gift from by Dr. Joel Elmquist's laboratory at UT Southwestern but are also commercially available from Jackson Laboratory (Jia et al., 2014). Animals were bred in house to maintain the transgenic line and pups were weaned between 21-28 days old, ear notched, and tail-clipped to

verify genotypes *via* polymerase chain reaction (PCR) (Figure 4.2B). All animals used in this study were homozygous for the TLR4^{Flox} gene. Cell-specific knockout mice, LysM^{TLR4Flox}, were heterozygous for the LysMcre gene; littermates WT for cre were used as wild type controls. Mice were group housed with 4-5 animals per cage (separated by sex at the time of weaning) in a temperature-controlled vivarium (20-25°C) and a 12-hour light/dark cycle (6 am-6 pm) with *ad libitum* access to standard rodent chow and water. Experimenters were blinded to sex (except for behavioral experiments), genotype, and treatment during behavioral testing, cell culture, tissue freezing, cryosectioning, staining, histological procedures, and image acquisition and image analysis.

Drugs

Stock paclitaxel (Sigma-Aldrich, T1912) was reconstituted at 5mg/ml in a 1:1 ratio of kolliphor oil (Sigma-Aldrich, C5135) and 100% ethanol (Thermo Fisher Scientific, 2701) (vehicle) and stored at 4°C until further use. Prior to administration, a working solution was prepared fresh by diluting the stock solution in 1× phosphate-buffered saline (PBS) (Thermo Fisher Scientific, BP3994). Animals received a 4 mg/kg intraperitoneal injection of paclitaxel every other day for a total of 4 injections and a total dose of 16 mg/kg (Toma et al., 2017). Vehicle treatments consisted of a 1:1 ratio of kolliphor oil and 100% ethanol were diluted in 1× PBS. Following injection, animals were closely monitored for signs of pain, illness, and bleeding and euthanized if in poor health (<1%).

Behavioral Experiments

Baseline readings for all behavioral assays were recorded before animals were randomly assigned to treatment groups based on sex and genotype. In brief, mice were placed in custom built (11 cm length x 10 cm width x 4.5 cm height) clear acrylic behavior racks above a wire mesh grid. Mice were allowed to habituate for minimally 2 hours and all behavioral testing was performed between 8 am and 4 pm, during the light cycle. Mechanical hypersensitivity was measured by von Frey filaments (Stoelting, 58011) using the up-down method and cold allodynia was measured with biology grade acetone (Thermo Fisher Scientific, AI6P-4) using the acetone test (Chaplan, 1994; Yoon, 1994). Mechanical hypersensitivity is represented as the average paw withdrawal in grams, and cold allodynia is represented as the average response to application of acetone over the course of 60 seconds. Mechanical hypersensitivity was always assessed prior to cold allodynia. Upon completion of behavioral testing, mice were returned to their home cages and the behavior racks were thoroughly cleaned with a 1:3 ratio of a plant-based deodorant free solution (Seventh Generation, 22719BK).

Behavioral data sets are also represented as effect sizes. Effect sizes were determined by calculating the cumulative difference between the value for each time point and the subsequent baseline value (Agalave et al., 2021; Szabo-Pardi et al., 2021). Calculated values were summed to obtain the effect size, which is represented as an absolute number for each group (Hassler et al., 2020).

Peritoneal Macrophage Isolation, Culture and Treatment

Naïve mice were deeply anesthetized with 100% isoflurane (Covetrus, 11695) and euthanized *via* cervical dislocation. Peritoneal macrophages were extracted by injecting 8 mL of sterile 1× PBS into the peritoneal cavity using a 27-gauge needle (BD, 305136) attached to a 10 mL syringe (BD, 300912). The periotoneal cavity was gently agitated for 30 seconds to dislodge macrophages adhered to the surface of organs. Four mLs of fluid from the peritoneum was then extracted using a 25-gauge needle (BD, 305122) attached to a 10 mL syringe, dispensed into a sterile 50 mL conical tube (VWR, 89039-658), and kept on ice. Isolated peritoneal macrophages were then spun down in a centrifuge for 4 min at 0.6 relative centrifugal force (RCF) to form a cell pellet. The remaining supernatant was decanted, and the cells were resuspended in 37ºC RPMI media (Hyclone, SH30605) supplemented by 5% fetal bovine serum (FBS) (R&D Systems, S12495) and 1% penicillin-streptomycin (PS) (Thermo Fisher Scientific, 15070063). The cells were then counted using an automatic cell counter and 100,000 cells were seeded on poly-d-lysine coated coverslips (Sigma-Aldrich, P0899) in a 24 well plate (VWR, 10861-558). The cultures were then stored at 37˚C in a humidified incubator and maintained to obtain 80% cellular confluency, after which macrophages were treated with 200 nM of paclitaxel (reconstituted as previously described), or vehicle (as previously described) diluted in 37˚C RPMI supplemented with 1% FBS and 1% PS for 24 hours. Following paclitaxel treatment, 20 uL (1.0 x 10^8) of opsonized fluorescein isothiocyanate (FITC) microbeads (1 µm diameter) were dispensed into each well and the cultures were incubated at 37˚C for 1 hour. After incubation, the cultures were washed three times with ice cold 1× PBS for 5 minutes each to stop phagocytic activity.

Immunocytochemistry

The peritoneal macrophage cultures treated with FITC microbeads were fixed with 4% paraformaldehyde (PFA) (Sigma-Aldrich, 158127) for 30 minutes and washed thrice with $1\times$ PBS for 5 minutes each. After washing, the fixed cultures were blocked for non-specific antibody binding and permeabilized at room temperature (RT) for 2 hours in a solution containing: $1\times$ PBS, 2% heat-inactivated normal goat serum (NGS) (Gibco, 16210-072), 1% BSA, 0.1% triton X-100 (Sigma-Aldrich, X100), 0.05% tween-20 (Sigma-Aldrich, P1379), and 0.05% sodium azide (Sigma-Aldrich, RTC0000068). The blocked and permeabilized cultures were then incubated with a primary antibody cocktail diluted in the previously described buffer at 4°C for 24 hours (see Table 4.1). Incubated cultures were washed three times with $1\times$ PBS at RT for 5 minutes each. After washing, cultures were incubated with a secondary antibody cocktail diluted in the previously described buffer at RT for 2 hours (see Table 4.1). Stained cultures were then washed once with $1\times$ PBS at RT for 5 minutes and treated with DAPI solution (Sigma-Aldrich, D9542) at RT for 5 minutes. Stained coverslips were then washed three times with $1\times$ PBS at RT for 5 minutes each and covered with Fluoroshield (Sigma-Aldrich, F6182) mounting medium and placed face down on a glass slide (Thermo Fisher Scientific, 12-544-7). Z-stack images for phagocytosis analysis and representation were taken using a Zeiss (Jena, Germany) Axio-Observer 7 epifluorescent microscope at 20x using 15 slices and a 1 μm step size. Light source power and exposure time were identical for all images used in quantitative analysis. Image analysis was performed using ImageJ version 1.53 (National Institutes of Health, Bethesda, MD) for Windows (Microsoft). In brief, phagocytic activity was measured *via* intracellular colocalization of FITC microbeads and cluster of differentiation 68 (CD68) positive cells. The Colocalization Image

Creator plugin was utilized to generate images measuring intracellular colocalization of fluorescent microbeads with CD68. Image thresholds were set and a 1 µm particle size filter was used to isolate objects of interest. The 3D Object Counter plugin provided counts of the FITC microbeads and CD68 positive macrophages colocalized in each Z-slice, compounding colocalization measures across the entire image to obtain a final value (Lunde & Glover, 2020). Data are represented as the ratio of intracellular microbeads to the total number of CD68 positive macrophages on the analyzed image. Lastly, the numerical average across three technical replicates was calculated and graphed per animal used in the experiment.

Immunohistochemistry

Ten days after paclitaxel treatment, mice were deeply anesthetized using 100% isoflurane and euthanized *via* cervical dislocation and subsequent decapitation. Lumbar (L3-5) DRG, and hind paws were isolated and collected in 4% PFA for 24 hours at 4˚C and cryoprotected in 30% sucrose (Sigma-Aldrich, S0389) for minimally 48 hours at 4˚C. DRG and paw skin were then embedded in optimal cutting temperature (OCT) medium (Thermo Fisher Scientific, 50-363-773) and cryosectioned at 16 and 20 µm, respectively, and mounted on positively charged glass slides (Thermo Fisher Scientific, 12-550-15). Mounted sections were allowed to dry for 30 minutes before being stored at -20˚C until further use. Prior to staining, mounted sections were thawed and dried at 30˚C for 5 minutes. Slides were then blocked for non-specific antibody binding and permeabilized at RT for 2 hours in a solution containing: 1× PBS, 2% heat-inactivated NGS, 1% BSA, 0.1% triton X-100, 0.05% tween-20, and 0.05% sodium azide. Slides were then incubated with a primary antibody cocktail diluted in the previously described buffer at 4˚C for 24 hours (see

Table 4.1). Slides were washed three times with $1\times$ PBS at RT for 5 minutes each. After washing, slides were incubated with a secondary antibody cocktail diluted in the previously described buffer at RT for 2 hours (see Table 4.1). Slides were then washed once with $1\times$ PBS at RT for 5 minutes and treated with DAPI solution at RT for 5 minutes. Slides were then washed three times with $1\times$ PBS at RT for 5 minutes each and covered with Fluoroshield mounting medium and a 1.5 mm glass coverslip (Thermo Fisher Scientific, 08-774-384). Z-stack images for DRG analysis and representation were taken using an Olympus (Tokyo, Japan) IX83 epifluorescent microscope at 20x using 15 slices and a 1 μm step size. Z-stack images for paw skin analysis and representation were taken using a Zeiss (Jena, Germany) Axio-Observer 7 epifluorescent microscope at 40x using 20 slices and a 1 μm step size. Light source power and exposure time were identical for all images used in quantitative analysis. Image analysis was performed using ImageJ version 1.53 (National Institutes of Health, Bethesda, MD) for Windows (Microsoft). In brief, CD68 and ATF3 upregulation in the DRG was analyzed by localization with DAPI. Image thresholds were obtained and a 5-100 μm particle filter was used to isolate objects of interest. In the DRG, data are represented as the ratio of CD68 positive cells to the total area (mm^2) of the analyzed DRG, or the total number of ATF3 positive cells. The numerical average across two technical replicates was calculated and graphed per animal used in the experiment. Intraepidermal nerve fiber density in the paw skin was measured by tracing protein gene product 9.5 (PGP9.5) staining and counting the number of fibers that crossed the basement membrane (Kennedy et al., 1996). In the paw skin, data are represented as the density of PGP9.5 positive fibers to the total distance (mm) of the analyzed section of paw skin. The numerical average across three technical replicates was calculated and graphed per animal used in the experiment.

Statistical Analysis

Data were assessed for statistical significance using GraphPad Prism software (version 9.3) and are expressed as mean ± standard error of the mean (SEM), unless otherwise specified. For all data sets, three-way ANOVAs were performed followed by Sidak's *post-hoc* for multiple comparisons to appropriately assess sex, genotype, and treatment effects. A *p* value of < 0.05 was considered statistically significant.

Table 4.1. Antibodies used for ICC and IHC.

Antibody	Company	Catalog number	Working Dilution
Antibodies used for IHC			
Anti-PGP9.5 (IHC)	CedarLane	CL7756AP-50	1:500
Anti-CD68 (IHC & ICC)	BioRad	MCA1957	1:1000
Anti-ATF3 (IHC)	Abcam	AB207434	1:500
Goat anti-rat Alexa Fluor 488 (IHC)	Invitrogen	A11006	1:500
Goat anti-rabbit Alexa Fluor 647 (IHC)	Invitrogen	A21245	1:500
Antibodies used for ICC			
Anti-CD68 (IHC & ICC)	BioRad	MCA1957	1:1000
Goat anti-rat Alexa Fluor 647 (ICC)	Invitrogen	A21247	1:500
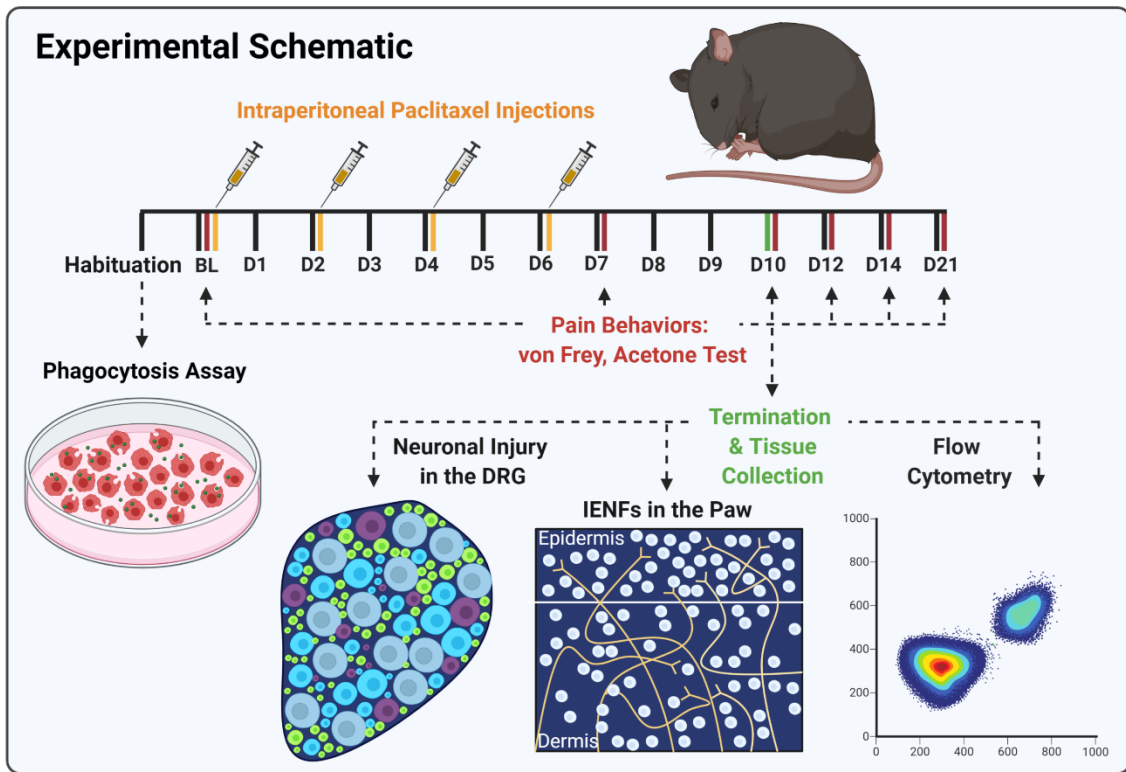
Figure 4.1. Schematic of the experimental timeline used in this study. Following habituation and behavioral baselines, mice were subjected to intraperitoneal injections of paclitaxel (4 mg/kg) on days: 0, 2, 4, and 6 to model CIPN. A subset of naïve mice was euthanized and used for peritoneal macrophages cultures and flow cytometry to assess phagocytic activity of cells after paclitaxel treatment. Behavioral assays (mechanical hypersensitivity and cold allodynia) were performed on days 7 to 35 after the start of paclitaxel treatment. A subset of mice was sacrificed on day 10 and peritoneal macrophages, lumbar DRG and hind paws were collected for flow cytometry and histology.

RESULTS

TLR4 signaling on Macrophages Mediates the Development of CIPN in males, but not Females.

It has previously been shown that paclitaxel, and many other chemotherapeutics, facilitate development of neuropathic behavioral phenotypes (Barginear et al., 2019; Staff et al., 2020). We asked whether TLR4 activation by paclitaxel on LysM positive macrophages was necessary for

the development of CIPN in both sexes, since paclitaxel is often used to treat metastatic breast cancer and is accompanied by dose-limiting pain comorbidities (Brady et al., 2021). To test this, we used a previously validated transgenic mouse line, LysM[TLR4Flox], which enabled us to selectively ablate TLR4 expression in peripheral macrophages and monocytes in a constitutive, cre-dependent manner (Figure 4.2B). Consistent with our previous study, and many others, male and female mice treated with a total dose of 16 mg/kg paclitaxel developed robust mechanical and thermal sensitivity by day 7, (Figure 4.2C-E, Table 2) (Agalave et al., 2021; Boyette-Davis et al., 2011; Li et al., 2017; Li et al., 2014; Zhang et al., 2016). Interestingly, removal of TLR4 from macrophages was associated with a protective behavioral phenotype, where development of mechanical but not thermal hypersensitivity in paclitaxel treated male mice was attenuated (Figure 4.2C & E, Table 2). This indicates that TLR4 signaling on macrophages is required for mediating the response to mechanical but not thermal stimuli after paclitaxel treatment in males. Conversely, we did not observe the same protective phenotype in female LysM[TLR4Flox] mice. This implies that paclitaxel acts through a different receptor or cell population in females since development of nociceptive phenotypes in wild type mice is similar between sex (Figure 4.2D & E, Table 2). Taken together, our data suggest that activation of TLR4 on macrophages by paclitaxel, specifically in males, is an important mechanism involved in CIPN development.
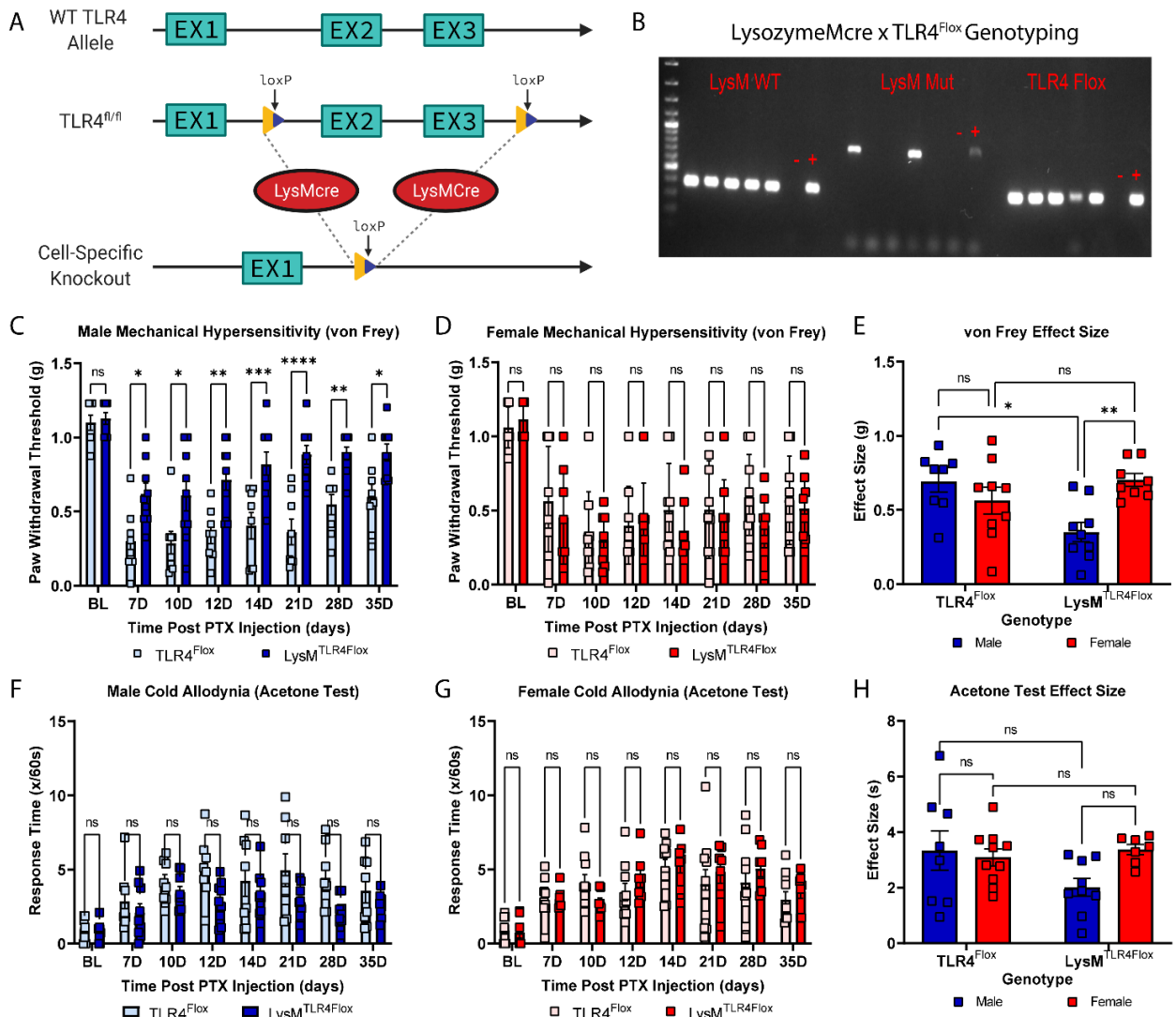
Figure 4.2. TLR4 signaling on Macrophages Mediates the Development of CIPN in males, but not Females. A) Schematic representing the murine genetic model, LysMcre[TLR4Flox]. **B)** Example PCR and gel electrophoresis for LysMcre[TLR4Flox] mice. – indicates negative control and + indicates positive control. **C-D)** Hind paw mechanical withdrawal thresholds were measured prior to PTX injection and on days: 7, 10, 12, 14, 21, 28 and 35 post injection in male (n=8) and female (n=9) TLR4[Flox] and male (n=9) and female (n=8) LysM[TLR4Flox] mice. **E)** Data for males and females are combined and shown as the total effect size during the experiment. **F-G)** Hind paw response to application of acetone was measured prior to PTX injection and on days: 7, 10, 12, 14, 21, 28 and 35 post injection in male (n=8) and female (n=9) TLR4[Flox] and male (n=9) and female (n=8) LysM[TLR4Flox] mice. **H)** Data for males and females are combined and shown as the total effect size during the experiment. Data were analyzed using a 2-way ANOVA and Sidak's *post-hoc* comparisons. * = $p < 0.05$, ** = $p < 0.005$, *** = $p < 0.0005$, **** = $p < 0.00005$.

90

Table 4.2. Statistical values corresponding to the data analysis in figure 4.2.

Šídák's multiple comparisons test	Predicted (LS) mean diff.	95.00% CI of diff.	Below threshold?	Summary	Adjusted P Value
Male von Frey					
TLR4^{Flox} - LysM^{TLR4Flox}					
BL	-0.02835	-0.3164 to 0.2597	No	ns	>0.9999
7D	-0.3193	-0.6074 to -0.03120	Yes	*	0.0206
10D	-0.3236	-0.6117 to -0.03552	Yes	*	0.0181
12D	-0.3684	-0.6565 to -0.08033	Yes	**	0.0044
14D	-0.4132	-0.7013 to -0.1252	Yes	***	0.0009
21D	-0.5212	-0.8093 to -0.2332	Yes	****	<0.0001
28D	-0.3439	-0.6320 to -0.05581	Yes	**	0.0097
35D	-0.2982	-0.5863 to -0.01017	Yes	*	0.0378
Female von Frey					
TLR4^{Flox} - LysM^{TLR4Flox}					
BL	-0.05505	-0.2544 to 0.1443	No	ns	0.9822
7D	0.1102	-0.4182 to 0.6386	No	ns	0.9971
10D	0.05118	-0.3072 to 0.4095	No	ns	0.9998
12D	-0.03917	-0.4305 to 0.3521	No	ns	>0.9999
14D	0.1423	-0.2642 to 0.5488	No	ns	0.9281
21D	0.07345	-0.3914 to 0.5383	No	ns	0.9996
28D	0.1905	-0.1940 to 0.5750	No	ns	0.6894
35D	0.0563	-0.3493 to 0.4619	No	ns	0.9998
Male Acetone					
TLR4^{Flox} - LysM^{TLR4Flox}					
BL	0.1854	-0.9313 to 1.302	No	ns	0.9994
7D	0.765	-2.164 to 3.694	No	ns	0.9868
10D	0.6692	-1.340 to 2.678	No	ns	0.9435
12D	2.231	-0.6162 to 5.078	No	ns	0.176
14D	0.8869	-3.133 to 4.906	No	ns	0.9936
21D	2.154	-2.100 to 6.407	No	ns	0.5857
28D	2.314	-0.4631 to 5.091	No	ns	0.1266
35D	0.9846	-2.077 to 4.046	No	ns	0.9276
Female Acetone					

TLR4^{Flox} - LysM^{TLR4Flox}					
BL	0.1186	-1.449 to 1.686	No	ns	>0.9999
7D	-0.01943	-1.591 to 1.553	No	ns	>0.9999
10D	1.311	-0.7686 to 3.391	No	ns	0.4001
12D	-0.933	-3.601 to 1.735	No	ns	0.9297
14D	-0.2633	-2.976 to 2.449	No	ns	>0.9999
21D	-0.839	-4.768 to 3.090	No	ns	0.9966
28D	-0.9316	-4.131 to 2.268	No	ns	0.975
35D	-0.5633	-2.844 to 1.717	No	ns	0.991
von Frey Effect Size					
TLR4^{Flox}:Male vs. TLR4^{Flox}:Female	0.1303	-0.1531 to 0.4136	No	ns	0.7482
TLR4^{Flox}:Male vs. LysM^{TLR4Flox}:Male	0.3413	0.05799 to 0.6247	Yes	*	0.0117
TLR4^{Flox}:Male vs. LysM^{TLR4Flox}:Female	-0.008335	-0.2999 to 0.2832	No	ns	>0.9999
TLR4^{Flox}:Female vs. LysM^{TLR4Flox}:Male	0.2111	-0.06380 to 0.4860	No	ns	0.2108
TLR4^{Flox}:Female vs. LysM^{TLR4Flox}:Female	-0.1386	-0.4219 to 0.1448	No	ns	0.6929
LysM^{TLR4Flox}:Male vs. LysM^{TLR4Flox}:Female	-0.3497	-0.6330 to -0.06633	Yes	**	0.0094
Acetone Effect Size					
TLR4^{Flox}:Male vs. TLR4^{Flox}:Female	0.2496	-1.400 to 1.900	No	ns	0.9988
TLR4^{Flox}:Male vs. LysM^{TLR4Flox}:Male	1.318	-0.3720 to 3.008	No	ns	0.1972
TLR4^{Flox}:Male vs. LysM^{TLR4Flox}:Female	-0.03587	-1.836 to 1.764	No	ns	>0.9999
TLR4^{Flox}:Female vs. LysM^{TLR4Flox}:Male	1.069	-0.5297 to 2.667	No	ns	0.3507
TLR4^{Flox}:Female vs. LysM^{TLR4Flox}:Female	-0.2855	-2.000 to 1.429	No	ns	0.9979
LysM^{TLR4Flox}:Male vs. LysM^{TLR4Flox}:Female	-1.354	-3.107 to 0.3989	No	ns	0.2055

Paclitaxel increases phagocytic behavior of male, but not female macrophages in a TLR4-dependent manner.

Measuring uptake of microbeads as a proxy of cell-to-cell signaling is an increasingly viable way to study mechanisms of macrophage biology, *in vitro* (Mohning et al., 2018). Paclitaxel has been

previously shown to significantly enhance phagocytic activity of macrophages derived from bone marrow, with recent evidence suggesting that TLR4 may regulate phagocytosis through one of its adaptor proteins, translocating chain-associated membrane protein (TRAM) (Li et al., 2008; Skjesol et al., 2019). It's possible that one mechanism of CIPN development is through interaction of paclitaxel and TLR4 to engage phagocytosis in macrophages. To test this hypothesis, we isolated and subsequently cultured peritoneal macrophages from male and female LysM$^{\text{TLR4Flox}}$ mice. Upon reaching appropriate confluency, the cells were treated with paclitaxel for 24 hours and incubated with opsonized fluorescent beads for one hour to measure phagocytic behavior (Figure 4.3A). We discovered a robust sex difference where paclitaxel treatment significantly increases bead uptake in male, but not female wild type macrophages. Moreover, conditional deletion of TLR4 from these isolated macrophages only prevents the paclitaxel-induced upregulation of phagocytic behavior in males (Figure 4.3B; Table 4.3). This suggests that the direct action of paclitaxel on male macrophages induces a pro-inflammatory phenotype and are dependent on TLR4 signaling, whereas female macrophages are less affected by paclitaxel.
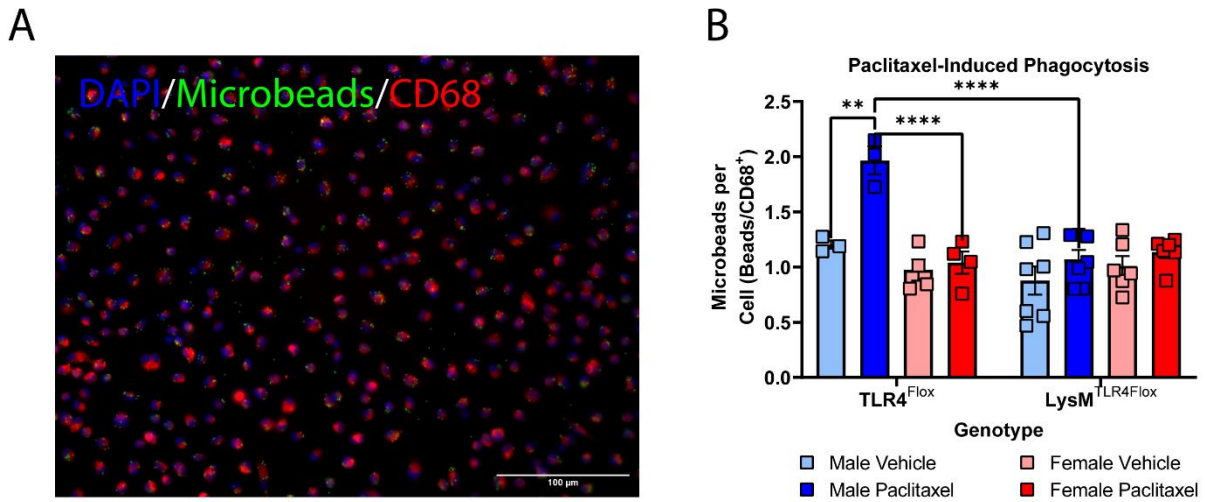
Figure 4.3. Paclitaxel treatment induces phagocytosis of FITC microbeads in cultured macrophages by a sex- and genotype-dependent manner. A) Representative image from a TLR4^{Flox} male treated with paclitaxel. Individual group sample sizes are as follows: Male Vehicle (TLR4^{Flox} n=3; LysM^{TLR4Flox} n=7), Male Paclitaxel (TLR4^{Flox} n=3; LysM^{TLR4Flox} n=7), Female Vehicle (TLR4^{Flox} n=4; LysM^{TLR4Flox} n=6), Female Paclitaxel (TLR4^{Flox} n=4; LysM^{TLR4Flox} n=6). Coverslips were stained with DAPI (405) and CD68 (568) and were imaged at 40x. FITC microbeads have inherent fluorescence on the 488 channel. **B)** Quantification of FITC microbead phagocytosis by cultured macrophages. The numerical average across 3 technical replicates per animal is represented in the graph. Data were analyzed using a 3-way ANOVA and Sidak's *post-hoc* comparisons. * = $p < 0.05$, ** = $p < 0.005$, *** = $p < 0.0005$, **** = $p < 0.00005$.

Table 4.3 Statistical values corresponding to the data analysis in figure 4.3.

Šídák's multiple comparisons test	Mean Diff.	95.00% CI of diff.	Below threshold?	Summary	Adjusted P Value
Phagocytosis Assay					
TLR4^{Flox}:Male Vehicle vs. LysM^{TLR4Flox}:Male Vehicle	0.3249	-0.1565 to 0.8063	No	ns	0.4312
TLR4^{Flox}:Male Paclitaxel vs. LysM^{TLR4Flox}:Male Paclitaxel	0.8935	0.4121 to 1.375	Yes	****	<0.0001
TLR4^{Flox}:Female Vehicle vs. LysM^{TLR4Flox}:Female Vehicle	-0.03502	-0.4853 to 0.4153	No	ns	>0.9999
TLR4^{Flox}:Female Paclitaxel vs. LysM^{TLR4Flox}:Female Paclitaxel	-0.09713	-0.5474 to 0.3532	No	ns	0.9998
TLR4^{Flox}:Male Vehicle vs. TLR4^{Flox}:Male Paclitaxel	-0.7622	-1.332 to -0.1926	Yes	**	0.003
TLR4^{Flox}:Female Vehicle vs. TLR4^{Flox}:Female Paclitaxel	-0.06523	-0.5585 to 0.4281	No	ns	>0.9999

LysM^{TLR4Flox}:Male Vehicle vs. LysM^{TLR4flox}:Male Paclitaxel	-0.1936	-0.5665 to 0.1793	No	ns	0.7842
LysM^{TLR4Flox}:Female Vehicle vs. LysM^{TLR4flox}:Female Paclitaxel	-0.1273	-0.5301 to 0.2754	No	ns	0.9929
TLR4^{Flox}:Male Vehicle vs. TLR4^{Flox}:Female Vehicle	0.2289	-0.3039 to 0.7617	No	ns	0.9266
TLR4^{Flox}:Male Paclitaxel vs. TLR4^{Flox}:Female Paclitaxel	0.9259	0.3931 to 1.459	Yes	****	<0.0001
LysM^{TLR4Flox}:Male Vehicle vs. LysM^{TLR4flox}:Female Vehicle	-0.1311	-0.5192 to 0.2571	No	ns	0.9876
LysM^{TLR4Flox}:Male Paclitaxel vs. LysM^{TLR4flox}:Female Paclitaxel	-0.06478	-0.4529 to 0.3233	No	ns	>0.9999

Immune Cell Infiltration and Neuronal Injury after Paclitaxel Treatment in the DRG is Mediated by TLR4 Activation on Male Macrophages.

It is well known that first-order pain processing occurs within the DRG by nociceptive neurons receiving sensory input from afferent fibers and modulatory signals from peripheral immune cells (Krames, 2015). Paclitaxel treatment has been shown to induce a neuroinflammatory phenotype in the DRG of human patients and in animal models (Akin et al., 2021; Li et al., 2021). We have previously shown, along with others, that a dose of 16 mg/kg of paclitaxel is sufficient to induce upregulation of ATF3 in the DRG of these mice between 2 and 10 days after initial dosing (Agalave et al., 2021; Peters et al., 2007). This upregulation of ATF3 may be interpreted as a biomarker for neuronal injury and is often associated with reprogramming of neuronal and immune phenotypes, indicating bi-directional communication between the nervous and immune systems in the periphery (Renthal et al., 2020; Tsujino et al., 2000). To better understand how modulatory signals from immune cells affect neuronal injury in the DRG we isolated lumbar DRGs from LysM^{TLR4flox} animals 10 days after paclitaxel treatment and performed immunohistochemical analyses to measure the upregulation of ATF3 in neurons and CD68 positive macrophages (Figure 4.4A & B). We found that the number of ATF3 positive neurons was significantly increased in the

DRG of male TLR4^{Flox} mice treated with paclitaxel. Interestingly, male LysM^{TLR4Flox} mice treated with paclitaxel had significantly reduced ATF3 positive neurons in the DRG as compared to male TLR4^{Flox} mice. These effects were not recapitulated in females of either genotype, indicating a sex- and genotype-dependent effect where TLR4 activation on macrophages by paclitaxel administration facilitates upregulation of a neuroinflammatory phenotype only in males (Figure 4.4C, Table 4.4). Moreover, analysis of CD68 positive macrophages in the DRG after paclitaxel treatment reveals significant sex-, treatment- and genotype-dependent effects. Both male and female TLR4^{Flox} mice treated with paclitaxel have significantly increased expression of CD68 positive macrophages in the DRG.-Intriguingly, paclitaxel treatment increased expression of CD68 positive macrophages in the DRG significantly more in males than in females. Lastly, removal of TLR4 from macrophages in the LysM^{TLR4Flox} male mice prevents the paclitaxel-dependent upregulation of CD68 positive macrophages in the DRG. These findings are also not recapitulated in females (Figure 4.4D, Table 4.4). These data show that paclitaxel may facilitate neuroinflammation and injury through TLR4 signaling on macrophages in males, but not females. This is indicative of a sex- and cell-specific difference in the mechanisms behind CIPN development.
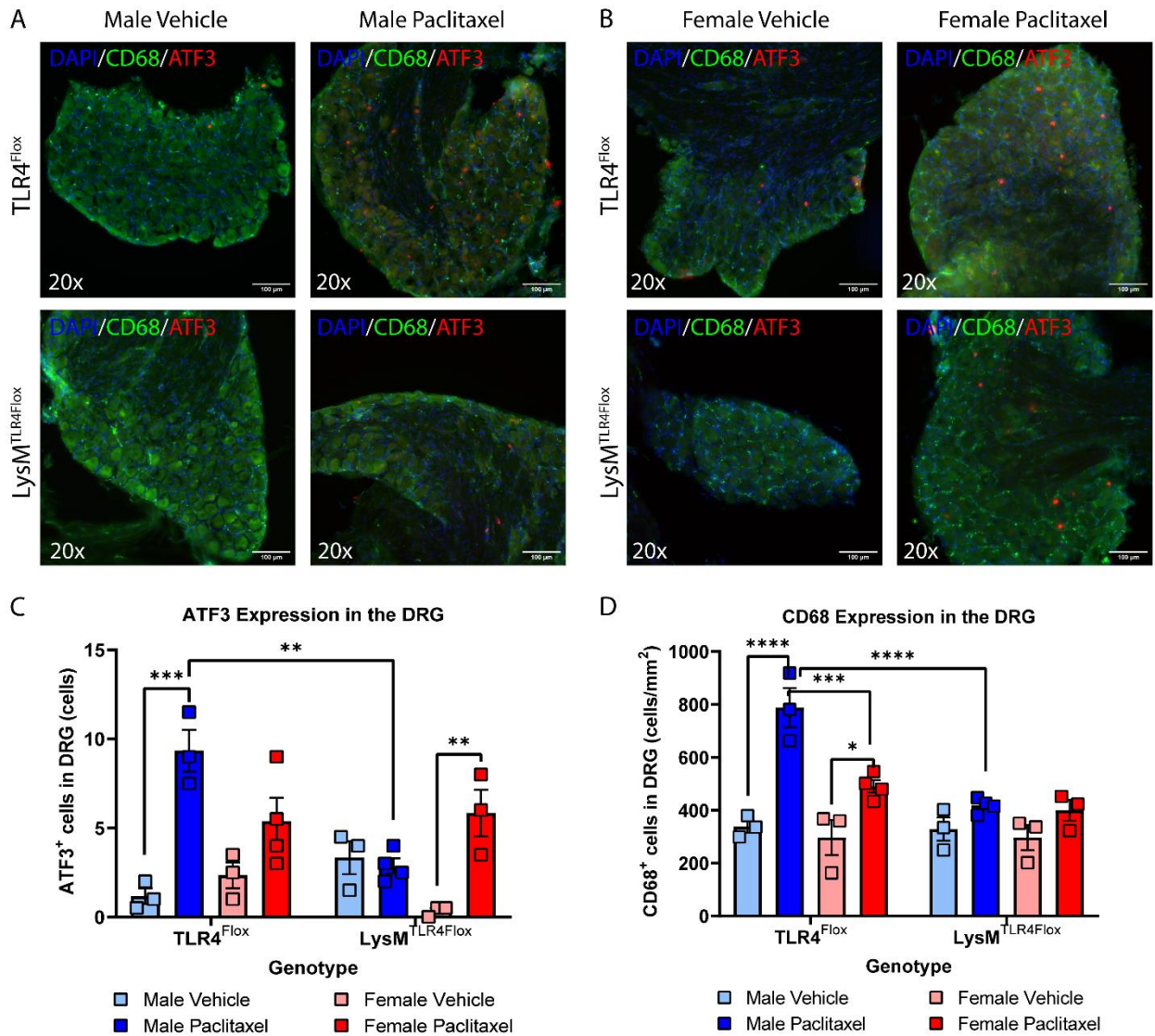
Figure 4.4. Infiltration of macrophages and incidence of neuronal injury in the DRG after paclitaxel treatment. A) Representative images from male vehicle (n=3) and paclitaxel (n=3) treated TLR4^{Flox} and male vehicle (n=3) and paclitaxel (n=4) treated LysM^{TLR4Flox} mice. Sections were stained with DAPI (blue), CD68 (green), and ATF3 (red) and imaged at 20x. **B)** Representative images from female vehicle (n=3) and paclitaxel (n=4) treated TLR4^{Flox} and female vehicle (n=3) and paclitaxel (n=3) treated LysM^{TLR4Flox} mice. Sections were stained with DAPI (blue), CD68 (green), and ATF3 (red) and imaged at 20x. **C)** Quantification of ATF3 positive neurons in the DRG. Data are expressed as the average of 2 technical replicates per animal. **D)** Quantification of CD68 positive macrophages in the DRG. Data are expressed as the average of 2 technical replicates per animal and normalized by the area measured in millimeters^2. Data were analyzed using a 3-way ANOVA and Sidak's *post-hoc* comparisons. * = $p < 0.05$, ** = $p < 0.005$, *** = $p < 0.0005$, **** = $p < 0.00005$.

**Table 4.4.** Statistical values corresponding to the data analysis in figure 4.4.

Šídák's multiple comparisons test	Mean Diff.	95.00% CI of diff.	Below threshold?	Summary	Adjusted P Value
ATF3 Expression					
TLR4^{Flox}:Male Vehicle vs. LysM^{TLR4Flox}:Male Vehicle	-2.167	-6.654 to 2.320	No	ns	0.8168
TLR4^{Flox}:Male Paclitaxel vs. LysM^{TLR4Flox}:Male Paclitaxel	6.458	2.261 to 10.66	Yes	**	0.001
TLR4^{Flox}:Female Vehicle vs. LysM^{TLR4Flox}:Female Vehicle	2	-2.487 to 6.487	No	ns	0.8807
TLR4^{Flox}:Female Paclitaxel vs. LysM^{TLR4Flox}:Female Paclitaxel	-0.4583	-4.656 to 3.739	No	ns	>0.9999
TLR4^{Flox}:Male Vehicle vs. TLR4^{Flox}:Male Paclitaxel	-8.167	-12.65 to -3.680	Yes	***	0.0002
TLR4^{Flox}:Female Vehicle vs. TLR4^{Flox}:Female Paclitaxel	-3.042	-7.239 to 1.156	No	ns	0.2996
LysM^{TLR4Flox}:Male Vehicle vs. LysM^{TLR4Flox}:Male Paclitaxel	0.4583	-3.739 to 4.656	No	ns	>0.9999
LysM^{TLR4Flox}:Female Vehicle vs. LysM^{TLR4Flox}:Female Paclitaxel	-5.5	-9.987 to -1.013	Yes	**	0.0099
TLR4^{Flox}:Male Vehicle vs. TLR4^{Flox}:Female Vehicle	-1.167	-5.654 to 3.320	No	ns	0.9981
TLR4^{Flox}:Male Paclitaxel vs. TLR4^{Flox}:Female Paclitaxel	3.958	-0.2389 to 8.156	No	ns	0.0743
LysM^{TLR4Flox}:Male Vehicle vs. LysM^{TLR4Flox}:Female Vehicle	3	-1.487 to 7.487	No	ns	0.4048
LysM^{TLR4Flox}:Male Paclitaxel vs. LysM^{TLR4Flox}:Female Paclitaxel	-2.958	-7.156 to 1.239	No	ns	0.3345
CD68 Expression					
TLR4^{Flox}:Male Vehicle vs. LysM^{TLR4Flox}:Male Vehicle	9.661	-195.2 to 214.6	No	ns	>0.9999
TLR4^{Flox}:Male Paclitaxel vs. LysM^{TLR4Flox}:Male Paclitaxel	370.1	178.4 to 561.7	Yes	****	<0.0001
TLR4^{Flox}:Female Vehicle vs. LysM^{TLR4Flox}:Female Vehicle	0.4017	-204.5 to 205.3	No	ns	>0.9999
TLR4^{Flox}:Female Paclitaxel vs. LysM^{TLR4Flox}:Female Paclitaxel	90.8	-100.9 to 282.5	No	ns	0.8338
TLR4^{Flox}:Male Vehicle vs. TLR4^{Flox}:Male Paclitaxel	-449.4	-654.3 to -244.5	Yes	****	<0.0001
TLR4^{Flox}:Female Vehicle vs. TLR4^{Flox}:Female Paclitaxel	-193.5	-385.2 to -1.832	Yes	*	0.0467

Comparison					
LysM^{TLR4Flox}:Male Vehicle vs. LysM^{TLR4Flox}:Male Paclitaxel	-89.01	-280.7 to 102.7	No	ns	0.8504
LysM^{TLR4Flox}:Female Vehicle vs. LysM^{TLR4Flox}:Female Paclitaxel	-103.1	-308.0 to 101.8	No	ns	0.7764
TLR4^{Flox}:Male Vehicle vs. TLR4^{Flox}:Female Vehicle	41.27	-163.6 to 246.2	No	ns	0.9998
TLR4^{Flox}:Male Paclitaxel vs. TLR4^{Flox}:Female Paclitaxel	297.2	105.5 to 488.9	Yes	***	0.001
LysM^{TLR4Flox}:Male Vehicle vs. LysM^{TLR4Flox}:Female Vehicle	32.01	-172.9 to 236.9	No	ns	>0.9999
LysM^{TLR4Flox}:Male Paclitaxel vs. LysM^{TLR4Flox}:Female Paclitaxel	17.91	-173.8 to 209.6	No	ns	>0.9999

Paclitaxel Treatment Reduces Intraepidermal Nerve Fiber Density in Both Sexes.

Paclitaxel treatment has been previously shown to reduce IENF density in males (Boyette-Davis et al., 2011). We sought to further investigate this by assessing the potential for sex differences in cell specific TLR4 signaling. To test our hypothesis, we utilized our genetic model, LysM^{TLR4Flox}, where we remove the ability for paclitaxel to act on TLR4 expressed by macrophages and monocytes. We then isolated hind limb skin 10 days after paclitaxel treatment and performed immunohistochemical analyses to measure the density of IENFs crossing the basement membrane in the paw (Figure 4.5A & B). Our initial findings recapitulate data shown in the previously mentioned studies, where paclitaxel treatment significantly reduces IENF density in the paw skin of male TLR4^{Flox} mice (Boyette-Davis et al., 2011). We also found that paclitaxel treatment reduces IENF density in the paw of female mice—an entirely novel finding. Interestingly, we demonstrate that reduction of IENF density in male mice is mediated by TLR4 signaling on macrophages. Male LysM^{TLR4Flox} mice treated with paclitaxel exhibit no significant change from vehicle counterparts, however; these effects are not recapitulated in female LysM^{TLR4Flox} mice

(Figure 4.5C, Table 4.5). We believe these data indicate a sex- and cell-specific difference in TLR4 signaling, meaning that males utilize TLR4 signaling on macrophages to facilitate inflammation in the DRG and paw skin. Conversely, paclitaxel acts on a different receptor and cell type to drive the effects we see in wild type females. Lastly, we observed a robust positive correlation between ATF3 expression in DRG nociceptors and CD68+ macrophages in a treatment, sex, genotype dependent manner. Moreover, these variables were also inversely correlated with IENF density, indicating that an increase in neuronal injury markers and macrophage infiltration facilitates IENF retraction in the paw (Figure 4.5D). These effects are attenuated in males lacking macrophage TLR4 but are not recapitulated in females.
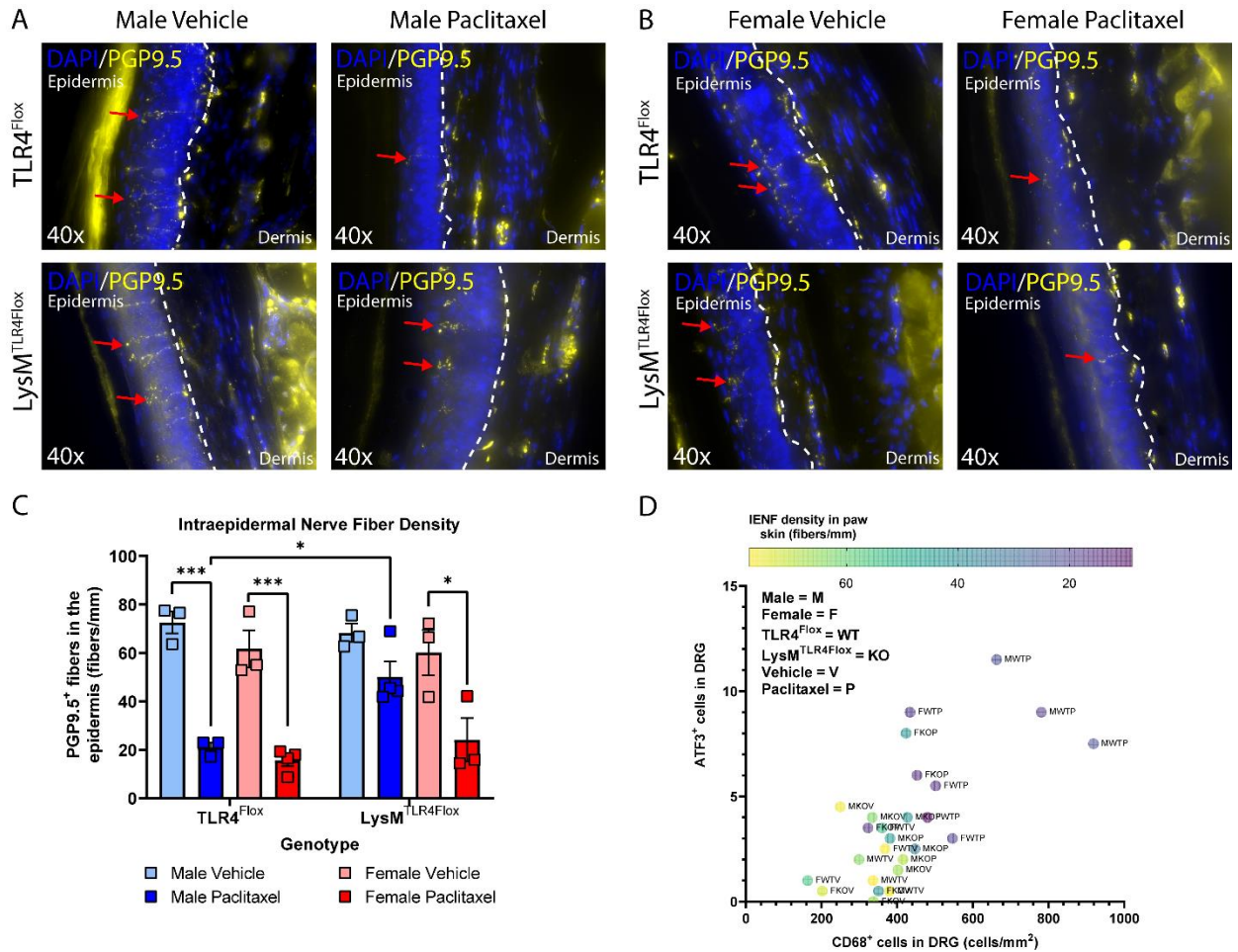
Figure 4.5. Intraepidermal nerve fiber density in the hind paw skin after paclitaxel treatment. A) Representative images from male vehicle (n=3) and paclitaxel (n=3) treated TLR4$^{\text{Flox}}$ and male vehicle (n=3) and paclitaxel (n=4) treated LysM$^{\text{TLR4Flox}}$ mice. Sections were stained with DAPI (blue) and PGP9.5 (yellow) and imaged at 40x. **B)** Representative images from female vehicle (n=3) and paclitaxel (n=4) treated TLR4$^{\text{Flox}}$ and female vehicle (n=3) and paclitaxel (n=3) treated LysM$^{\text{TLR4Flox}}$ mice. Sections were stained with DAPI (blue) and PGP9.5 (yellow) and imaged at 40x. **C)** Quantification of PGP9.5 positive fibers crossing the basement membrane. Data are expressed as the average of 3 technical replicates per animal and normalized by the length of area measured in millimeters. **D)** Multivariate plot between CD68, ATF3, and IENF expression. Averages of duplicates (CD68, ATF3) and triplicates (IENFs) are graphed in opposition to represent the correlation between CD68 and ATF3. Individual dots are color-coded to represent the density of IENFs per animal. Data were analyzed using a 3-way ANOVA and Sidak's *post-hoc* comparisons. * = $p < 0.05$, ** = $p < 0.005$, *** = $p < 0.0005$, **** = $p < 0.00005$.

Table 4.5. Statistical values corresponding to the data analysis in figure 4.5.

Šídák's multiple comparisons test	Mean Diff.	95.00% CI of diff.	Below threshold?	Summary	Adjusted P Value
IENF Density					
TLR4^{Flox}:Male Vehicle vs. LysM^{TLR4Flox}:Male Vehicle	4.246	-24.82 to 33.31	No	ns	>0.9999
TLR4^{Flox}:Male Paclitaxel vs. LysM^{TLR4Flox}:Male Paclitaxel	-29.18	-56.36 to -1.991	Yes	*	0.0297
TLR4^{Flox}:Female Vehicle vs. LysM^{TLR4Flox}:Female Vehicle	1.534	-27.53 to 30.60	No	ns	>0.9999
TLR4^{Flox}:Female Paclitaxel vs. LysM^{TLR4Flox}:Female Paclitaxel	-8.538	-35.72 to 18.65	No	ns	0.9899
TLR4^{Flox}:Male Vehicle vs. TLR4^{Flox}:Male Paclitaxel	51.57	22.51 to 80.63	Yes	***	0.0002
TLR4^{Flox}:Female Vehicle vs. TLR4^{Flox}:Female Paclitaxel	46.06	18.88 to 73.24	Yes	***	0.0004
LysM^{TLR4Flox}:Male Vehicle vs. LysM^{TLR4Flox}:Male Paclitaxel	18.15	-9.037 to 45.33	No	ns	0.4069
LysM^{TLR4Flox}:Female Vehicle vs. LysM^{TLR4Flox}:Female Paclitaxel	35.99	6.927 to 65.05	Yes	**	0.009
TLR4^{Flox}:Male Vehicle vs. TLR4^{Flox}:Female Vehicle	10.86	-18.20 to 39.93	No	ns	0.9614
TLR4^{Flox}:Male Paclitaxel vs. TLR4^{Flox}:Female Paclitaxel	5.356	-21.83 to 32.54	No	ns	0.9999
LysM^{TLR4Flox}:Male Vehicle vs. LysM^{TLR4Flox}:Female Vehicle	8.153	-20.91 to 37.21	No	ns	0.9962
LysM^{TLR4Flox}:Male Paclitaxel vs. LysM^{TLR4Flox}:Female Paclitaxel	25.99	-1.191 to 53.18	No	ns	0.0679

DISCUSSION

Our study was designed and powered with the intent to uncover the sex- and cell-specific contributions of macrophage TLR4 signaling in response to paclitaxel-induced peripheral neuropathy. Using our murine genetic tool, LysM^{TLR4Flox}, we discovered that the development of mechanical hypersensitivity during CIPN is mediated by signaling processes of TLR4 activation on male macrophages but these findings were not recapitulated in female mice. In addition, we found that inflammatory polarization and antigen presentation in macrophages after paclitaxel treatment is mediated by TLR4 activation only in males. Moreover, a TLR4 mediated increase in

phagocytic activity of macrophages after paclitaxel treatment is exclusive to males. Lastly, retraction of IENFs in the paw skin after paclitaxel treatment occurs in both sexes, but only male mice lacking TLR4 on their macrophages are protected against this.

In line with our previously published work and other literature, both male and female mice develop mechanical and thermal hypersensitivity following paclitaxel administration (Agalave et al., 2021; Hwang et al., 2012; Illias et al., 2022). However, our results showed a potent protective effect where conditional knockout of TLR4 from peripheral macrophages attenuated mechanical but not cold hypersensitivity development after paclitaxel treatment. Moreover, the observed behavioral differences were sex dependent. This led us to believe that macrophage specific activation of TLR4 by paclitaxel facilitates inflammatory mechanisms in males which drives neuropathic pain development. For example, whole-body deletion of TLR4, MyD88 and TRIF prevents CIPN development in both sexes (Woller et al., 2015). Also, infiltration of monocytes in the DRG of male rats following paclitaxel is shown to mediate mechanical hypersensitivity. Depletion of peripheral macrophages using clodronate-filled liposomes reverses the paclitaxel-induced mechanical hypersensitivity and decreases inflammatory cytokine expression (Zhang et al., 2016). While these studies provide clear evidence that TLR4 is necessary for CIPN, our results suggest that sex differences in the macrophage response to paclitaxel underlies this phenotype. These results raised several questions that formed the basis of follow-up experiments throughout this study.

It has previously been shown that paclitaxel treatment facilitates macrophage upregulation and recruitment to the DRG (Jimenez-Andrade et al., 2006; Zhang et al., 2016). Further investigation revealed that these effects were mediated by TLR4 signaling, as intrathecal administration of LPS-RS, a TLR4 antagonist, reversed the paclitaxel-induced upregulation of DRG macrophages in males (Li et al., 2014). While these studies provide ample evidence that connects TLR4 signaling to the macrophage response during CIPN, they raise important questions about the implications of macrophage TLR4 and its role in neuroinflammation within the peripheral nervous system. Interestingly, novel data suggest that activation of TLR4 can initiate macrophage infiltration through upregulation of cluster of differentiation 68 (CD68) and promote polarization towards a pro-inflammatory, or M1 phenotype (Shao et al., 2019; Wanderley et al., 2018). A critical component missing from these studies is the consideration of sex as a variable. We, among many others, have shown that both immune and neuronal cells have sexually divergent mechanisms that regulate pain (Agalave et al., 2021; Mogil, 2020; Szabo-Pardi et al., 2021). Specifically, female macrophages adopt a more anti-inflammatory, or M2, phenotype in response to infection and tissue injury (Keselman et al., 2017; Li et al., 2009). The intricate relationship these cells have with DRG nociceptors dictate changes in homeostatic balance, and dysregulation of feedback systems lead to rampant inflammation and maladaptive neuronal plasticity (Szabo-Pardi, 2021). As such, we cannot assume that downstream outcomes are similar between males and females. In a previous study, we had shown that 10 days after paclitaxel administration ATF3 expression is induced in DRG neurons (Agalave et al., 2021). These data indicate a stressed neuronal phenotype in response to paclitaxel, in both sexes. Unclear, however, was whether paclitaxel acts directly on nociceptors through TLR4, an alternative mechanism, or if bidirectional communication between infiltrated

macrophages and nociceptors exacerbates the injured neuronal phenotype. Thus, we designed an experiment to assess how macrophage activation by TLR4 in response to paclitaxel alters recruitment to the DRG, and how this affects neuronal injury in a sex-dependent manner. Our data suggests that removal of TLR4 from macrophages reduces their magnitude of infiltration in the DRGs, as well as upregulation of neuronal ATF3, in males but not females. Moreover, we demonstrate that direct activation of cultured macrophages by paclitaxel only induces elevated phagocytic behavior in males through TLR4-dependent mechanisms. Thus, we believe inflammatory cytokine signaling from TLR4 activation on macrophages induces neuronal ATF3 upregulation in males, however; females rely on a direct neuronal mechanism of cellular injury. This may be due, in part, to the ability of paclitaxel to interact with, and change the intrinsic excitability of transient receptor potential ankyrin 1 (TRPA1) channels on nociceptive sensory neurons (Zhang & Dougherty, 2014). Opening of TRPA1 channels can modulate action potentials during neuronal activation, and increasing excitability works to amplify afferent signals from nociceptive and sensory nerve fibers in the skin. Persistent signals from these fibers can activate intracellular machinery that leads to neuronal plasticity underlying chronic pain (Alles & Smith, 2018).

Loss of IENFs is a ubiquitous characteristic of neuropathic pain conditions. Decreases in IENF density are often correlated with neuropathy and neuronal hyperexcitability (Cheng et al., 2015). Administration of paclitaxel has been previously shown to reduce IENF density in the paw skin in males, which is often predictive of CIPN development (Boyette-Davis et al., 2011). Since then, many advances have been made in the field providing additional clarity as to the mechanisms that

regulate IENF loss. Specifically, DRG macrophages have been proven to facilitate IENF loss through rampant inflammation. Interestingly, blocking the actions of TLR4 with LPS-RS in the spinal cord prevents the loss of IENFs after paclitaxel treatment (Zhang et al., 2016). While this information provides valuable insights as to the role of glia and immune cells in CIPN, the results prove difficult to interpret since chemotactic signals in the periphery, such as C-C motif chemokine ligand 2 (CCL2), arise from sensory neurons in the DRG, as opposed to the spinal cord. However, ablation of peripheral macrophages using minocycline or clodronate-filled liposomes yields similar effects (Liu et al., 2010). The direct mechanisms involved in IENF loss are still poorly understood, however; expression of inflammatory cytokines has been shown to be robustly correlated with IENF loss (Wang et al., 2012). Exposure to chemotherapeutics increases levels of inflammatory cytokines such as tumor necrosis factor-α (TNFα), interleukin-1β (IL-1β), and interleukin-6 (IL-6), all of which are implicated in neuroinflammation and upregulation of cellular injury markers like ATF3 (Zaks-Zilberman et al., 2001). Many of these cytokines are produced as a result of nuclear factor kappa B (NF-κB) phosphorylation and nuclear localization, which is directly downstream of TLR4 activation by paclitaxel. Nevertheless, we believe it to be necessary to demonstrate the direct effects of TLR4 activation on peripheral macrophages to accurately assess their role in paclitaxel-induced neuropathy and IENF retraction. Our data suggests that removal of TLR4 from macrophages prevents the paclitaxel-induced loss of IENFs in the paw of males. Importantly, female IENF density is unaffected by removal of macrophage TLR4. Moreover, we demonstrate a strong positive correlation between CD68 and ATF3 expression in the DRG after paclitaxel treatment. This corroborates data previously published by our group, and others, that suggests DRG macrophages drive inflammation and neuronal plasticity during CIPN

106

(Agalave et al., 2021; Huang et al., 2014; Zhang et al., 2016). Interestingly, IENF density possesses a robust inverse correlation with these two markers and is modulated by macrophage TLR4 expression in males only. Therefore, we believe that preservation of IENFs by reducing macrophage TLR4 signaling in males may contribute to the reversal of mechanical hypersensitivity induced by paclitaxel. It is likely that one of the mechanisms by which this occurs is through mitochondrial dysfunction in DRG neurons, where paclitaxel-mediated dysregulation of mitochondrial transport and accumulation in axons is compounded by the inability of macrophages to shift towards an anti-inflammatory phenotype (Krukowski et al., 2015; Wanderley et al., 2018). Alternatively, it is possible that females utilize a direct method of nociceptor activation through TLR4, or an alternative mechanism, as it has been shown that paclitaxel increases expression of voltage-gated T-type calcium channels ($Ca_v3.2$) in the DRG which is linked to behavioral nociceptive phenotypes (Li et al., 2017). This, coupled with previously mentioned studies that indicate paclitaxel may also act through TRPA1 sensitization, provides a clear direction for future studies investing female-specific mechanisms of CIPN.

Despite the limitations, our study reveals novel insights involving the sex- and cell-specific mechanisms of paclitaxel-induced peripheral neuropathy, which may open new avenues of neuroimmune research and highlight novel treatment strategies. Overall, our data suggest that macrophages mediate neuroimmune interactions through activation of TLR4 by paclitaxel treatment in males, but not in females. While we observed macrophage TLR4-dependent changes in behavioral phenotypes and cellular physiology after paclitaxel treatment in males, females still exhibit the majority of treatment-induced effects in the absence of TLR4. This suggests that the mechanisms and cell types involved in engendering the nociceptive behavioral phenotypes,

107

neuronal injury and IENF retraction differ between sex. While our study begins to unravel the complex mechanisms behind sex differences in CIPN, more work is necessary to fully elucidate female-specific pathways.

CHAPTER 5

SENSORY NEURON TLR4 MEDIATES THE DEVELOPMENT OF NERVE-INJURY INDUCED MECHANICAL HYPERSENSITIVITY IN FEMALE MICE

Authors – Thomas A. Szabo-Pardi, Luz R. Barron, Melissa E. Lenert, Michael D. Burton

The Department of Neuroscience, BSB10.537

The University of Texas at Dallas

800 West Campbell Road

Richardson, Texas 75080-3021

ABSTRACT

Recent studies have brought to light the necessity to discern sex-specific differences in various pain states and different cell-types that mediate these differences. These studies have uncovered the role of neuroimmune interactions to mediate pain states in a sex-specific fashion. While investigating immune function in pain development, we discovered that females utilize immune components of sensory neurons to mediate neuropathic pain development. We utilized two novel transgenic mouse models that either restore expression of toll-like receptor (TLR) 4 in $Na_v1.8$ nociceptors on a TLR4-null background (TLR4^{LoxTB}) or remove TLR4 specifically from $Na_v1.8$ nociceptors (TLR4$^{fl/fl}$). After spared nerve injury (SNI), a model of neuropathic injury, we observed a robust female-specific onset of mechanical hypersensitivity in our transgenic animals. Female $Na_v1.8$-TLR4$^{fl/fl}$ knockout animals were less mechanically sensitive than *cre*-negative TLR4$^{fl/fl}$ littermates. Conversely, female $Na_v1.8$-TLR4^{LoxTB} reactivated animals were as mechanically sensitive as their wild-type counterparts. These sex and cell-specific effects were not recapitulated in male animals of either strain. Additionally, we find the danger associated molecular pattern, high mobility group box-1 (HGMB1), a potent TLR4 agonist, localization and ATF3 expression in females is dependent on TLR4 expression in dorsal root ganglia (DRG) populations following SNI. These experiments provide novel evidence toward sensory neuron specific modulation of pain in a sex-dependent manner.

INTRODUCTION

The CDC lists chronic pain as a leading cause of long-term disability, with current treatments remaining ineffective (Dahlhamer et al., 2018). Grim side effects have tallied over 600,000 opioid-

related deaths, with 64% of these cases linked to chronic pain patients since 2010 (Seth et al., 2018). These issues become more complex with females being more susceptible to certain forms of chronic pain (Joseph et al., 2003). Neuropathic pain results from disease or trauma to the nervous system, with injury-induced neuropathic pain estimated to occur in 20–50% of patients following routine operations (Kehlet, 2006). Sufferers often report a significantly reduced quality of life, and the prevalence of chronic pain continues to rise as the number of effective therapeutics remain limited (McDermott et al., 2006). Recent literature highlighting sexual dimorphisms in the onset and chronicity of pain states have begun to alter the way researchers and clinicians approach mechanisms in pain and potential therapeutics. Therefore, a dire need exists to bolster research efforts to identify crucial therapeutic time windows as well as novel and effective alternatives for the treatment and abatement of chronic pain. Here we hope to identify early time-points in the development of neuropathic pain that could represent a viable therapeutic window.

Toll-like receptors (TLRs) are pattern recognition receptors (PRRs) that initiate responses to infection and tissue injury that lead to inflammation and nocifensive behaviors (Hanamsagar et al., 2012; Nicotra et al., 2012; Xiang et al., 2015). TLR4 plays a pivotal role in chronic pain through the activation of pro-inflammatory cytokine production in non-neuronal cells. Pro-inflammatory mediators have been shown to directly sensitize neurons in the dorsal root ganglia (DRG) and exacerbate maladaptive plasticity (Ma et al., 2006). The dynamics of TLR4-mediated activation via microglia is well established where pharmacological inhibition of spinal TLR4 attenuates mechanical hypersensitivity in male, but not female mice (Sorge, 2011; Woller et al., 2016). Moreover, the role for T-cells regulating development of neuropathic pain in females has been

alluded to, however, recent evidence leads us to believe that nociceptive sensory neurons are the primary facilitators of chronic pain etiology (Lopes, 2017). Differential expression of genes involved in nociceptive pathways have been identified with females expressing upregulated genetic markers that correlate with increased inflammation, synaptic transmission, and extracellular matrix (ECM) reorganization (Mecklenburg et al., 2020; Wangzhou et al., 2021).

In the periphery, direct TLR4 stimulation is involved in dental pain via sensitization of trigeminal ganglion neurons (Diogenes et al., 2011), while TLR4 in dorsal root ganglia (DRG) cultures are implicated in chemotherapy-induced neuropathy (Li, Adamek, et al., 2015). Recent studies suggest that TLR4 on peripheral monocytes may play a role in female-specific nociceptive states (Huck et al., 2021), while others refute this claim (Peng, 2016; Yu, 2020). Due to its expression pattern in immune, mesenchymal, and neuronal cell populations, peripheral TLR4 signaling remains an elusive topic and important in both sexes. Importantly, the sex-specific role of TLR4 signaling in DRG neurons is unclear (Allette et al., 2014; Feldman et al., 2012; Hutchinson et al., 2008; Rudjito, 2020). In this study, we ask how endogenous TLR4 activation on peripheral nociceptors mediates the development of neuropathic pain.

Tissue injury upregulates danger-associated molecular patterns (DAMPs) (Man et al., 2015; Wan et al., 2016). High-mobility group box 1 (HMGB1) is a DAMP capable of initiating inflammatory cascades via TLR4 (Yamasoba et al., 2016). HMGB1 is a nuclear-bound redox sensitive cytokine, that is released from the cell upon activation, during tissue damage and changes to oxidative states; disulfide HMGB1 (dsHMGB1), is the predominant species that has affinity for TLR4 (Agalave &

112

Svensson, 2015; Yamasoba et al., 2016). Intrathecal administration of HMGB1 has been shown to produce robust mechanical allodynia (Agalave, 2020; O'Connor et al., 2003). Elevated levels of circulating HMGB1 promote activation and priming states of immune cells; however, its action on neurons that express TLR4 to elicit pain behavior has not been assessed (Bestall et al., 2018). The notion of neuronal TLR signaling remains contentious as emerging evidence suggests DRG macrophages are involved in communication with sensory neurons following nerve injury in both sexes (Yu et al., 2020). Interestingly, this does not relegate the fact that sensory neurons are activated and directly interact with immune cells (reverse communication). While the magnitude of neuropathic pain may not differ between sexes, the mechanisms which drive its development are clearly different. The timing and mode of communication between immune cells and neurons may help elucidate the mechanisms by which males and females differ.

Utilizing recently developed and validated transgenic models, we were able to specifically remove or reactivate TLR4 on $Na_v1.8^+$ nociceptors in a cre dependent fashion (Jia et al., 2021; Jia et al., 2014). We identified a distinct neuronal-mediated pathway in female mice which contributes to the early onset of peripheral nerve injury-induced mechanical hypersensitivity in addition to uncovering a direct mechanism of neuronal sensitization. We demonstrated that TLR4, expressed specifically on $Na_v1.8^+$ peripheral nociceptors, is responsible for mechanical hypersensitivity during the onset of peripheral nerve injury in female, but not male mice. Additionally, HMGB1 localization and autocrine signaling via these nociceptors, as well as paracrine action on large diameter sensory neurons in the DRG, contribute to pain sensitization in female mice. We believe TLR4 activation on $Na_v1.8^+$ nociceptors is one mechanism of pain sensitization unique to females.

MATERIALS AND METHODS

Animals

All animal experiments were carried out in accordance with protocols approved by the Institutional Animal Care and Use Committee of the University of Texas at Dallas. Mice were housed (4–5 per cage) in a temperature-controlled facility and maintained on a 12-hour light/dark cycle (lights on: 7am/ lights off 7 pm). Mice had *ad-libitum* access to food and water and were eight to twelve-weeks-old during the experiments (male, 25–30 g: female 20–25 g). Transgenic mice expressing Cre recombinase under control of the Scn10a (Na$_v$1.8) promoter were obtained initially from Professor John Wood (University College London), but are commercially available from Ifrafrontier (EMMA ID: 04582). Characterization of these mice showed that heterozygous cre animals have no pain phenotype and normal electrophysiological properties (Stirling et al., 2005). Genetically modified TLR4 floxed animals (has loxP sites flanking exon 2 and 3; TLR4$^{fl/fl}$) (Jia et al., 2014)and TLR4 null-reactivatable animals (has a transcriptional blocker inserted into the TLR4 gene in between exon 2 and 3; TLR4^{LoxTB}) (Jia et al., 2021) were a gift from Joel K. Elmquist, (UT Southwestern Medical Center) were bred with Na$_v$1.8^{cre} animals in-house (Na$_v$1.8cre × TLR4$^{fl/fl}$, TLR4$^{fl/fl}$, Na$_v$1.8cre × TLR4^{LoxTB}, TLR4^{LoxTB}) and used for all behavioral and biochemical assays (Jia et al., 2021; Jia et al., 2014). All cell-specific knockout (Na$_v$1.8$^{TLR4fl/fl}$) or cell-specific reactivated (Na$_v$1.8^{TLR4LoxTB}) mice are heterozygous for the Na$_v$1.8-cre (Na$_v$1.8^{cre}) and are homozygous for the TLR4$^{fl/fl}$ or TLR4^{LoxTB} gene, respectively. Phenotypically normal littermates lack Na$_v$1.8^{cre} and are homozygous for the TLR4$^{fl/fl}$ gene. Whole-body null or knockout mice (TLR4$^{TB/TB}$) lack Na$_v$1.8^{cre} and are homozygous for the TLR4^{LoxTB} gene. We purchased ROSA26^{LSLtdtomato} (tdtomato) animals from Jackson lab (stock no. 007909) and crossed them with

Nav1.8^{cre} animals (Nav1.8^{tdT+}) for reporter, IHC, and flow cytometry experiments. All strains were backcrossed at least eight generations to maintain C57BL/6J genetic background with animals from Jackson Lab (stock no. 000664). We used in-house bred C57BL/6J animals as wild-type (WT) controls.

Surgical procedures

The spared nerve injury (SNI) model of neuropathic pain was used. Mice were anesthetized under isoflurane anesthesia (1.0–2.5%). The ipsilateral thigh was shaved and cleaned with betadine (Dynarex, 1425) and 70% ethanol (Decon Labs, 2701). The skin and muscle of the left thigh were incised with a #11 scalpel blade (Thermo, 22–079-691) and the sciatic nerve along with its three branches (common peroneal, tibial, and sural) was exposed. A tight ligature using a 5–0 silk suture (VWR, MV-682) was placed around the proximal tibial and common peroneal branches, after which the nerve distal to the ligature was transected, taking care to not stretch or damage the sural nerve (Decosterd, 2000). Sham surgeries were done identically to the SNI surgery; however, no portion of the sciatic nerve was ligated or transected. The skin was closed using an auto clip (Fine Science Tools, 12022-09) and mice were then given a subcutaneous injection of 5 mg/mL Gentamicin (Sigma, G1272) as a preventative antibiotic and returned to their home cages to recover (Decosterd, 2000). Mice were monitored daily for the duration of the experiment. Mechanical hypersensitivity and cold allodynia were then assessed on postoperative days 1, 3, 5 and 7. Baseline values were taken 24 h prior to surgery.

Behavioral testing

To measure mechanical hypersensitivity, mice were individually placed on an elevated wire grid inside acrylic behavior racks and allowed to habituate for approximately 2 h. The ipsilateral hind paw was then stimulated with von Frey filaments (Stoelting, 58011) using the up-down experimental paradigm (Chaplan, 1994). To assess cold allodynia in our SNI model, mice were individually placed on the same elevated wire grid and behavior racks and allowed to habituate for approximately 2 h before testing. Approximately 100 μL of biology grade acetone (Fisher, AI6P-4) was then applied to the ipsilateral hind paw using a 1 mL syringe (VWR, 309659) attached to a 25 G needle (VWR, 305125). Latency of behavioral response over a 60 s period was measured (Yoon, 1994). Behavior racks were cleaned with a 1:3 ratio of a plant-based deodorant-free cleaner (Seventh Generation[TM], 22719BK-5) to eliminate odor cues between each reading, baseline, and experiment. Baseline values were taken 24 h prior to performing surgery. Mechanical hypersensitivity and cold allodynia were then measured on postoperative days 1, 3, 5, and 7. Mechanical measures were always taken before thermal. All behavioral testing was done between 10 a.m. and 2:00p.m. All behavior data sets are additionally represented as effect sizes. It is determined by calculating the cumulative difference between the value for each time point and the baseline value (Agalave et al., 2021; Hassler et al., 2020). Behavioral experiments were performed by T.A.S., L.R.B., and M.D.B. Experimenters were blinded to genotype, surgical condition, or both.

Immunohistochemistry

Three days post SNI, mice were anesthetized using 100% isoflurane and were subsequently euthanized via decapitation. Dorsal root ganglia (L3-5) were extracted and post-fixed in 4%

paraformaldehyde made in $1 \times$ phosphate buffered saline (PBS) (Sigma, 158127) for 4 h and then cryoprotected for 48 h in a 30% sucrose (Sigma, S0389) solution made in $1 \times$ (PBS). Frozen tissues (DRGs: 16 µm) were then transversally sectioned on a cryostat and mounted onto SuperFrost Plus (Fisher, 12–544-7) charged microscope slides. Slides were then allowed to dry for 1 h before being placed in the $-80°$ C freezer overnight. Slides were then rehydrated in $1 \times$ PBS for 5 min before being incubated in a blocking/permeabilization solution consisting of: $1 \times$ PBS, 2% heat-inactivated normal goat serum (Sigma, G9023), 1% bovine serum albumin (Sigma, A9576-50ML) 0.1% Triton (Sigma, X100), 0.05% Tween-20 (Sigma, P1379) and 0.05% sodium azide (Ricca Chemical, R7144800). Slides were then incubated overnight at $4°$ C in a primary antibody cocktail diluted in blocking/permeabilization solution. The following day slides were washed three times for 5 min each in $1 \times$ PBS + 0.05% Tween-20 and incubated for 2 h at room temperature in their respective secondary antibodies diluted in blocking/permeabilization solution. Slides were then washed three times for 5 min each in $1 \times$ PBS + 0.05% Tween-20 and mounted using Prolong gold (Thermo, P36974) mounting media and a 1.5 mm glass coverslip (Thermo, 08–774-384). Slides were stored at $4°$ C until imaging. Images used for analysis and quantification were taken on a Zeiss Axiobserver 7 epifluorescent Microscope at 20x. Representative images were taken at 20x (ATF3 and tdTomato images) or 40x (HMGB1 images) using an Olympus FluoView 3000 RS confocal microscope. Analysis of images was done using ImageJ Version 1.48 (National Institutes of Health, Bethesda, MD) for Mac OS X (Apple). Immunohistochemistry (IHC) experiments and analyses were performed by T.A.S., and L.R.B. Experimenters were blinded to sex, genotype, and surgical condition. For a complete list of antibodies used refer to Table 1.

Flow cytometry

Flow cytometric analysis of isolated DRGs was performed based on previous protocols with some modifications (Chiu et al., 2014). In brief, ipsilateral and contralateral DRGs (L3-4) were collected in ice cold sterile $1 \times$ DPBS (Hyclone, SH30028). Samples were centrifuged at $400 \times g$ for 3 min. Supernatants were removed and samples were treated with Collagenase A (Sigma, 10103586001) and incubated in a 37 °C water bath for 20 min. Samples were then centrifuged at $400 \times g$ for 3 min. Supernatants were removed and the samples were treated with Collagenase D (Sigma, 1188866001) and a 10% v/v of papain (Roche, 10108014001) in HBSS for another 20 min. Cells were centrifuged at $400 \times g$ and the pellet were resuspended in Enzyme T (Sigma, 10109886001) (soybean trypsin inhibitor made in 1:1 bovine serum albumin and DMEM/F12 media (Thermo, 10565161) supplemented with 10% fetal bovine serum (FBS) (Hyclone, SH30088.03) and 1% pen/strep (Sigma, P4333)) to stop the enzymatic reaction. Digested tissues were triturated using a 1 mL fire-polished Pasteur pipette tip and passed through a 70-µm nylon mesh cell strainer (Sigma, CLS431751-50EA), with a subsequent wash using flow buffer (0.5% bovine serum albumin with 0.02% glucose (Sigma, G7528) made in $1 \times$ DPBS). Resultant suspension was centrifuged at $400 \times g$ for 3 min and resuspended in flow blocking buffer (anti-CD16/32 purified antibody diluted in flow buffer) for 20 min to block fc receptors. Samples were incubated with pre-conjugated extracellular flow antibodies (CD45 & TLR4) for 45 min. Samples were then washed with flow buffer, then centrifuged at $400 \times g$ for 3 min and resuspended in a fixation/permeabilization buffer (BD Biosciences, 555028) for 45 min. Samples were then centrifuged at $400 \times g$ for 3 min and were washed twice using the manufacturer provided wash buffer ($1 \times$). Samples were incubated with pre-conjugated intracellular flow antibodies (NeuN)

for 60 min and washed with DAPI for 5 min. Samples were then centrifuged at $400 \times g$ for 3 min and were washed twice using wash buffer and were then resuspended in flow buffer. Appropriate compensation controls and isotypes were used for determination and gating. After gating DAPI positive cells (to determine debris), immune cells were identified with gating for CD45 and were further gated to identify expression of TLR4. Neurons were initially identified with gating for NeuN and were further gated to identify expression of TLR4. Stained samples were analyzed using a Special Order (4-laser) Becton-Dickinson Fortessa analyzer (Red Oaks, CA) and data were analyzed using FlowJo and FCS Express software (De Novo Software, Los Angeles, CA). Flow cytometry experiments and analyses were performed by T.A.S., M.E.L., and M.D.B. Experimenters were blinded to genotype and surgical condition. For a complete list of antibodies used refer to Table 1.

Statistical analysis

Prism 8.01 software (GraphPad, San Diego, CA, USA) was utilized to generate all graphs and statistical analysis. Behavioral data was analyzed using repeated measures Two-Way ANOVA with Tukey's *post hoc* tests. Effect size, immunohistochemical, and flow cytometric data were analyzed using Ordinary Two-Way ANOVA with Tukey's *post hoc* tests. All data are represented as the standard error of the mean (SEM). A *p*-value of < 0.05 was used to determine statistical significance. All statistical values and corresponding tests can be found in Table 2, Table 3, Table 4, Table 5, Table 6, and Table 7. All behavioral, immunohistochemical, and flow cytometric experiments and analyses were performed by blinded experimenters.

Table 5.1. Information for antibodies used in experiments.

Antibody	Company	Catalog number	Working dilution
Antibodies used for IHC			
Anti-Nav1.8 sodium channel	Neuromab	75-166	0.388888889
Anti-Neurofilament 200	Millipore Sigma	MAB5266	0.736111111
Anti-HMGB1	Abcam	AB79823	0.388888889
Anti-ATF3	Abcam	AB207434	0.388888889
Goat anti-mouse Alexa Fluor 488	Invitrogen	A21131	0.736111111
Goat anti-mouse Alexa Fluor 647	Invitrogen	A21240	0.736111111
Goat anti-rabbit Alexa Fluor 568	Invitrogen	A11011	0.736111111
Antibodies used for flow			
Anti-CD45 Super Bright 645 conjugate	eBioscience	64-0451-82	0.180555556
Anti-TLR4/MD-2 Complex APC conjugate	eBioscience	17-9924-82	0.180555556
Anti-CD16/32	eBioscience	16016185	0.736111111
Anti-NeuN Alexa Fluor 488 conjugate	Millipore Sigma	MAB377X	0.180555556

RESULTS

The severity of mechanical hypersensitivity and cold allodynia in a neuropathic pain model is similar between males and females, but protein expression levels in the lumbar DRG are different

To establish if any sexual dimorphisms exist in the magnitude of pain following neuropathic injury, SNI was performed on both male and female WT mice. No significant differences were found between male and female SNI groups in either mechanical hypersensitivity or cold allodynia (Fig. 5.1A-D, Table 5.2). Emerging evidence suggests that the mechanisms that mediate neuronal sensitization during the early onset of neuropathic pain differ between sexes (Ross et al., 2018;

Tajerian et al., 2015). Myeloid-derived immune cells are strongly implicated in driving the early onset of pain following injury, however; differences between sexes in direct neuronal sensitization in the lumbar DRG are poorly understood (Peng et al., 2016). To test the hypothesis that neuronal injury after SNI is different between males and females we first utilized our $Na_v1.8^{tdT}$ reporter line to verify colocalization between our $Na_v1.8$ antibody and cre-mediated tdTomato expression in $Na_v1.8^+$ nociceptors. Naïve male and female $Na_v1.8^{tdT}$ lumbar DRGs (L3-5) were immunoassayed with $Na_v1.8$ and NF200 antibody (Fig. .1E, Table 5.2). They were then assessed for colocalization with tdTomato. We found there to be a high degree of colocalization (75%) between $Na_v1.8$ antibody and tdTomato expression (Fig. 5.1F, Table 5.2). This indicates robust specificity of the $Na_v1.8$ antibody with endogenous expression of tdTomato. Next, we used histochemical markers to identify small ($Na_v1.8$) and large (NF200) diameter nociceptors in the DRG (L3-5) of male and female WT mice. We then examined HMGB1 cytosolic localization and ATF3 expression in these distinct neuronal populations 3 days post SNI (Fig. 5.1G-J, Table 5.2). We discovered a sexual dimorphism where both male and female small diameter nociceptors ($Na_v1.8^+$) exhibit significantly elevated expression of ATF3 3 days post SNI, but females have significantly more ATF3 expressed as compared to males. (Fig. 5.1K, Table 5.2). Both males and females have significantly increased ATF3 expression in their large diameter sensory neurons (NF200$^+$) 3 days post SNI as compared to sham controls (Fig. 5.1L, Table .2). It is evident that these neuronal subpopulations exhibit signs of cellular injury in both males and females after SNI. We then measured cellular localization of HMGB1 in these neuronal subpopulations. Only female WT mice exhibit significantly elevated cytosolic localization of HMGB1 3 days post SNI in their $Na_v1.8^+$ nociceptors as compared to sham controls (Fig. 5.1M, Table 5.2). Additionally, only

female WT mice exhibit significantly elevated cytosolic localization of HMGB1 3 days post SNI in their NF200^{+} neurons as compared to sham controls (Fig. 5.1N, Table 5.2). Taken together, our data reveals an inherent sexual dimorphism in both inflammatory signaling and neuronal injury in the context of neuropathic pain. This simple, yet enlightening finding pushed us to further investigate the dichotomy of sex and cell-specific sensitization in the peripheral nervous system.
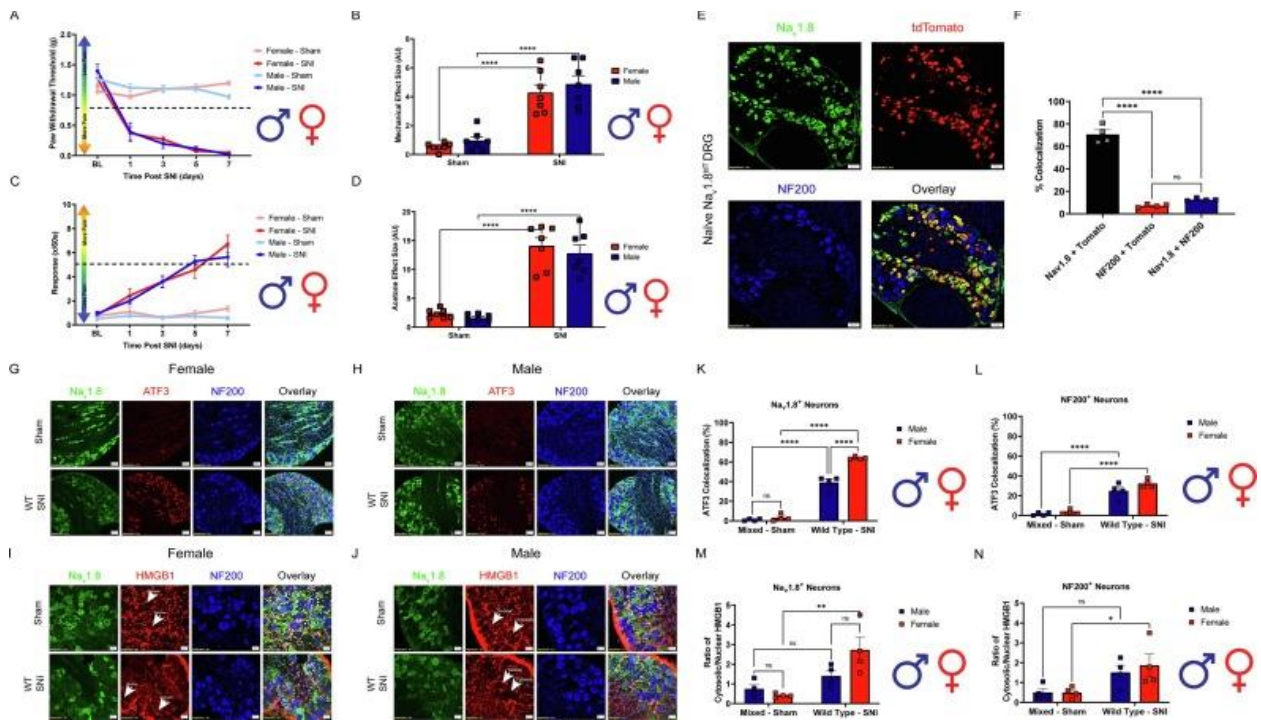
Figure 5.1. The magnitude of pain after SNI does not differ between sexes following SNI, however; the mechanisms during its onset at the level of the lumbar (L3-5) DRGs are. Spared-nerve injury was performed on the left hindlimb of male and female mice. *A,* Hind paw mechanical withdrawal thresholds were measured prior to surgery and on days: 1, 3, 5, and 7 post-surgery in both male and female sham (n = 7) and SNI (n = 7) wild type mice. *B,* Data for males and females combined shown as mechanical effect size. *C,* Hind paw response to application of acetone were measured prior to surgery and on days: 1, 3, 5, and 7 post-surgery in both male and female sham (n = 7) and SNI (n = 7) mice. *D,* Data for males and females combined shown as acetone effect size. *E,* Naïve $Na_v1.8^{tdT}$ female and male lumbar (L3-5) DRGs were immunostained with $Na_v1.8$ (green), tdTomato (red) and NF200 (Blue); representative images from n = 4 mice). Scale bar: 50 µm. Magnification: 20x. *F,* Quantification of colocalization between $Na_v1.8$, tdTomato and NF200 (n = 4). *G-H* Female and male WT lumbar DRGs (L3-5) were immunostained 3D post SNI with DAPI (teal), $Na_v1.8$ (green), ATF3 (red) and NF200 (blue; representative images from n = 4 mice). Scale bar: 50 µm. Magnification: 20x. *K,* Quantification of ATF3 colocalization with

122

Na$_v$1.8$^+$ neurons of both sexes 3 days after SNI (n = 4 per group). *L,* Quantification of ATF3 colocalization with NF200$^+$ neurons of both sexes 3 days after SNI (n = 4 per group). *I-J,* Female, and male WT lumbar DRGs (L3-5) were immunostained 3D post SNI with DAPI (teal), Na$_v$1.8 (green), HMGB1 (red) and NF200 (blue; representative images from n = 4 mice). White arrows point to an example of nuclear or cytosolic localization of HMGB1. Scale bar: 20 µm. Magnification: 40x. *M,* Quantification of HMGB1 cytosolic localization in Na$_v$1.8$^+$ neurons of both sexes 3 days after SNI (n = 4 per group). *N,* Quantification of HMGB1 cytosolic localization in NF200$^+$ neurons of both sexes 3 days after SNI (n = 4 per group). *p < 0.05; **p < 0.01; ****p < 0.0001. BL = Baseline. (For interpretation of the references to colour in this figure legend, the reader is referred to the web version of this article.)

Table 5.2. Statistical values corresponding to the data in Figure 5.1.

Tukey's multiple comparisons test	Mean Diff.	95.00% CI of diff.	Below threshold?	Summary	Adjusted P Value
Colocalization					
Nav1.8 + Tomato vs. NF200 + Tomato	63.56	54.33 to 72.78	Yes	****	<0.0001
Nav1.8 + Tomato vs. Nav1.8 + NF200	58.16	48.93 to 67.39	Yes	****	<0.0001
NF200 + Tomato vs. Nav1.8 + NF200	-5.395	-14.62 to 3.831	No	ns	0.2819
Nav1.8 HMGB1 Colocalization					
Mixed - Sham:Male vs. Mixed - Sham:Female	0.33	-1.186 to 1.846	No	ns	0.9148
Mixed - Sham:Male vs. Wild Type - SNI:Male	-0.66	-2.176 to 0.8558	No	ns	0.5843
Mixed - Sham:Male vs. Wild Type - SNI:Female	-1.98	-3.496 to -0.4642	Yes	*	0.0102
Mixed - Sham:Female vs. Wild Type - SNI:Male	-0.99	-2.506 to 0.5258	No	ns	0.2634
Mixed - Sham:Female vs. Wild Type - SNI:Female	-2.31	-3.826 to -0.7942	Yes	**	0.0034
Wild Type - SNI:Male vs. Wild Type - SNI:Female	-1.32	-2.836 to 0.1958	No	ns	0.0959
Nav1.8 ATF3 Colocalization					
Mixed - Sham:Male vs. Mixed - Sham:Female	-2	-10.18 to 6.176	No	ns	0.8847
Mixed - Sham:Male vs. Wild Type - SNI:Male	-38	-46.18 to -29.82	Yes	****	<0.0001
Mixed - Sham:Male vs. Wild Type - SNI:Female	-63	-71.18 to -54.82	Yes	****	<0.0001
Mixed - Sham:Female vs. Wild Type - SNI:Male	-36	-44.18 to -27.82	Yes	****	<0.0001

Mixed - Sham:Female vs. Wild Type - SNI:Female	-61	-69.18 to -52.82	Yes	****	<0.0001
Wild Type - SNI:Male vs. Wild Type - SNI:Female	-25	-33.18 to -16.82	Yes	****	<0.0001
NF200 HMGB1 Colocalization					
Male	-1.013	-2.288 to 0.2630	No	ns	0.1267
Female	-1.38	-2.656 to -0.1045	Yes	*	0.0341
NF200 ATF3 Colocalization					
Male	-23.25	-31.81 to -14.69	Yes	****	<0.0001
Female	-28.75	-37.31 to -20.19	Yes	****	<0.0001
Mechanical Behavior					
BL					
Male Sham vs. Male SNI	-0.1337	-0.5438 to 0.2764	No	ns	0.7619
Male Sham vs. Female Sham	0.1984	-0.08117 to 0.4781	No	ns	0.1918
Male Sham vs. Female SNI	-0.001043	-0.4333 to 0.4312	No	ns	>0.9999
Male SNI vs. Female Sham	0.3321	-0.05009 to 0.7143	No	ns	0.0898
Male SNI vs. Female SNI	0.1326	-0.3485 to 0.6138	No	ns	0.8444
Female Sham vs. Female SNI	-0.1995	-0.6082 to 0.2092	No	ns	0.4393
1					
Male Sham vs. Male SNI	0.7314	0.2025 to 1.260	Yes	**	0.0093
Male Sham vs. Female Sham	0.1479	-0.08396 to 0.3798	No	ns	0.2586
Male Sham vs. Female SNI	0.7536	0.3829 to 1.124	Yes	***	0.0004
Male SNI vs. Female Sham	-0.5835	-1.109 to -0.05840	Yes	*	0.0317
Male SNI vs. Female SNI	0.02214	-0.5343 to 0.5786	No	ns	0.9993
Female Sham vs. Female SNI	0.6057	0.2531 to 0.9582	Yes	**	0.003
3					
Male Sham vs. Male SNI	0.9052	0.6015 to 1.209	Yes	****	<0.0001
Male Sham vs. Female Sham	0.0008	-0.2449 to 0.2465	No	ns	>0.9999
Male Sham vs. Female SNI	0.8335	0.5845 to 1.083	Yes	****	<0.0001
Male SNI vs. Female Sham	-0.9044	-1.179 to -0.6299	Yes	****	<0.0001
Male SNI vs. Female SNI	-0.07171	-0.3488 to 0.2053	No	ns	0.857
Female Sham vs. Female SNI	0.8327	0.6361 to 1.029	Yes	****	<0.0001
5					

Male Sham vs. Male SNI	0.9866	0.8022 to 1.171	Yes	****	<0.0001
Male Sham vs. Female Sham	-0.02881	-0.2286 to 0.1710	No	ns	0.9725
Male Sham vs. Female SNI	1.026	0.8538 to 1.198	Yes	****	<0.0001
Male SNI vs. Female Sham	-1.015	-1.195 to -0.8363	Yes	****	<0.0001
Male SNI vs. Female SNI	0.03921	-0.1008 to 0.1792	No	ns	0.832
Female Sham vs. Female SNI	1.055	0.8890 to 1.220	Yes	****	<0.0001
7					
Male Sham vs. Male SNI	0.9506	0.8375 to 1.064	Yes	****	<0.0001
Male Sham vs. Female Sham	-0.2262	-0.3642 to -0.08825	Yes	**	0.0019
Male Sham vs. Female SNI	0.9186	0.8033 to 1.034	Yes	****	<0.0001
Male SNI vs. Female Sham	-1.177	-1.290 to -1.063	Yes	****	<0.0001
Male SNI vs. Female SNI	-0.03207	-0.09057 to 0.02642	No	ns	0.3642
Female Sham vs. Female SNI	1.145	1.029 to 1.260	Yes	****	<0.0001
Acetone Behavior					
BL					
Male Sham vs. Male SNI	-0.4286	-1.233 to 0.3761	No	ns	0.4227
Male Sham vs. Female Sham	-0.24	-0.8906 to 0.4106	No	ns	0.6857
Male Sham vs. Female SNI	-0.3029	-1.291 to 0.6855	No	ns	0.7891
Male SNI vs. Female Sham	0.1886	-0.5352 to 0.9124	No	ns	0.8519
Male SNI vs. Female SNI	0.1257	-0.8935 to 1.145	No	ns	0.9817
Female Sham vs. Female SNI	-0.06286	-1.007 to 0.8810	No	ns	0.9964
1					
Male Sham vs. Male SNI	-1.241	-2.353 to -0.1296	Yes	*	0.0293
Male Sham vs. Female Sham	-0.3271	-1.610 to 0.9561	No	ns	0.8437
Male Sham vs. Female SNI	-1.674	-3.673 to 0.3240	No	ns	0.1
Male SNI vs. Female Sham	0.9143	-0.5426 to 2.371	No	ns	0.2917
Male SNI vs. Female SNI	-0.4329	-2.484 to 1.619	No	ns	0.9116
Female Sham vs. Female SNI	-1.347	-3.445 to 0.7508	No	ns	0.2647
3					
Male Sham vs. Male SNI	-2.963	-4.654 to -1.272	Yes	**	0.0027
Male Sham vs. Female Sham	-0.004286	-0.5961 to 0.5876	No	ns	>0.9999
Male Sham vs. Female SNI	-2.976	-4.562 to -1.389	Yes	**	0.0017
Male SNI vs. Female Sham	2.959	1.269 to 4.649	Yes	**	0.0031
Male SNI vs. Female SNI	-0.01286	-2.010 to 1.984	No	ns	>0.9999

Female Sham vs. Female SNI	-2.971	-4.556 to -1.387	Yes	**	0.002
5					
Male Sham vs. Male SNI	-4.576	-6.231 to -2.920	Yes	***	0.0001
Male Sham vs. Female Sham	-0.2386	-1.214 to 0.7372	No	ns	0.8808
Male Sham vs. Female SNI	-3.864	-6.238 to -1.491	Yes	**	0.0044
Male SNI vs. Female Sham	4.337	2.647 to 6.027	Yes	****	<0.0001
Male SNI vs. Female SNI	0.7114	-1.824 to 3.247	No	ns	0.8305
Female Sham vs. Female SNI	-3.626	-6.007 to -1.245	Yes	**	0.0056
7					
Male Sham vs. Male SNI	-5.054	-7.874 to -2.235	Yes	**	0.0028
Male Sham vs. Female Sham	-0.7643	-1.607 to 0.07836	No	ns	0.0796
Male Sham vs. Female SNI	-6.14	-8.668 to -3.612	Yes	***	0.0005
Male SNI vs. Female Sham	4.29	1.472 to 7.108	Yes	**	0.0064
Male SNI vs. Female SNI	-1.086	-4.352 to 2.181	No	ns	0.7586
Female Sham vs. Female SNI	-5.376	-7.903 to -2.848	Yes	***	0.0009
Mechanical Effect Size					
Female	-3.743	-5.170 to -2.316	Yes	****	<0.0001
Male	-3.914	-5.341 to -2.488	Yes	****	<0.0001
Acetone Effect Size					
Female	-11.76	-15.16 to -8.358	Yes	****	<0.0001
Male	-11.21	-14.61 to -7.816	Yes	****	<0.0001

Sensory neuron and immune cell expression of TLR4

To investigate baseline and surgery-induced levels of TLR4 on DRG cell populations, ipsilateral and contralateral DRGs (L3-L5) were isolated from males and females 3 days post SNI (Chiu et al., 2014). Moreover, we verified protein expression of our null-re-expression animals when we added whole-body null (TLR4^{LoxTB}) and cell-specific re-expression (Na$_v$1.8^{TLR4LoxTB}) groups to the study. Neuronal (NeuN$^+$) and immune cell (CD45$^+$) populations were identified and assessed for TLR4 at various stages and genotypes (Fig. 5.2A). We determined that there were no significant

sex or surgery-induced differences in TLR4 protein expression patterns in DRG neurons in ipsilateral DRGs, compared to contralateral DRGs, with roughly 30% of the neurons expressing TLR4 in males and females (Fig. 5.2B & 2C; Table 5.3). We saw that our whole-body null animals expressed minimum amounts of TLR4 across the neuronal populations, as expected (Fig. 5.2B & 2C; Table 5.3). Opposingly, we observed a male-driven sex-dependent upregulation of ipsilateral TLR4 expression in CD45^{+} immune cells 3 days post SNI (Fig. 5.2E; Table 5.3), but no female differences. This data juxtaposes recent findings of no sex-differences in DRG immune cells after neuropathic injury (Yu et al., 2020). Apparently, it is imperative to understand not only the cell population amount, but the expression pattern of those cells in the DRG.
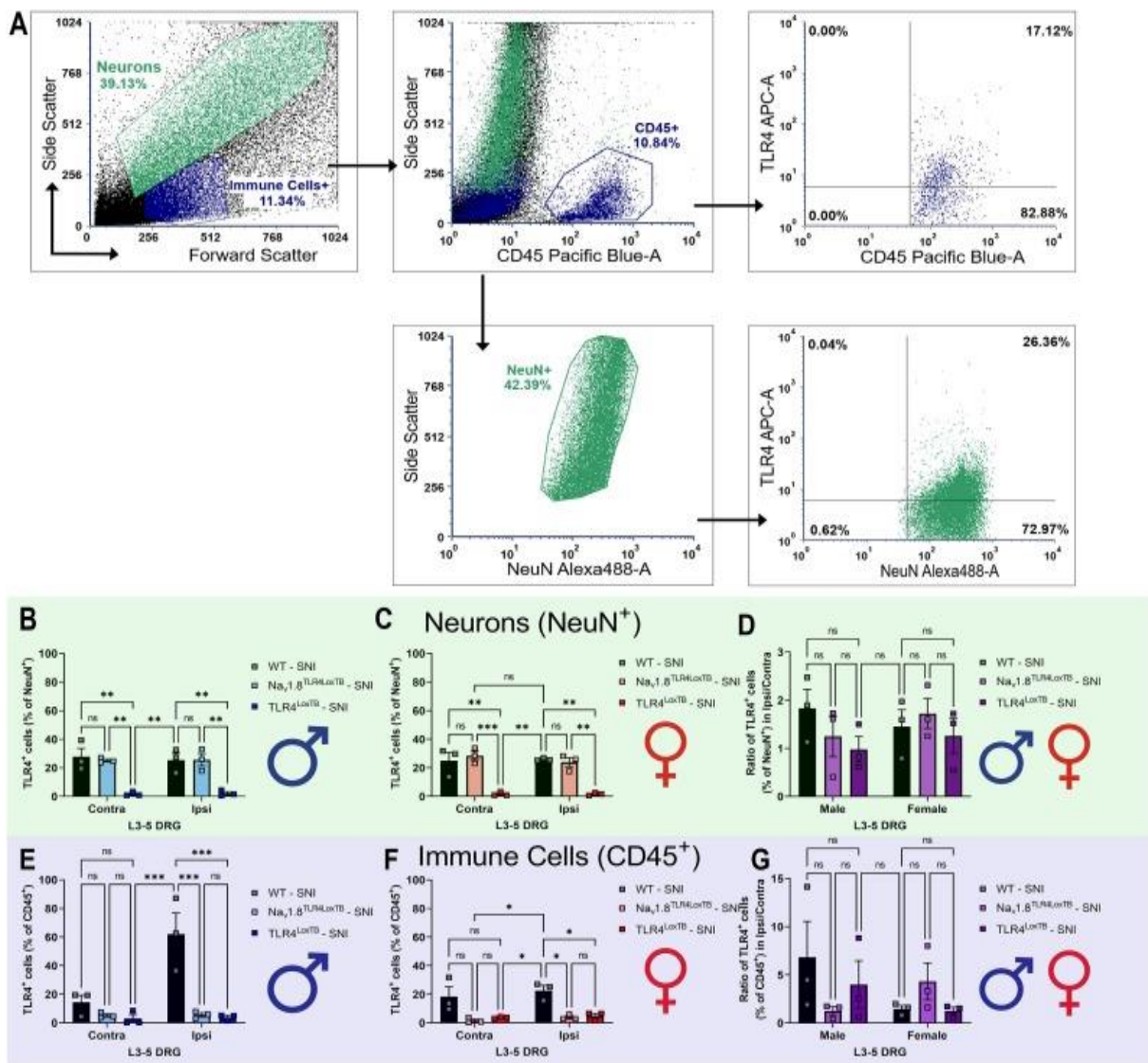
Figure 5.2. There are no basal or surgery-induced sex differences in TLR4 expression in sensory neurons and a surgery-induced upregulation of TLR4 in DRG immune cells 3D post SNI. *A,* Lumbar DRGs (L3-5) were enzymatically dissociated, stained with TLR4, NeuN, and DAPI and subjected to flow cytometry. After gating on both neurons and immune cells based on forward and side scatter, NeuN$^+$ and CD45$^+$ cells were further gated to TLR4$^+$ populations. *B,* NeuN$^+$/TLR4$^+$ cells in control (contra) and surgerized DRGs (ipsi) 3D post SNI in males. *C,* NeuN$^+$/TLR4$^+$ cells in control (contra) and surgerized DRGs (ipsi) 3D post SNI in females. *D,* Combined male and female data; ratio of ipsilateral-to-contralateral NeuN$^+$/TLR4$^+$ DRG cells 3D post SNI. *E,* CD45$^+$/TLR4$^+$ cells in control (contra) and surgerized DRGs (ipsi) 3D post SNI in males. *F,* CD45$^+$/TLR4$^+$ cells in control (contra) and surgerized DRGs (ipsi) 3D post SNI in females. *G,* Combined male and female data; ratio of ipsilateral-to-contralateral CD45$^+$/TLR4$^+$ DRG cells 3D post SNI. Asterisks on the bar graphs indicate significant differences between the groups. $*p < 0.05$; $**p < 0.01$; $***p < 0.001$, (n = 3–4).

128

Table 5.3. Statistical values corresponding to the data in Figure 5.2.

Tukey's multiple comparisons test	Mean Diff.	95.00% CI of diff.	Below threshold?	Summary	Adjusted P Value
Males					
Contra:WT - SNI vs. Contra:Na$_v$1.8^{TLR4LoxTB} - SNI	9.147	-21.62 to 39.91	No	ns	0.9097
Contra:WT - SNI vs. Contra:TLR4^{LoxTB} - SNI	11.43	-19.34 to 42.19	No	ns	0.8062
Contra:WT - SNI vs. Ipsi:WT - SNI	-47.69	-78.45 to -16.93	Yes	**	0.0023
Contra:WT - SNI vs. Ipsi:Na$_v$1.8^{TLR4LoxTB} - SNI	8.777	-21.99 to 39.54	No	ns	0.9226
Contra:WT - SNI vs. Ipsi:TLR4^{LoxTB} - SNI	10.53	-20.23 to 41.30	No	ns	0.8513
Contra:Na$_v$1.8^{TLR4LoxTB} - SNI vs. Contra:TLR4^{LoxTB} - SNI	2.28	-28.48 to 33.04	No	ns	0.9998
Contra:Na$_v$1.8^{TLR4LoxTB} - SNI vs. Ipsi:WT - SNI	-56.84	-87.60 to -26.07	Yes	***	0.0005
Contra:Na$_v$1.8^{TLR4LoxTB} - SNI vs. Ipsi:Na$_v$1.8^{TLR4LoxTB} - SNI	-0.37	-31.13 to 30.39	No	ns	>0.9999
Contra:Na$_v$1.8^{TLR4LoxTB} - SNI vs. Ipsi:TLR4^{LoxTB} - SNI	1.387	-29.38 to 32.15	No	ns	>0.9999
Contra:TLR4^{LoxTB} - SNI vs. Ipsi:WT - SNI	-59.12	-89.88 to -28.35	Yes	***	0.0003
Contra:TLR4^{LoxTB} - SNI vs. Ipsi:Na$_v$1.8^{TLR4LoxTB} - SNI	-2.65	-33.41 to 28.11	No	ns	0.9996
Contra:TLR4^{LoxTB} - SNI vs. Ipsi:TLR4^{LoxTB} - SNI	-0.8933	-31.66 to 29.87	No	ns	>0.9999
Ipsi:WT - SNI vs. Ipsi:Na$_v$1.8^{TLR4LoxTB} - SNI	56.47	25.70 to 87.23	Yes	***	0.0005
Ipsi:WT - SNI vs. Ipsi:TLR4^{LoxTB} - SNI	58.22	27.46 to 88.99	Yes	***	0.0004
Ipsi:Na$_v$1.8^{TLR4LoxTB} - SNI vs. Ipsi:TLR4^{LoxTB} - SNI	1.757	-29.01 to 32.52	No	ns	>0.9999
Females					
Contra:WT - SNI vs. Contra:Na$_v$1.8^{TLR4LoxTB} - SNI	16.78	-0.08247 to 33.64	No	ns	0.0517
Contra:WT - SNI vs. Contra:TLR4^{LoxTB} - SNI	14.69	-2.169 to 31.55	No	ns	0.1189
Contra:WT - SNI vs. Ipsi:WT - SNI	-4.153	-21.01 to 12.71	No	ns	>0.9999
Contra:WT - SNI vs. Ipsi:Na$_v$1.8^{TLR4LoxTB} - SNI	14.56	-2.299 to 31.42	No	ns	0.1253
Contra:WT - SNI vs. Ipsi:TLR4^{LoxTB} - SNI	13.48	-3.382 to 30.34	No	ns	0.1938

Contra:Na$_v$1.8^{TLR4LoxTB} - SNI vs. Contra:TLR4^{LoxTB} - SNI	-2.087	-18.95 to 14.77	No	ns	>0.9999
Contra:Na$_v$1.8^{TLR4LoxTB} - SNI vs. Ipsi:WT - SNI	-20.93	-37.79 to -4.071	Yes	*	0.0103
Contra:Na$_v$1.8^{TLR4LoxTB} - SNI vs. Ipsi:Na$_v$1.8^{TLR4LoxTB} - SNI	-2.217	-19.08 to 14.64	No	ns	>0.9999
Contra:Na$_v$1.8^{TLR4LoxTB} - SNI vs. Ipsi:TLR4^{LoxTB} - SNI	-3.3	-20.16 to 13.56	No	ns	>0.9999
Contra:TLR4^{LoxTB} - SNI vs. Ipsi:WT - SNI	-18.84	-35.70 to -1.984	Yes	*	0.023
Contra:TLR4^{LoxTB} - SNI vs. Ipsi:Na$_v$1.8^{TLR4LoxTB} - SNI	-0.13	-16.99 to 16.73	No	ns	>0.9999
Contra:TLR4^{LoxTB} - SNI vs. Ipsi:TLR4^{LoxTB} - SNI	-1.213	-18.07 to 15.65	No	ns	>0.9999
Ipsi:WT - SNI vs. Ipsi:Na$_v$1.8^{TLR4LoxTB} - SNI	18.71	1.854 to 35.57	Yes	*	0.0241
Ipsi:WT - SNI vs. Ipsi:TLR4^{LoxTB} - SNI	17.63	0.7709 to 34.49	Yes	*	0.0369
Ipsi:Na$_v$1.8^{TLR4LoxTB} - SNI vs. Ipsi:TLR4^{LoxTB} - SNI	-1.083	-17.94 to 15.78	No	ns	>0.9999
Ratio with Sexes Combined					
Male:WT - SNI vs. Male:Na$_v$1.8^{TLR4LoxTB} - SNI	5.585	-3.942 to 15.11	No	ns	0.4108
Male:WT - SNI vs. Male:TLR4^{LoxTB} - SNI	2.853	-6.673 to 12.38	No	ns	0.9072
Male:WT - SNI vs. Female:WT - SNI	5.38	-4.147 to 14.91	No	ns	0.4479
Male:WT - SNI vs. Female:Na$_v$1.8^{TLR4LoxTB} - SNI	2.526	-7.001 to 12.05	No	ns	0.9417
Male:WT - SNI vs. Female:TLR4^{LoxTB} - SNI	5.573	-3.954 to 15.10	No	ns	0.4129
Male:Na$_v$1.8^{TLR4LoxTB} - SNI vs. Male:TLR4^{LoxTB} - SNI	-2.731	-12.26 to 6.795	No	ns	0.9212
Male:Na$_v$1.8^{TLR4LoxTB} - SNI vs. Female:WT - SNI	-0.205	-9.731 to 9.321	No	ns	>0.9999
Male:Na$_v$1.8^{TLR4LoxTB} - SNI vs. Female:Na$_v$1.8^{TLR4LoxTB} - SNI	-3.059	-12.59 to 6.467	No	ns	0.8808
Male:Na$_v$1.8^{TLR4LoxTB} - SNI vs. Female:TLR4^{LoxTB} - SNI	-0.01195	-9.538 to 9.514	No	ns	>0.9999
Male:TLR4^{LoxTB} - SNI vs. Female:WT - SNI	2.526	-7.000 to 12.05	No	ns	0.9416
Male:TLR4^{LoxTB} - SNI vs. Female:Na$_v$1.8^{TLR4LoxTB} - SNI	-0.3278	-9.854 to 9.199	No	ns	>0.9999
Male:TLR4^{LoxTB} - SNI vs. Female:TLR4^{LoxTB} - SNI	2.719	-6.807 to 12.25	No	ns	0.9225
Female:WT - SNI vs. Female:Na$_v$1.8^{TLR4LoxTB} - SNI	-2.854	-12.38 to 6.672	No	ns	0.9071
Female:WT - SNI vs. Female:TLR4^{LoxTB} - SNI	0.193	-9.333 to 9.719	No	ns	>0.9999

Female:Na$_v$1.8^{TLR4LoxTB} - SNI vs. Female:TLR4^{LoxTB} - SNI	3.047	-6.479 to 12.57	No	ns	0.8824

Sensory neuron TLR4 is necessary during the onset of neuropathic mechanical hypersensitivity in female mice

Investigating the cell-specific implications of TLR4 activation in behavioral pain phenotypes is necessary to understand the biological relevance of cell-molecule interactions. Danger signals are released by both neuronal and non-neuronal cells in response to tissue injury, where neuronally expressed TLR4 allows for rapid detection of these proteins (Liu et al., 2014). Here, we asked if there are sex differences in the response to neuropathic tissue injury by neuronally expressed TLR4. To test this, we used transgenic male and female mice that lack TLR4 on their Na$_v$1.8$^+$ nociceptors combined with a spared nerve injury (SNI) model of peripheral neuropathic injury (Fig. 5.3A). Genotypes for Na$_v$1.8$^{TLR4fl/fl}$ mice are confirmed using polymerase chain reaction (PCR) and gel electrophoresis (Fig. 5.3B, C). We assessed the onset of neuropathic pain by measuring mechanical hypersensitivity and cold allodynia and our data reveals robust sex and genotype-dependent behavioral effects (Mecklenburg et al., 2020). Our data demonstrates the role of TLR4 in nociceptors and their female-specific role in regulating neuropathic pain development. Male Na$_v$1.8$^{TLR4fl/fl}$ mice exhibit similar mechanical withdrawal thresholds to their TLR4$^{fl/fl}$ littermates after SNI (Fig. 5.3D, Table 5.4). Female Na$_v$1.8$^{TLR4fl/fl}$ mice exhibit reduced mechanical withdrawal thresholds days 1, 3 and 5 after SNI as compared to their TLR4$^{fl/fl}$ littermates (Fig. 5.3E, Table 5.4). Sexes are directly compared using effect sizes (Fig. 5.3F, Table 5.4). Interestingly, male but not female mice show reduced cold allodynia on day 3 post-surgery as compared to their TLR4$^{fl/fl}$ littermates (Fig. 5.3G-H, Table 5.4). Sexes are directly

compared using effect sizes (Fig. 5.3I, Table 5.4). This demonstrates a distinction in the role of

TLR4 in mechanical vs. thermal during neuropathic pain development. It is possible that the

mechanisms which mediate cold and mechanical hypersensitivity are sexually dimorphic in nature,

and a distinguished subset of transient receptor potential (TRP)[+] sensory neurons in the DRG

differ mechanistically between males and females in a neuropathic state, however; this was not the

focus of the current study.
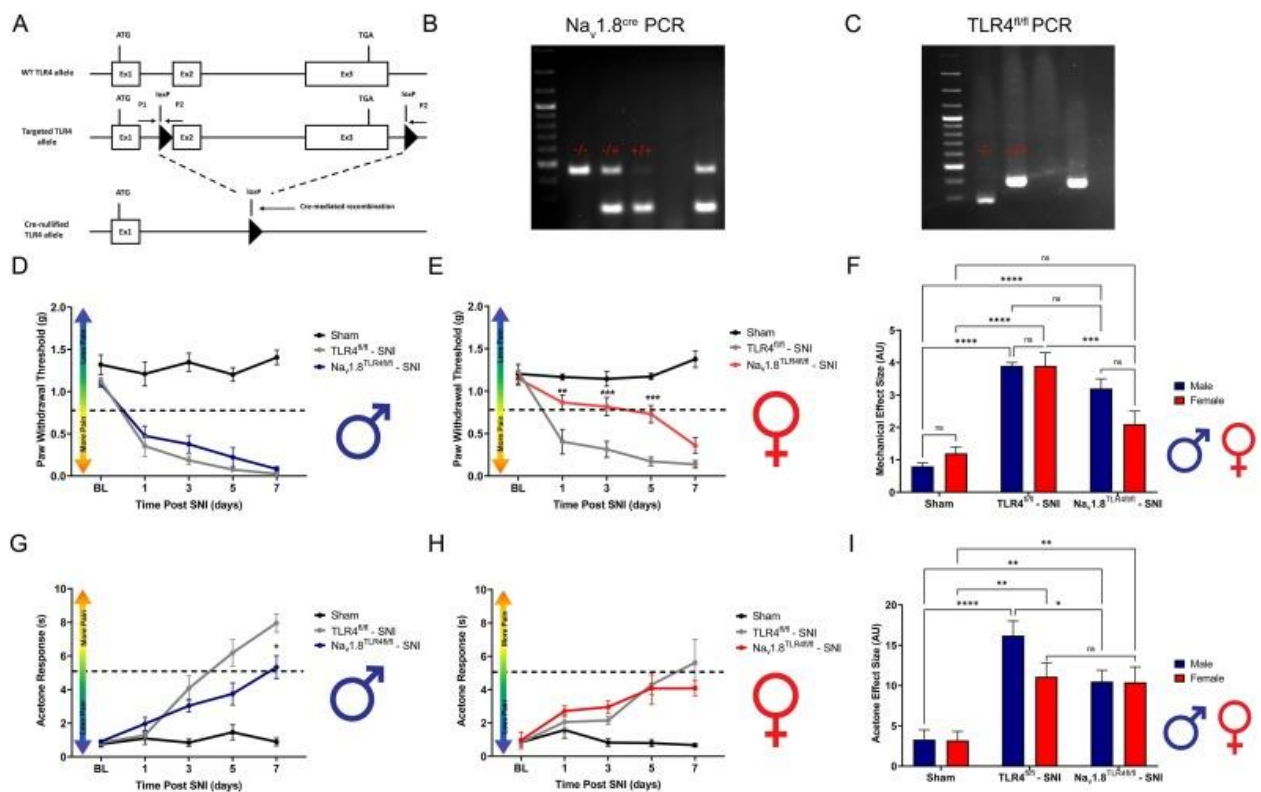
Figure 5.3. Development of neuropathic pain is attenuated in $Na_v1.8^{TLR4fl/fl}$ female, but not male mice. Spared-nerve injury was performed on the left hindlimb of male and female mice. *A*, Schematic representing the murine genetic model, $Na_v1.8^{TLR4fl/fl}$. *B*, Example PCR, and gel electrophoresis for $Na_v1.8$cre. A – indicates homozygous WT mice, a -/+ indicates heterozygous $Na_v1.8$cre mice, a +/+ indicates homozygous $Na_v1.8$cre. *C*, Example PCR, and gel electrophoresis for TLR4fl/fl. A - indicates homozygous WT mice, a -/+ indicates heterozygous TLR4fl/fl mice, a +/+ indicates homozygous TLR4fl/fl mice. *D-E*, Hind paw mechanical withdrawal thresholds were measured prior to surgery and on days: 1, 3, 5, and 7 post-surgery in both male and female sham (n = 8), TLR4fl/fl (n = 9), $Na_v1.8^{TLR4fl/fl}$ (n = 8) mice. *F*, Data for males and females combined shown as mechanical effect size. *G-H*, Hind paw response to application of acetone were measured

prior to surgery and on days: 1, 3, 5, and 7 post-surgery in both male and female sham (n = 8), TLR4$^{fl/fl}$ (n = 9) and Na$_v$1.8$^{TLR4fl/fl}$ (n = 8) mice. *I,* Data for males and females combined shown as acetone effect size. Asterisks on the line graphs indicate significant differences between the Na$_v$1.8$^{TLR4fl/fl}$ and TLR4$^{fl/fl}$ groups. $*p < 0.05$; $**p < 0.01$; $***p < 0.001$; $****p < 0.0001$. BL = Baseline.

Table 5.4. Statistical values corresponding to the data in Figure 5.3.

Tukey's multiple comparisons test	Predicted (LS) mean diff.	95.00% CI of diff.	Below threshold?	Summary	Adjusted P Value
Mechanical Males					
BL					
TLR4$^{fl/fl}$ - SNI vs. Na$_v$1.8$^{TLR4fl/fl}$ - SNI	0.03582	-0.1061 to 0.1778	No	ns	0.7957
TLR4$^{fl/fl}$ - SNI vs. Sham	-0.1915	-0.5364 to 0.1535	No	ns	0.3123
Na$_v$1.8$^{TLR4fl/fl}$ - SNI vs. Sham	-0.2273	-0.5714 to 0.1168	No	ns	0.2072
1					
TLR4$^{fl/fl}$ - SNI vs. Na$_v$1.8$^{TLR4fl/fl}$ - SNI	-0.1208	-0.5548 to 0.3131	No	ns	0.7581
TLR4$^{fl/fl}$ - SNI vs. Sham	-0.8543	-1.348 to -0.3603	Yes	**	0.0013
Na$_v$1.8$^{TLR4fl/fl}$ - SNI vs. Sham	-0.7334	-1.216 to -0.2510	Yes	**	0.0036
3					
TLR4$^{fl/fl}$ - SNI vs. Na$_v$1.8$^{TLR4fl/fl}$ - SNI	-0.1912	-0.4969 to 0.1144	No	ns	0.2611
TLR4$^{fl/fl}$ - SNI vs. Sham	-1.162	-1.490 to -0.8339	Yes	****	<0.0001
Na$_v$1.8$^{TLR4fl/fl}$ - SNI vs. Sham	-0.9707	-1.357 to -0.5842	Yes	****	<0.0001
5					
TLR4$^{fl/fl}$ - SNI vs. Na$_v$1.8$^{TLR4fl/fl}$ - SNI	-0.1471	-0.4642 to 0.1700	No	ns	0.4406
TLR4$^{fl/fl}$ - SNI vs. Sham	-1.127	-1.369 to -0.8854	Yes	****	<0.0001
Na$_v$1.8$^{TLR4fl/fl}$ - SNI vs. Sham	-0.98	-1.340 to -0.6199	Yes	****	<0.0001
7					
TLR4$^{fl/fl}$ - SNI vs. Na$_v$1.8$^{TLR4fl/fl}$ - SNI	-0.05637	-0.1399 to 0.02712	No	ns	0.2021
TLR4$^{fl/fl}$ - SNI vs. Sham	-1.38	-1.632 to -1.127	Yes	****	<0.0001
Na$_v$1.8$^{TLR4fl/fl}$ - SNI vs. Sham	-1.323	-1.578 to -1.068	Yes	****	<0.0001

Mechanical Females					
BL					
TLR4$^{fl/fl}$ - SNI vs. Na$_v$1.8$^{TLR4fl/fl}$ - SNI	0.08263	-0.2105 to 0.3757	No	ns	0.7533
TLR4$^{fl/fl}$ - SNI vs. Sham	0.02842	-0.3391 to 0.3960	No	ns	0.9777
Na$_v$1.8$^{TLR4fl/fl}$ - SNI vs. Sham	-0.0542	-0.4124 to 0.3040	No	ns	0.9158
1					
TLR4$^{fl/fl}$ - SNI vs. Na$_v$1.8$^{TLR4fl/fl}$ - SNI	-0.4613	-0.9066 to -0.01599	Yes	*	0.0419
TLR4$^{fl/fl}$ - SNI vs. Sham	-0.7622	-1.172 to -0.3522	Yes	**	0.0012
Na$_v$1.8$^{TLR4fl/fl}$ - SNI vs. Sham	-0.3009	-0.5650 to -0.03676	Yes	*	0.0266
3					
TLR4$^{fl/fl}$ - SNI vs. Na$_v$1.8$^{TLR4fl/fl}$ - SNI	-0.5024	-0.8703 to -0.1345	Yes	**	0.0074
TLR4$^{fl/fl}$ - SNI vs. Sham	-0.8303	-1.160 to -0.5006	Yes	****	<0.0001
Na$_v$1.8$^{TLR4fl/fl}$ - SNI vs. Sham	-0.3279	-0.6895 to 0.03376	No	ns	0.0783
5					
TLR4$^{fl/fl}$ - SNI vs. Na$_v$1.8$^{TLR4fl/fl}$ - SNI	-0.5576	-0.8597 to -0.2554	Yes	***	0.001
TLR4$^{fl/fl}$ - SNI vs. Sham	-1	-1.161 to -0.8401	Yes	****	<0.0001
Na$_v$1.8$^{TLR4fl/fl}$ - SNI vs. Sham	-0.4428	-0.7389 to -0.1468	Yes	**	0.0054
7					
TLR4$^{fl/fl}$ - SNI vs. Na$_v$1.8$^{TLR4fl/fl}$ - SNI	-0.2225	-0.4929 to 0.04788	No	ns	0.112
TLR4$^{fl/fl}$ - SNI vs. Sham	-1.239	-1.535 to -0.9431	Yes	****	<0.0001
Na$_v$1.8$^{TLR4fl/fl}$ - SNI vs. Sham	-1.016	-1.364 to -0.6688	Yes	****	<0.0001
Acetone Males					
BL					
TLR4$^{fl/fl}$ - SNI vs. Na$_v$1.8$^{TLR4fl/fl}$ - SNI	-0.07268	-0.5843 to 0.4390	No	ns	0.9249
TLR4$^{fl/fl}$ - SNI vs. Sham	0.08607	-0.5122 to 0.6843	No	ns	0.9239
Na$_v$1.8$^{TLR4fl/fl}$ - SNI vs. Sham	0.1588	-0.4053 to 0.7228	No	ns	0.7419
1					
TLR4$^{fl/fl}$ - SNI vs. Na$_v$1.8$^{TLR4fl/fl}$ - SNI	-0.6825	-1.912 to 0.5474	No	ns	0.3318
TLR4$^{fl/fl}$ - SNI vs. Sham	0.1925	-0.9330 to 1.318	No	ns	0.893

$Na_v1.8^{TLR4fl/fl}$ - SNI vs. Sham	0.875	-0.4850 to 2.235	No	ns	0.245
3					
$TLR4^{fl/fl}$ - SNI vs. $Na_v1.8^{TLR4fl/fl}$ - SNI	1.038	-1.282 to 3.358	No	ns	0.4565
$TLR4^{fl/fl}$ - SNI vs. Sham	3.23	0.9615 to 5.499	Yes	**	0.01
$Na_v1.8^{TLR4fl/fl}$ - SNI vs. Sham	2.193	1.025 to 3.360	Yes	***	0.001
5					
$TLR4^{fl/fl}$ - SNI vs. $Na_v1.8^{TLR4fl/fl}$ - SNI	2.438	-0.3153 to 5.192	No	ns	0.085
$TLR4^{fl/fl}$ - SNI vs. Sham	4.727	2.206 to 7.248	Yes	**	0.0013
$Na_v1.8^{TLR4fl/fl}$ - SNI vs. Sham	2.289	0.1718 to 4.406	Yes	*	0.034
7					
$TLR4^{fl/fl}$ - SNI vs. $Na_v1.8^{TLR4fl/fl}$ - SNI	2.63	0.3141 to 4.946	Yes	*	0.026
$TLR4^{fl/fl}$ - SNI vs. Sham	7.066	5.366 to 8.767	Yes	****	<0.0001
$Na_v1.8^{TLR4fl/fl}$ - SNI vs. Sham	4.436	2.409 to 6.464	Yes	***	0.0005
Acetone Females					
BL					
$TLR4^{fl/fl}$ - SNI vs. $Na_v1.8^{TLR4fl/fl}$ - SNI	-0.1198	-1.667 to 1.427	No	ns	0.9718
$TLR4^{fl/fl}$ - SNI vs. Sham	-0.0025	-0.6707 to 0.6657	No	ns	>0.9999
$Na_v1.8^{TLR4fl/fl}$ - SNI vs. Sham	0.1173	-1.441 to 1.676	No	ns	0.9749
1					
$TLR4^{fl/fl}$ - SNI vs. $Na_v1.8^{TLR4fl/fl}$ - SNI	-0.6584	-2.083 to 0.7662	No	ns	0.4576
$TLR4^{fl/fl}$ - SNI vs. Sham	0.4813	-1.238 to 2.200	No	ns	0.7482
$Na_v1.8^{TLR4fl/fl}$ - SNI vs. Sham	1.14	-0.3990 to 2.678	No	ns	0.1593
3					
$TLR4^{fl/fl}$ - SNI vs. $Na_v1.8^{TLR4fl/fl}$ - SNI	-0.8046	-1.953 to 0.3434	No	ns	0.1864
$TLR4^{fl/fl}$ - SNI vs. Sham	1.328	0.4808 to 2.174	Yes	**	0.0029
$Na_v1.8^{TLR4fl/fl}$ - SNI vs. Sham	2.132	1.010 to 3.254	Yes	**	0.001
5					
$TLR4^{fl/fl}$ - SNI vs. $Na_v1.8^{TLR4fl/fl}$ - SNI	0.227	-2.866 to 3.319	No	ns	0.9781

TLR4$^{fl/fl}$ - SNI vs. Sham	3.509	1.750 to 5.267	Yes	***	0.0009
Na$_v$1.8$^{TLR4fl/fl}$ - SNI vs. Sham	3.282	0.3289 to 6.235	Yes	*	0.0325
7					
TLR4$^{fl/fl}$ - SNI vs. Na$_v$1.8$^{TLR4fl/fl}$ - SNI	1.531	-2.631 to 5.693	No	ns	0.5727
TLR4$^{fl/fl}$ - SNI vs. Sham	4.946	0.8181 to 9.074	Yes	*	0.0228
Na$_v$1.8$^{TLR4fl/fl}$ - SNI vs. Sham	3.415	2.054 to 4.776	Yes	***	0.0004
Mechanical Effect Size					
Sham:Male vs. Sham:Female	-0.4	-1.747 to 0.9467	No	ns	0.9493
Sham:Male vs. TLR4$^{fl/fl}$ - SNI:Male	-3.1	-4.409 to -1.791	Yes	****	<0.0001
Sham:Male vs. TLR4$^{fl/fl}$ - SNI:Female	-3.1	-4.378 to -1.822	Yes	****	<0.0001
Sham:Male vs. Na$_v$1.8$^{TLR4fl/fl}$ - SNI:Male	-2.4	-3.678 to -1.122	Yes	****	<0.0001
Sham:Male vs. Na$_v$1.8$^{TLR4fl/fl}$ - SNI:Female	-1.3	-2.578 to -0.02245	Yes	*	0.0439
Sham:Female vs. TLR4$^{fl/fl}$ - SNI:Male	-2.7	-4.009 to -1.391	Yes	****	<0.0001
Sham:Female vs. TLR4$^{fl/fl}$ - SNI:Female	-2.7	-3.978 to -1.422	Yes	****	<0.0001
Sham:Female vs. Na$_v$1.8$^{TLR4fl/fl}$ - SNI:Male	-2	-3.278 to -0.7224	Yes	***	0.0004
Sham:Female vs. Na$_v$1.8$^{TLR4fl/fl}$ - SNI:Female	-0.9	-2.178 to 0.3776	No	ns	0.3098
TLR4$^{fl/fl}$ - SNI:Male vs. TLR4$^{fl/fl}$ - SNI:Female	0	-1.237 to 1.237	No	ns	>0.9999
TLR4$^{fl/fl}$ - SNI:Male vs. Na$_v$1.8$^{TLR4fl/fl}$ - SNI:Male	0.7	-0.5375 to 1.937	No	ns	0.5528
TLR4$^{fl/fl}$ - SNI:Male vs. Na$_v$1.8$^{TLR4fl/fl}$ - SNI:Female	1.8	0.5625 to 3.037	Yes	**	0.001
TLR4$^{fl/fl}$ - SNI:Female vs. Na$_v$1.8$^{TLR4fl/fl}$ - SNI:Male	0.7	-0.5045 to 1.904	No	ns	0.5235
TLR4$^{fl/fl}$ - SNI:Female vs. Na$_v$1.8$^{TLR4fl/fl}$ - SNI:Female	1.8	0.5955 to 3.004	Yes	***	0.0007
Na$_v$1.8$^{TLR4fl/fl}$ - SNI:Male vs. Na$_v$1.8$^{TLR4fl/fl}$ - SNI:Female	1.1	-0.1045 to 2.304	No	ns	0.0918
Acetone Effect Size					
Male					
Sham vs. TLR4$^{fl/fl}$ - SNI	-12.9	-18.32 to -7.475	Yes	****	<0.0001
Sham vs. Na$_v$1.8$^{TLR4fl/fl}$ - SNI	-7.2	-12.44 to -1.959	Yes	**	0.0043
TLR4$^{fl/fl}$ - SNI vs. Na$_v$1.8$^{TLR4fl/fl}$ - SNI	5.7	0.2754 to 11.12	Yes	*	0.0368

Female					
Sham vs. TLR4$^{fl/fl}$ - SNI	-7.9	-13.14 to -2.659	Yes	**	0.0016
Sham vs. Na$_v$1.8$^{TLR4fl/fl}$ - SNI	-7.2	-12.62 to -1.775	Yes	**	0.006
TLR4$^{fl/fl}$ - SNI vs. Na$_v$1.8$^{TLR4fl/fl}$ - SNI	0.7	-4.725 to 6.125	No	ns	0.9843

Sensory neuron TLR4 is sufficient during the onset of neuropathic mechanical hypersensitivity in female mice

Whole body TLR4 has been shown to influence recovery from a non-terminal neuropathic injury (Stokes et al., 2013). Moreover, TLR4 knockout mice have reduced mechanical and thermal hypersensitivity in response to neuropathic injury (Piao et al., 2018). It is still unclear what specific populations of cells that express TLR4 contribute to these behavioral effects. To investigate the direct action of TLR4 on peripheral sensory neurons, we utilized Na$_v$1.8^{TLR4LoxTB} mice combined with an SNI model of neuropathic pain (Fig. 5.4A). Genotypes for Na$_v$1.8^{TLR4LoxTB} mice are confirmed using PCR and gel electrophoresis (Fig. 5.4B, C). Here, we tested the sufficiency of TLR4 expressed only on Na$_v$1.8$^+$ DRG neurons to produce a neuropathic behavioral pain phenotype similar to wild type mice. Analysis reveals significant genotype-dependent behavioral phenotypes and robust sex differences. Male TLR4^{LoxTB} mice show significantly diminished mechanical withdrawal thresholds during days 1, 3 and 5 post-surgery as compared to WT littermates. Interestingly, male Na$_v$1.8^{TLR4LoxTB} mice do not recapitulate the severe mechanical hypersensitivity seen in WT littermates on days 1, 3 and 5 post-surgery (Fig. 5.4D, Table 5.5). Female TLR4^{LoxTB} mice show significantly diminished mechanical withdrawal thresholds during days 1, 3 and 5 post-surgery as compared to WT littermates, however; only female Na$_v$1.8^{TLR4LoxTB} mice recapitulate the severe mechanical hypersensitivity seen in WT littermates on days 1, 3 and 5 post-surgery (Fig. 5.4E, Table 5.5). Sexes are directly compared using effect

sizes (Fig. 5.4F, Table 5.5). Surprisingly, no sex or genotype-dependent effects are seen across time in cold allodynia development (Fig. 5.4G-H, Table 5.5). Sexes are directly compared using effect sizes (Fig. 5.4I, Table 5.5). These data suggest direct activation of neuronally expressed TLR4 by endogenous danger signals released during injury is enough to cause a neuropathic behavioral pain phenotype only in female mice.
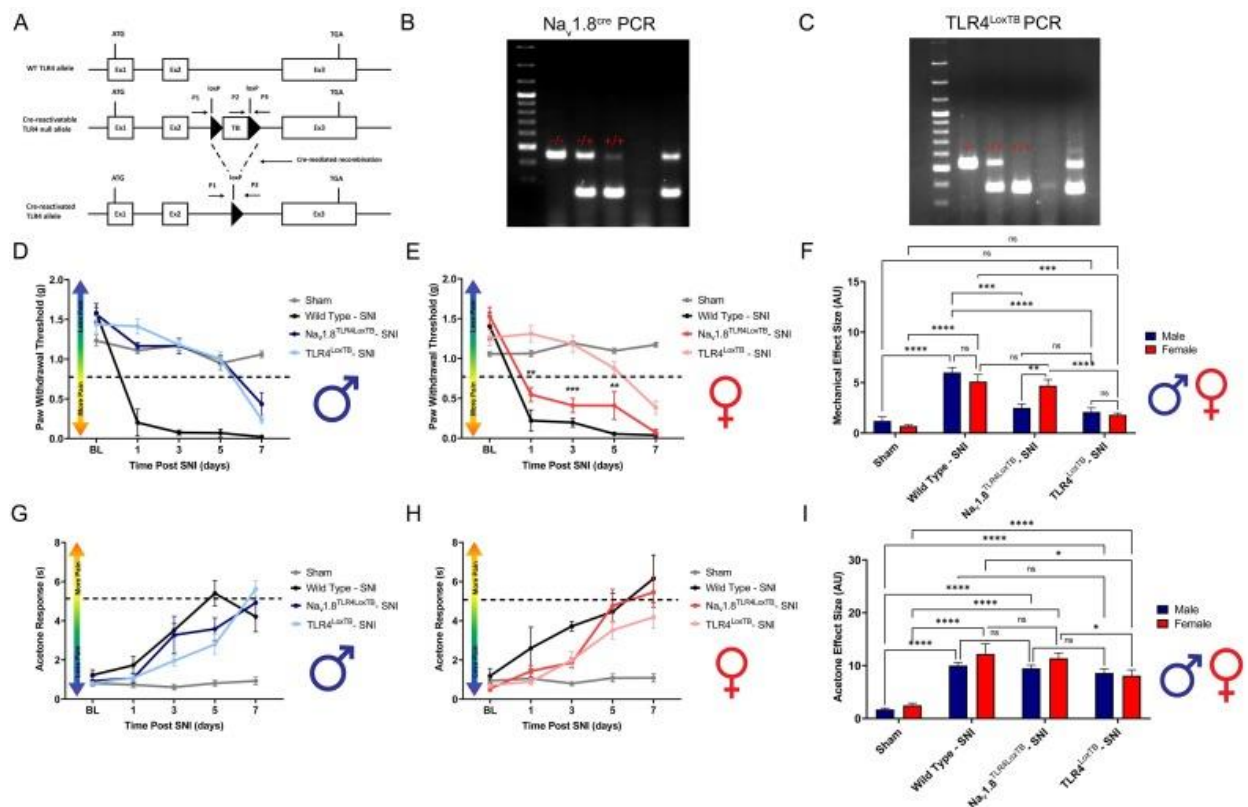
Figure 5.4. Development of neuropathic pain is phenotypically normal in Na$_v$1.8^{TLR4LoxTB} female, but not male mice. Spared-nerve injury was performed on the left hindlimb of male and female mice. *A*, Schematic representing the murine genetic model, Na$_v$1.8^{TLR4LoxTB}. *B,* Example PCR, and gel electrophoresis for Na$_v$1.8cre. A - indicates homozygous WT mice, a -/+ indicates heterozygous Na$_v$1.8cre mice, a +/+ indicates homozygous Na$_v$1.8cre. *C,* Example PCR, and gel electrophoresis for TLR4^{LoxTB}. A – indicates homozygous WT mice, a -/+ indicates heterozygous TLR4^{LoxTB} mice, a +/+ indicates homozygous TLR4^{LoxTB} mice. *D-E,* Hind paw mechanical withdrawal thresholds were measured prior to surgery and on days: 1, 3, 5, and 7 post-surgery in both male and female sham (n = 12), wild type (n = 4), TLR4^{LoxTB} (n = 9), *F,* Data for males and females combined shown as mechanical effect size. *G-H,* Hind paw response to application of acetone were measured prior to surgery and on days: 1, 3, 5, and 7 post-surgery in both male and female sham (n = 12), wild type (n = 4),

138

TLR4^{LoxTB} (n = 9), Na$_v$1.8^{TLR4LoxTB} (n = 7) mice. *I,* Data for males and females combined shown as acetone effect size. Asterisks on the line graphs indicate significant differences between the Na$_v$1.8^{TLR4LoxTB} and TLR4^{LoxTB} groups. *p* < 0.05; **p* < 0.01; ***p* < 0.001; ****p* < 0.0001. BL = Baseline.

Table 5.5. Statistical values corresponding to the data in Figure 5.4.

Tukey's multiple comparisons test	Mean Diff.	95.00% CI of diff.	Below threshold?	Summary	Adjusted P Value
Male Mechanical					
BL					
TLR4^{LoxTB}- SNI vs. Na$_v$1.8^{TLR4LoxTB}- SNI	-0.1254	-0.5228 to 0.2719	No	ns	0.7958
TLR4^{LoxTB}- SNI vs. Wild Type - SNI	-0.1422	-0.6485 to 0.3642	No	ns	0.8051
TLR4^{LoxTB}- SNI vs. Sham	0.2076	-0.1602 to 0.5753	No	ns	0.3918
Na$_v$1.8^{TLR4LoxTB}- SNI vs. Wild Type - SNI	-0.01671	-0.5141 to 0.4806	No	ns	0.9994
Na$_v$1.8^{TLR4LoxTB}- SNI vs. Sham	0.333	0.007778 to 0.6582	Yes	*	0.0441
Wild Type - SNI vs. Sham	0.3497	-0.1408 to 0.8402	No	ns	0.1559
1					
TLR4^{LoxTB}- SNI vs. Na$_v$1.8^{TLR4LoxTB}- SNI	0.2482	-0.06082 to 0.5572	No	ns	0.131
TLR4^{LoxTB}- SNI vs. Wild Type - SNI	1.212	0.4947 to 1.930	Yes	**	0.006
TLR4^{LoxTB}- SNI vs. Sham	0.3036	-0.004680 to 0.6119	No	ns	0.054
Na$_v$1.8^{TLR4LoxTB}- SNI vs. Wild Type - SNI	0.9642	0.1846 to 1.744	Yes	*	0.0266
Na$_v$1.8^{TLR4LoxTB}- SNI vs. Sham	0.05543	-0.1185 to 0.2294	No	ns	0.798
Wild Type - SNI vs. Sham	#VALUE!	-1.687 to -0.1308	Yes	*	0.0316
3					
TLR4^{LoxTB}- SNI vs. Na$_v$1.8^{TLR4LoxTB}- SNI	0.01439	-0.3518 to 0.3806	No	ns	0.9994
TLR4^{LoxTB}- SNI vs. Wild Type - SNI	1.106	0.8578 to 1.354	Yes	****	<0.0001
TLR4^{LoxTB}- SNI vs. Sham	0.004208	-0.2762 to 0.2846	No	ns	>0.9999
Na$_v$1.8^{TLR4LoxTB}- SNI vs. Wild Type - SNI	1.091	0.7534 to 1.429	Yes	****	<0.0001
Na$_v$1.8^{TLR4LoxTB}- SNI vs. Sham	-0.01018	-0.3612 to 0.3408	No	ns	0.9997
Wild Type - SNI vs. Sham	-1.101	-1.307 to -0.8958	Yes	****	<0.0001

5					
TLR4^{LoxTB}- SNI vs. Na$_v$1.8^{TLR4LoxTB}- SNI	0.0005444	-0.3088 to 0.3099	No	ns	>0.9999
TLR4^{LoxTB}- SNI vs. Wild Type - SNI	0.9319	0.6189 to 1.245	Yes	****	<0.0001
TLR4^{LoxTB}- SNI vs. Sham	0.05397	-0.3028 to 0.4108	No	ns	0.9731
Na$_v$1.8^{TLR4LoxTB}- SNI vs. Wild Type - SNI	0.9314	0.7091 to 1.154	Yes	****	<0.0001
Na$_v$1.8^{TLR4LoxTB}- SNI vs. Sham	0.05342	-0.2329 to 0.3398	No	ns	0.9497
Wild Type - SNI vs. Sham	-0.878	-1.168 to -0.5878	Yes	****	<0.0001
7					
TLR4^{LoxTB}- SNI vs. Na$_v$1.8^{TLR4LoxTB}- SNI	-0.1972	-0.6948 to 0.3003	No	ns	0.595
TLR4^{LoxTB}- SNI vs. Wild Type - SNI	0.2171	0.05414 to 0.3801	Yes	*	0.011
TLR4^{LoxTB}- SNI vs. Sham	-0.8229	-1.008 to -0.6375	Yes	****	<0.0001
Na$_v$1.8^{TLR4LoxTB}- SNI vs. Wild Type - SNI	0.4143	-0.08474 to 0.9134	No	ns	0.1004
Na$_v$1.8^{TLR4LoxTB}- SNI vs. Sham	-0.6257	-1.123 to -0.1289	Yes	*	0.0171
Wild Type - SNI vs. Sham	-1.04	-1.165 to -0.9149	Yes	****	<0.0001
Female Mechanical					
BL					
TLR4^{LoxTB} - SNI vs. Na$_v$1.8^{TLR4LoxTB}- SNI	-0.2735	-0.7064 to 0.1594	No	ns	0.2939
TLR4^{LoxTB} - SNI vs. Wild Type - SNI	-0.1485	-0.8880 to 0.5909	No	ns	0.8767
TLR4^{LoxTB} - SNI vs. Sham	0.2006	-0.1158 to 0.5170	No	ns	0.2686
Na$_v$1.8^{TLR4LoxTB}- SNI vs. Wild Type - SNI	0.1249	-0.6144 to 0.8643	No	ns	0.9267
Na$_v$1.8^{TLR4LoxTB}- SNI vs. Sham	0.474	0.09376 to 0.8543	Yes	*	0.0181
Wild Type - SNI vs. Sham	0.3491	-0.4738 to 1.172	No	ns	0.3563
1					
TLR4^{LoxTB} - SNI vs. Na$_v$1.8^{TLR4LoxTB}- SNI	0.7621	0.3685 to 1.156	Yes	***	0.0003
TLR4^{LoxTB} - SNI vs. Wild Type - SNI	1.087	0.5200 to 1.654	Yes	**	0.0019
TLR4^{LoxTB} - SNI vs. Sham	0.2476	-0.08732 to 0.5825	No	ns	0.1743
Na$_v$1.8^{TLR4LoxTB}- SNI vs. Wild Type - SNI	0.3251	-0.2434 to 0.8936	No	ns	0.2831
Na$_v$1.8^{TLR4LoxTB}- SNI vs. Sham	-0.5145	-0.8207 to -0.2083	Yes	**	0.0026
Wild Type - SNI vs. Sham	-0.8396	-1.447 to -0.2320	Yes	*	0.0182

3					
TLR4^{LoxTB} - SNI vs. Na_v1.8^{TLR4LoxTB}- SNI	0.7705	0.3640 to 1.177	Yes	***	0.0004
TLR4^{LoxTB} - SNI vs. Wild Type - SNI	0.9845	0.6180 to 1.351	Yes	****	<0.0001
TLR4^{LoxTB} - SNI vs. Sham	-0.01248	-0.3587 to 0.3338	No	ns	0.9994
Na_v1.8^{TLR4LoxTB}- SNI vs. Wild Type - SNI	0.214	-0.1155 to 0.5435	No	ns	0.2463
Na_v1.8^{TLR4LoxTB}- SNI vs. Sham	-0.783	-1.090 to -0.4761	Yes	***	0.0003
Wild Type - SNI vs. Sham	-0.997	-1.240 to -0.7542	Yes	***	0.0002
5					
TLR4^{LoxTB} - SNI vs. Na_v1.8^{TLR4LoxTB}- SNI	0.4685	-0.1297 to 1.067	No	ns	0.1353
TLR4^{LoxTB} - SNI vs. Wild Type - SNI	0.823	0.5648 to 1.081	Yes	****	<0.0001
TLR4^{LoxTB} - SNI vs. Sham	-0.2184	-0.4787 to 0.04181	No	ns	0.1102
Na_v1.8^{TLR4LoxTB}- SNI vs. Wild Type - SNI	0.3545	-0.2399 to 0.9489	No	ns	0.2698
Na_v1.8^{TLR4LoxTB}- SNI vs. Sham	-0.687	-1.280 to -0.09346	Yes	*	0.0265
Wild Type - SNI vs. Sham	-1.041	-1.170 to -0.9129	Yes	****	<0.0001
7					
TLR4^{LoxTB} - SNI vs. Na_v1.8^{TLR4LoxTB}- SNI	0.313	0.02860 to 0.5974	Yes	*	0.0299
TLR4^{LoxTB} - SNI vs. Wild Type - SNI	0.346	0.07311 to 0.6188	Yes	*	0.0147
TLR4^{LoxTB} - SNI vs. Sham	-0.789	-1.064 to -0.5137	Yes	****	<0.0001
Na_v1.8^{TLR4LoxTB}- SNI vs. Wild Type - SNI	0.03298	-0.1195 to 0.1855	No	ns	0.8959
Na_v1.8^{TLR4LoxTB}- SNI vs. Sham	-1.102	-1.260 to -0.9438	Yes	****	<0.0001
Wild Type - SNI vs. Sham	-1.135	-1.238 to -1.032	Yes	****	<0.0001
Male Acetone					
BL					
TLR4^{LoxTB}- SNI vs. Na_v1.8^{TLR4LoxTB}- SNI	-0.1183	-0.8556 to 0.6191	No	ns	0.9576
TLR4^{LoxTB}- SNI vs. Wild Type - SNI	-0.4186	-1.591 to 0.7543	No	ns	0.5393
TLR4^{LoxTB}- SNI vs. Sham	0.004722	-0.5525 to 0.5620	No	ns	>0.9999
Na_v1.8^{TLR4LoxTB}- SNI vs. Wild Type - SNI	-0.3004	-1.449 to 0.8481	No	ns	0.8149
Na_v1.8^{TLR4LoxTB}- SNI vs. Sham	0.123	-0.6591 to 0.9051	No	ns	0.966
Wild Type - SNI vs. Sham	0.4233	-0.7015 to 1.548	No	ns	0.5732

1					
TLR4^{LoxTB}- SNI vs. Na$_v$1.8^{TLR4LoxTB}- SNI	0.01857	-0.8802 to 0.9173	No	ns	>0.9999
TLR4^{LoxTB}- SNI vs. Wild Type - SNI	-0.6375	-2.632 to 1.357	No	ns	0.601
TLR4^{LoxTB}- SNI vs. Sham	0.3625	-0.2636 to 0.9886	No	ns	0.3785
Na$_v$1.8^{TLR4LoxTB}- SNI vs. Wild Type - SNI	-0.6561	-2.584 to 1.271	No	ns	0.6146
Na$_v$1.8^{TLR4LoxTB}- SNI vs. Sham	0.3439	-0.5178 to 1.206	No	ns	0.625
Wild Type - SNI vs. Sham	1	-1.048 to 3.048	No	ns	0.3007
3					
TLR4^{LoxTB}- SNI vs. Na$_v$1.8^{TLR4LoxTB}- SNI	-1.316	-4.604 to 1.972	No	ns	0.5759
TLR4^{LoxTB}- SNI vs. Wild Type - SNI	-1.56	-2.971 to -0.1493	Yes	*	0.032
TLR4^{LoxTB}- SNI vs. Sham	1.348	0.4592 to 2.236	Yes	**	0.0033
Na$_v$1.8^{TLR4LoxTB}- SNI vs. Wild Type - SNI	-0.2443	-3.551 to 3.062	No	ns	0.9946
Na$_v$1.8^{TLR4LoxTB}- SNI vs. Sham	2.663	-0.6330 to 5.959	No	ns	0.1112
Wild Type - SNI vs. Sham	2.908	1.462 to 4.353	Yes	**	0.0039
5					
TLR4^{LoxTB}- SNI vs. Na$_v$1.8^{TLR4LoxTB}- SNI	-0.7862	-3.015 to 1.443	No	ns	0.7327
TLR4^{LoxTB}- SNI vs. Wild Type - SNI	-2.606	-5.357 to 0.1457	No	ns	0.0625
TLR4^{LoxTB}- SNI vs. Sham	1.984	0.3604 to 3.608	Yes	*	0.0172
Na$_v$1.8^{TLR4LoxTB}- SNI vs. Wild Type - SNI	-1.82	-4.661 to 1.022	No	ns	0.2385
Na$_v$1.8^{TLR4LoxTB}- SNI vs. Sham	2.77	0.8055 to 4.735	Yes	**	0.0095
Wild Type - SNI vs. Sham	4.59	1.600 to 7.580	Yes	*	0.0135
7					
TLR4^{LoxTB}- SNI vs. Na$_v$1.8^{TLR4LoxTB}- SNI	0.6913	-1.729 to 3.112	No	ns	0.8198
TLR4^{LoxTB}- SNI vs. Wild Type - SNI	1.406	-1.858 to 4.669	No	ns	0.4515
TLR4^{LoxTB}- SNI vs. Sham	4.689	3.327 to 6.051	Yes	****	<0.0001
Na$_v$1.8^{TLR4LoxTB}- SNI vs. Wild Type - SNI	0.7143	-2.644 to 4.073	No	ns	0.8953
Na$_v$1.8^{TLR4LoxTB}- SNI vs. Sham	3.998	1.661 to 6.335	Yes	**	0.0033
Wild Type - SNI vs. Sham	3.283	-0.2474 to 6.814	No	ns	0.0615

Female Acetone					
BL					
TLR4^{LoxTB}- SNI vs. Na$_v$1.8^{TLR4LoxTB}- SNI	0.1705	-0.4573 to 0.7983	No	ns	0.857
TLR4^{LoxTB}- SNI vs. Wild Type - SNI	-0.4792	-2.097 to 1.138	No	ns	0.6584
TLR4^{LoxTB}- SNI vs. Sham	-0.2317	-0.7954 to 0.3320	No	ns	0.6547
Na$_v$1.8^{TLR4LoxTB}- SNI vs. Wild Type - SNI	-0.6496	-2.268 to 0.9689	No	ns	0.4585
Na$_v$1.8^{TLR4LoxTB}- SNI vs. Sham	-0.4021	-0.9841 to 0.1798	No	ns	0.2301
Wild Type - SNI vs. Sham	0.2475	-1.400 to 1.895	No	ns	0.9163
1					
TLR4^{LoxTB}- SNI vs. Na$_v$1.8^{TLR4LoxTB}- SNI	-0.539	-1.582 to 0.5043	No	ns	0.4368
TLR4^{LoxTB}- SNI vs. Wild Type - SNI	-1.711	-6.753 to 3.331	No	ns	0.4968
TLR4^{LoxTB}- SNI vs. Sham	-0.1558	-0.9861 to 0.6745	No	ns	0.9513
Na$_v$1.8^{TLR4LoxTB}- SNI vs. Wild Type - SNI	-1.172	-6.070 to 3.726	No	ns	0.733
Na$_v$1.8^{TLR4LoxTB}- SNI vs. Sham	0.3832	-0.7016 to 1.468	No	ns	0.732
Wild Type - SNI vs. Sham	1.555	-3.429 to 6.539	No	ns	0.561
3					
TLR4^{LoxTB}- SNI vs. Na$_v$1.8^{TLR4LoxTB}- SNI	0.1365	-1.330 to 1.603	No	ns	0.9923
TLR4^{LoxTB}- SNI vs. Wild Type - SNI	-1.723	-3.218 to -0.2274	Yes	*	0.0233
TLR4^{LoxTB}- SNI vs. Sham	1.2	-0.1897 to 2.589	No	ns	0.0951
Na$_v$1.8^{TLR4LoxTB}- SNI vs. Wild Type - SNI	-1.859	-2.970 to -0.7490	Yes	**	0.003
Na$_v$1.8^{TLR4LoxTB}- SNI vs. Sham	1.063	0.2162 to 1.910	Yes	*	0.0155
Wild Type - SNI vs. Sham	2.923	1.866 to 3.979	Yes	***	0.0009
5					
TLR4^{LoxTB}- SNI vs. Na$_v$1.8^{TLR4LoxTB}- SNI	-1.24	-4.207 to 1.727	No	ns	0.5887
TLR4^{LoxTB}- SNI vs. Wild Type - SNI	-0.9361	-5.017 to 3.144	No	ns	0.8123
TLR4^{LoxTB}- SNI vs. Sham	2.449	0.9483 to 3.949	Yes	**	0.0022
Na$_v$1.8^{TLR4LoxTB}- SNI vs. Wild Type - SNI	0.3036	-3.855 to 4.462	No	ns	0.9948
Na$_v$1.8^{TLR4LoxTB}- SNI vs. Sham	3.689	0.7828 to 6.594	Yes	*	0.0169
Wild Type - SNI vs. Sham	3.385	-1.042 to 7.812	No	ns	0.103

TLR4^{LoxTB}- SNI vs. Na$_v$1.8^{TLR4LoxTB}- SNI	-1.278	-4.122 to 1.567	No	ns	0.5554
TLR4^{LoxTB}- SNI vs. Wild Type - SNI	-1.973	-7.166 to 3.221	No	ns	0.5127
TLR4^{LoxTB}- SNI vs. Sham	3.091	1.296 to 4.885	Yes	**	0.0016
Na$_v$1.8^{TLR4LoxTB}- SNI vs. Wild Type - SNI	-0.695	-5.784 to 4.394	No	ns	0.9593
Na$_v$1.8^{TLR4LoxTB}- SNI vs. Sham	4.368	1.699 to 7.038	Yes	**	0.0042
Wild Type - SNI vs. Sham	5.063	-0.5829 to 10.71	No	ns	0.0673
Mechanical Effect Size					
Sham:Male vs. Sham:Female	0.5	-0.9117 to 1.912	No	ns	0.9508
Sham:Male vs. Wild Type - SNI:Male	-4.8	-6.796 to -2.804	Yes	****	<0.0001
Sham:Male vs. Wild Type - SNI:Female	-3.9	-5.896 to -1.904	Yes	****	<0.0001
Sham:Male vs. Na$_v$1.8^{TLR4LoxTB}- SNI:Male	-1.3	-2.945 to 0.3446	No	ns	0.2216
Sham:Male vs. Na$_v$1.8^{TLR4LoxTB}- SNI:Female	-3.5	-5.145 to -1.855	Yes	****	<0.0001
Sham:Male vs. TLR4^{LoxTB}- SNI:Male	-0.9	-2.425 to 0.6248	No	ns	0.5843
Sham:Male vs. TLR4^{LoxTB}- SNI:Female	-0.6	-2.125 to 0.9248	No	ns	0.9165
Sham:Female vs. Wild Type - SNI:Male	-5.3	-7.296 to -3.304	Yes	****	<0.0001
Sham:Female vs. Wild Type - SNI:Female	-4.4	-6.396 to -2.404	Yes	****	<0.0001
Sham:Female vs. Na$_v$1.8^{TLR4LoxTB}- SNI:Male	-1.8	-3.445 to -0.1554	Yes	*	0.0226
Sham:Female vs. Na$_v$1.8^{TLR4LoxTB}- SNI:Female	-4	-5.645 to -2.355	Yes	****	<0.0001
Sham:Female vs. TLR4^{LoxTB}- SNI:Male	-1.4	-2.925 to 0.1248	No	ns	0.094
Sham:Female vs. TLR4^{LoxTB}- SNI:Female	-1.1	-2.625 to 0.4248	No	ns	0.3275
Wild Type - SNI:Male vs. Wild Type - SNI:Female	0.9	-1.545 to 3.345	No	ns	0.9401
Wild Type - SNI:Male vs. Na$_v$1.8^{TLR4LoxTB}- SNI:Male	3.5	1.333 to 5.667	Yes	***	0.0001
Wild Type - SNI:Male vs. Na$_v$1.8^{TLR4LoxTB}- SNI:Female	1.3	-0.8674 to 3.467	No	ns	0.5644
Wild Type - SNI:Male vs. TLR4^{LoxTB}- SNI:Male	3.9	1.822 to 5.978	Yes	****	<0.0001
Wild Type - SNI:Male vs. TLR4^{LoxTB}- SNI:Female	4.2	2.122 to 6.278	Yes	****	<0.0001
Wild Type - SNI:Female vs. Na$_v$1.8^{TLR4LoxTB}- SNI:Male	2.6	0.4326 to 4.767	Yes	**	0.0086

Wild Type - SNI:Female vs. Na$_v$1.8^{TLR4LoxTB}- SNI:Female	0.4	-1.767 to 2.567	No	ns	0.999
Wild Type - SNI:Female vs. TLR4^{LoxTB}- SNI:Male	3	0.9220 to 5.078	Yes	***	0.0007
Wild Type - SNI:Female vs. TLR4^{LoxTB}- SNI:Female	3.3	1.222 to 5.378	Yes	***	0.0002
Na$_v$1.8^{TLR4LoxTB}- SNI:Male vs. Na$_v$1.8^{TLR4LoxTB}- SNI:Female	-2.2	-4.048 to -0.3516	Yes	**	0.0094
Na$_v$1.8^{TLR4LoxTB}- SNI:Male vs. TLR4^{LoxTB}- SNI:Male	0.4	-1.343 to 2.143	No	ns	0.9959
Na$_v$1.8^{TLR4LoxTB}- SNI:Male vs. TLR4^{LoxTB}- SNI:Female	0.7	-1.043 to 2.443	No	ns	0.9079
Na$_v$1.8^{TLR4LoxTB}- SNI:Female vs. TLR4^{LoxTB}- SNI:Male	2.6	0.8573 to 4.343	Yes	***	0.0004
Na$_v$1.8^{TLR4LoxTB}- SNI:Female vs. TLR4^{LoxTB}- SNI:Female	2.9	1.157 to 4.643	Yes	****	<0.0001
TLR4^{LoxTB}- SNI:Male vs. TLR4^{LoxTB}- SNI:Female	0.3	-1.330 to 1.930	No	ns	0.999
Acetone Effect Size					
Male					
Sham vs. Wild Type - SNI	-8.3	-11.72 to -4.884	Yes	****	<0.0001
Sham vs. Na$_v$1.8^{TLR4LoxTB}- SNI	-7.8	-10.61 to -4.986	Yes	****	<0.0001
Sham vs. TLR4^{LoxTB}- SNI	-6.9	-9.509 to -4.291	Yes	****	<0.0001
Wild Type - SNI vs. Na$_v$1.8^{TLR4LoxTB}- SNI	0.5	-3.209 to 4.209	No	ns	0.9843
Wild Type - SNI vs. TLR4^{LoxTB}- SNI	1.4	-2.156 to 4.956	No	ns	0.7256
Na$_v$1.8^{TLR4LoxTB}- SNI vs. TLR4^{LoxTB}- SNI	0.9	-2.082 to 3.882	No	ns	0.8547
Female					
Sham vs. Wild Type - SNI	-9.7	-13.12 to -6.284	Yes	****	<0.0001
Sham vs. Na$_v$1.8^{TLR4LoxTB}- SNI	-8.9	-11.60 to -6.199	Yes	****	<0.0001
Sham vs. TLR4^{LoxTB}- SNI	-5.6	-8.209 to -2.991	Yes	****	<0.0001
Wild Type - SNI vs. Na$_v$1.8^{TLR4LoxTB}- SNI	0.8	-2.824 to 4.424	No	ns	0.9364
Wild Type - SNI vs. TLR4^{LoxTB}- SNI	4.1	0.5442 to 7.656	Yes	*	0.0177
Na$_v$1.8^{TLR4LoxTB}- SNI vs. TLR4^{LoxTB}- SNI	3.3	0.4247 to 6.175	Yes	*	0.0183

Injury marker, ATF3, in small diameter neurons is upregulated in a sex specific and TLR4 fashion

To investigate the sexual dimorphisms driving the development of neuropathic pain we used a neuronal marker of injury, ATF3, and assessed colocalization with small diameter nociceptors ($Na_v1.8^+$) and large diameter neurons ($NF200^+$) (Fig. 5.5A-B, Table 5.6). In female $Na_v1.8^{TLR4LoxTB}$ mice, we show significantly upregulated ATF3 expression in their $Na_v1.8^+$ DRG neurons 3 days post-SNI as compared to $TLR4^{LoxTB}$ mice. Conversely, in male $Na_v1.8^{TLR4LoxTB}$ mice there is no significant upregulation of ATF3 3 days post-SNI in their $Na_v1.8^+$ DRG neurons as compared to $TLR4^{LoxTB}$ counterparts. There is, however, a significant upregulation in both male and female WT mice 3 days after SNI as compared to shams (Fig. 5.5C, Table 5.6). This sets a precedent that endogenous TLR4 activation on $Na_v1.8^+$ nociceptors after nerve injury regulates transcription factors (ATF3) that are important in neuronal injury in female, but not male mice. Both male and female $Na_v1.8^{TLR4LoxTB}$ mice exhibit no significant differences in ATF3 expression after SNI as compared to $TLR4^{LoxTB}$ counterparts in $NF200^+$ neurons. There is, however, a significant upregulation in both male and female WT mice 3 days after SNI as compared to shams (Fig. 5.5.D, Table 5.6). This data demonstrates that TLR4 has an important role in regulating neuronal injury after neuropathic injury in both sexes, but the cell types that express TLR4 which are responsible for these effects differ between males and females. This interesting finding led us to investigate the downstream implications of TLR4 activation on these small diameter nociceptors via HMGB1 localization.
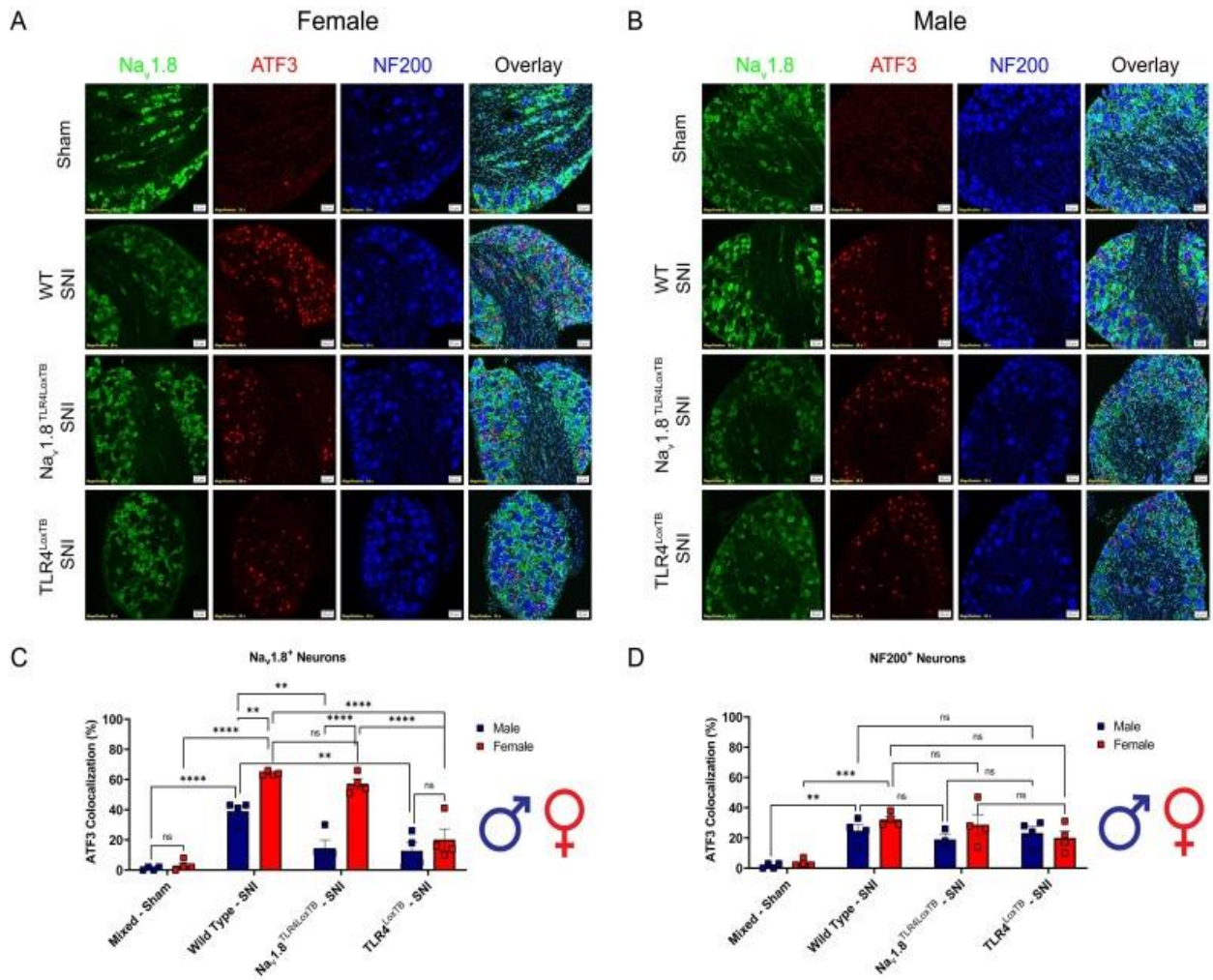
Figure 5.5. The injury marker, ATF3, is upregulated in small diameter nociceptors in a sex and genotype dependent manner via TLR4 expression. *A,* Female sham (mixed genotypes), WT, $Na_v1.8^{TLR4LoxTB}$, and $TLR4^{LoxTB}$ lumbar (L3-5) DRGs were immunostained 3D post SNI with DAPI (teal), $Na_v1.8$ (green), ATF3 (red) and NF200 (blue; representative images from n = 4 mice). ***B,*** Male sham (mixed genotypes), WT, $Na_v1.8^{TLR4LoxTB}$, and $TLR4^{LoxTB}$ lumbar (L3-5) DRGs were immunostained 3D post SNI with DAPI (teal), $Na_v1.8$ (green), ATF3 (red) and NF200 (blue; representative images from n = 4 mice). ***C,*** Quantification of ATF3 colocalization with $Na_v1.8^+$ neurons of both sexes (n = 4 per group). ***D,*** Quantification of ATF3 colocalization with $NF200^+$ neurons of both sexes (n = 4 per group). Scale bar: 50 µm. Magnification: 20x. *$p < 0.05$; **$p < 0.01$; ***$p < 0.001$; ****$p < 0.0001$. ns = not significant. (For interpretation of the references to colour in this figure legend, the reader is referred to the web version of this article.)

147

**Table 5.6.** Statistical values corresponding to the data in Figure 5.5.

Tukey's multiple comparisons test	Predicted (LS) mean diff.	95.00% CI of diff.	Below threshold?	Summary	Adjusted P Value
NF200 ATF3 Colocalization					
Male					
Mixed - Sham vs. Wild Type - SNI	-23.25	-38.34 to -8.164	Yes	**	0.0015
Mixed - Sham vs. Na$_v$1.8^{TLR4LoxTB} - SNI	-17.5	-33.79 to -1.206	Yes	*	0.0322
Mixed - Sham vs. TLR4^{LoxTB} - SNI	-21.75	-36.84 to -6.664	Yes	**	0.003
Wild Type - SNI vs. Na$_v$1.8^{TLR4LoxTB} - SNI	5.75	-10.54 to 22.04	No	ns	0.764
Wild Type - SNI vs. TLR4^{LoxTB} - SNI	1.5	-13.59 to 16.59	No	ns	0.9925
Na$_v$1.8^{TLR4LoxTB} - SNI vs. TLR4^{LoxTB} - SNI	-4.25	-20.54 to 12.04	No	ns	0.8874
Female					
Mixed - Sham vs. Wild Type - SNI	-28.75	-43.84 to -13.66	Yes	***	0.0001
Mixed - Sham vs. Na$_v$1.8^{TLR4LoxTB} - SNI	-25.25	-40.34 to -10.16	Yes	***	0.0006
Mixed - Sham vs. TLR4^{LoxTB} - SNI	-16.5	-31.59 to -1.414	Yes	*	0.0285
Wild Type - SNI vs. Na$_v$1.8^{TLR4LoxTB} - SNI	3.5	-11.59 to 18.59	No	ns	0.9172
Wild Type - SNI vs. TLR4^{LoxTB} - SNI	12.25	-2.836 to 27.34	No	ns	0.1405
Na$_v$1.8^{TLR4LoxTB} - SNI vs. TLR4^{LoxTB} - SNI	8.75	-6.336 to 23.84	No	ns	0.3955
Nav1.8 ATF3 Colocalization					
Mixed - Sham:Male vs. Mixed - Sham:Female	-2	-21.30 to 17.30	No	ns	>0.9999
Mixed - Sham:Male vs. Wild Type - SNI:Male	-38	-57.30 to -18.70	Yes	****	<0.0001
Mixed - Sham:Male vs. Wild Type - SNI:Female	-63	-82.30 to -43.70	Yes	****	<0.0001
Mixed - Sham:Male vs. Na$_v$1.8^{TLR4LoxTB} - SNI:Male	-13.5	-32.80 to 5.795	No	ns	0.325
Mixed - Sham:Male vs. Na$_v$1.8^{TLR4LoxTB} - SNI:Female	-56.25	-75.55 to -36.95	Yes	****	<0.0001
Mixed - Sham:Male vs. TLR4^{LoxTB} - SNI:Male	-11.75	-31.05 to 7.545	No	ns	0.4919
Mixed - Sham:Male vs. TLR4^{LoxTB} - SNI:Female	-19.25	-38.55 to 0.04533	No	ns	0.0508

Comparison					
Mixed - Sham:Female vs. Wild Type - SNI:Male	-36	-55.30 to -16.70	Yes	****	<0.0001
Mixed - Sham:Female vs. Wild Type - SNI:Female	-61	-80.30 to -41.70	Yes	****	<0.0001
Mixed - Sham:Female vs. $Na_v1.8^{TLR4LoxTB}$ - SNI:Male	-11.5	-30.80 to 7.795	No	ns	0.5181
Mixed - Sham:Female vs. $Na_v1.8^{TLR4LoxTB}$ - SNI:Female	-54.25	-73.55 to -34.95	Yes	****	<0.0001
Mixed - Sham:Female vs. $TLR4^{LoxTB}$ - SNI:Male	-9.75	-29.05 to 9.545	No	ns	0.7031
Mixed - Sham:Female vs. $TLR4^{LoxTB}$ - SNI:Female	-17.25	-36.55 to 2.045	No	ns	0.1037
Wild Type - SNI:Male vs. Wild Type - SNI:Female	-25	-44.30 to -5.705	Yes	**	0.0052
Wild Type - SNI:Male vs. $Na_v1.8^{TLR4LoxTB}$ - SNI:Male	24.5	5.205 to 43.80	Yes	**	0.0064
Wild Type - SNI:Male vs. $Na_v1.8^{TLR4LoxTB}$ - SNI:Female	-18.25	-37.55 to 1.045	No	ns	0.0731
Wild Type - SNI:Male vs. $TLR4^{LoxTB}$ - SNI:Male	26.25	6.955 to 45.55	Yes	**	0.0031
Wild Type - SNI:Male vs. $TLR4^{LoxTB}$ - SNI:Female	18.75	-0.5453 to 38.05	No	ns	0.0611
Wild Type - SNI:Female vs. $Na_v1.8^{TLR4LoxTB}$ - SNI:Male	49.5	30.20 to 68.80	Yes	****	<0.0001
Wild Type - SNI:Female vs. $Na_v1.8^{TLR4LoxTB}$ - SNI:Female	6.75	-12.55 to 26.05	No	ns	0.936
Wild Type - SNI:Female vs. $TLR4^{LoxTB}$ - SNI:Male	51.25	31.95 to 70.55	Yes	****	<0.0001
Wild Type - SNI:Female vs. $TLR4^{LoxTB}$ - SNI:Female	43.75	24.45 to 63.05	Yes	****	<0.0001
$Na_v1.8^{TLR4LoxTB}$ - SNI:Male vs. $Na_v1.8^{TLR4LoxTB}$ - SNI:Female	-42.75	-62.05 to -23.45	Yes	****	<0.0001
$Na_v1.8^{TLR4LoxTB}$ - SNI:Male vs. $TLR4^{LoxTB}$ - SNI:Male	1.75	-17.55 to 21.05	No	ns	>0.9999
$Na_v1.8^{TLR4LoxTB}$ - SNI:Male vs. $TLR4^{LoxTB}$ - SNI:Female	-5.75	-25.05 to 13.55	No	ns	0.972
$Na_v1.8^{TLR4LoxTB}$ - SNI:Female vs. $TLR4^{LoxTB}$ - SNI:Male	44.5	25.20 to 63.80	Yes	****	<0.0001
$Na_v1.8^{TLR4LoxTB}$ - SNI:Female vs. $TLR4^{LoxTB}$ - SNI:Female	37	17.70 to 56.30	Yes	****	<0.0001
$TLR4^{LoxTB}$ - SNI:Male vs. $TLR4^{LoxTB}$ - SNI:Female	-7.5	-26.80 to 11.80	No	ns	0.8948

TLR4 expression in small diameter neurons mediates HMGB1 translocation from the nucleus to the cytosol of the cell

We demonstrated the sufficiency of TLR4 to upregulate the injury marker, ATF3, in $Na_v1.8^+$ DRG neurons in female, but not male mice. Now that we have established a significant role for TLR4 in regulating neuronal injury, we further investigated the downstream implication of TLR4 signaling in these populations of small and large diameter DRG neurons. Here, we immunoassayed lumbar DRGs (L3-5) from female and male $Na_v1.8^{TLR4LoxTB}$, $TLR4^{LoxTB}$, and WT mice 3 days post-SNI for cellular localization of HMGB1, a DAMP, in both small ($Na_v1.8^+$) and large ($NF200^+$) diameter neurons (Fig. 5.6A, B). We found there to be a trend of increased cytosolic HMGB1 in female $Na_v1.8^+$ DRG neurons of $Na_v1.8^{TLR4LoxTB}$ mice as compared to $TLR4^{LoxTB}$ mice. Interestingly, male $Na_v1.8^{TLR4LoxTB}$ mice do not show significantly increased cytosolic HMGB1 in their $Na_v1.8^+$ DRG neurons 3 days after SNI as compared to $TLR4^{LoxTB}$ mice. These results are recapitulated only in female WT mice, indicating direct activation of TLR4 on $Na_v1.8^+$ DRG neurons through endogenous DAMP signaling is sufficient to induce mobilization of HMGB1 to the cytosol of the cell (Fig. 5.6C, Table 5.7). We find no significant differences between both male and female $Na_v1.8^{TLR4LoxTB}$ and $TLR4^{LoxTB}$ mice regarding cytosolic HMGB1 localization in $NF200^+$ large diameter DRG neurons 3 days after SNI (Fig. 5.6D, Table 5.7). These highly sex and genotype dependent results indicate that endogenous activation of TLR4 on sensory neurons in the DRG of female mice after neuropathic injury initiates cytosolic mobilization of HMGB1. This, taken together with the upregulation of ATF3 expression in nociceptors indicates females utilize a TLR4-dependent pathway to facilitate pain behaviors during a neuropathic injury.
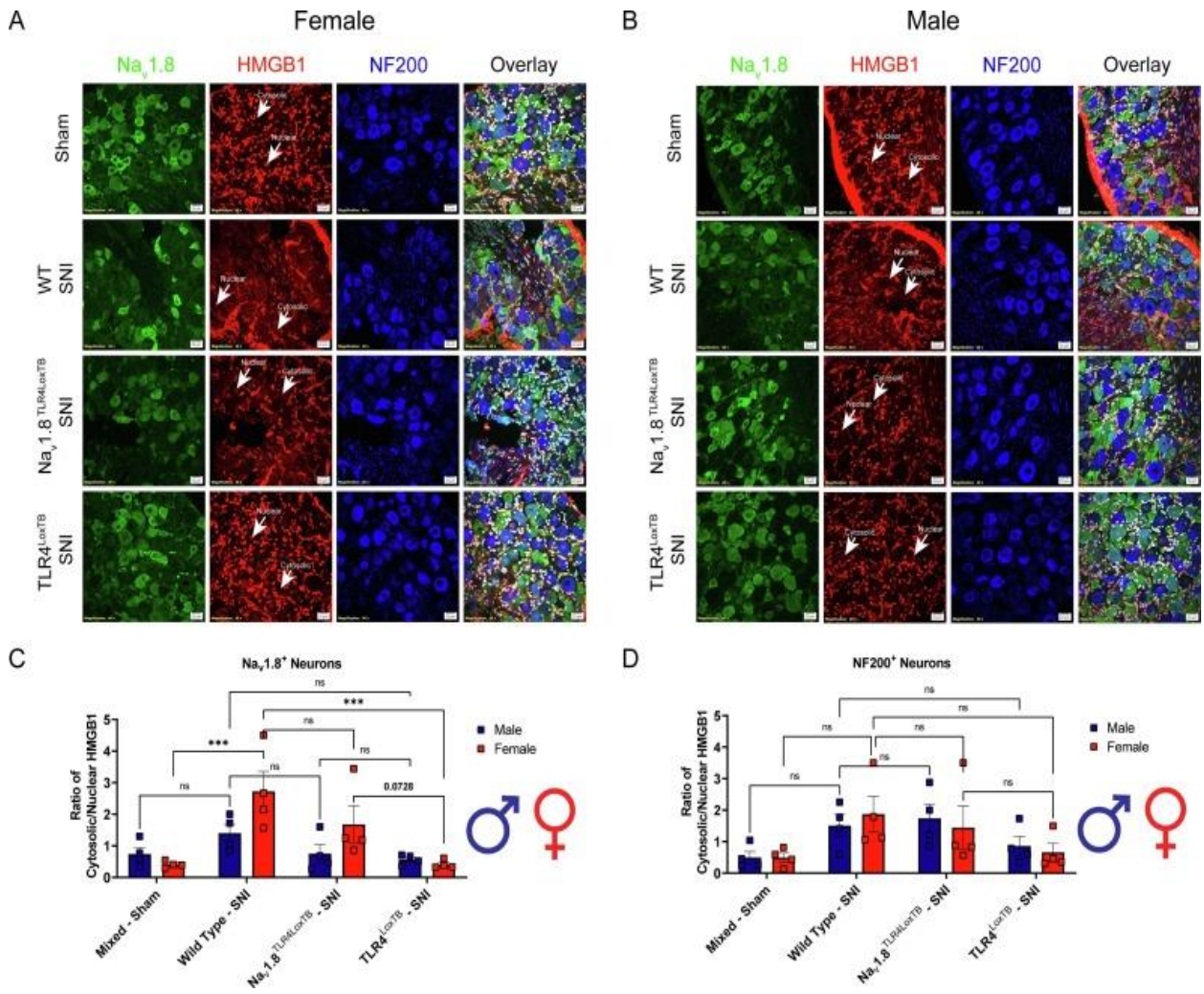
Figure 5.6. HMGB1 translocation following neuropathic injury is upregulated in a sex and genotype dependent manner in small diameter nociceptors and is mediated by TLR4. *A,* Female sham (mixed genotypes), WT, $Na_v1.8^{TLR4LoxTB}$, and $TLR4^{LoxTB}$ lumbar (L3-5) DRGs were immunostained 3D post SNI with DAPI (teal), $Na_v1.8$ (green), HGMB1 (red) and NF200 (blue; representative images from n = 4 mice). White arrows point to an example of nuclear or cytosolic localization of HMGB1. *B,* Male sham (mixed genotypes), WT, $Na_v1.8^{TLR4LoxTB}$, and $TLR4^{LoxTB}$ lumbar (L3-5) DRGs were immunostained 3D post SNI with DAPI (teal), $Na_v1.8$ (green), HGMB1 (red) and NF200 (blue; representative images from n = 4 mice). White arrows point to an example of nuclear or cytosolic localization of HMGB1. *C,* Quantification of cytosolic localization of HMGB1 in $Na_v1.8^+$ neurons of both sexes (n = 4 per group). *D,* Quantification of cytosolic localization of HMGB1 in $NF200^+$ neurons of both sexes (n = 4 per group). Scale bar: 20 µm. Magnification: 40x. *$p < 0.05$; **$p < 0.01$; ****$p < 0.0001$. ns = not significant. (For interpretation of the references to colour in this figure legend, the reader is referred to the web version of this article.)

151

**Table 5.7.** Statistical values corresponding to the data in Figure 5.6.

Tukey's multiple comparisons test	Mean Diff.	95.00% CI of diff.	Below threshold?	Summary	Adjusted P Value
NF200 HMGB1 Localization					
Male					
Mixed - Sham vs. Wild Type - SNI	-1.013	-2.613 to 0.5877	No	ns	0.3233
Mixed - Sham vs. Na$_v$1.8^{TLR4LoxTB} - SNI	-1.243	-2.843 to 0.3577	No	ns	0.1687
Mixed - Sham vs. TLR4^{LoxTB} - SNI	-0.3675	-1.968 to 1.233	No	ns	0.9202
Wild Type - SNI vs. Na$_v$1.8^{TLR4LoxTB} - SNI	-0.23	-1.830 to 1.370	No	ns	0.9784
Wild Type - SNI vs. TLR4^{LoxTB} - SNI	0.645	-0.9552 to 2.245	No	ns	0.6859
Na$_v$1.8^{TLR4LoxTB} - SNI vs. TLR4^{LoxTB} - SNI	0.875	-0.7252 to 2.475	No	ns	0.4483
Female					
Mixed - Sham vs. Wild Type - SNI	-1.38	-2.980 to 0.2202	No	ns	0.1085
Mixed - Sham vs. Na$_v$1.8^{TLR4LoxTB} - SNI	-0.955	-2.555 to 0.6452	No	ns	0.373
Mixed - Sham vs. TLR4^{LoxTB} - SNI	-0.1675	-1.768 to 1.433	No	ns	0.9914
Wild Type - SNI vs. Na$_v$1.8^{TLR4LoxTB} - SNI	0.425	-1.175 to 2.025	No	ns	0.883
Wild Type - SNI vs. TLR4^{LoxTB} - SNI	1.213	-0.3877 to 2.813	No	ns	0.1849
Na$_v$1.8^{TLR4LoxTB} - SNI vs. TLR4^{LoxTB} - SNI	0.7875	-0.8127 to 2.388	No	ns	0.5369
Nav1.8 HMGB1 Localization					
Male					
Mixed - Sham vs. Wild Type - SNI	-0.66	-2.071 to 0.7513	No	ns	0.7231
Mixed - Sham vs. Na$_v$1.8^{TLR4LoxTB} - SNI	-0.01	-1.421 to 1.401	No	ns	>0.9999
Mixed - Sham vs. TLR4^{LoxTB} - SNI	0.175	-1.236 to 1.586	No	ns	0.9996
Wild Type - SNI vs. Na$_v$1.8^{TLR4LoxTB} - SNI	0.65	-0.7613 to 2.061	No	ns	0.7364
Wild Type - SNI vs. TLR4^{LoxTB} - SNI	0.835	-0.5763 to 2.246	No	ns	0.4787
Na$_v$1.8^{TLR4LoxTB} - SNI vs. TLR4^{LoxTB} - SNI	0.185	-1.226 to 1.596	No	ns	0.9994
Female					
Mixed - Sham vs. Wild Type - SNI	-2.31	-3.721 to -0.8987	Yes	***	0.0005

Mixed - Sham vs. Na$_v$1.8^{TLR4LoxTB} - SNI	-1.268	-2.679 to 0.1438	No	ns	0.0958
Mixed - Sham vs. TLR4^{LoxTB} - SNI	0.0025	-1.409 to 1.414	No	ns	>0.9999
Wild Type - SNI vs. Na$_v$1.8^{TLR4LoxTB} - SNI	1.043	-0.3688 to 2.454	No	ns	0.2405
Wild Type - SNI vs. TLR4^{LoxTB} - SNI	2.313	0.9012 to 3.724	Yes	***	0.0005
Na$_v$1.8^{TLR4LoxTB} - SNI vs. TLR4^{LoxTB} - SNI	1.27	-0.1413 to 2.681	No	ns	0.0948

DISCUSSION

In the nociceptive system, bi-directional communication between neuronal and non-neuronal cells is a core mechanism in mediating the response to injury (Iwata, 2017; Szabo-Pardi, 2021). Emerging evidence suggests that both sexes utilize myeloid-derived immune cells in the central and peripheral nervous system to drive cytokine production and subsequent neuronal sensitization (Peng, 2016; Yu et al., 2020). Currently, little is known about direct neuronal response to activation by endogenous DAMP signaling during injury. Here, we report that female mice utilize a specific pathway where direct activation of TLR4 by endogenous danger signals on small diameter nociceptors in the DRG leads to upregulation of stress-induced ATF3 and DAMPs (HMGB1) in the lumbar DRG. Additionally, these molecular changes lead to a delay in the onset of neuropathic pain associated with peripheral nerve injury in a TLR4 dependent manner (Fig. 5.7). Our genetic and histological experiments demonstrate a robust sexual dimorphism wherein peripheral nociceptors expressing TLR4 mediate the early onset of neuropathic mechanical hypersensitivity in female mice, in addition to regulating molecular changes in peripheral nervous tissue. Moreover, TLR4 expression on Na$_v$1.8$^+$ DRG neurons is both necessary and sufficient for the behavioral response to neuropathic injury. Use of this genetic model has allowed us to elucidate a novel pathway to neuronal injury in female mice. Our results support the

idea that TLR4 signaling on peripheral nociceptors plays an important role in direct sensitization through the up-regulation of stress-induced transcription factors and DAMPs in these cells. In our view, this identifies a novel mechanism of direct neuronal sensitization in female mice crucial for the early onset of neuropathic pain. This provides novel evidence for the dissection of the sexually dimorphic response to tissue injury (Anwar et al., 2019).
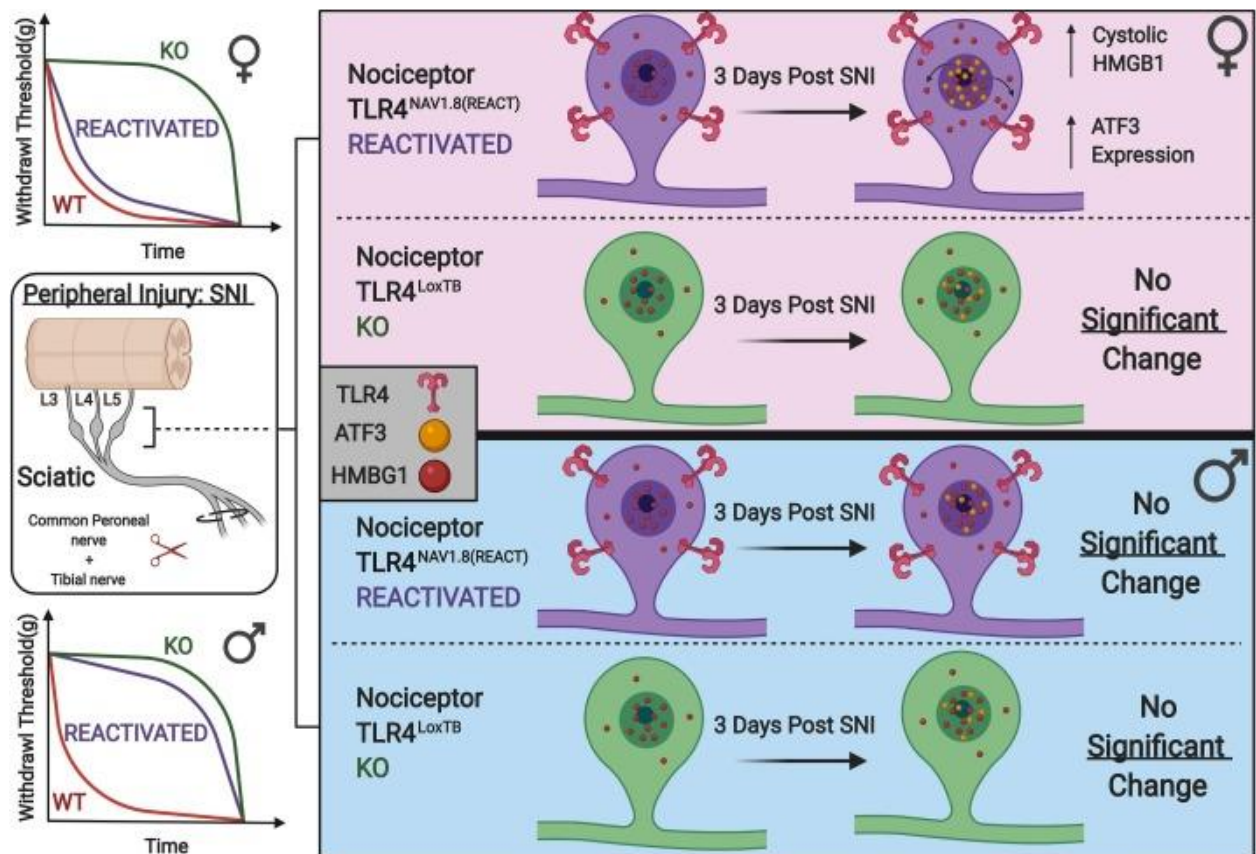
Figure 5.7. Schematic model indicated that TLR4 expressed on Na$_v$1.8$^+$ nociceptors in the lumbar DRGs (L3-5) plays an important role in regulating the localization of HMGB1 in response to neuropathic injury in females, but not males. This is both behaviorally and molecularly significant, as female mice lacking TLR4 expression on their Na$_v$1.8 + nociceptors exhibit reduced mechanical hypersensitivity following SNI. Moreover, re-expression of TLR4 only on these Na$_v$1.8 nociceptors recapitulates a behavioral phenotype similar to that of wild type mice. This effect is not present in male mice of either genotype.

Women are found to have a higher incidence of neuropathic pain as compared to males, in addition to lowered efficacy of common therapeutics (DiBonaventura et al., 2017). As such, there exists a need to understand the core mechanisms that differentiate male and female nociceptive circuitry. Compared with the well-documented behavioral phenotypes seen after SNI, we show that male and female wild type mice exhibit no differences in the magnitude of both mechanical hypersensitivity and cold allodynia (Bravo-Caparrós et al., 2019; Sorge, 2015). Interestingly, evidence suggests a fundamental disconnect between the mechanisms involved in the onset of neuropathic pain (Mogil, 2020). For example, male mice lacking chemokine receptor 1 (CX3CR1) expressing immune cells exhibit delayed development of been shown that neuronally expressed NOD-like receptor protein 3 (NLRP3) inflammasome has sex specific effects in pain, where females are dependent on NLRP3 in sensory neurons to facilitate mechanical hypersensitivity (Cowie et al., 2019). NLRP3 inflammasome activation is enhanced via intracellular cascades initiated through TLR4 activation (Bauernfeind et al., 2009). Importantly, inflammasome activation in tissue injury increases production of IL-1β, which plays a prominent role in pain, specifically mechanical hypersensitivity (Chen, 2015). Sensory neurons express large amounts of interleukin (IL) −1β receptor, which leads us to believe that autocrine signaling through the TLR4 and NLRP3 pathways in sensory neurons presents a point of sexually divergent mechanisms of pain sensitization.

In response to this, we sought to characterize endogenous DAMP signaling and chose to focus on HMGB1, specifically, as it has been implicated by numerous studies in chronic pain development (Campana et al., 2009; O'Connor et al., 2003; Zhao et al., 2015). HMGB1 is localized

in the nucleus of cells in homeostasis, however; with adequate stimulation, hyperacetylation of the protein causes translocation to the cytosolic and subsequent release in both neuronal and non-neuronal cells (Lotze & Tracey, 2005). Secreted HMGB1 acts on a variety of receptors, namely the receptor for advanced glycation and end products (RAGE), TLR2, TLR4 and TLR5 all of which are involved in immunomodulation and neuroinflammation (Das et al., 2016; Frasnelli et al., 2015). Interestingly, HMGB1 is capable of upregulating canonical NLRP3 activation, both of which are dependent on the nuclear factor (NF)-κB pathway which is directly linked to TLR4 signaling (Chi et al., 2015). Downstream consequences of neuronally-expressed TLR4 activation are poorly understood, however; evidence does suggest that neurons are able to produce cytokines through its activation (Leow-Dyke et al., 2012). Moreover, it has been demonstrated that activation of TLRs on sensory neurons does promote the production of neuropeptides and chemokines which may facilitate neuronal sensitization (Diogenes et al., 2011). To our surprise, we have identified a robust sexual dimorphism in the lumbar DRG 3 days after SNI. Wild type female mice exhibit elevated cytosolic localization of HMGB1 in $Na_v1.8$ expressing nociceptors. Cytosolic localization of HMGB1 after injury is decreased in both male and female TLR4 knockouts, but only females with TLR4 reactivated in their $Na_v1.8$ neurons see an increase that trends towards a wild type phenotype. Moreover, this same population of peripheral nociceptors in females express higher levels of neuronal injury measured by upregulated ATF3 expression. We demonstrate that this increase in ATF3 expression is linked to TLR4 expression, as both male and female TLR4 knockouts have lower expression of ATF3 after injury. ATF3 has been shown to be a negative regulator of TLR4 activity by dampening the activity of NF-κB. Although co-expression of ATF3 and HMGB1 were not performed, it is a potential that the increase in ATF3 localization within

Na$_v$1.8$^+$ neurons is due to endogenous TLR4 activation from tissue injury (Kwon et al., 2015; Rao et al., 2015). These data provide evidence that neuronally-expressed HMGB1 is involved in the onset of neuropathic pain in females, however; in future experiments it may be necessary to distinguish specific subsets of nociceptor populations (isolectin b4 (IB4) vs. calcitonin gene related peptide (CGRP)) that express HMGB1 to enhance granularity as to the specific circuitry involved. Nonetheless, this novel finding leads us to believe that females utilize more neuronally-driven mechanisms to facilitate chronic pain development.

To better understand the implications of direct neuronal activation through endogenous TLR4 signaling, we use two recently developed transgenic lines wherein TLR4 is either deleted (Na$_v$1.8$^{TLR4fl/fl}$) or reactivated (Na$_v$1.8^{TLR4LoxTB}) constitutively in a cre dependent manner (Jia et. Al., 2020). Evidence suggests TLR4 plays a major role in regulating the onset of neuropathic mechanical hypersensitivity, but not it's persistence (Hu et al., 2018). Here, we investigate the nocifensive response to SNI in both male and female mice using mechanical and thermal measures. Interestingly, removal of TLR4 only on Na$_v$1.8$^+$ nociceptors delay the onset of mechanical hypersensitivity but not cold allodynia in female mice. Additionally, re-expression of TLR4 on these same nociceptors confers a phenotype that recapitulates a wild type behavioral response to neuropathic injury only in females. Lastly, whole body knockouts of TLR4 in both sexes behave similarly, conferring necessity during the onset of neuropathic pain in both sexes. Together, these data indicate that neuronally-expressed TLR4 is both necessary and sufficient during the onset of neuropathic mechanical hypersensitivity. The involvement of TLR4 signaling in thermal hyperalgesia is unclear. TLR4 deficiency has been shown to reduce mechanical allodynia, but not

157

thermal hyperalgesia in a model of trigeminal neuropathic pain (Hu et al., 2018). Conversely, administration of a TLR4 antagonist, lipopolysaccharide (LPS)-RS, after chronic constriction injury (CCI) reduced both mechanical allodynia and thermal hyperalgesia (Jurga et al., 2016). We report no significant differences in cold allodynia, measured by behavioral response to acetone application, throughout the entirety of our behavioral experiments, independent of both sex and genotype. Interestingly, a recent study highlights how over 80% of cold-sensitive neurons in the DRG do not express $Na_v1.8$ (Luiz et al., 2019). As we study the role of TLR4 in the $Na_v1.8$ expressing neuronal population, it is a potential that co-expression between TLR4 and cold sensitive neurons (TRPM8) is not high enough to confer biological relevant behavioral changes in a murine model of neuropathic pain.

A major unanswered question from this work is how the spontaneous ectopic activity of $Nav1.8^+$ DRG neurons is affected by direct TLR4 activity following neuropathic injury. Our histological data provides some insights as to what molecular changes these neurons undergo soon after injury, however; changes in their excitability are unknown. Following SNI, there is a large increase in the spontaneous activity of DRG neurons in addition to afferent fibers in the injured sciatic nerve (Seltzer et al., 1990; Wall & Gutnick, 1974). As seen in our model and consistent with others, whole body knockouts of TLR4 exhibit attenuated pain responses following injury (Piao et al., 2018; Tanga et al., 2005). While we currently cannot pinpoint the effects of direct TLR4 activation on DRG neuron excitability, there is evidence in the brain where TLR4 activation leads to increased neuronal excitability in the dentate gyrus after injury (Li, Korgaonkar, et al., 2015). Although not directly translatable, this does provide compelling

evidence that TLR4 can modulate neuronal excitability. Therefore, understanding the role of TLR4 in regulating the spontaneous activity and subsequent excitability of DRG nociceptors will yield significant insights as to how the transient changes in behavior we see evolves into long-term nociceptor plasticity. This is a research endeavor we plan on pursuing as a follow-up to the present study.

In conclusion, we have identified a novel and sexually dimorphic mechanism of neuronal injury in a murine model of neuropathic pain. Female, but not male mice utilize endogenous TLR4 activation on their $Na_v1.8$ expressing nociceptors to facilitate the onset of mechanical hypersensitivity following SNI. Additionally, TLR4 expression on $Na_v1.8$ expressing nociceptors plays an important role in regulating neuronal localization of HMGB1 in female mice. Taken together, these data indicate a unique mechanism of neuronal injury and behavioral output following peripheral injury in female mice. This work is poised as an initial endeavor into the sexually dimorphic mechanisms that regulate pain plasticity.

CHAPTER 6

SUMMARY AND SIGNIFIGANCE

In the last few years there has been a significant push towards uncovering the mechanisms that facilitate sex differences in pain. With the increased focus on including biological sex as a variable in pre-clinical studies numerous studies have provided valuable insights as to how the cellular mechanisms between males and females differ. Microglia were initially ascribed as the primary mediator of sex-dependent differences in pain development (Sorge, 2011; Sorge, 2015). However, numerous studies that followed suite have provided robust evidence that the peripheral immune and nervous systems influence these nociceptive circuits in a sex-dependent manner more than we previously believed (Lopes, 2017; Peng, 2016; Szabo-Pardi et al., 2021; Woller et al., 2015; Woller et al., 2016; Yu, 2020; Zhang et al., 2016). Signals that arise from the DRG are modulated by a plethora of neuro and immunomodulatory molecules which rely on bidirectional communication between the nervous and immune systems. Inflammatory mediates such as CSF1, CCL2, HMGB1, IL-6, IL-1β and TNFα are all upregulated to varying degrees during CIPN, surgery-induced neuropathy and inflammation and modulate the nociceptive system in various sex- and cell-specific ways. Our lab and others have demonstrated that robust sex differences related to TLR4 signaling exist in both central and peripheral systems which are responsible for mediating chronic pain development (Agalave et al., 2021; Agalave, 2020; Huck et al., 2021; Sorge, 2011; Szabo-Pardi et al., 2021; Woller et al., 2016).

Literature over the last few decades as shown a significant correlation between expression, upregulation, and modulation of HMGB1 and various forms of chronic pain (Lotze & Tracey,

2005; O'Connor et al., 2003; Park et al., 2004; Yamasoba et al., 2016). We, and others, believe that endogenous danger signals such as HMGB1 have a prominent sex- and cell-specific role in mediating the development of neuropathic pain (Agalave et al., 2014; Agalave, 2020; Rudjito, 2020; Szabo-Pardi et al., 2021). The data presented throughout this dissertation suggests that the inflammatory signaling pathways differ between sexes where TLR4 activation on male peripheral macrophages mediates inflammation and neuropathic pain development, whereas direct activation of TLR4 on female nociceptors is responsible for these effects. This work serves as a foundation in the Burton Lab for future research aimed at dissecting sex- and cell-specific mechanisms of chronic pain development and subsequent therapeutic targets.

REFERENCES

Ackland, G. L., Kazymov, V., Marina, N., Singer, M., & Gourine, A. V. (2013). Peripheral neural detection of danger-associated and pathogen-associated molecular patterns. *Crit Care Med*, *41*(6), e85-92. https://doi.org/10.1097/CCM.0b013e31827c0b05

Agalave, N. M., Larsson, M., Abdelmoaty, S., Su, J., Baharpoor, A., Lundbäck, P., . . . Svensson, C. I. (2014). Spinal HMGB1 induces TLR4-mediated long-lasting hypersensitivity and glial activation and regulates pain-like behavior in experimental arthritis. *Pain*, *155*(9), 1802-1813. https://doi.org/10.1016/j.pain.2014.06.007

Agalave, N. M., Mody, P. H., Szabo-Pardi, T. A., Jeong, H. S., & Burton, M. D. (2021). Neuroimmune Consequences of eIF4E Phosphorylation on Chemotherapy-Induced Peripheral Neuropathy. *Front Immunol*, *12*, 642420. https://doi.org/10.3389/fimmu.2021.642420

Agalave, N. M., & Svensson, C. I. (2015). Extracellular high-mobility group box 1 protein (HMGB1) as a mediator of persistent pain. *Mol Med*, *20*, 569-578. https://doi.org/10.2119/molmed.2014.00176

Agalave, N. M. a. R. R. a. F. A. B. a. K. P. E. a. S. K. a. N. Y. a. S.-P. T. A. a. U. C. M. a. (2020). Sex-dependent role of microglia in disulfide HMGB1-mediated mechanical hypersensitivity. *Pain*. https://doi.org/10.1097/j.pain.0000000000002033

Ajibade, A. A., Wang, H. Y., & Wang, R. F. (2013). Cell type-specific function of TAK1 in innate immune signaling. *Trends Immunol*, *34*(7), 307-316. https://doi.org/10.1016/j.it.2013.03.007

Ajibade, A. A., Wang, Q., Cui, J., Zou, J., Xia, X., Wang, M., . . . Wang, R. F. (2012). TAK1 negatively regulates NF-κB and p38 MAP kinase activation in Gr-1+CD11b+ neutrophils. *Immunity*, *36*(1), 43-54. https://doi.org/10.1016/j.immuni.2011.12.010

Akin, E. J., Alsaloum, M., Higerd, G. P., Liu, S., Zhao, P., Dib-Hajj, F. B., . . . Dib-Hajj, S. D. (2021). Paclitaxel increases axonal localization and vesicular trafficking of Nav1.7. *Brain*, *144*(6), 1727-1737. https://doi.org/10.1093/brain/awab113

Akira, S., & Takeda, K. (2004). Toll-like receptor signalling. *Nat Rev Immunol*, *4*(7), 499-511. https://doi.org/10.1038/nri1391

Alles, S. R. A., & Smith, P. A. (2018). Etiology and Pharmacology of Neuropathic Pain. *Pharmacol Rev*, *70*(2), 315-347. https://doi.org/10.1124/pr.117.014399

Allette, Y. M., Due, M. R., Wilson, S. M., Feldman, P., Ripsch, M. S., Khanna, R., & White, F. A. (2014). Identification of a functional interaction of HMGB1 with Receptor for Advanced Glycation End-products in a model of neuropathic pain. *Brain Behav Immun*, *42*, 169-177. https://doi.org/10.1016/j.bbi.2014.06.199

Alshawaf, A. J., Viventi, S., Qiu, W., D'Abaco, G., Nayagam, B., Erlichster, M., . . . Dottori, M. (2018). Phenotypic and Functional Characterization of Peripheral Sensory Neurons derived from Human Embryonic Stem Cells. *Sci Rep*, *8*(1), 603. https://doi.org/10.1038/s41598-017-19093-0

Alvarez, B., Revilla, C., Chamorro, S., López-Fraga, M., Alonso, F., Domínguez, J., & Ezquerra, A. (2006). Molecular cloning, characterization and tissue expression of porcine Toll-like receptor 4. *Dev Comp Immunol*, *30*(4), 345-355. https://doi.org/10.1016/j.dci.2005.06.020

Anderson, K. V., Jürgens, G., & Nüsslein-Volhard, C. (1985). Establishment of dorsal-ventral polarity in the Drosophila embryo: genetic studies on the role of the Toll gene product. *Cell*, *42*(3), 779-789. https://doi.org/10.1016/0092-8674(85)90274-0

Anwar, M. A., Shah, M., Kim, J., & Choi, S. (2019). Recent clinical trends in Toll-like receptor targeting therapeutics. *Med Res Rev*, *39*(3), 1053-1090. https://doi.org/10.1002/med.21553

Araya, E. I., Barroso, A. R., Turnes, J. M., Radulski, D. R., Jaganaught, J. A., Zampronio, A. R., & Chichorro, J. G. (2020). Toll-like receptor 4 (TLR4) signaling in the trigeminal ganglion mediates facial mechanical and thermal hyperalgesia in rats. *Physiol Behav*, *226*, 113127. https://doi.org/10.1016/j.physbeh.2020.113127

Barginear, M., Dueck, A. C., Allred, J. B., Bunnell, C., Cohen, H. J., Freedman, R. A., . . . Jatoi, A. (2019). Age and the Risk of Paclitaxel-Induced Neuropathy in Women with Early-Stage Breast Cancer (Alliance A151411): Results from 1,881 Patients from Cancer and Leukemia Group B (CALGB) 40101. *Oncologist*, *24*(5), 617-623. https://doi.org/10.1634/theoncologist.2018-0298

Barrett, A. C. (2006). Low efficacy opioids: implications for sex differences in opioid antinociception. *Exp Clin Psychopharmacol*, *14*(1), 1-11. https://doi.org/10.1037/1064-1297.14.1.1

Bartley, E. J., & Fillingim, R. B. (2013). Sex differences in pain: a brief review of clinical and experimental findings. *Br J Anaesth*, *111*(1), 52-58. https://doi.org/10.1093/bja/aet127

Basbaum, A. I. a. B. D. M. a. S. G. a. J. D. (2009). Cellular and Molecular Mechanisms of Pain. In.

Bauer, R. N., Diaz-Sanchez, D., & Jaspers, I. (2012). Effects of air pollutants on innate immunity: the role of Toll-like receptors and nucleotide-binding oligomerization domain-like receptors. *J Allergy Clin Immunol*, *129*(1), 14-24; quiz 25-16. https://doi.org/10.1016/j.jaci.2011.11.004

Bauernfeind, F. G., Horvath, G., Stutz, A., Alnemri, E. S., MacDonald, K., Speert, D., . . . Latz, E. (2009). Cutting edge: NF-kappaB activating pattern recognition and cytokine receptors license NLRP3 inflammasome activation by regulating NLRP3 expression. *J Immunol*, *183*(2), 787-791. https://doi.org/10.4049/jimmunol.0901363

Belle, M. a. G. D. a. C. G. a. M. S. A. a. C. F. a. G. P. a. C. A. (2017). Tridimensional Visualization and Analysis of Early Human Development. *Cell*. https://doi.org/10.1016/j.cell.2017.03.008

Bennett, M. L., Bennett, F. C., Liddelow, S. A., Ajami, B., Zamanian, J. L., Fernhoff, N. B., . . . Barres, B. A. (2016). New tools for studying microglia in the mouse and human CNS. *Proc Natl Acad Sci U S A*, *113*(12), E1738-1746. https://doi.org/10.1073/pnas.1525528113

Bertani, F. R. a. M. P. a. F. M. a. I. M. a. R. G. a. P. F. a. S. D. a. T. G. a. T. M. a. B. L. a. (2017). Classification of M1/M2-polarized human macrophages by label-free hyperspectral reflectance confocal microscopy and multivariate analysis. *Scientific Reports , pmid = 28827726*. https://doi.org/10.1038/s41598-017-08121-8

Bestall, S. M., Hulse, R. P., Blackley, Z., Swift, M., Ved, N., Paton, K., . . . Donaldson, L. F. (2018). Sensory neuronal sensitisation occurs through HMGB-1-RAGE and TRPV1 in high-glucose conditions. *J Cell Sci*, *131*(14). https://doi.org/10.1242/jcs.215939

Bettoni, I., Comelli, F., Rossini, C., Granucci, F., Giagnoni, G., Peri, F., & Costa, B. (2008). Glial TLR4 receptor as new target to treat neuropathic pain: efficacy of a new receptor antagonist in a model of peripheral nerve injury in mice. *Glia*, *56*(12), 1312-1319. https://doi.org/10.1002/glia.20699

Bhattacharyya, S., Wang, W., Qin, W., Cheng, K., Coulup, S., Chavez, S., . . . Varga, J. (2018). TLR4-dependent fibroblast activation drives persistent organ fibrosis in skin and lung. *JCI Insight*, *3*(13). https://doi.org/10.1172/jci.insight.98850

Black, J. A., Nikolajsen, L., Kroner, K., Jensen, T. S., & Waxman, S. G. (2008). Multiple sodium channel isoforms and mitogen-activated protein kinases are present in painful human neuromas. *Ann Neurol*, *64*(6), 644-653. https://doi.org/10.1002/ana.21527

Bowman, C. C., Rasley, A., Tranguch, S. L., & Marriott, I. (2003). Cultured astrocytes express toll-like receptors for bacterial products. *Glia*, *43*(3), 281-291. https://doi.org/10.1002/glia.10256

Boyette-Davis, J., Xin, W., Zhang, H., & Dougherty, P. M. (2011). Intraepidermal nerve fiber loss corresponds to the development of taxol-induced hyperalgesia and can be prevented by treatment with minocycline. *Pain*, *152*(2), 308-313. https://doi.org/10.1016/j.pain.2010.10.030

Brady, B. L., Lucci, M., Wilson, K., Fox, K. M., Wojtynek, J., Cooper, C., . . . Dokubo, I. (2021). Chemotherapy-induced peripheral neuropathy in metastatic breast cancer patients initiating intravenous paclitaxel/nab-paclitaxel. *Am J Manag Care*, *27*(1 Spec. No.), SP37-SP43. https://doi.org/10.37765/ajmc.2021.88562

Bravo-Caparrós, I., Perazzoli, G., Yeste, S., Cikes, D., Baeyens, J. M., Cobos, E. J., & Nieto, F. R. (2019). Sigma-1 Receptor Inhibition Reduces Neuropathic Pain Induced by Partial Sciatic Nerve Transection in Mice by Opioid-Dependent and -Independent Mechanisms. *Front Pharmacol*, *10*, 613. https://doi.org/10.3389/fphar.2019.00613

Bronte, V. a. M. P. J. (2015). Understanding local macrophage phenotypes in disease: Modulating macrophage function to treat cancer. In.

Byrd-Leifer, C. A., Block, E. F., Takeda, K., Akira, S., & Ding, A. (2001). The role of MyD88 and TLR4 in the LPS-mimetic activity of Taxol. *Eur J Immunol*, *31*(8), 2448-2457. https://doi.org/10.1002/1521-4141(200108)31:8

Calil, I. L., Zarpelon, A. C., Guerrero, A. T., Alves-Filho, J. C., Ferreira, S. H., Cunha, F. Q., . . . Verri, W. A. (2014). Lipopolysaccharide induces inflammatory hyperalgesia triggering a TLR4/MyD88-dependent cytokine cascade in the mice paw. *PLoS One*, *9*(3), e90013. https://doi.org/10.1371/journal.pone.0090013

Campana, L., Bosurgi, L., Bianchi, M. E., Manfredi, A. A., & Rovere-Querini, P. (2009). Requirement of HMGB1 for stromal cell-derived factor-1/CXCL12-dependent migration of macrophages and dendritic cells. *J Leukoc Biol*, *86*(3), 609-615. https://doi.org/10.1189/jlb.0908576

Carpenter, T. S., Parkin, J., & Khalid, S. (2016). The Free Energy of Small Solute Permeation through the Escherichia coli Outer Membrane Has a Distinctly Asymmetric Profile. *J Phys Chem Lett*, *7*(17), 3446-3451. https://doi.org/10.1021/acs.jpclett.6b01399

Chaplan, S. R. a. B. F. W. a. P. J. W. a. C. J. M. a. Y. T. L. (1994). Quantitative assessment of tactile allodynia in the rat paw. *Journal of Neuroscience Methods*. https://doi.org/10.1016/0165-0270(94)90144-9

Chase, M. A., Wheeler, D. S., Lierl, K. M., Hughes, V. S., Wong, H. R., & Page, K. (2007). Hsp72 induces inflammation and regulates cytokine production in airway epithelium through a TLR4- and NF-kappaB-dependent mechanism. *J Immunol*, *179*(9), 6318-6324. https://doi.org/10.4049/jimmunol.179.9.6318

Chen, B. L., Li, Y. Q., Xie, D. H., He, Q. L., & Yang, X. X. (2012). Blocking TNF-α with infliximab alleviates ovariectomy induced mechanical and thermal hyperalgesia in rats. *Neurol Sci*, *33*(3), 527-533. https://doi.org/10.1007/s10072-011-0743-9

Chen, P. a. P. X. a. B. P. (2015). Role of macrophages in Wallerian degeneration and axonal regeneration after peripheral nerve injury. In.

Chen, Z. J. (2012). Ubiquitination in signaling to and activation of IKK. *Immunol Rev*, *246*(1), 95-106. https://doi.org/10.1111/j.1600-065X.2012.01108.x

Cheng, X. L., Liu, H. Q., Wang, Q., Huo, J. G., Wang, X. N., & Cao, P. (2015). Chemotherapy-induced peripheral neurotoxicity and complementary and alternative medicines: progress and perspective. *Front Pharmacol*, *6*, 234. https://doi.org/10.3389/fphar.2015.00234

Chernykh, E. R. a. S. E. Y. a. S. N. M. a. M. S. A. a. D. M. N. a. M. E. V. a. O. A. A. (2016). Safety and therapeutic potential of m2 macrophages in stroke treatment. *Cell Transplantation*. https://doi.org/10.3727/096368915X690279

Chi, W., Chen, H., Li, F., Zhu, Y., Yin, W., & Zhuo, Y. (2015). HMGB1 promotes the activation of NLRP3 and caspase-8 inflammasomes via NF-κB pathway in acute glaucoma. *J Neuroinflammation*, *12*, 137. https://doi.org/10.1186/s12974-015-0360-2

Chiappini, S., & Schifano, F. (2016). A Decade of Gabapentinoid Misuse: An Analysis of the European Medicines Agency's 'Suspected Adverse Drug Reactions' Database. *CNS Drugs*, *30*(7), 647-654. https://doi.org/10.1007/s40263-016-0359-y

Chiu, I. M., Barrett, L. B., Williams, E. K., Strochlic, D. E., Lee, S., Weyer, A. D., . . . Woolf, C. J. (2014). Transcriptional profiling at whole population and single cell levels reveals somatosensory neuron molecular diversity. *Elife*, *3*. https://doi.org/10.7554/eLife.04660

Chou, P. L., Fang, S. Y., Sun, J. L., Rau, K. M., & Lee, B. O. (2018). Gender Difference in Cancer Patients' Adherence to Analgesics and Related Outcomes of Pain Management. *Cancer Nurs*, *41*(6), E11-E18. https://doi.org/10.1097/NCC.0000000000000532

Clausen, B. E. a. B. C. a. R. W. a. R. R. a. F. I. (1999). Conditional gene targeting in macrophages and granulocytes using LysMcre mice. *Transgenic Research*. https://doi.org/10.1023/A:1008942828960

Cobos, E. J. a. N. C. A. a. G. F. a. C. V. a. B.-C. I. a. G.-C. R. a. R. P. a. A. N. A. a. L. (2018). Mechanistic Differences in Neuropathic Pain Modalities Revealed by Correlating Behavior with Global Expression Profiling. *Cell Reports*. https://doi.org/10.1016/j.celrep.2018.01.006

Cowie, A. M., Menzel, A. D., O'Hara, C., Lawlor, M. W., & Stucky, C. L. (2019). NOD-like receptor protein 3 inflammasome drives postoperative mechanical pain in a sex-dependent manner. *Pain*, *160*(8), 1794-1816. https://doi.org/10.1097/j.pain.0000000000001555

Dahlhamer, J., Lucas, J., Zelaya, C., Nahin, R., Mackey, S., DeBar, L., . . . Helmick, C. (2018). Prevalence of Chronic Pain and High-Impact Chronic Pain Among Adults - United States, 2016. *MMWR Morb Mortal Wkly Rep*, *67*(36), 1001-1006. https://doi.org/10.15585/mmwr.mm6736a2

Das, N., Dewan, V., Grace, P. M., Gunn, R. J., Tamura, R., Tzarum, N., . . . Yin, H. (2016). HMGB1 Activates Proinflammatory Signaling via TLR5 Leading to Allodynia. *Cell Rep*, *17*(4), 1128-1140. https://doi.org/10.1016/j.celrep.2016.09.076

De Paoli, F., Staels, B., & Chinetti-Gbaguidi, G. (2014). Macrophage phenotypes and their modulation in atherosclerosis. *Circ J*, *78*(8), 1775-1781. https://doi.org/10.1253/circj.cj-14-0621

Decosterd, I. a. W. C. J. (2000). Spared nerve injury: An animal model of persistent peripheral neuropathic pain. *Pain*. https://doi.org/10.1016/S0304-3959(00)00276-1

DeLeo, J. A., Tanga, F. Y., & Tawfik, V. L. (2004). Neuroimmune activation and neuroinflammation in chronic pain and opioid tolerance/hyperalgesia. *Neuroscientist*, *10*(1), 40-52. https://doi.org/10.1177/1073858403259950

DiBonaventura, M. D., Sadosky, A., Concialdi, K., Hopps, M., Kudel, I., Parsons, B., . . . Farrar, J. T. (2017). The prevalence of probable neuropathic pain in the US: results from a multimodal general-population health survey. *J Pain Res*, *10*, 2525-2538. https://doi.org/10.2147/JPR.S127014

Diogenes, A., Ferraz, C. C., Akopian, A. N., Henry, M. A., & Hargreaves, K. M. (2011). LPS sensitizes TRPV1 via activation of TLR4 in trigeminal sensory neurons. *J Dent Res*, *90*(6), 759-764. https://doi.org/10.1177/0022034511400225

Du, X., Poltorak, A., Silva, M., & Beutler, B. (1999). Analysis of Tlr4-mediated LPS signal transduction in macrophages by mutational modification of the receptor. *Blood Cells Mol Dis*, *25*(5-6), 328-338. https://doi.org/10.1006/bcmd.1999.0262

Duitama, M., Vargas-López, V., Casas, Z., Albarracin, S. L., Sutachan, J. J., & Torres, Y. P. (2020). TRP Channels Role in Pain Associated With Neurodegenerative Diseases. *Front Neurosci*, *14*, 782. https://doi.org/10.3389/fnins.2020.00782

Echeverry, S. a. W. Y. a. Z. J. (2013). Selectively reducing cytokine/chemokine expressing macrophages in injured nerves impairs the development of neuropathic pain. *Experimental Neurology*. https://doi.org/10.1016/j.expneurol.2012.11.013

Ellis, A., Grace, P. M., Wieseler, J., Favret, J., Springer, K., Skarda, B., . . . Watkins, L. R. (2016). Morphine amplifies mechanical allodynia via TLR4 in a rat model of spinal cord injury. *Brain Behav Immun*, *58*, 348-356. https://doi.org/10.1016/j.bbi.2016.08.004

Feldman, P., Due, M. R., Ripsch, M. S., Khanna, R., & White, F. A. (2012). The persistent release of HMGB1 contributes to tactile hyperalgesia in a rodent model of neuropathic pain. *J Neuroinflammation*, *9*, 180. https://doi.org/10.1186/1742-2094-9-180

Ferreiro, D. U., & Komives, E. A. (2010). Molecular mechanisms of system control of NF-kappaB signaling by IkappaBalpha. *Biochemistry*, *49*(8), 1560-1567. https://doi.org/10.1021/bi901948j

Fillingim, R. B. a. K. C. D. a. R.-D. M. C. a. R.-W. B. a. R. J. L. (2009). Sex, Gender, and Pain: A Review of Recent Clinical and Experimental Findings. In.

Finnerup, N. B. (2015). Advances in pain management and research presented at the 2015 Scientific Meeting of the Scandinavian Association for the Study of Pain (SASP). In.

Finnerup, N. B. (2019). Nonnarcotic Methods of Pain Management. *N Engl J Med*, *380*(25), 2440-2448. https://doi.org/10.1056/NEJMra1807061

Fitzgerald, K. A., McWhirter, S. M., Faia, K. L., Rowe, D. C., Latz, E., Golenbock, D. T., . . . Maniatis, T. (2003). IKKepsilon and TBK1 are essential components of the IRF3 signaling pathway. *Nat Immunol*, *4*(5), 491-496. https://doi.org/10.1038/ni921

Frasnelli, S. C., de Medeiros, M. C., Bastos, A. e. S., Costa, D. L., Orrico, S. R., & Rossa Junior, C. (2015). Modulation of immune response by RAGE and TLR4 signalling in PBMCs of diabetic and non-diabetic patients. *Scand J Immunol*, *81*(1), 66-71. https://doi.org/10.1111/sji.12241

Furlan, A., Chaparro, L. E., Irvin, E., & Mailis-Gagnon, A. (2011). A comparison between enriched and nonenriched enrollment randomized withdrawal trials of opioids for chronic noncancer pain. *Pain Res Manag*, *16*(5), 337-351. https://doi.org/10.1155/2011/465281

Gaskin, D. J., & Richard, P. (2012). The economic costs of pain in the United States. *J Pain*, *13*(8), 715-724. https://doi.org/10.1016/j.jpain.2012.03.009

Gay, N. J., & Keith, F. J. (1991). Drosophila Toll and IL-1 receptor. *Nature*, *351*(6325), 355-356. https://doi.org/10.1038/351355b0

Gewandter, J. S., Kleckner, A. S., Marshall, J. H., Brown, J. S., Curtis, L. H., Bautista, J., . . . Mustian, K. M. (2020). Chemotherapy-induced peripheral neuropathy (CIPN) and its treatment: an NIH Collaboratory study of claims data. *Support Care Cancer*, *28*(6), 2553-2562. https://doi.org/10.1007/s00520-019-05063-x

Ghasemlou, N. a. C. I. M. a. J. J. P. a. W. C. J. (2015). CD11b+Ly6G- myeloid cells mediate mechanical inflammatory pain hypersensitivity. *Proceedings of the National Academy of Sciences of the United States of America*. https://doi.org/10.1073/pnas.1501372112

Ghosh, S., Gifford, A. M., Riviere, L. R., Tempst, P., Nolan, G. P., & Baltimore, D. (1990). Cloning of the p50 DNA binding subunit of NF-kappa B: homology to rel and dorsal. *Cell*, *62*(5), 1019-1029. https://doi.org/10.1016/0092-8674(90)90276-k

Gmez-Gaviro, M. V. a. S. D. a. R. J. a. D. M. (2020). Biomedical Applications of Tissue Clearing and Three-Dimensional Imaging in Health and Disease. In.

Goldberg, D. S., & McGee, S. J. (2011). Pain as a global public health priority. *BMC Public Health*, *11*, 770. https://doi.org/10.1186/1471-2458-11-770

Gondokaryono, S. P., Ushio, H., Niyonsaba, F., Hara, M., Takenaka, H., Jayawardana, S. T., . . . Ogawa, H. (2007). The extra domain A of fibronectin stimulates murine mast cells via toll-like receptor 4. *J Leukoc Biol*, *82*(3), 657-665. https://doi.org/10.1189/jlb.1206730

Goren, I. a. A. N. a. Y. N. a. S. C. a. L. A. a. H. M. a. W. A. a. P. J. a. F. S. (2009). A transgenic mouse model of inducible macrophage depletion: Effects of diphtheria toxin-driven lysozyme m-specific cell lineage ablation on wound inflammatory, angiogenic, and contractive processes. *American Journal of Pathology , pmid = 19528348*. https://doi.org/10.2353/ajpath.2009.081002

Grace, P. M., Strand, K. A., Galer, E. L., Urban, D. J., Wang, X., Baratta, M. V., . . . Watkins, L. R. (2016). Morphine paradoxically prolongs neuropathic pain in rats by amplifying spinal NLRP3 inflammasome activation. *Proc Natl Acad Sci U S A*, *113*(24), E3441-3450. https://doi.org/10.1073/pnas.1602070113

Graham, G. G., Davies, M. J., Day, R. O., Mohamudally, A., & Scott, K. F. (2013). The modern pharmacology of paracetamol: therapeutic actions, mechanism of action, metabolism, toxicity and recent pharmacological findings. *Inflammopharmacology*, *21*(3), 201-232. https://doi.org/10.1007/s10787-013-0172-x

Guan, Z., Kuhn, J. A., Wang, X., Colquitt, B., Solorzano, C., Vaman, S., . . . Basbaum, A. I. (2016). Injured sensory neuron-derived CSF1 induces microglial proliferation and DAP12-dependent pain. *Nat Neurosci*, *19*(1), 94-101. https://doi.org/10.1038/nn.4189

Gunnell, L. M., Jonason, J. H., Loiselle, A. E., Kohn, A., Schwarz, E. M., Hilton, M. J., & O'Keefe, R. J. (2010). TAK1 regulates cartilage and joint development via the MAPK and BMP signaling pathways. *J Bone Miner Res*, *25*(8), 1784-1797. https://doi.org/10.1002/jbmr.79

Guo, L. H., & Schluesener, H. J. (2007). The innate immunity of the central nervous system in chronic pain: the role of Toll-like receptors. *Cell Mol Life Sci*, *64*(9), 1128-1136. https://doi.org/10.1007/s00018-007-6494-3

Hadi, M. A., McHugh, G. A., & Closs, S. J. (2019). Impact of Chronic Pain on Patients' Quality of Life: A Comparative Mixed-Methods Study. *J Patient Exp*, *6*(2), 133-141. https://doi.org/10.1177/2374373518786013

Hadjicharalambous, C., Alexaki, V. I., Alpantaki, K., & Chatzinikolaidou, M. (2016). Effects of NSAIDs on the osteogenic differentiation of human adipose tissue-derived stromal cells. *J Pharm Pharmacol*, *68*(11), 1403-1408. https://doi.org/10.1111/jphp.12595

Hama, H. a. H. H. a. N. K. a. H. T. a. K. H. a. I. F. a. K. T. a. A. T. a. S. T. a. S. T. a. M. (2015). ScaleS: An optical clearing palette for biological imaging. *Nature Neuroscience , pmid = 26368944*. https://doi.org/10.1038/nn.4107

Hanamsagar, R., Hanke, M. L., & Kielian, T. (2012). Toll-like receptor (TLR) and inflammasome actions in the central nervous system. *Trends Immunol*, *33*(7), 333-342. https://doi.org/10.1016/j.it.2012.03.001

Hassler, S. N., Kume, M., Mwirigi, J. M., Ahmad, A., Shiers, S., Wangzhou, A., . . . Price, T. J. (2020). The cellular basis of protease-activated receptor 2-evoked mechanical and affective pain. *JCI Insight*, *5*(11). https://doi.org/10.1172/jci.insight.137393

Hayden, M. S., & Ghosh, S. (2004). Signaling to NF-kappaB. *Genes Dev*, *18*(18), 2195-2224. https://doi.org/10.1101/gad.1228704

Heiman, A., Pallottie, A., Heary, R. F., & Elkabes, S. (2014). Toll-like receptors in central nervous system injury and disease: a focus on the spinal cord. *Brain Behav Immun*, *42*, 232-245. https://doi.org/10.1016/j.bbi.2014.06.203

Hershman, D. L., Till, C., Wright, J. D., Awad, D., Ramsey, S. D., Barlow, W. E., . . . Unger, J. (2016). Comorbidities and Risk of Chemotherapy-Induced Peripheral Neuropathy Among Participants 65 Years or Older in Southwest Oncology Group Clinical Trials. *J Clin Oncol*, *34*(25), 3014-3022. https://doi.org/10.1200/JCO.2015.66.2346

Hori, O., Brett, J., Slattery, T., Cao, R., Zhang, J., Chen, J. X., . . . Nitecki, D. (1995). The receptor for advanced glycation end products (RAGE) is a cellular binding site for amphoterin. Mediation of neurite outgrowth and co-expression of rage and amphoterin in the developing nervous system. *J Biol Chem*, *270*(43), 25752-25761. https://doi.org/10.1074/jbc.270.43.25752

Hoshino, K., Takeuchi, O., Kawai, T., Sanjo, H., Ogawa, T., Takeda, Y., . . . Akira, S. (1999). Cutting edge: Toll-like receptor 4 (TLR4)-deficient mice are hyporesponsive to lipopolysaccharide: evidence for TLR4 as the Lps gene product. *J Immunol*, *162*(7), 3749-3752.

Hu, T. T., Wang, R. R., Tang, Y. Y., Wu, Y. X., Yu, J., Hou, W. W., . . . Chen, Z. (2018). TLR4 deficiency abrogated widespread tactile allodynia, but not widespread thermal hyperalgesia and trigeminal neuropathic pain after partial infraorbital nerve transection. *Pain*, *159*(2), 273-283. https://doi.org/10.1097/j.pain.0000000000001100

Huang, Z. Z., Li, D., Liu, C. C., Cui, Y., Zhu, H. Q., Zhang, W. W., . . . Xin, W. J. (2014). CX3CL1-mediated macrophage activation contributed to paclitaxel-induced DRG neuronal apoptosis and painful peripheral neuropathy. *Brain Behav Immun*, *40*, 155-165. https://doi.org/10.1016/j.bbi.2014.03.014

Huck, N. A., Siliezar-Doyle, J., Haight, E. S., Ishida, R., Forman, T. E., Wu, S., . . . Tawfik, V. L. (2021). Temporal Contribution of Myeloid-Lineage TLR4 to the Transition to Chronic Pain: A Focus on Sex Differences. *J Neurosci*, *41*(19), 4349-4365. https://doi.org/10.1523/JNEUROSCI.1940-20.2021

Hutchinson, M. R., Zhang, Y., Brown, K., Coats, B. D., Shridhar, M., Sholar, P. W., . . . Watkins, L. R. (2008). Non-stereoselective reversal of neuropathic pain by naloxone and naltrexone: involvement of toll-like receptor 4 (TLR4). *Eur J Neurosci*, *28*(1), 20-29. https://doi.org/10.1111/j.1460-9568.2008.06321.x

Hwang, B. Y., Kim, E. S., Kim, C. H., Kwon, J. Y., & Kim, H. K. (2012). Gender differences in paclitaxel-induced neuropathic pain behavior and analgesic response in rats. *Korean J Anesthesiol*, *62*(1), 66-72. https://doi.org/10.4097/kjae.2012.62.1.66

Illias, A. M., Yu, K. J., Hwang, S. H., Solis, J., Zhang, H., Velasquez, J. F., . . . Dougherty, P. M. (2022). Dorsal root ganglion toll-like receptor 4 signaling contributes to oxaliplatin-induced peripheral neuropathy. *Pain*, *163*(5), 923-935. https://doi.org/10.1097/j.pain.0000000000002454

Inoue, K., & Tsuda, M. (2018). Microglia in neuropathic pain: cellular and molecular mechanisms and therapeutic potential. *Nat Rev Neurosci*, *19*(3), 138-152. https://doi.org/10.1038/nrn.2018.2

Inyang, K. E. a. S.-P. T. a. W. E. a. M. T. A. a. D. G. a. B. M. D. a. P. T. J. (2019). The antidiabetic drug metformin prevents and reverses neuropathic pain and spinal cord microglial activation in male but not female mice. *Pharmacological Research*. https://doi.org/10.1016/j.phrs.2018.10.027

Iwata, K. a. K. A. a. S. M. (2017). Neuron-glia interaction is a key mechanism underlying persistent orofacial pain. In.

Jensen, K. H. R. a. B. R. W. (2017). Advances and perspectives in tissue clearing using CLARITY. In.

Jia, L., Lee, S., Tierney, J. A., Elmquist, J. K., Burton, M. D., & Gautron, L. (2021). TLR4 Signaling Selectively and Directly Promotes CGRP Release from Vagal Afferents in the Mouse. *eNeuro*, *8*(1). https://doi.org/10.1523/ENEURO.0254-20.2020

Jia, L., Vianna, C. R., Fukuda, M., Berglund, E. D., Liu, C., Tao, C., . . . Elmquist, J. K. (2014). Hepatocyte Toll-like receptor 4 regulates obesity-induced inflammation and insulin resistance. *Nat Commun*, *5*, 3878. https://doi.org/10.1038/ncomms4878

Jiang, Z., Ninomiya-Tsuji, J., Qian, Y., Matsumoto, K., & Li, X. (2002). Interleukin-1 (IL-1) receptor-associated kinase-dependent IL-1-induced signaling complexes phosphorylate TAK1 and TAB2 at the plasma membrane and activate TAK1 in the cytosol. *Mol Cell Biol*, *22*(20), 7158-7167. https://doi.org/10.1128/MCB.22.20.7158-7167.2002

Jimenez-Andrade, J. M., Peters, C. M., Mejia, N. A., Ghilardi, J. R., Kuskowski, M. A., & Mantyh, P. W. (2006). Sensory neurons and their supporting cells located in the trigeminal, thoracic and lumbar ganglia differentially express markers of injury following intravenous administration of paclitaxel in the rat. *Neurosci Lett*, *405*(1-2), 62-67. https://doi.org/10.1016/j.neulet.2006.06.043

Joseph, E. K., Parada, C. A., & Levine, J. D. (2003). Hyperalgesic priming in the rat demonstrates marked sexual dimorphism. *Pain*, *105*(1-2), 143-150. https://doi.org/10.1016/s0304-3959(03)00175-1

Jurga, A. M., Rojewska, E., Piotrowska, A., Makuch, W., Pilat, D., Przewlocka, B., & Mika, J. (2016). Blockade of Toll-Like Receptors (TLR2, TLR4) Attenuates Pain and Potentiates Buprenorphine Analgesia in a Rat Neuropathic Pain Model. *Neural Plast*, *2016*, 5238730. https://doi.org/10.1155/2016/5238730

Kagan, J. C., Su, T., Horng, T., Chow, A., Akira, S., & Medzhitov, R. (2008). TRAM couples endocytosis of Toll-like receptor 4 to the induction of interferon-beta. *Nat Immunol*, *9*(4), 361-368. https://doi.org/10.1038/ni1569

Kaur, S., Benton, W. L., Tongkhuya, S. A., Lopez, C. M. C., Uphouse, L., & Averitt, D. L. (2018). Sex Differences and Estrous Cycle Effects of Peripheral Serotonin-Evoked Rodent Pain Behaviors. *Neuroscience*, *384*, 87-100. https://doi.org/10.1016/j.neuroscience.2018.05.017

Kawai, T., Adachi, O., Ogawa, T., Takeda, K., & Akira, S. (1999). Unresponsiveness of MyD88-deficient mice to endotoxin. *Immunity*, *11*(1), 115-122. https://doi.org/10.1016/s1074-7613(00)80086-2

Kawai, T., & Akira, S. (2010). The role of pattern-recognition receptors in innate immunity: update on Toll-like receptors. *Nat Immunol*, *11*(5), 373-384. https://doi.org/10.1038/ni.1863

Kawasaki, T., & Kawai, T. (2014). Toll-like receptor signaling pathways. *Front Immunol*, *5*, 461. https://doi.org/10.3389/fimmu.2014.00461

Kehlet, H. a. J. T. S. a. W. C. J. (2006). Persistent postsurgical pain: risk factors and prevention. In.

Kennedy, W. R., Wendelschafer-Crabb, G., & Johnson, T. (1996). Quantitation of epidermal nerves in diabetic neuropathy. *Neurology*, *47*(4), 1042-1048. https://doi.org/10.1212/wnl.47.4.1042

Keselman, A., Fang, X., White, P. B., & Heller, N. M. (2017). Estrogen Signaling Contributes to Sex Differences in Macrophage Polarization during Asthma. *J Immunol*, *199*(5), 1573-1583. https://doi.org/10.4049/jimmunol.1601975

Ketloy, C., Engering, A., Srichairatanakul, U., Limsalakpetch, A., Yongvanitchit, K., Pichyangkul, S., & Ruxrungtham, K. (2008). Expression and function of Toll-like receptors on dendritic cells and other antigen presenting cells from non-human primates. *Vet Immunol Immunopathol*, *125*(1-2), 18-30. https://doi.org/10.1016/j.vetimm.2008.05.001

Kiguchi, N., Kobayashi, D., Saika, F., Matsuzaki, S., & Kishioka, S. (2018). Inhibition of peripheral macrophages by nicotinic acetylcholine receptor agonists suppresses spinal microglial activation and neuropathic pain in mice with peripheral nerve injury. *J Neuroinflammation*, *15*(1), 96. https://doi.org/10.1186/s12974-018-1133-5

Kim, H. I., Lim, H., & Moon, A. (2018). Sex Differences in Cancer: Epidemiology, Genetics and Therapy. *Biomol Ther (Seoul)*, *26*(4), 335-342. https://doi.org/10.4062/biomolther.2018.103

Kolb, J. P., Casella, C. R., SenGupta, S., Chilton, P. M., & Mitchell, T. C. (2014). Type I interferon signaling contributes to the bias that Toll-like receptor 4 exhibits for signaling mediated by the adaptor protein TRIF. *Sci Signal*, *7*(351), ra108. https://doi.org/10.1126/scisignal.2005442

Kollewe, C., Mackensen, A. C., Neumann, D., Knop, J., Cao, P., Li, S., . . . Martin, M. U. (2004). Sequential autophosphorylation steps in the interleukin-1 receptor-associated kinase-1 regulate its availability as an adapter in interleukin-1 signaling. *J Biol Chem*, *279*(7), 5227-5236. https://doi.org/10.1074/jbc.M309251200

Krames, E. S. (2015). The dorsal root ganglion in chronic pain and as a target for neuromodulation: a review. *Neuromodulation*, *18*(1), 24-32; discussion 32. https://doi.org/10.1111/ner.12247

Krukowski, K., Nijboer, C. H., Huo, X., Kavelaars, A., & Heijnen, C. J. (2015). Prevention of chemotherapy-induced peripheral neuropathy by the small-molecule inhibitor pifithrin-μ. *Pain*, *156*(11), 2184-2192. https://doi.org/10.1097/j.pain.0000000000000290

Kuhn, J. A., Vainchtein, I. D., Braz, J., Hamel, K., Bernstein, M., Craik, V., . . . Basbaum, A. I. (2021). Regulatory T-cells inhibit microglia-induced pain hypersensitivity in female mice. *Elife*, *10*. https://doi.org/10.7554/eLife.69056

Kwak, M. S., Kim, H. S., Lee, B., Kim, Y. H., Son, M., & Shin, J. S. (2020). Immunological Significance of HMGB1 Post-Translational Modification and Redox Biology. *Front Immunol*, *11*, 1189. https://doi.org/10.3389/fimmu.2020.01189

Kwon, J. W., Kwon, H. K., Shin, H. J., Choi, Y. M., Anwar, M. A., & Choi, S. (2015). Activating transcription factor 3 represses inflammatory responses by binding to the p65 subunit of NF-κB. *Sci Rep*, *5*, 14470. https://doi.org/10.1038/srep14470

Kwon, M. J. a. K. J. a. S. H. a. J. S. R. a. K. Y. M. a. C. J. Y. a. H. D. H. a. K. B. G. (2013). Contribution of macrophages to enhanced regenerative capacity of dorsal root ganglia sensory neurons by conditioning injury. *Journal of Neuroscience , pmid = 24048840*. https://doi.org/10.1523/JNEUROSCI.0278-13.2013

Lemaitre, B., Nicolas, E., Michaut, L., Reichhart, J. M., & Hoffmann, J. A. (1996). The dorsoventral regulatory gene cassette spätzle/Toll/cactus controls the potent antifungal response in Drosophila adults. *Cell*, *86*(6), 973-983. https://doi.org/10.1016/s0092-8674(00)80172-5

Leow-Dyke, S., Allen, C., Denes, A., Nilsson, O., Maysami, S., Bowie, A. G., . . . Pinteaux, E. (2012). Neuronal Toll-like receptor 4 signaling induces brain endothelial activation and neutrophil transmigration in vitro. *J Neuroinflammation*, *9*, 230. https://doi.org/10.1186/1742-2094-9-230

Li, C. L., Li, K. C., Wu, D., Chen, Y., Luo, H., Zhao, J. R., . . . Zhang, X. (2016). Somatosensory neuron types identified by high-coverage single-cell RNA-sequencing and functional heterogeneity. *Cell Res*, *26*(8), 967. https://doi.org/10.1038/cr.2016.90

Li, J., Csakai, A., Jin, J., Zhang, F., & Yin, H. (2016). Therapeutic Developments Targeting Toll-like Receptor-4-Mediated Neuroinflammation. *ChemMedChem*, *11*(2), 154-165. https://doi.org/10.1002/cmdc.201500188

Li, K., Xu, W., Guo, Q., Jiang, Z., Wang, P., Yue, Y., & Xiong, S. (2009). Differential macrophage polarization in male and female BALB/c mice infected with coxsackievirus B3 defines susceptibility to viral myocarditis. *Circ Res*, *105*(4), 353-364. https://doi.org/10.1161/CIRCRESAHA.109.195230

Li, K. a. X. W. a. G. Q. a. J. Z. a. W. P. a. Y. Y. a. X. S. (2009). Differential macrophage polarization in male and female BALB/c mice infected with coxsackievirus B3 defines susceptibility to viral myocarditis. *Circulation Research*. https://doi.org/10.1161/CIRCRESAHA.109.195230

Li, L., We, H., Chen, J., & Zhao, Y. (2008). [Effects of paclitaxel on the macrophages derived from bone marrow cells in vitro]. *Xi Bao Yu Fen Zi Mian Yi Xue Za Zhi*, *24*(12), 1137-1139.

Li, Y., Adamek, P., Zhang, H., Tatsui, C. E., Rhines, L. D., Mrozkova, P., . . . Dougherty, P. M. (2015). The Cancer Chemotherapeutic Paclitaxel Increases Human and Rodent Sensory Neuron Responses to TRPV1 by Activation of TLR4. *J Neurosci*, *35*(39), 13487-13500. https://doi.org/10.1523/JNEUROSCI.1956-15.2015

Li, Y., Korgaonkar, A. A., Swietek, B., Wang, J., Elgammal, F. S., Elkabes, S., & Santhakumar, V. (2015). Toll-like receptor 4 enhancement of non-NMDA synaptic currents increases dentate excitability after brain injury. *Neurobiol Dis*, *74*, 240-253. https://doi.org/10.1016/j.nbd.2014.11.021

Li, Y., Tatsui, C. E., Rhines, L. D., North, R. Y., Harrison, D. S., Cassidy, R. M., . . . Dougherty, P. M. (2017). Dorsal root ganglion neurons become hyperexcitable and increase expression of voltage-gated T-type calcium channels (Cav3.2) in paclitaxel-induced peripheral neuropathy. *Pain*, *158*(3), 417-429. https://doi.org/10.1097/j.pain.0000000000000774

Li, Y., Yin, C., Liu, B., Nie, H., Wang, J., Zeng, D., . . . Jiang, Y. (2021). Transcriptome profiling of long noncoding RNAs and mRNAs in spinal cord of a rat model of paclitaxel-induced peripheral neuropathy identifies potential mechanisms mediating neuroinflammation and pain. *J Neuroinflammation*, *18*(1), 48. https://doi.org/10.1186/s12974-021-02098-y

Li, Y., Zhang, H., Kosturakis, A. K., Jawad, A. B., & Dougherty, P. M. (2014). Toll-like receptor 4 signaling contributes to Paclitaxel-induced peripheral neuropathy. *J Pain*, *15*(7), 712-725. https://doi.org/10.1016/j.jpain.2014.04.001

Lindborg, J. A. a. N. J. P. a. H. M. A. a. L. K. W. a. M. C. Z. a. M. D. a. Z. R. E. (2018). Molecular and cellular identification of the immune response in peripheral ganglia following nerve injury. *Journal of Neuroinflammation*. https://doi.org/10.1186/s12974-018-1222-5

Liu, C. C., Lu, N., Cui, Y., Yang, T., Zhao, Z. Q., Xin, W. J., & Liu, X. G. (2010). Prevention of paclitaxel-induced allodynia by minocycline: Effect on loss of peripheral nerve fibers and infiltration of macrophages in rats. *Mol Pain*, *6*, 76. https://doi.org/10.1186/1744-8069-6-76

Liu, X. J., Zhang, Y., Liu, T., Xu, Z. Z., Park, C. K., Berta, T., . . . Ji, R. R. (2014). Nociceptive neurons regulate innate and adaptive immunity and neuropathic pain through MyD88 adapter. *Cell Res*, *24*(11), 1374-1377. https://doi.org/10.1038/cr.2014.106

Lluis, J. M., Nachbur, U., Cook, W. D., Gentle, I. E., Moujalled, D., Moulin, M., . . . Vaux, D. L. (2010). TAK1 is required for survival of mouse fibroblasts treated with TRAIL, and does so by NF-kappaB dependent induction of cFLIPL. *PLoS One*, *5*(1), e8620. https://doi.org/10.1371/journal.pone.0008620

Lopes, D. M. a. M. N. a. E. M. a. J. S. B. a. M. S. a. M. S. B. a. D. F. (2017). Sex differences in peripheral not central immune responses to pain-inducing injury. *Scientific Reports , pmid = 29184144*. https://doi.org/10.1038/s41598-017-16664-z

Lotze, M. T., & Tracey, K. J. (2005). High-mobility group box 1 protein (HMGB1): nuclear weapon in the immune arsenal. *Nat Rev Immunol*, *5*(4), 331-342. https://doi.org/10.1038/nri1594

Lu, Z., Li, Y., Jin, J., Zhang, X., Lopes-Virella, M. F., & Huang, Y. (2012). Toll-like receptor 4 activation in microvascular endothelial cells triggers a robust inflammatory response and cross talk with mononuclear cells via interleukin-6. *Arterioscler Thromb Vasc Biol*, *32*(7), 1696-1706. https://doi.org/10.1161/ATVBAHA.112.251181

Luiz, A. P., MacDonald, D. I., Santana-Varela, S., Millet, Q., Sikandar, S., Wood, J. N., & Emery, E. C. (2019). Cold sensing by Na. *Proc Natl Acad Sci U S A*, *116*(9), 3811-3816. https://doi.org/10.1073/pnas.1814545116

Lunde, A., & Glover, J. C. (2020). A versatile toolbox for semi-automatic cell-by-cell object-based colocalization analysis. *Sci Rep*, *10*(1), 19027. https://doi.org/10.1038/s41598-020-75835-7

Ma, C., Greenquist, K. W., & Lamotte, R. H. (2006). Inflammatory mediators enhance the excitability of chronically compressed dorsal root ganglion neurons. *J Neurophysiol*, *95*(4), 2098-2107. https://doi.org/10.1152/jn.00748.2005

Man, L. L., Liu, F., Wang, Y. J., Song, H. H., Xu, H. B., Zhu, Z. W., & Zhang, Q. (2015). The HMGB1 signaling pathway activates the inflammatory response in Schwann cells. *Neural Regen Res*, *10*(10), 1706-1712. https://doi.org/10.4103/1673-5374.167773

Martinez, F. O., & Gordon, S. (2014). The M1 and M2 paradigm of macrophage activation: time for reassessment. *F1000Prime Rep*, *6*, 13. https://doi.org/10.12703/P6-13

McDermott, A. M., Toelle, T. R., Rowbotham, D. J., Schaefer, C. P., & Dukes, E. M. (2006). The burden of neuropathic pain: results from a cross-sectional survey. *Eur J Pain*, *10*(2), 127-135. https://doi.org/10.1016/j.ejpain.2005.01.014

McWhorter, F. Y. a. W. T. a. N. P. a. C. T. a. L. W. F. (2013). Modulation of macrophage phenotype by cell shape. *Proceedings of the National Academy of Sciences of the United States of America , pmid = 24101477*. https://doi.org/10.1073/pnas.1308887110

Mecklenburg, J., Zou, Y., Wangzhou, A., Garcia, D., Lai, Z., Tumanov, A. V., . . . Akopian, A. N. (2020). Transcriptomic sex differences in sensory neuronal populations of mice. *Sci Rep*, *10*(1), 15278. https://doi.org/10.1038/s41598-020-72285-z

Medzhitov, R., Preston-Hurlburt, P., & Janeway, C. A. (1997). A human homologue of the Drosophila Toll protein signals activation of adaptive immunity. *Nature*, *388*(6640), 394-397. https://doi.org/10.1038/41131

Megat, S., Ray, P. R., Moy, J. K., Lou, T. F., Barragán-Iglesias, P., Li, Y., . . . Price, T. J. (2019). Nociceptor Translational Profiling Reveals the Ragulator-Rag GTPase Complex as a Critical Generator of Neuropathic Pain. *J Neurosci*, *39*(3), 393-411. https://doi.org/10.1523/JNEUROSCI.2661-18.2018

Mellegers, M. A., Furlan, A. D., & Mailis, A. (2001). Gabapentin for neuropathic pain: systematic review of controlled and uncontrolled literature. *Clin J Pain*, *17*(4), 284-295. https://doi.org/10.1097/00002508-200112000-00002

Mendoza-Coronel, E., & Ortega, E. (2017). Macrophage Polarization Modulates FcγR- and CD13-Mediated Phagocytosis and Reactive Oxygen Species Production, Independently of Receptor Membrane Expression. *Front Immunol*, *8*, 303. https://doi.org/10.3389/fimmu.2017.00303

Min, H., Cho, W. H., Lee, H., Choi, B., Kim, Y. J., Lee, H. K., . . . Lee, S. J. (2018). Association of TRPV1 and TLR4 through the TIR domain potentiates TRPV1 activity by blocking activation-induced desensitization. *Mol Pain*, *14*, 1744806918812636. https://doi.org/10.1177/1744806918812636

Modhiran, N., Watterson, D., Muller, D. A., Panetta, A. K., Sester, D. P., Liu, L., . . . Young, P. R. (2015). Dengue virus NS1 protein activates cells via Toll-like receptor 4 and disrupts endothelial cell monolayer integrity. *Sci Transl Med*, *7*(304), 304ra142. https://doi.org/10.1126/scitranslmed.aaa3863

Mogil, J. S. (2012). Sex differences in pain and pain inhibition: multiple explanations of a controversial phenomenon. *Nat Rev Neurosci*, *13*(12), 859-866. https://doi.org/10.1038/nrn3360

Mogil, J. S. (2020). Qualitative sex differences in pain processing: emerging evidence of a biased literature. *Nat Rev Neurosci*, *21*(7), 353-365. https://doi.org/10.1038/s41583-020-0310-6

Mohning, M. P., Thomas, S. M., Barthel, L., Mould, K. J., McCubbrey, A. L., Frasch, S. C., . . . Janssen, W. J. (2018). Phagocytosis of microparticles by alveolar macrophages during acute lung injury requires MerTK. *Am J Physiol Lung Cell Mol Physiol*, *314*(1), L69-L82. https://doi.org/10.1152/ajplung.00058.2017

Mosser, D. M. a. E. J. P. (2008). Exploring the full spectrum of macrophage activation. In.
Murray, P. J. (2017). Macrophage Polarization. *Annu Rev Physiol*, *79*, 541-566. https://doi.org/10.1146/annurev-physiol-022516-034339

Müller, S., Ronfani, L., & Bianchi, M. E. (2004). Regulated expression and subcellular localization of HMGB1, a chromatin protein with a cytokine function. *J Intern Med*, *255*(3), 332-343. https://doi.org/10.1111/j.1365-2796.2003.01296.x

Naji-Esfahani, H., Vaseghi, G., Safaeian, L., Pilehvarian, A. A., Abed, A., & Rafieian-Kopaei, M. (2016). Gender differences in a mouse model of chemotherapy-induced neuropathic pain. *Lab Anim*, *50*(1), 15-20. https://doi.org/10.1177/0023677215575863

Nicholas, D. A., Zhang, K., Hung, C., Glasgow, S., Aruni, A. W., Unternaehrer, J., . . . De Leon, M. (2017). Palmitic acid is a toll-like receptor 4 ligand that induces human dendritic cell secretion of IL-1β. *PLoS One*, *12*(5), e0176793. https://doi.org/10.1371/journal.pone.0176793

Nicotra, L., Loram, L. C., Watkins, L. R., & Hutchinson, M. R. (2012). Toll-like receptors in chronic pain. *Exp Neurol*, *234*(2), 316-329. https://doi.org/10.1016/j.expneurol.2011.09.038

O'Brien, J. M., Wewers, M. D., Moore, S. A., & Allen, J. N. (1995). Taxol and colchicine increase LPS-induced pro-IL-1 beta production, but do not increase IL-1 beta secretion. A role for microtubules in the regulation of IL-1 beta production. *J Immunol*, *154*(8), 4113-4122.

O'Connor, K. A., Hansen, M. K., Rachal Pugh, C., Deak, M. M., Biedenkapp, J. C., Milligan, E. D., . . . Watkins, L. R. (2003). Further characterization of high mobility group box 1 (HMGB1) as a proinflammatory cytokine: central nervous system effects. *Cytokine*, *24*(6), 254-265. https://doi.org/10.1016/j.cyto.2003.08.001

Olson, J. K., & Miller, S. D. (2004). Microglia initiate central nervous system innate and adaptive immune responses through multiple TLRs. *J Immunol*, *173*(6), 3916-3924. https://doi.org/10.4049/jimmunol.173.6.3916

Oun, R., Moussa, Y. E., & Wheate, N. J. (2018). Correction: The side effects of platinum-based chemotherapy drugs: a review for chemists. *Dalton Trans*, *47*(23), 7848. https://doi.org/10.1039/c8dt90088d

Park, H. J., & Choi, J. M. (2017). Sex-specific regulation of immune responses by PPARs. *Exp Mol Med*, *49*(8), e364. https://doi.org/10.1038/emm.2017.102

Park, J. S., Svetkauskaite, D., He, Q., Kim, J. Y., Strassheim, D., Ishizaka, A., & Abraham, E. (2004). Involvement of toll-like receptors 2 and 4 in cellular activation by high mobility group box 1 protein. *J Biol Chem*, *279*(9), 7370-7377. https://doi.org/10.1074/jbc.M306793200

Paul, D. a. C. A. E. a. G. S. a. P. J. S. (2013). Novel 3D analysis of Claudin-5 reveals significant endothelial heterogeneity among CNS microvessels. *Microvascular Research , pmid = 23261753*. https://doi.org/10.1016/j.mvr.2012.12.001

Peng, J., Gu, N., Zhou, L., B Eyo, U., Murugan, M., Gan, W. B., & Wu, L. J. (2016). Microglia and monocytes synergistically promote the transition from acute to chronic pain after nerve injury. *Nat Commun*, *7*, 12029. https://doi.org/10.1038/ncomms12029

Peng, J. a. G. N. a. Z. L. a. (2016). Microglia and monocytes synergistically promote the transition from acute to chronic pain after nerve injury. *Nature Communications , pmid = 27349690*. https://doi.org/10.1038/ncomms12029

Peters, C. M., Jimenez-Andrade, J. M., Jonas, B. M., Sevcik, M. A., Koewler, N. J., Ghilardi, J. R., . . . Mantyh, P. W. (2007). Intravenous paclitaxel administration in the rat induces a peripheral sensory neuropathy characterized by macrophage infiltration and injury to sensory neurons and their supporting cells. *Exp Neurol*, *203*(1), 42-54. https://doi.org/10.1016/j.expneurol.2006.07.022

Piao, Y., Gwon, D. H., Kang, D. W., Hwang, T. W., Shin, N., Kwon, H. H., . . . Kim, D. W. (2018). TLR4-mediated autophagic impairment contributes to neuropathic pain in chronic constriction injury mice. *Mol Brain*, *11*(1), 11. https://doi.org/10.1186/s13041-018-0354-y

Pinho-Ribeiro, F. A., Verri, W. A., & Chiu, I. M. (2017). Nociceptor Sensory Neuron-Immune Interactions in Pain and Inflammation. *Trends Immunol*, *38*(1), 5-19. https://doi.org/10.1016/j.it.2016.10.001

Poltorak, A., He, X., Smirnova, I., Liu, M. Y., Van Huffel, C., Du, X., . . . Beutler, B. (1998). Defective LPS signaling in C3H/HeJ and C57BL/10ScCr mice: mutations in Tlr4 gene. *Science*, *282*(5396), 2085-2088. https://doi.org/10.1126/science.282.5396.2085

Qin, S., Wang, H., Yuan, R., Li, H., Ochani, M., Ochani, K., . . . Yang, H. (2006). Role of HMGB1 in apoptosis-mediated sepsis lethality. *J Exp Med*, *203*(7), 1637-1642. https://doi.org/10.1084/jem.20052203

Quarato, G., Guy, C. S., Grace, C. R., Llambi, F., Nourse, A., Rodriguez, D. A., . . . Green, D. R. (2016). Sequential Engagement of Distinct MLKL Phosphatidylinositol-Binding Sites Executes Necroptosis. *Mol Cell*, *61*(4), 589-601. https://doi.org/10.1016/j.molcel.2016.01.011

Raetz, C. R., Garrett, T. A., Reynolds, C. M., Shaw, W. A., Moore, J. D., Smith, D. C., . . . Dennis, E. A. (2006). Kdo2-Lipid A of Escherichia coli, a defined endotoxin that activates macrophages via TLR-4. *J Lipid Res*, *47*(5), 1097-1111. https://doi.org/10.1194/jlr.M600027-JLR200

Raghavendra, V., Tanga, F. Y., & DeLeo, J. A. (2004). Complete Freunds adjuvant-induced peripheral inflammation evokes glial activation and proinflammatory cytokine expression in the CNS. *Eur J Neurosci*, *20*(2), 467-473. https://doi.org/10.1111/j.1460-9568.2004.03514.x

Rajput, S., Volk-Draper, L. D., & Ran, S. (2013). TLR4 is a novel determinant of the response to paclitaxel in breast cancer. *Mol Cancer Ther*, *12*(8), 1676-1687. https://doi.org/10.1158/1535-7163.MCT-12-1019

Ransohoff, R. M. (2016). A polarizing question: do M1 and M2 microglia exist? *Nat Neurosci*, *19*(8), 987-991. https://doi.org/10.1038/nn.4338

Rao, J., Qian, X., Li, G., Pan, X., Zhang, C., Zhang, F., . . . Lu, L. (2015). ATF3-mediated NRF2/HO-1 signaling regulates TLR4 innate immune responses in mouse liver ischemia/reperfusion injury. *Am J Transplant*, *15*(1), 76-87. https://doi.org/10.1111/ajt.12954

Raoof, R. a. W. H. L. D. M. a. E. N. (2018). Divergent roles of immune cells and their mediators in pain. In.

Renier, N. a. W. Z. a. S. D. J. a. Y. J. a. A. P. a. T.-L. M. (2014). IDISCO: A simple, rapid method to immunolabel large tissue samples for volume imaging. *Cell , pmid = 25417164*. https://doi.org/10.1016/j.cell.2014.10.010

Renthal, W., Tochitsky, I., Yang, L., Cheng, Y. C., Li, E., Kawaguchi, R., . . . Woolf, C. J. (2020). Transcriptional Reprogramming of Distinct Peripheral Sensory Neuron Subtypes after Axonal Injury. *Neuron*, *108*(1), 128-144.e129. https://doi.org/10.1016/j.neuron.2020.07.026

Resman, N., Gradisar, H., Vasl, J., Keber, M. M., Pristovsek, P., & Jerala, R. (2008). Taxanes inhibit human TLR4 signaling by binding to MD-2. *FEBS Lett*, *582*(28), 3929-3934. https://doi.org/10.1016/j.febslet.2008.10.037

Ristoiu, V. (2013). Contribution of macrophages to peripheral neuropathic pain pathogenesis. *Life Sci*, *93*(23), 870-881. https://doi.org/10.1016/j.lfs.2013.10.005

Rittner, H. L. (2005). Leukocytes in the regulation of pain and analgesia. *Journal of Leukocyte Biology , pmid = 16204636*. https://doi.org/10.1189/jlb.0405223

Ross, J. L., Queme, L. F., Lamb, J. E., Green, K. J., & Jankowski, M. P. (2018). Sex differences in primary muscle afferent sensitization following ischemia and reperfusion injury. *Biol Sex Differ*, *9*(1), 2. https://doi.org/10.1186/s13293-017-0163-5

Ruau, D., Liu, L. Y., Clark, J. D., Angst, M. S., & Butte, A. J. (2012). Sex differences in reported pain across 11,000 patients captured in electronic medical records. *J Pain*, *13*(3), 228-234. https://doi.org/10.1016/j.jpain.2011.11.002

Rudjito, R. a. A. N. M. a. F. A. B. a. L. P. a. S.-P. T. A. a. P. T. J. a. H. H. E. a. B. M. D. (2020). Sex- and cell-dependent contribution of peripheral high mobility group box 1 and TLR4 in arthritis-induced pain. *Pain*. https://doi.org/10.1097/j.pain.0000000000002034

Scarpignato, C., Lanas, A., Blandizzi, C., Lems, W. F., Hermann, M., Hunt, R. H., & Group, I. N. C. (2015). Safe prescribing of non-steroidal anti-inflammatory drugs in patients with osteoarthritis--an expert consensus addressing benefits as well as gastrointestinal and cardiovascular risks. *BMC Med*, *13*, 55. https://doi.org/10.1186/s12916-015-0285-8

Schmid, A. B. a. C. M. W. a. R. M. J. a. M. E. M. (2013). Local and remote immune-mediated inflammation after mild peripheral nerve compression in rats. *Journal of Neuropathology and Experimental Neurology*. https://doi.org/10.1097/NEN.0b013e318298de5b

Seltzer, Z., Dubner, R., & Shir, Y. (1990). A novel behavioral model of neuropathic pain disorders produced in rats by partial sciatic nerve injury. *Pain*, *43*(2), 205-218. https://doi.org/10.1016/0304-3959(90)91074-S

Sen, D. a. J. S. M. a. O. E. M. a. P. H. a. C. K. a. K. M. F. (2016). Tracking the spatial and functional gradient of monocyte-to-macrophage differentiation in inflamed lung. *PLoS ONE , pmid = 27755611*. https://doi.org/10.1371/journal.pone.0165064

Seretny, M., Currie, G. L., Sena, E. S., Ramnarine, S., Grant, R., MacLeod, M. R., . . . Fallon, M. (2014). Incidence, prevalence, and predictors of chemotherapy-induced peripheral neuropathy: A systematic review and meta-analysis. *Pain*, *155*(12), 2461-2470. https://doi.org/10.1016/j.pain.2014.09.020

Seth, P., Rudd, R. A., Noonan, R. K., & Haegerich, T. M. (2018). Quantifying the Epidemic of Prescription Opioid Overdose Deaths. *Am J Public Health*, *108*(4), 500-502. https://doi.org/10.2105/AJPH.2017.304265

Shao, Y. X., Gong, Q., Qi, X. M., Wang, K., & Wu, Y. G. (2019). Paeoniflorin Ameliorates Macrophage Infiltration and Activation by Inhibiting the TLR4 Signaling Pathway in Diabetic Nephropathy. *Front Pharmacol*, *10*, 566. https://doi.org/10.3389/fphar.2019.00566

Shi, H., Kokoeva, M. V., Inouye, K., Tzameli, I., Yin, H., & Flier, J. S. (2006). TLR4 links innate immunity and fatty acid-induced insulin resistance. *J Clin Invest*, *116*(11), 3015-3025. https://doi.org/10.1172/JCI28898

Shibasaki, M., Sasaki, M., Miura, M., Mizukoshi, K., Ueno, H., Hashimoto, S., . . . Amaya, F. (2010). Induction of high mobility group box-1 in dorsal root ganglion contributes to pain hypersensitivity after peripheral nerve injury. *Pain*, *149*(3), 514-521. https://doi.org/10.1016/j.pain.2010.03.023

Shiers, S., Pradhan, G., Mwirigi, J., Mejia, G., Ahmad, A., Kroener, S., & Price, T. (2018). Neuropathic Pain Creates an Enduring Prefrontal Cortex Dysfunction Corrected by the Type II Diabetic Drug Metformin But Not by Gabapentin. *J Neurosci*, *38*(33), 7337-7350. https://doi.org/10.1523/JNEUROSCI.0713-18.2018

Sills, G. J., & Rogawski, M. A. (2020). Mechanisms of action of currently used antiseizure drugs. *Neuropharmacology*, *168*, 107966. https://doi.org/10.1016/j.neuropharm.2020.107966

Skjesol, A., Yurchenko, M., Bösl, K., Gravastrand, C., Nilsen, K. E., Grøvdal, L. M., . . . Husebye, H. (2019). The TLR4 adaptor TRAM controls the phagocytosis of Gram-negative bacteria by interacting with the Rab11-family interacting protein 2. *PLoS Pathog*, *15*(3), e1007684. https://doi.org/10.1371/journal.ppat.1007684

Smith, T. J., & Hillner, B. E. (2019). The Cost of Pain. *JAMA Netw Open*, *2*(4), e191532. https://doi.org/10.1001/jamanetworkopen.2019.1532

Son, S., Shim, D. W., Hwang, I., Park, J. H., & Yu, J. W. (2019). Chemotherapeutic Agent Paclitaxel Mediates Priming of NLRP3 Inflammasome Activation. *Front Immunol*, *10*, 1108. https://doi.org/10.3389/fimmu.2019.01108

Song, M. Y., & Yuan, J. X. (2010). Introduction to TRP channels: structure, function, and regulation. *Adv Exp Med Biol*, *661*, 99-108. https://doi.org/10.1007/978-1-60761-500-2_6

Sorge, R. E. a. L.-F. M. L. a. T. A. H. a. S. S. G. a. A. J. S. a. R. J. a. C. M. L. a. G. (2011). Spinal cord toll-like receptor 4 mediates inflammatory and neuropathic hypersensitivity in male but not female mice. *Journal of Neuroscience , pmid = 22031891*. https://doi.org/10.1523/JNEUROSCI.3859-11.2011

Sorge, R. E. a. M. J. C. S. a. R. S. a. B. S. a. T. S. a. A. J. K. a. M. L. J. a. A. J. S. (2015). Different immune cells mediate mechanical pain hypersensitivity in male and female mice. *Nature Neuroscience , pmid = 26120961*. https://doi.org/10.1038/nn.4053

Srivastava, M., Saqib, U., Naim, A., Roy, A., Liu, D., Bhatnagar, D., . . . Baig, M. S. (2017). The TLR4-NOS1-AP1 signaling axis regulates macrophage polarization. *Inflamm Res*, *66*(4), 323-334. https://doi.org/10.1007/s00011-016-1017-z

Staff, N. P., Fehrenbacher, J. C., Caillaud, M., Damaj, M. I., Segal, R. A., & Rieger, S. (2020). Pathogenesis of paclitaxel-induced peripheral neuropathy: A current review of in vitro and in vivo findings using rodent and human model systems. *Exp Neurol*, *324*, 113121. https://doi.org/10.1016/j.expneurol.2019.113121

Steimle, A., Autenrieth, I. B., & Frick, J. S. (2016). Structure and function: Lipid A modifications in commensals and pathogens. *Int J Med Microbiol*, *306*(5), 290-301. https://doi.org/10.1016/j.ijmm.2016.03.001

Steingrímsdóttir, Ó., Landmark, T., Macfarlane, G. J., & Nielsen, C. S. (2017). Defining chronic pain in epidemiological studies: a systematic review and meta-analysis. *Pain*, *158*(11), 2092-2107. https://doi.org/10.1097/j.pain.0000000000001009

Stephens, K. E., Zhou, W., Ji, Z., Chen, Z., He, S., Ji, H., . . . Taverna, S. D. (2019). Sex differences in gene regulation in the dorsal root ganglion after nerve injury. *BMC Genomics*, *20*(1), 147. https://doi.org/10.1186/s12864-019-5512-9

Stirling, L. C., Forlani, G., Baker, M. D., Wood, J. N., Matthews, E. A., Dickenson, A. H., & Nassar, M. A. (2005). Nociceptor-specific gene deletion using heterozygous NaV1.8-Cre recombinase mice. *Pain*, *113*(1-2), 27-36. https://doi.org/10.1016/j.pain.2004.08.015

Stokes, J. A., Cheung, J., Eddinger, K., Corr, M., & Yaksh, T. L. (2013). Toll-like receptor signaling adapter proteins govern spread of neuropathic pain and recovery following nerve injury in male mice. *J Neuroinflammation*, *10*, 148. https://doi.org/10.1186/1742-2094-10-148

183

Szabo-Pardi, T. A., Barron, L. R., Lenert, M. E., & Burton, M. D. (2021). Sensory Neuron TLR4 mediates the development of nerve-injury induced mechanical hypersensitivity in female mice. *Brain Behav Immun*, *97*, 42-60. https://doi.org/10.1016/j.bbi.2021.06.011

Szabo-Pardi, T. A. a. A. N. M. a. A. A. T. a. B. M. D. (2019). In vivo two-color 2-photon imaging of genetically-tagged reporter cells in the skin. *Journal of Visualized Experiments*. https://doi.org/10.3791/59647

Szabo-Pardi, T. a. A. N. a. B. M. (2021). The role of microglia versus peripheral macrophages in maladaptive plasticity after nerve injury. In.

Szajnik, M., Szczepanski, M. J., Czystowska, M., Elishaev, E., Mandapathil, M., Nowak-Markwitz, E., . . . Whiteside, T. L. (2009). TLR4 signaling induced by lipopolysaccharide or paclitaxel regulates tumor survival and chemoresistance in ovarian cancer. *Oncogene*, *28*(49), 4353-4363. https://doi.org/10.1038/onc.2009.289

Taguchi, T., Mitcham, J. L., Dower, S. K., Sims, J. E., & Testa, J. R. (1996). Chromosomal localization of TIL, a gene encoding a protein related to the Drosophila transmembrane receptor Toll, to human chromosome 4p14. *Genomics*, *32*(3), 486-488. https://doi.org/10.1006/geno.1996.0150

Tajerian, M., Sahbaie, P., Sun, Y., Leu, D., Yang, H. Y., Li, W., . . . David Clark, J. (2015). Sex differences in a Murine Model of Complex Regional Pain Syndrome. *Neurobiol Learn Mem*, *123*, 100-109. https://doi.org/10.1016/j.nlm.2015.06.004

Talbot, S., Foster, S. L., & Woolf, C. J. (2016). Neuroimmunity: Physiology and Pathology. *Annu Rev Immunol*, *34*, 421-447. https://doi.org/10.1146/annurev-immunol-041015-055340

Tang, S. C., Arumugam, T. V., Xu, X., Cheng, A., Mughal, M. R., Jo, D. G., . . . Mattson, M. P. (2007). Pivotal role for neuronal Toll-like receptors in ischemic brain injury and functional deficits. *Proc Natl Acad Sci U S A*, *104*(34), 13798-13803. https://doi.org/10.1073/pnas.0702553104

Tanga, F. Y., Nutile-McMenemy, N., & DeLeo, J. A. (2005). The CNS role of Toll-like receptor 4 in innate neuroimmunity and painful neuropathy. *Proc Natl Acad Sci U S A*, *102*(16), 5856-5861. https://doi.org/10.1073/pnas.0501634102

Tauer, U. (2002). Advantages and risks of multiphoton microscopy in physiology. *Experimental Physiology , pmid = 12530403*. https://doi.org/10.1113/eph8702464

Taves, S., Berta, T., Liu, D. L., Gan, S., Chen, G., Kim, Y. H., . . . Ji, R. R. (2016). Spinal inhibition of p38 MAP kinase reduces inflammatory and neuropathic pain in male but not female mice: Sex-dependent microglial signaling in the spinal cord. *Brain Behav Immun*, *55*, 70-81. https://doi.org/10.1016/j.bbi.2015.10.006

Templeton, K. J. (2020). Sex and Gender Issues in Pain Management. *J Bone Joint Surg Am*, *102 Suppl 1*, 32-35. https://doi.org/10.2106/JBJS.20.00237

Thomas, A. V., Broers, A. D., Vandegaart, H. F., & Desmecht, D. J. (2006). Genomic structure, promoter analysis and expression of the porcine (Sus scrofa) TLR4 gene. *Mol Immunol*, *43*(6), 653-659. https://doi.org/10.1016/j.molimm.2005.04.001

Thorburn, J., Horita, H., Redzic, J., Hansen, K., Frankel, A. E., & Thorburn, A. (2009). Autophagy regulates selective HMGB1 release in tumor cells that are destined to die. *Cell Death Differ*, *16*(1), 175-183. https://doi.org/10.1038/cdd.2008.143

Toma, W., Kyte, S. L., Bagdas, D., Alkhlaif, Y., Alsharari, S. D., Lichtman, A. H., . . . Damaj, M. I. (2017). Effects of paclitaxel on the development of neuropathy and affective behaviors in the mouse. *Neuropharmacology*, *117*, 305-315. https://doi.org/10.1016/j.neuropharm.2017.02.020

Tsuda, M. (2019). Microglia-Mediated Regulation of Neuropathic Pain: Molecular and Cellular Mechanisms. *Biol Pharm Bull*, *42*(12), 1959-1968. https://doi.org/10.1248/bpb.b19-00715

Tsujino, H., Kondo, E., Fukuoka, T., Dai, Y., Tokunaga, A., Miki, K., . . . Noguchi, K. (2000). Activating transcription factor 3 (ATF3) induction by axotomy in sensory and motoneurons: A novel neuronal marker of nerve injury. *Mol Cell Neurosci*, *15*(2), 170-182. https://doi.org/10.1006/mcne.1999.0814

Uematsu, S., & Akira, S. (2008). Toll-Like receptors (TLRs) and their ligands. *Handb Exp Pharmacol*(183), 1-20. https://doi.org/10.1007/978-3-540-72167-3_1

Ulevitch, R. J., & Tobias, P. S. (1995). Receptor-dependent mechanisms of cell stimulation by bacterial endotoxin. *Annu Rev Immunol*, *13*, 437-457. https://doi.org/10.1146/annurev.iy.13.040195.002253

Venereau, E., Schiraldi, M., Uguccioni, M., & Bianchi, M. E. (2013). HMGB1 and leukocyte migration during trauma and sterile inflammation. *Mol Immunol*, *55*(1), 76-82. https://doi.org/10.1016/j.molimm.2012.10.037

Verriotis, M., Jones, L., Whitehead, K., Laudiano-Dray, M., Panayotidis, I., Patel, H., . . . Fitzgerald, M. (2018). The distribution of pain activity across the human neonatal brain is sex dependent. *Neuroimage*, *178*, 69-77. https://doi.org/10.1016/j.neuroimage.2018.05.030

Vina, E. R., Ran, D., Ashbeck, E. L., & Kwoh, C. K. (2020). Widespread Pain Is Associated with Increased Risk of No Clinical Improvement After TKA in Women. *Clin Orthop Relat Res*, *478*(7), 1453. https://doi.org/10.1097/CORR.0000000000001001

Wall, P. D., & Gutnick, M. (1974). Ongoing activity in peripheral nerves: the physiology and pharmacology of impulses originating from a neuroma. *Exp Neurol*, *43*(3), 580-593. https://doi.org/10.1016/0014-4886(74)90197-6

Wan, W., Cao, L., Khanabdali, R., Kalionis, B., Tai, X., & Xia, S. (2016). The Emerging Role of HMGB1 in Neuropathic Pain: A Potential Therapeutic Target for Neuroinflammation. *J Immunol Res*, *2016*, 6430423. https://doi.org/10.1155/2016/6430423

Wan, Y. Y. (2010). Regulatory T cells: immune suppression and beyond. *Cell Mol Immunol*, *7*(3), 204-210. https://doi.org/10.1038/cmi.2010.20

Wanderley, C. W., Colón, D. F., Luiz, J. P. M., Oliveira, F. F., Viacava, P. R., Leite, C. A., . . . Cunha, F. Q. (2018). Paclitaxel Reduces Tumor Growth by Reprogramming Tumor-Associated Macrophages to an M1 Profile in a TLR4-Dependent Manner. *Cancer Res*, *78*(20), 5891-5900. https://doi.org/10.1158/0008-5472.CAN-17-3480

Wang, X., Han, L., & Yang, J. (2022). Evaluation of efficacy and safety of aspirin combination treatment in treating patients with coronary heart disease: A protocol for systematic review and meta-analysis. *Medicine (Baltimore)*, *101*(7), e28848. https://doi.org/10.1097/MD.0000000000028848

Wang, X. M., Lehky, T. J., Brell, J. M., & Dorsey, S. G. (2012). Discovering cytokines as targets for chemotherapy-induced painful peripheral neuropathy. *Cytokine*, *59*(1), 3-9. https://doi.org/10.1016/j.cyto.2012.03.027

Wangzhou, A., Paige, C., Ray, P. R., Dussor, G., & Price, T. J. (2021). Diversity of Receptor Expression in Central and Peripheral Mouse Neurons Estimated from Single Cell RNA Sequencing. *Neuroscience*, *463*, 86-96. https://doi.org/10.1016/j.neuroscience.2021.03.017

Weber, L., Yeomans, D. C., & Tzabazis, A. (2017). Opioid-induced hyperalgesia in clinical anesthesia practice: what has remained from theoretical concepts and experimental studies? *Curr Opin Anaesthesiol*, *30*(4), 458-465. https://doi.org/10.1097/ACO.0000000000000485

Werling, D., Jann, O. C., Offord, V., Glass, E. J., & Coffey, T. J. (2009). Variation matters: TLR structure and species-specific pathogen recognition. *Trends Immunol*, *30*(3), 124-130. https://doi.org/10.1016/j.it.2008.12.001

Werling, D., & Jungi, T. W. (2003). TOLL-like receptors linking innate and adaptive immune response. *Vet Immunol Immunopathol*, *91*(1), 1-12. https://doi.org/10.1016/s0165-2427(02)00228-3

Wiesenfeld-Hallin, Z. (2005). Sex differences in pain perception. *Gend Med*, *2*(3), 137-145. https://doi.org/10.1016/s1550-8579(05)80042-7

Wolf, S. L., Barton, D. L., Qin, R., Wos, E. J., Sloan, J. A., Liu, H., . . . Loprinzi, C. L. (2012). The relationship between numbness, tingling, and shooting/burning pain in patients with chemotherapy-induced peripheral neuropathy (CIPN) as measured by the EORTC QLQ-CIPN20 instrument, N06CA. *Support Care Cancer*, *20*(3), 625-632. https://doi.org/10.1007/s00520-011-1141-9

Woller, S. A., Corr, M., & Yaksh, T. L. (2015). Differences in cisplatin-induced mechanical allodynia in male and female mice. *Eur J Pain*, *19*(10), 1476-1485. https://doi.org/10.1002/ejp.679

Woller, S. A., Ravula, S. B., Tucci, F. C., Beaton, G., Corr, M., Isseroff, R. R., . . . Yaksh, T. L. (2016). Systemic TAK-242 prevents intrathecal LPS evoked hyperalgesia in male, but not female mice and prevents delayed allodynia following intraplantar formalin in both male and female mice: The role of TLR4 in the evolution of a persistent pain state. *Brain Behav Immun*, *56*, 271-280. https://doi.org/10.1016/j.bbi.2016.03.026

Wright, A., Luedtke, K. E., & Vandenberg, C. (2010). Duloxetine in the treatment of chronic pain due to fibromyalgia and diabetic neuropathy. *J Pain Res*, *4*, 1-10. https://doi.org/10.2147/JPR.S12866

Wu, Y., Wang, Y., Wang, J., Fan, Q., Zhu, J., Yang, L., & Rong, W. (2019). TLR4 mediates upregulation and sensitization of TRPV1 in primary afferent neurons in 2,4,6-trinitrobenzene sulfate-induced colitis. *Mol Pain*, *15*, 1744806919830018. https://doi.org/10.1177/1744806919830018

Xiang, W., Chao, Z. Y., & Feng, D. Y. (2015). Role of Toll-like receptor/MYD88 signaling in neurodegenerative diseases. *Rev Neurosci*, *26*(4), 407-414. https://doi.org/10.1515/revneuro-2014-0067

Xie, M. X., Zhang, X. L., Xu, J., Zeng, W. A., Li, D., Xu, T., . . . Liu, X. G. (2019). Nuclear Factor-kappaB Gates Na. *iScience*, *19*, 623-633. https://doi.org/10.1016/j.isci.2019.08.017

Yamasoba, D., Tsubota, M., Domoto, R., Sekiguchi, F., Nishikawa, H., Liu, K., . . . Kawabata, A. (2016). Peripheral HMGB1-induced hyperalgesia in mice: Redox state-dependent distinct roles of RAGE and TLR4. *J Pharmacol Sci*, *130*(2), 139-142. https://doi.org/10.1016/j.jphs.2016.01.005

Yang, H., Zeng, Q., Silverman, H. A., Gunasekaran, M., George, S. J., Devarajan, A., . . . Tracey, K. J. (2021). HMGB1 released from nociceptors mediates inflammation. *Proc Natl Acad Sci U S A*, *118*(33). https://doi.org/10.1073/pnas.2102034118

Yang, S., Sugawara, S., Monodane, T., Nishijima, M., Adachi, Y., Akashi, S., . . . Takada, H. (2001). Micrococcus luteus teichuronic acids activate human and murine monocytic cells in a CD14- and toll-like receptor 4-dependent manner. *Infect Immun*, *69*(4), 2025-2030. https://doi.org/10.1128/IAI.69.4.2025-2030.2001

Yoon, C. a. (1994). Behavioral signs of ongoing pain and cold allodynia in a rat model of neuropathic pain. *Pain*. https://doi.org/10.1016/0304-3959(94)90023-X

Youn, J. H., & Shin, J. S. (2006). Nucleocytoplasmic shuttling of HMGB1 is regulated by phosphorylation that redirects it toward secretion. *J Immunol*, *177*(11), 7889-7897. https://doi.org/10.4049/jimmunol.177.11.7889

Yu, M., Wang, H., Ding, A., Golenbock, D. T., Latz, E., Czura, C. J., . . . Yang, H. (2006). HMGB1 signals through toll-like receptor (TLR) 4 and TLR2. *Shock*, *26*(2), 174-179. https://doi.org/10.1097/01.shk.0000225404.51320.82

Yu, X., Liu, H., Hamel, K. A., Morvan, M. G., Yu, S., Leff, J., . . . Basbaum, A. I. (2020). Dorsal root ganglion macrophages contribute to both the initiation and persistence of neuropathic pain. *Nat Commun*, *11*(1), 264. https://doi.org/10.1038/s41467-019-13839-2

Yu, X. a. L. H. a. H. K. A. a. M. M. G. a. Y. S. a. L. J. a. G. Z. a. B. J. M. a. B. A. I. (2020). Dorsal root ganglion macrophages contribute to both the initiation and persistence of neuropathic pain. *Nature Communications , pmid = 31937758*. https://doi.org/10.1038/s41467-019-13839-2

Zaks-Zilberman, M., Zaks, T. Z., & Vogel, S. N. (2001). Induction of proinflammatory and chemokine genes by lipopolysaccharide and paclitaxel (Taxol) in murine and human breast cancer cell lines. *Cytokine*, *15*(3), 156-165. https://doi.org/10.1006/cyto.2001.0935

Zanoni, I., Ostuni, R., Marek, L. R., Barresi, S., Barbalat, R., Barton, G. M., . . . Kagan, J. C. (2011). CD14 controls the LPS-induced endocytosis of Toll-like receptor 4. *Cell*, *147*(4), 868-880. https://doi.org/10.1016/j.cell.2011.09.051

Zhang, H., & Dougherty, P. M. (2014). Enhanced excitability of primary sensory neurons and altered gene expression of neuronal ion channels in dorsal root ganglion in paclitaxel-induced peripheral neuropathy. *Anesthesiology*, *120*(6), 1463-1475. https://doi.org/10.1097/ALN.0000000000000176

Zhang, H., Li, Y., de Carvalho-Barbosa, M., Kavelaars, A., Heijnen, C. J., Albrecht, P. J., & Dougherty, P. M. (2016). Dorsal Root Ganglion Infiltration by Macrophages Contributes to Paclitaxel Chemotherapy-Induced Peripheral Neuropathy. *J Pain*, *17*(7), 775-786. https://doi.org/10.1016/j.jpain.2016.02.011

Zhang, W., Wu, H., Xu, Q., Chen, S., Sun, L., Jiao, C., . . . Chen, X. (2020). Estrogen modulation of pain perception with a novel 17β-estradiol pretreatment regime in ovariectomized rats. *Biol Sex Differ*, *11*(1), 2. https://doi.org/10.1186/s13293-019-0271-5

Zhao, H., Alam, A., Chen, Q., A Eusman, M., Pal, A., Eguchi, S., . . . Ma, D. (2017). The role of microglia in the pathobiology of neuropathic pain development: what do we know? *Br J Anaesth*, *118*(4), 504-516. https://doi.org/10.1093/bja/aex006

Zhao, X. H., Zhang, T., & Li, Y. Q. (2015). The up-regulation of spinal Toll-like receptor 4 in rats with inflammatory pain induced by complete Freund's adjuvant. *Brain Res Bull*, *111*, 97-103. https://doi.org/10.1016/j.brainresbull.2015.01.002

Zheng, Y., Liu, P., Bai, L., Trimmer, J. S., Bean, B. P., & Ginty, D. D. (2019). Deep Sequencing of Somatosensory Neurons Reveals Molecular Determinants of Intrinsic Physiological Properties. *Neuron*, *103*(4), 598-616.e597. https://doi.org/10.1016/j.neuron.2019.05.039

Zhu, L., & Chen, L. (2019). Progress in research on paclitaxel and tumor immunotherapy. *Cell Mol Biol Lett*, *24*, 40. https://doi.org/10.1186/s11658-019-0164-y

Zhuo, M. a. W. G. a. W. L. J. (2011). Neuronal and microglial mechanisms of neuropathic pain. In.

BIOGRAPHICAL SKETCH

Thomas is currently enrolled in the PhD program at The University of Texas at Dallas and is pursuing a career as a technical applications scientist in the industrial sector. His meticulous attention to detail and desire to discover optimal and efficient solutions for not only research endeavors, but also scientific protocols, has prepared him to improve the research community by providing support and guidance as he takes a step away from the bench. His desire to study neuroimmunology stems from an early exposure to pre-clinical research during his time spent working in Drs. Theodore Price and Gregory Dussor's Pain Neurobiology Research Group. As an undergraduate researcher, he worked closely with graduate and post-doc mentors on NIH funded research projects modulating the activity of cellular metabolism and determining its efficacy in treating both acute and chronic pain. The opportunity to work closely with well renowned investigators in the field as an undergraduate researcher helped him develop a strong foundation of not only technical skills, but also life skills necessary to pursue a successful career in science, as well as the knowledge to provide meaningful contributions to the field along the way. To that end, the positive experiences he encountered during his undergraduate education inspired him to pursue a doctoral degree in neuroscience under the tutelage of Dr. Michael Burton, whose primary research interests included the intersection of both the nervous system and immune system, with a focus on the interconnected dynamics of neuroimmune signaling in mediating chronic pain. His diverse background and experiences allowed Thomas to pursue both of his passions, neuroscience and immunology, to their fullest potential.

Over the past 5 years as a graduate student, Thomas has worked on numerous projects tailored towards understanding how cell-specific mechanisms during the development of chronic pain are

sexually dimorphic by nature. Until a recent NIH mandate, pre-clinical pain research had been conducted in almost exclusively male subjects, creating an immense void in knowledge considering the mechanistic differences in cellular machinery between males and females. Under the shadow of the current opioid crisis, the lack in efficacy of non-opioid based pain therapeutics in the clinic leaves many questions unanswered. Thomas' research sought to provide a better understanding of the inherent mechanistic differences between sexes that mediate chronic pain development. This dissertation has provided robust preclinical evidence that suggests there are numerous sex differences in the cellular response during chronic pain development. Specifically, a dichotomy exists between sexes in their neuronal and immune-mediated response to tissue injury and inflammation. His experiences thus far have exposed him to the highest caliber of neuroscience research and have provided the necessary skillset to pursue a professional career in science.

Thomas Alexander Szabo-Pardi
Behavioral and Brain Sciences
The University of Texas at Dallas
800 W Campbell Road, Richardson, TX 75080

Chronology of Education:

2017-2022   Doctor of Philosophy
      The University of Texas at Dallas
      Mentor: Michael D. Burton, Ph.D.
      Field of Study: Neuroscience

2017-present   Master of Science
      The University of Texas at Dallas
      Mentor: Michael D. Burton, Ph.D.
      Field of Study: Neuroscience

2013-2017   Bachelor of Science
      The University of Texas at Dallas
      Mentor: Theodore J. Price, Ph.D.
      Field of Study: Neuroscience

Chronology of Employment

2020-2022   Graduate Teaching Assistant
      The University of Texas at Dallas
      Department of Behavioral and Brain Sciences

2019-2020   Graduate Research Assistant
      The University of Texas at Dallas
      Mentor: Michael D. Burton, Ph.D.
      Field of Study: Neuroscience

2017-2019   Graduate Teaching Assistant
      The University of Texas at Dallas
      Department of Behavioral and Brain Sciences

2016-2017   Research Intern
      The University of Texas at Dallas
      Mentors: Theodore J. Price & Gregory O. Dussor
      Field of Study: Neuroscience

2014-2016   Volunteer Undergraduate Researcher

The University of Texas at Dallas
Mentors: Theodore J. Price & Gregory O. Dussor
Field of Study: Neuroscience

Academic and Professional Honors

2020	Santrock Conference Travel Award
2019	Brain and Behavioral Sciences Ph.D. Travel Award
2017	PVST Brain and Behavioral Sciences Scholarship

Grant Applications

2021	F31 Ruth L. Kirschstein National Research Service Award (NRSA) predoctoral fellowship (not funded)
2020	F31 Ruth L. Kirschstein National Research Service Award (NRSA) predoctoral fellowship (not funded)

Professional Collaborations

2021-2022	Abbott Laboratories

Professional Societies

2018-present	International Association for the Study of Pain
2017-present	American Pain Society
2016-present	Society for Neuroscience

Publications

1. **Szabo-Pardi TA**, Barron LR, Lenert ME, Burton MD. Sensory Neuron TLR4 mediates the development of nerve-injury induced mechanical hypersensitivity in female mice. Brain Behav Immun. 2021 Oct;97:42-60. doi: 10.1016/j.bbi.2021.06.011. Epub 2021 Jun 23. PubMed PMID: 34174335; PubMed Central PMCID: PMC8453057.

2. **Szabo-Pardi TA**, Agalave NM, Burton MD. The role of microglia *versus* peripheral macrophages in maladaptive plasticity after nerve injury. Neural Regen Res. 2021 Jun;16(6):1202-1203. doi: 10.4103/1673-5374.300438. PubMed PMID: 33269776; PubMed Central PMCID: PMC8224119.

3. Agalave NM, Mody PH, **Szabo-Pardi TA**, Jeong HS, Burton MD. Neuroimmune Consequences of eIF4E Phosphorylation on Chemotherapy-Induced Peripheral Neuropathy. FrontImmunol. 2021;12:642420. doi: 10.3389/fimmu.2021.642420. eCollection 2021. PubMed PMID: 33912169; PubMed Central PMCID: PMC8071873.

4. **Szabo-Pardi TA**, Syed UM, Castillo ZW, Burton MD. Use of Integrated Optical Clearing and 2-Photon Imaging to Investigate Sex Differences in Neuroimmune Interactions After Peripheral Nerve Injury. Front Cell Dev Biol. 2021;9:624201. doi:

10.3389/fcell.2021.624201. eCollection 2021. PubMed PMID: 34178976; PubMed Central PMCID: PMC8221108.

5. Rudjito R, Agalave NM, Farinotti AB, Lundbäck P, **Szabo-Pardi TA**, Price TJ, Harris HE, Burton MD, Svensson CI. Sex- and cell-dependent contribution of peripheral high mobility group box 1 and TLR4 in arthritis-induced pain. Pain. 2021 Feb 1;162(2):459-470. doi: 10.1097/j.pain.0000000000002034. PubMed PMID: 32796317; PubMed Central PMCID: PMC7808351.

6. Agalave NM, Rudjito R, Farinotti AB, Khoonsari PE, Sandor K, Nomura Y, **Szabo-Pardi TA**, Urbina CM, Palada V, Price TJ, Erlandsson Harris H, Burton MD, Kultima K, Svensson CI. Sex-dependent role of microglia in disulfide high mobility group box 1 protein-mediated mechanical hypersensitivity. Pain. 2021 Feb 1;162(2):446-458. doi: 10.1097/j.pain.0000000000002033. PubMed PMID: 32773600; PubMed Central PMCID: PMC7808363.

7. Agalave NM, Lane BT, Mody PH, **Szabo-Pardi TA**, Burton MD. Isolation, culture, and downstream characterization of primary microglia and astrocytes from adult rodent brain and spinal cord. J Neurosci Methods. 2020 Jul 1;340:108742. doi: 10.1016/j.jneumeth.2020.108742. Epub 2020 Apr 19. PubMed PMID: 32315669; PubMed Central PMCID: PMC7293863.

8. Milligan AL, **Szabo-Pardi TA**, Burton MD. Cannabinoid Receptor Type 1 and Its Role as an Analgesic: An Opioid Alternative?. J Dual Diagn. 2020 Jan-Mar;16(1):106-119. doi: 10.1080/15504263.2019.1668100. Epub 2019 Oct 9. Review. PubMed PMID: 31596190; PubMed Central PMCID: PMC7007359.

9. Inyang KE, Burton MD, **Szabo-Pardi T**, Wentworth E, McDougal TA, Ramirez ED, Pradhan G, Dussor G, Price TJ. Indirect AMP-Activated Protein Kinase Activators Prevent Incision-Induced Hyperalgesia and Block Hyperalgesic Priming, Whereas Positive Allosteric Modulators Block Only Priming in Mice. J Pharmacol Exp Ther. 2019 Oct;371(1):138-150. doi: 10.1124/jpet.119.258400. Epub 2019 Jul 19. PubMed PMID: 31324647; PubMed Central PMCID: PMC6750189.

10. **Szabo-Pardi TA**, Agalave NM, Andrew AT, Burton MD. In Vivo Two-Color 2-Photon Imaging of Genetically-Tagged Reporter Cells in the Skin. J Vis Exp. 2019 Jul 11;(149). doi: 10.3791/59647. PubMed PMID: 31355792.

11. Moy JK, **Szabo-Pardi T**, Tillu DV, Megat S, Pradhan G, Kume M, Asiedu MN, Burton MD, Dussor G, Price TJ. Temporal and sex differences in the role of BDNF/TrkB signaling in hyperalgesic priming in mice and rats. Neurobiol Pain. 2019 Jan-Jul;5:100024. doi: 10.1016/j.ynpai.2018.10.001. eCollection 2019 Jan-Jul. PubMed PMID: 31194015; PubMed Central PMCID: PMC6550116.

12. Inyang KE, **Szabo-Pardi T**, Wentworth E, McDougal TA, Dussor G, Burton MD, Price TJ. The antidiabetic drug metformin prevents and reverses neuropathic pain and spinal cord microglial activation in male but not female mice. Pharmacol Res. 2019 Jan;139:1-16. doi: 10.1016/j.phrs.2018.10.027. Epub 2018 Nov 1. PubMed PMID: 30391353; PubMed Central PMCID: PMC6447087.

13. Moy JK, Kuhn JL, **Szabo-Pardi TA**, Pradhan G, Price TJ. eIF4E phosphorylation regulates ongoing pain, independently of inflammation, and hyperalgesic priming in the mouse CFA model. Neurobiol Pain. 2018 Aug-Dec;4:45-50. doi: 10.1016/j.ynpai.2018.03.001. Epub 2018 Mar 15. PubMed PMID: 30211343; PubMed Central PMCID: PMC6130839.

Presentations
1. **Szabo-Pardi, T.A**., Barron, L.R., Agalave, N.M., Burton, M.D. (2019) Toll-like receptor 4 expressed on lysozmeM^{+} immune cells mediates neuropathic mechanical hypersensitivity development in male, but not female mice. *Society for Neuroscience Meeting.* Chicago, IL.

2. Burton, M. D., Astarbadi, M., Syed, U., **Szabo-Pardi, T. A**., Price, T. J., Thompson, L. T. (2019). Delayed onset of neuropathic pain in the aged after peripheral nerve injury. *NIH Pain Consortium Symposium, Washington, D.C.*

3. Burton, M., **Szabo-Pardi, T**., Garner, K., Tierney, J., & Price, T. (2019). Uncovering Cell-Specific Mechanisms in Sex Differences in TLR4-Dependent Pain. *The Journal of Pain*, *20*(4), S1.

4. **Szabo-Pardi, T.A**., Agalave, N.M., Lindquist, K.A., Burton, M.D. (2018) Sex differences in cell-specific toll-like receptor 4 signaling on neuropathic pain development. *Society for Neuroscience Meeting, San Diego, CA.*

5. Tierney, J., **Szabo-Pardi, T.A**., Burton, M.D., (2018). Palmitic acid induces pain behavior via toll-like receptor 4 on sensory neurons. *Society for Neuroscience Meeting, San Diego, CA.*

6. **Szabo-Pardi, T.A**., Burton, M.D., Cruz, I., Megat, S., Price. T. (2018). Paclitaxel-induced neuropathic pain relies on TLR4 on macrophages in males only. *International Association for the Study of Pain Meeting, Boston, MA.*

7. Burton, M., **Szabo-Pardi, T**., Milligan, A., Castorena, C., Dussor, G., Elmquist, J., & Price, T. (2018). Peripheral nociceptors are not responsible for mediating the analgesic actions of CB1R. *The Journal of Pain*, *19*(3), S3.

8. Burton, M., **Szabo-Pardi, T**., Garner, K., Asiedu, M., Mejia, G., Megat, S., ... & Price, T. (2017). (131) TLR4-dependent pain depends on different cell types in males and females. *The Journal of Pain*, *18*(4), S9.

9. Inyang, K.E., Burton M.D., **Szabo-Pardi, T**., Wentworth, E., Dussor, G., Price, T.J. (2017). Metformin reverses neuropathic and post-surgical pain and spinal microglial activation specifically in male mice. *Society for Neuroscience Meeting, Washington D.C.*

10. Inyang, K., **Szabo-Pardi, T**., & Price, T. (2016). Treatment of Chronic pain: long term effects of Metformin on chronic neuropathic pain and microglial activation. *The Journal of Pain*, *17*(4), S53.